universität wien

DISSERTATION

Titel der Dissertation

„Synthesis of Novel PET-Tracers for the Norepinephrine Transporter“

verfasst von

Christina Rami-Mark, Bakk. MSc.

angestrebter akademischer Grad

Doktorin der Naturwissenschaften (Dr. rer. nat.)

Wien, 2015

Studienkennzahl lt. Studienblatt:	A 796 605 419
Dissertationsgebiet lt. Studienblatt:	Chemie
Betreut von:	Assoc. Prof. Mag. Dr. Wolfgang Wadsak

“Discovery consists of looking at the same thing as everyone else and thinking something different.”

— Albert Szent-Györgyi

ACKNOWLEDGEMENTS

"You don't write because you want to say something;
you write because you've got something to say."

-F. Scott Fitzgerald

Most of all, I would like to thank my supervisor and mentor Prof. Dr. Wolfgang Wadsak for his endless support, understanding, guidance and discussions. He gave me the possibility to take my own path, to learn a lot and has placed his trust on me all the way.
Danke Wolfgang, dass du mich immer unterstützt hast, danke für deinen Rat und Hilfe, wenn mal was nicht so funktioniert hat und für dein Vertrauen in mich.

I would also like to express my gratitude to Prof. Dr. Markus Mitterhauser for his support and bracing discussions.
Danke Markus, für all die inspirierenden Meetings und deine Unterstützung.

Thanks to Dr. Johanna Obermair, she made me learning a lot.
Danke Jo, für alles was du mir beigebracht hast.

To all my teammates and friends at the Radiochemistry and Biomarker Development unit, helping me survive all this stress in the orange world of the AKH by always cheering me up. Thanks for your patience when knocking on your doors asking for help.
You all have become good friends.
Danke euch allen für all die unzähligen Stunden die wir gemeinsam verbracht haben, den Spaß und eure offenen Ohren. Danke an euch Chrysou, Cécile, Moni, Resi, Sarah, Neydher, Luki – für all den gemeinsamen Unsinn und die sinnvollen Experimente den wir in all den Jahren gemacht haben. Ich hab euch sehr liebgewonnen.

Last but not least, I want to express my gratitude to my family, for their everlasting support to follow my ambitions. Thank you Michael for all your unceasing support, encouragement and understanding in the hard and easy times.
Danke, von ganzem Herzen.

TABLE OF CONTENTS

ABSTRACT (english)

A vast number of psychiatric, neurodegenerative and cardiac diseases are characterized by a perturbation of the norepinephrine transporter (NET) indicating its substantial relevance in medical research.

Thus, non-invasive imaging techniques, as for instance positron emission tomography (PET), are the method of choice in order to gain thorough insight into the molecular changes of the NET involved in these pathologies. By intravenous injection of radiolabeled compounds in sub-nanomolar quantities, PET imaging allows the visualization of molecular information revealing transporter or receptor densities within a living subject. These substances are widely known as PET tracers.

The objectives of this thesis were the development, radiolabelling and evaluation of novel PET-tracers for the NET which are not based on the Reboxetine scaffold. Additionally, already existing Reboxetine-derived NET-PET tracers were further improved. Concomitantly, several new lead structures were identified, as well as tested for their NET-affinity, selectivity and pharmacokinetic suitability. Subsequently a structure-activity relationship database was introduced.

Upon a successful accomplishment of the prerequisites, a radiolabelling with the positron emitting radionuclides carbon-11 and fluorine-18 was performed and optimized. The optimum parameters were transferred to an automated synthesizer and a feasible, remotely controlled, automated radiosynthesis presented a constant product quality, while reducing the radiation exposure to a minimum. To ensure highest quality and safety of the radiotracers, a radiopharmaceutical quality control following European guidelines was established.

The binding behavior of the three most promising compounds – [^{11}C]Me@APPI, [^{11}C]Me@HAPTHI and [^{18}F]FMeNER-D2 - was evaluated in human and murine tissue samples using *in vitro* autoradiography. Furthermore, their specificity and selectivity was proven in competition experiments with known NET-ligands. To reinforce the outcomes from the ex vivo tissue autoradiography, binding behavior was tested on a cellular level using hNET expressing membranes in competition experiments. Moreover, metabolic stability of the NET-PET tracers was tested in vitro using human and rat enzymes and plasma.

All trialed parameters indicated that both newly developed NET-PET tracers [^{11}C]Me@APPI and [^{11}C]Me@HAPTHI show highly favorable properties. Their excellent affinity, selectivity as well as enhanced metabolic stability were elucidated within this thesis. Hence, both novel carbon-11 labelled tracers will soon be tested *in vivo* in small animal PET studies. As a future prospective, both radiotracers, [^{11}C]Me@APPI and [^{11}C]Me@HAPTHI, might facilitate a more precise quantification of the NET in humans and show high potential to enhance the comprehension of the NET for clinical issues.

Overall, this manuscript comprises 6 peer reviewed publications and 4 chapters of, so far, unpublished material.

ABSTRACT (german)

Das noradrenerge System, und insbesondere der Norepinephrin Transporters (NET), hat einen sehr starken Einfluss bei einer Vielzahl von psychiatrischen, neurodegenerativen und kardialen Erkrankungen. Um ein besseres Verständnis der Krankheitsbilder und deren Ursachen auf molekularer Ebene zu erhalten, kann man mittels nicht-invasiver Bildgebung diese Stoffwechselvorgänge darstellen. Eine dieser Bildgebungsarten ist die Positronen-Emissions-Tomographie (PET), bei der Substanzen, die radioaktive, kurzlebige Nuklide enthalten, injiziert werden. Diese sogenannten PET-Tracer werden in subnanomolarer Menge eingesetzt und ermöglichen eine *in vivo* Visualisierung der jeweiligen Zielregion.
Um eine Bildgebung des NET mittels PET zu ermöglichen, bedarf es geeigneter, selektiver und spezifischer Moleküle, die anschließend mit Positronen-emittierenden Radionukliden markiert werden.

Ziel dieser Arbeit, war die Entwicklung, Radiosynthese sowie präklinische Evaluierung neuartiger NET-PET-Tracer, sowie die Weiterentwicklung und Optimierung von bereits bestehenden, auf der Reboxetin-Grundstruktur basierend NET-Radioliganden. Es wurde eine Vielzahl neuer Substanzen entwickelt, welche auf Affinität und Selektivität, Lipophilie, Bluthirnschranken-Penetration sowie Stabilität getestet wurden. Daraus wurde eine Struktur-Aktivitäts-Beziehung abgeleitet.
Für jene Substanzen mit geeigneten pharmakokinetischen Eigenschaften, wurde eine Radiomarkierung mit den PET-Nukliden Kohlenstoff-11 und Fluor-18 durchgeführt. Die Synthese wurde zuerst in kleinem Maßstab optimiert und daraufhin wurden die optimierten Bedingungen auf ein voll-automatisiertes Synthesemodul übertragen. Mittels dieser automatisierten Radiomarkierungsmethode kann man größtmögliche Reproduzierbarkeit, hohe Ausbeuten und konstante Produktqualität erhalten, bei gleichzeitig minimaler Strahlenbelastung für die durchführende Person. Zusätzlich wurde für jede radiomarkierte Substanz eine geeignete radiopharmazeutische Qualitätskontrolle aufgesetzt, die dem europäischen Arzneibuch entspricht.
Die vielversprechendsten NET-PET-Tracer wurden *in vitro* auf ihr Bindungsverhalten mittels Autoradiographie auf humanem und murinem Gewebe getestet und in Kompetitionsexperimenten die Spezifität und Selektivität der Bindung bestimmt. Um die autoradiographischen Ergebnisse mit Zellexperimenten zu korrelieren, wurden weitere Bindungsstudien auf humanen NET exprimierenden Membranen durchgeführt. Weiters wurde die metabolische Stabilität in Untersuchungen mit humanen und murinen Enzymen und Plasma bestimmt.
Alle bisher erhaltenen Daten verdeutlichen die Eignung von sowohl [^{11}C]Me@HAPTHI als auch [^{11}C]Me@APPI als potentielle NET-PET-Tracer, da sie herausragende Affinität, Selektivität und Stabilität zeigen. Da auch die logD und Permeabilitätswerte auf eine sehr wahrscheinliche passive Diffusion über die Bluthirnschranke hindeuten, werden in Zukunft beide Radioliganden *in vivo* angewendet werden und könnten Aufschluss über den Einfluss des NET bei den verschiedensten Krankheitsbildern beim Menschen liefern.
Die gesamte Dissertation umfasst 6 publizierte Arbeiten in internationalen Journalen, sowie 4 Kapitel zu noch nicht veröffentlichten Daten.

1. INTRODUCTION

1.1. RADIOCHEMISTRY FOR MOLECULAR IMAGING

1.1.1. Positron emission tomography

In the last 5 decades, positron emission tomography (PET) has become a vital non-invasive molecular imaging technique in clinical diagnostics and preclinical research [1-3]. This functional, nuclear medicine technique enables a tracing of biological and biochemical processes *in vivo* by generation of a 3D image. This molecular imaging modality facilitates not only a 'real-time' monitoring of disease and investigation of drug interactions, but also fosters a deeper understanding in the biochemical processes involved in pathophysiology and neurobiology [4]. Moreover, a quantification of receptors and transporters is possible, even when applied in a subnanomolar (or picomolar) range [2, 4].

For PET imaging, biologically relevant substances are labeled with positron emitting nuclides. These radionuclides decay by emission of a neutrino and a positron (β^+-decay), which subsequently annihilates with an electron (figure 1). This annihilation event culminates in a simultaneous ejection of 2 photons (γ-quants) with 511keV in a 180° angle. The distance, which the positron travels before encountering an electron, is known as positron range. This range is dependent on the energy emitted by the positron and varies for each radionuclide. The larger the distance traveled, the poorer the spatial resolution of the PET scan [4]. The pair of emitted photons is localized along the line of coincidence (or line of response, LOR) by the surrounding detectors of the PET scanner (figure 2). Numerous decay events and therefore LORs enable a localization of the origin of the annihilation. Reconstruction of all registered events leads to the final PET image as a function of time.

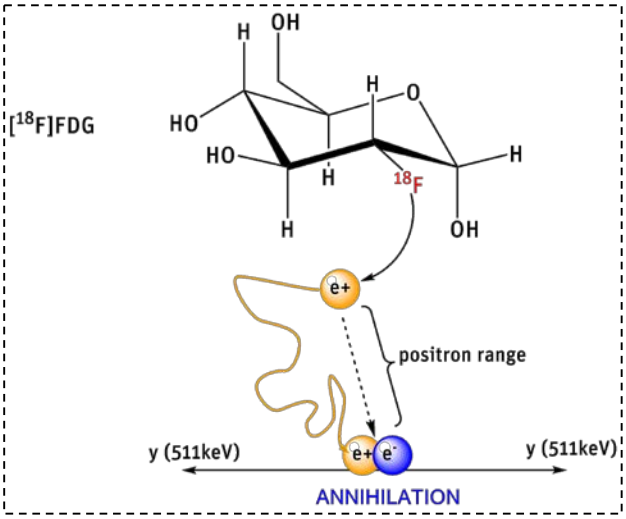

Figure 1: Principle of positron emission tomography imaging: ^{18}F-atom in the radiolabelled glucose molecule ([18F]FDG) decays to a positron (orange). Annihilation occurs upon hitting of an electron (blue). (modified, Chem Rev. 2008, 108,5, 1503)

Since the PET imaging modality provides only a functional information about physiological processes, it has been additionally enhanced by coupling to non-invasive anatomical imaging techniques for morphological allocation of the PET-signal. Thus, fusion images obtained by dual scanners, like PET/CT (computed tomography) or PET/MR (magnet resonance), are replacing more and more 'PET-only' scanners. This development of multimodal imaging enhances the clinical outcome for patient care tremendously by providing additional structural details and improvement of the localization of the PET signal [5-7].

For PET imaging, positron emitters are incorporated into endogeneous molecules or artificial receptor/transporter ligands, enabling an *in vivo* tracking of huge number of biological processes by 'tailoring' of a proper PET probe (so called PET tracers) for each distinct application. One of the prime benefits of the PET imaging technique is the possibility of isotopic substitution of carbon, fluorine,

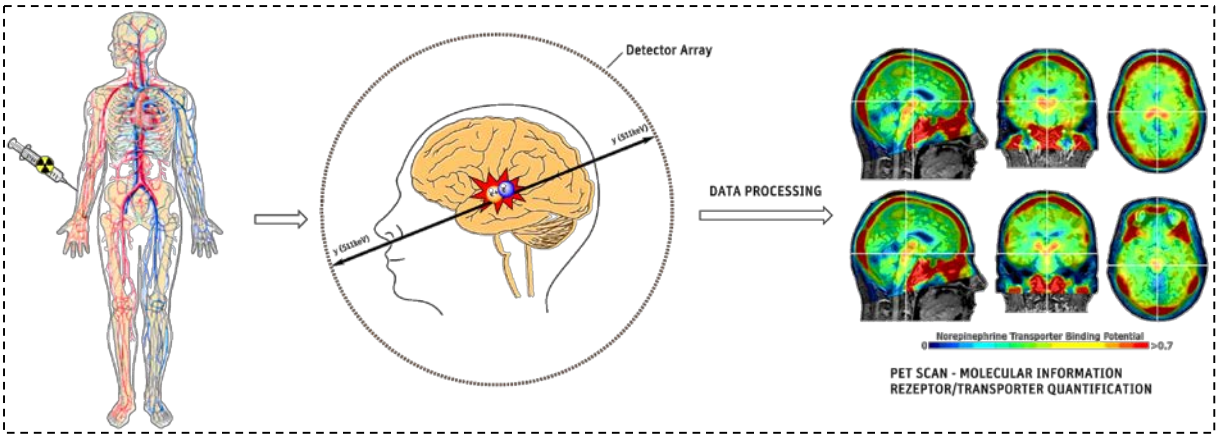

Figure 2: Principle of a PET scan – injection of the radiotracer, detection of coincident photons, data processing

nitrogen or oxygen in biomolecules by their respective radioactive isotope – leading to chemically indistinguishable compounds. Thus, their binding characteristics and physicochemical properties remain unchanged (neglecting a minor isotopic effect) [4]. Unfortunately, the radiochemical labeling of the vast majority of substances with these nuclides is not feasibly accomplished without changing the molecular structure, due to steric or electronical hindrance or lack of suitable radiolabelling synthons. In consequence, the choice of the radionuclide urges a compromise between chemical authenticity, appropriate half-life and reasonable target-binding kinetics. Particularly the bioisosteric replacement of a hydrogen atom or a hydroxyl-group by fluorine-18 leads to an altered lipophilicity and steric perturbations [2, 4, 8]. However, these minor changes in physicochemical and biological behavior are largely acceptable, since their van der Waal's radii are comparable (H: 1.20Å, OH: 1.40 Å, F: 1.35Å) [9]. Moreover, introduction of an additional fluorine label in a position susceptible to metabolic degradation can even enhance the *in vivo* stability of the compound.

1.1.2. Radiochemistry and Radiopharmaceuticals for PET-imaging

PET radiopharmaceuticals are consisting of two (or three) parts: the biological active molecule for target interactions, (a spacer, linker or chelator) and the proper radioactive nuclide. The suitability of positron emitting nuclides for radiolabelling of PET-tracers is limited by their ionic radius and electronegativity, their half-life and β+ energy and their accessibility within a reasonable timeframe. In table 1, the most common positron emitters used for PET imaging are outlined. The short-lived PET radionuclides are predominantly produced within a cyclotron by bombardment of the respective target with accelerated protons or deuterons. The sole accessibility by cyclotron-production puts constraints on their applicability and suitability for routine applications (high efforts, high costs). Especially for the very short-lived PET nuclides oxygen-15 ($t_{1/2}$=2.03min) and nitrogen-13 ($t_{1/2}$=9.98min), but also for carbon-11 ($t_{1/2}$=20.4min) a radiochemical facility is required on site. In contrast, gallium-68 is easily amenable through its generator-production route. Therefore, remote PET centers frequently opt for the ^{68}Ge/^{68}Ga generators, and ^{68}Ga-PET radiochemistry is thriving more and more.

Nevertheless, fluorine-18 and carbon-11 are the most frequently used PET radionuclides, each presenting relative low molecular weights, ideal β^+-energies and ideal half-lifes for diagnostic purposes [4, 7]. Therefore, this thesis will focus primarily on them.

Table 1: Selected PET radionuclides in nuclear medicine [2]

RADIONUCLIDE	HALF LIFE	β^+ ENERGY	PRODUCTION	COMMON TRACERS
Carbon - 11	20.4 min	0,96 MeV	^{14}N (p,α) ^{11}C (O_2) ^{14}N (p,α) ^{11}C (H_2) ^{11}B (p,n) ^{11}C ^{10}B (d,n) ^{11}C	[^{11}C]acetate, [^{11}C]methionin
Fluorine - 18	109.77 min	0.69 MeV	^{18}O (p,n) ^{18}F (F-) ^{20}Ne (d,α) ^{18}F (F_2) ^{18}O (p,n) ^{18}F (F_2) ^{16}O (^{3}He,p) ^{18}F (F_2)	[^{18}F]FDG, [^{18}F]FDOPA, [^{18}F]FET
Nitrogen - 13	9.98 min	1.7 MeV	^{16}O (d,α) ^{13}N	[^{13}N]NH_3
Oxygen - 15	2.03 min	1.19 MeV	^{14}N (d,n) ^{15}O	[^{15}O]H_2O
Gallium - 68	68.3 min	1.9 MeV	68Ge/68Ga generator	^{68}Ga-DOTANOC, ^{68}Ga-PSMA
Copper - 64	12.7 h	0.66 MeV	^{64}Ni (p,n) ^{64}Cu	[^{64}Cu]CXCR4
Rubidium - 82	1.25 min	0.069 MeV	82Sr/82Rb generator	[^{82}Rb]$RbCl_2$

The short half-lives of the PET nuclides urge short radiosynthesis times of the PET tracers. Ideally, the overall synthesis - including purification and quality control time - should not exceed two to three half-lives of the respective radionuclide used [4]. Therefore, the introduction of the radioactive label should be performed latest possible in the synthetic route, and long or complex multistep reactions should be, if possible, avoided. Unfortunately, most synthetic strategies oblige two or more reaction steps and/or include frequently a cleavage of protective groups for sensitive functional groups [4]. To drive equilibrium of the radiochemical reaction towards the product side, a 10^3-10^5 fold excess of the precursor (non-radioactive synthon) is applied. This stoichiometric imbalance leads to a 'pseudo-first-order' reaction kinetics, resulting in increased turn-over rates and decreased reaction times/temperatures [4]. Further reduction of reaction times can be reached by microwave assisted syntheses or microfluidic approaches [10].

Moreover, the question where and how to label a new compound is raised. Generally, there is more than one contrivable labeling strategy existing for a new candidate tracer. And even when the molecular structure of a substance already comprises a carbon or fluorine atom, it does not necessarily imply that a labeling at this position is viable. The following sections will address these issues by outlining all radiosynthetic strategies for fluorine-18 and carbon-11 radiolabeling.

i. Fluorine-18

Fluorine with its electron configuration [He] $1s^2 2s^2 2p^5$ belongs to the halogen elements. The isotope F-19 has 100% abundance, and is naturally occurring as highly reactive, extremely toxic, pale yellow F_2-gas. Its most common oxidation state is -1, which leads to highly polarized C-F bonds and it exerts the uppermost electronegativity of all elements [10]. These special properties put some constraints on its amenability in radiolabelling, especially when additionally taking in mind the production routes for its radioactive isotope ^{18}F (either as $^{18}F_2$ gas, or aqueous $^{18}F^-$). Nevertheless, fluorine-18 is the most important radionuclide for PET imaging. Its ideal 'clean' decay modes (97% b^+, 3% EC) and its comparatively long half-life ($t_{1/2}$=109.77 min) favor multi-step reactions and high resolution PET scans [4, 10].

Cyclotron production of fluorine-18 is predominantly performed by the bombardment of ^{18}O-enriched water with accelerated protons (^{18}O (p,n) ^{18}F) leading to ^{18}F-fluoride. The target bodies need to tolerate the high pressure and the harsh conditions during the bombardment. The target yield of [^{18}F]HF is dependent on the target volume, the grade of the ^{18}O-enrichment and the proton energy. The maximum cross-section energy is found for 15MeV protons. Classic cyclotrons operate between 10-18MeV protons, yielding in up to 100GBq ^{18}F-fluoride within 60min of bombardment [10].

The second production route of fluorine-18 is achieved by cyclotron-bombardment of a neon target with accelerated deuterons (^{20}Ne (d,α) ^{18}F). This pathway leads to the preparation of $^{18}F_2$, unfortunately 0.1%-2% of $^{19}F_2$ gas are indispensably added to the target material, to enable a recovery of the produced $^{18}F_2$ from the target-body walls. In fact, the resulting radioactive product consist of therefore ^{18}F-^{19}F (carrier added). Thus, all labeling strategies allow only a maximum of 50% labeling efficiency [4, 10] and lead to a significant deterioration of specific activity. More recently, Bishop and coworkers identified two other possibilities to obtain electrophilic fluorine by irradiation of an oxygen-18 or oxygen-16 gas target [11-15].

In general, the radiofluorination reactions can be divided into two basic radiolabelling routes: nucleophilic (aliphatic or sp^3 hybridized carbon-fluorine bonds) or electrophilic (non-sp^3 hybridized carbon-fluorine bond) bond formation reactions [16].

Nucleophilic radiofluorinations:

Nucleophilic ^{18}F-fluoride is produced in ^{18}O-enriched water in the cyclotron (table 1). Unfortunately, fluoride is known to be a poor nucleophile in any aqueous media, and nucleophilic substitutions are hampered by traces of moisture. To achieve a strictly anhydrous environment, every nucleophilic radiofluorination starts with the removal of residual target water from the fluoride-18 by transferal over a strong anion exchange cartridge. The fluoride-18 is retained on the resin, whereas the target water can be recycled. The activation and elution of the fluoride-18 with amino polyethers, discovered by Coenen and Hamacher, is achieved in combination with alkali metals or quaternary ammonium carbonates, hydroxides or bicarbonates [17-20]. The most

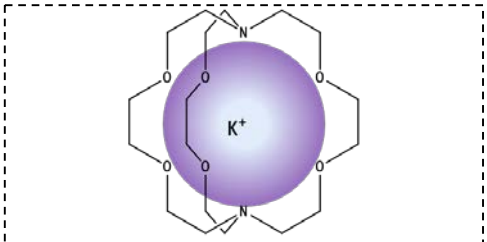

Figure 3: Amino polyether Kryptofix K222 forming its potassium complex.

common cryptand in radiochemistry is 4,7,13,16,21,24-hexaoxa-1,10-diazabicyclo[8.8.8]hexacosane (kryptofix K 2.2.2.) (figure 3) in combination with K_2CO_3 [4, 17, 21-23]. The cavity of kryptofix K2.2.2. is perfectly tailored for the ionic radius of the potassium cation.

Thus, the K2.2.2./K+ complex is employed as counter-ion for the release of the fixed ^{18}F-fluoride from the anion exchange cartridge, and strongly activates its nucleophilicity ('naked fluoride'). Moreover, it enables a partial dissolving of hydrophilic [^{18}F]fluoride in organic solvents (acetonitrile, DMSO, DMF). Alternatively, tetra-alkyl ammonium salts can be used as phase transfer catalysts, often resulting in reduced reaction times [4, 20, 24]. Residual trace amounts of water are removed by repeatedly drying of the [^{18}F]fluoride with acetonitrile (ACN), since the positive azeotrop of water and ACN decreases the boiling point to 76°C [25]. Hence, a repeated addition of small portions of dry ACN keenly supports the complete removal of remaining water vestiges. Recently, Wessmann et al. propounded the dispensability of the azeotropic drying step when the [^{18}F]F- is dried by ACN flushing before release with the K2.2.2./K^+ [26]. Current research is concerned with the use of protic solvents [7, 16, 27], or ionic liquids [28, 29] replacing the traditional reaction media.

For *aliphatic nucleophilic* substitutions, the reaction proceeds via SN_2 mechanism. Favorably SN_2 reactions are preferably performed in aprotic, polar solvents. Aliphatic compounds showed best conversion rates in acetonitrile. To avoid competing reactions (i.e. elimination reactions), the basicity of the reaction mixture needs to be monitored carefully. Leaving groups in the precursive substances are predominantly halides (Br, I) or bulky esters (figure 4, triflates, tosylates, nosylates, sulfonylates) [4, 10, 30, 31].

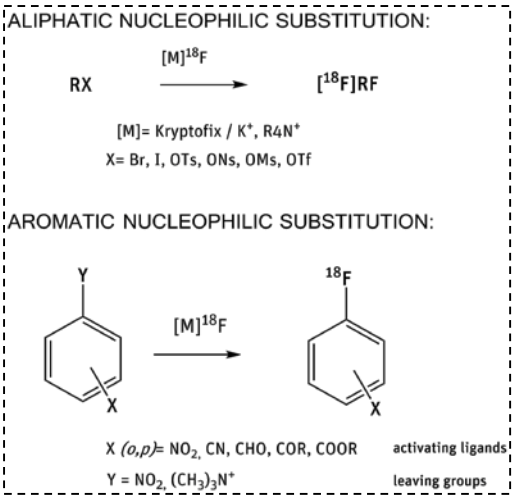

Figure 4: Overview on nucleophilic substitution reactions (modified, [4])

The utmost important and prominent PET radiopharmaceutical is a fluorine-18 labelled glucose derivative: 2-desoxy-2-[^{18}F]fluoro-D-glucose ([^{18}F]FDG) (figure 1). It is prepared via SN_2 reaction (figure 5) and subsequently used for the *in vivo* investigation of the glucose metabolism and transport in the human brain – known to be highly up-regulated in tumor tissue and inflammation areas. Thereby, it enabled for the first time *in vivo* cancer diagnosis and initiated the basic field of neuroimaging [32, 33]. [^{18}F]FDG was first described by Ido et al in 1978 in a cooperation between the NIH, the University of Pennsylvania and the Brookhaven National Laboratory [33, 34]. A later modification by Hamacher et al. was significantly improving the radiosynthesis by introduction of an amino polyether (figure 3 & 5) to support the nucleophilic substitution [17]. It allowed a preparation of [^{18}F]FDG with 50% radiochemical yield (not corrected for decay), which enabled a broad clinical

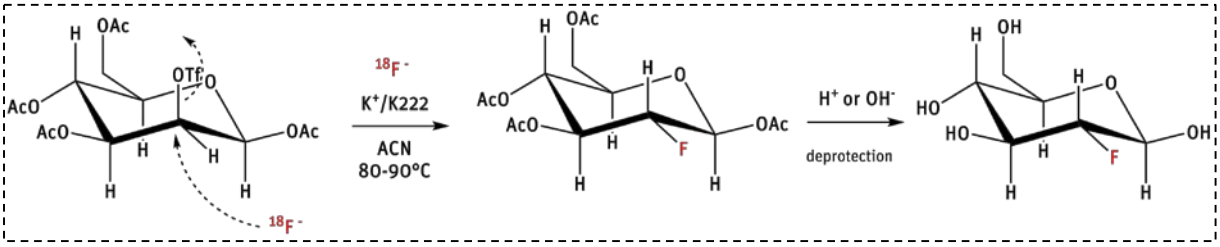

Figure 5: [^{18}F]FDG synthesis by nucleophilic substitution

application and satellite delivery, thereby starting it's triumph [10].

Current research proposed an aliphatic SN_2 reaction without a precomplexation with the metal cation of a phase transfer catalysts. Hereby arylsulfonate nucleophile assisting leaving groups (NALGs) are facilitating the nucleophilic radio-halogenation by stabilization of the charge in the transitions state [35].

Aromatic nucleophilic substitutions (SN_{AR}) are supported by activating ligands (figure 4) in the precursory molecule in *ortho*- or *para*-position [36-39]. Preferably strong electron-withdrawing groups are used for the activation of the leaving groups (NO_2, $(CH_3)_3N^+$) to stabilize the Meisenheimer complex in the sigma transition state [40, 41].

However, direct labelling of the precursor is not always viable. Hence, two-step [^{18}F]fluoroalkylation strategies are utilized for either sensitive compounds, which are prone to decomposition in the harsh labeling conditions, or for compounds not accessible in a direct labeling route. Therefore, several methods for the radiofluorination via prosthetic groups have been developed. Small [^{18}F]fluoroalkylation synthons, like [^{18}F]fluoromethyl bromide, [^{18}F]fluoroethyl bromide, [^{18}F]fluoromethyl triflate, [^{18}F]fluoroethyl triflate, [^{18}F]fluoromethyl tosylates or [^{18}F]fluoroethyl tosylates, are prepared by nucleophilic aliphatic substitution [4, 10, 42-45]. Subsequently, these [18F]fluoroalkylation probes are introduced into the desired molecule (e.g. in the synthesis of [^{18}F]fluorocholin, [^{18}F]fluoromethylcholin, [^{18}F]FECIT, [^{18}F]FET [^{18}F]FMeNER-D2) [31, 42, 46-60]. Some of these reactions require a pre-purification of the labeling synthon by distillation, putting some constraints on their routine availability [31, 56, 59, 61, 62]. Nevertheless, the radiochemical yield and purity of the second alkylation step is increased tremendously by this separation procedure. As an example, the two-step [^{18}F]fluoro(deutero)methylation of [^{18}F]FMeNER-D2 is presented in figure 6.

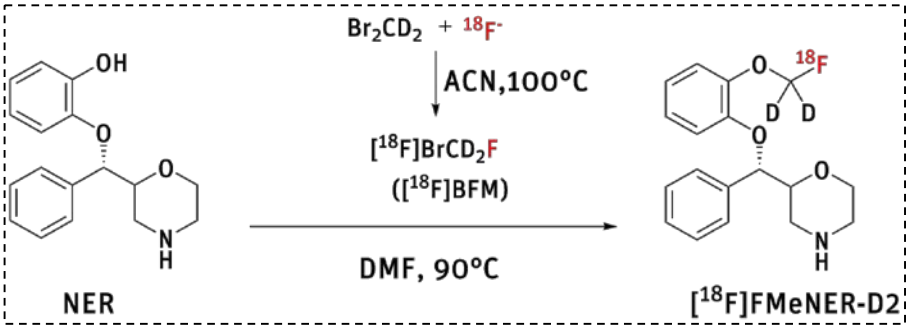

Figure 6: Radiochemical [^{18}F]fluoroalkylation of NER, resulting in the PET tracer [^{18}F]FMeNER-D2

To overcome the issues of labeling of electron-rich arenes without activating groups, where common SN_{AR} reactions are not feasible, promising methods were described using diarlyiodonium salts and [^{18}F]fluoride [63-66]. These complex radiosynthetic mechanisms are hitherto not fully understood, but there is confirmatory evidence that *ortho*-substituents can be replaced by [^{18}F]F^- [63].
Further development of 4-[^{18}F]fluoro-1-iodobenzene as labeling reagent was done by Wuest et al. [67-69]. This synthon is prepared from a diaryldiiodonium triflate and [^{18}F]fluoride, resulting in the respective 4-[^{18}F]fluoro-1-iodobenzene. This versatile radiolabeling probe can be used for cross coupling reactions with stannylated precursors via Stille coupling, or employed in Buchwald-Hartwig-type reactions under Pd-catalysis [70].

Electrophilic radiofluorinations:

For the production of electrophile [^{18}F]fluorine, there are basically two processes available. Originally, for electrophilic fluorination reactions [^{18}F]F_2 was used directly produced from the cyclotrone (table1) [7, 10, 16]. This production route requires the addition of $^{19}F_2$ as a carrier (c.a., carrier added) to reach a complete retrieval of the produced fluorine-18. Unfortunately this process leads to an isotope exchange, and therefore, highly reduced maximum radiochemical yields and specific activity is observed. However, the major drawback of electrophilic fluorinations using [^{18}F]F_2 is its low regioselectivity due to its strong reactivity [10, 16]. Substitution of the precursors with electron donating groups was shown to reduce significantly the formation of side products [31, 71]. Also substitution of organometallic precursors yields in a further enhanced regioselectivity (figure 8) [31, 71-74]. Alternatively, [^{18}F]F_2 can be used for generation of subsequent fluorination reagents (figure 7). It can be converted into the more selective [^{18}F]perchloric fluoride [4], [^{18}F]acetyl hypofluorite [71, 75], [^{18}F]xenon difluoride [76] or [^{18}F]fluorosulfonamide [77].

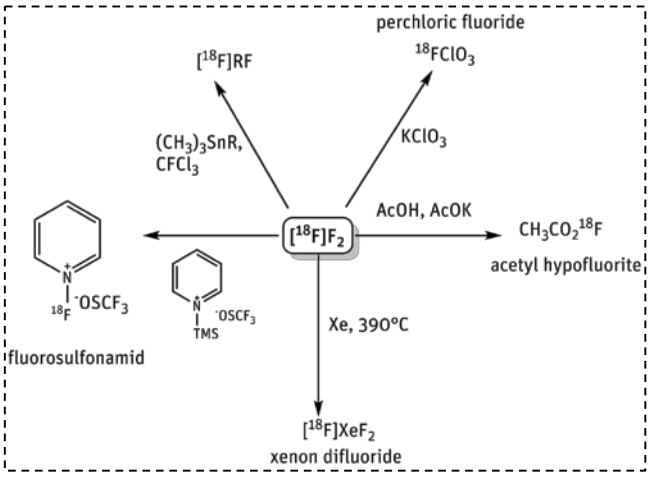

Figure 7: Electrophilic [^{18}F]labeled reagent pathways, (modified, [4])

The acetyl [^{18}F]hypofluorite was initially developed in the 1980s for the preparation of [^{18}F]FDG [78], but was promptly replaced by a nucleophilic substitution reaction. The most prominent example of an electrophilic [^{18}F]fluorination is presented in the synthesis of [^{18}F]F-DOPA (figure 8), a PET-radiotracer for imaging of Parkinson's disease [23, 79-81].

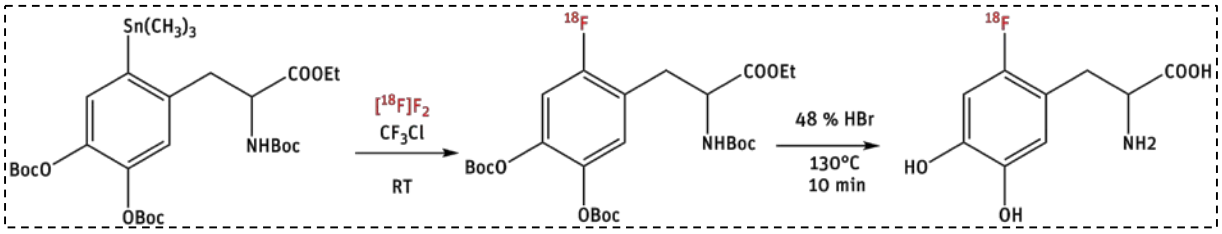

Figure 8: [^{18}F]FDOPA synthesis by electrophilic substitution [25,78-80]

Click chemistry:

Very recently, the field of ^{18}F-click chemistry started to spread in PET-radiochemistry. Yet still in its infancy, it shows encouraging results for the radiochemical labeling of a manifold of substances [4, 82-84]. These new click reactions favor selective labeling of biomolecules with high yield under biological conditions [85].

Moreover, the use of a bio-orthogonal labeling strategy for the radiolabeling of biomolecules has attracted increasing interest, facilitating a tracking of covalent chemical reaction in the native environment of the eobiotic compounds [84, 86].

ii. Carbon-11

Apart from fluorine-18, the most frequently used PET nuclide is carbon-11, with its ideal positron energy, clean β^+ decay mode and short half-life ($T_{1/2}$=20.38min). Carbon is a non-metallic tetravalent element, forming covalent bonds. Naturally two isotopes are predominantly existing (^{12}C, ^{13}C). The high abundance of carbon in biomolecules and drugs offers a huge leeway for radiolabeling, without alteration of the chemical structure of the target substance. Thus, a 'carbon-11-copy' of the chosen molecule is generated [10]. Especially in CNS tracer development, there is ample support for this 'model-compound' PET-tracer imaging. Moreover, the ^{11}C-labeling provides theoretically the complete reaction portfolio of conventional organic chemistry [10].

However, there are some negative premises to be taken into account. One of the prime limitations is the restricted access for secluded institutions. The short half-life does not permit a satellite distribution of ^{11}C-labeled PET-tracers. Moreover, the involvement of radioactive, gaseous intermediates requires a fully automated, rapid radiosynthesis in a closed, lead shielded environment. The total reaction time should be aimed at a maximum of 3 half-lives (including purification and formulation), to ensure sufficient yield for a latter application in research or clinics. Thus, the number of involved reactions steps should be considerably low, and the purification efforts and time are urged to be crisp and concise.

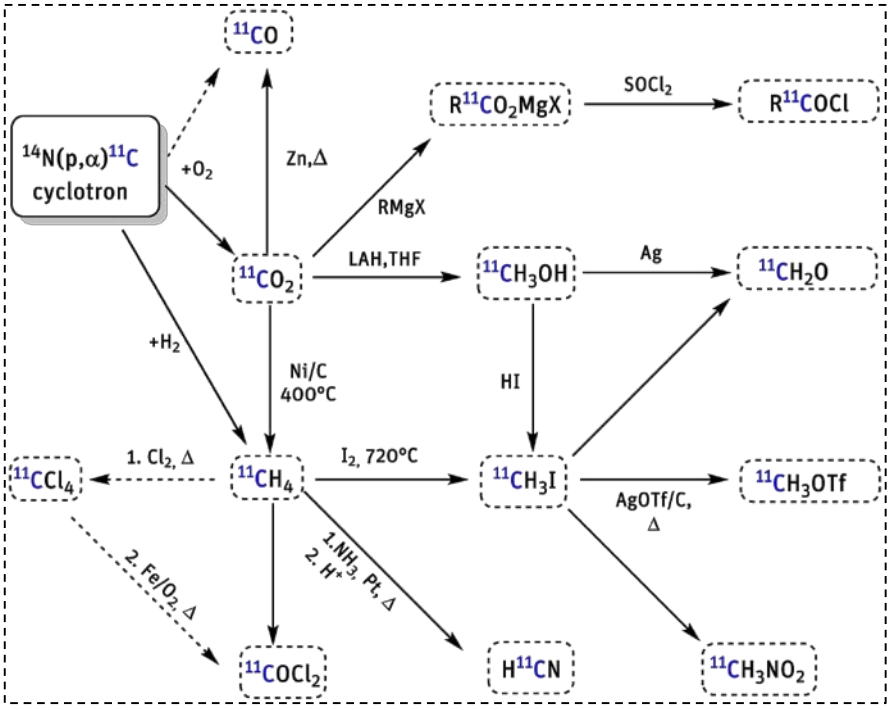

Figure 9: Strategies to access the different carbon 11 labelling reagents [4,12]

From the multitude of nuclear reactions for ^{11}C-production, the bombardment of $^{14}N_2$ with accelerated protons in the cyclotron is the most prevalent [4, 87, 88]. As depicted in figure 9, there are two main ^{11}C-radiolabelling progenitors directly accessible by cyclotron production: $[^{11}C]CH_4$ or $[^{11}C]CO_2$, dependent on the target gas mixture ($^{14}N_2$+ <2%O_2 or +5-10%H_2) [4, 89]. These two primary labeling precursors are offering a plentitude of derived ^{11}C-labeling synthons (figure 9).

^{11}C-Methylation reactions:

Nucleophilic ^{11}C-methylations are presenting the vast majority of ^{11}C-radiolabeling reactions, thus being versatile for the radiolabeling of probes bearing a hydroxyl, carboxyl, thiol or amine function. In general, the most commonly used radiolabeling agent is [^{11}C]CH_3I, developed by Comar in 1973 as so called 'wet-method' [4, 90, 91] (figure 10). Hereby, the cyclotron produced [^{11}C]CO_2 is first reduced with lithium aluminium hydride (LAH, $LiAlH_4$) to the alcohol, and subsequently converted with hydrogen iodide into the respective halide. Over 20 years later, Larsen et al. propounded the alternative 'gas-phase' or 'dry' method for the preparation of [^{11}C]methyliodide (figure 10) [92, 93]. Hereby, the [^{11}C]CO_2 is converted by a Nickle-catalyzed hydrogenation into [^{11}C]CH_4. Free radical iodination of the [^{11}C]methane with elementary iodine at highly elevated temperatures gives the desired [^{11}C]CH_3I. Overall, the gas-phase reaction is progressively evolving as the method of choice of the preparation for the preparation of [^{11}C]CH_3I. To increase the reactivity of the radio-methylation agent, on-line conversion of [^{11}C]CH_3I to [^{11}C]CH_3OTf can be accomplished by passage through a AgOTf impregnated charcoal column at 190°C [94, 95]. With the resulting [^{11}C]methyl triflate a methylation of less reactive nucleophiles can be reached.

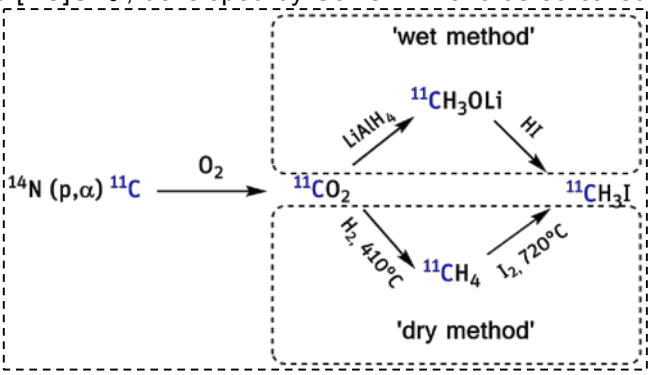

Figure 10: Wet and dry methods to prepare [^{11}C]CH_3I

^{11}C-Grignard reactions:

The preparation of ^{11}C-acyl halides and subsequent ^{11}C-grignard acylation of suitable progenitors presents a further strategy for ^{11}C-radiolabelling [96-101]. Reaction of a Grignard reagent RMgX with [^{11}C]CO_2 yields a [^{11}C]carboxymagnesium halide, which can be either hydrolysed to the respective [^{11}C]carboxylic acid or converted into reactive [^{11}C]acid halide (figure 11) [10, 102]. The trapping of [^{11}C]CO_2 in the dissolved Grignard reagent must be done with a distinct flowrate (<10ml/min) to ensure quantitative conversion. Moreover, a strictly anhydrous environment has to be provided throughout the whole synthesis. For the [^{11}C]-carboxylation reactions a 'wet' (vial-based) [98, 103] and an 'in-loop' (coiled polyethylene tubing, thin film of RMgX) [99, 101, 104] method have been proposed. Further reactions of [^{11}C]acyl chlorides with aliphatic or aromatic amines to the respective amides include the preparation of the PET tracers [^{11}C]WAY-100635, [^{11}C]PHNO or [^{11}C]Zofenoprilat [97, 101].

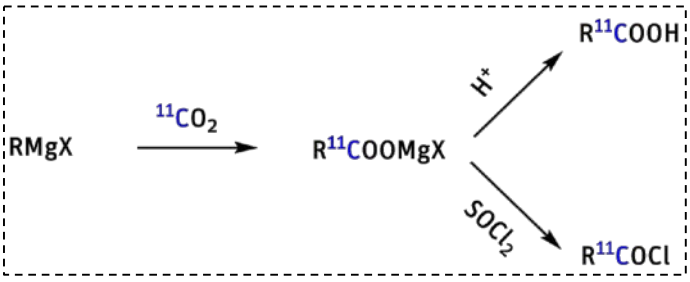

Figure 11: Reaction of a Grignard reagent with [^{11}C]CO_2

Additional ^{11}C-reactions:

Recent trends in ^{11}C-radiochemistry point towards organometallic-mediated ^{11}C-C bond forming reactions. Amongst these, either Pd-mediated ^{11}CO insertions, Pd-mediated Stille coupling of [^{11}C]CH_3I and Suzuki cross-coupling reactions are showing promising results [10, 105-107].

iii. Automation of Radiosyntheses

The rapidly growing field of PET and PET-radiochemistry raised the need for fast, safe and reproducible radiosyntheses. Therefore, automated radiochemical synthesizers (so called modules) for the production of PET-tracers were developed and implemented in daily routine preparations [108-110]. Aiming at flexible, multipurpose automated apparatus, a multitude of versatile modules have been developed for radiolabeling and purification of the radiopharmaceuticals [108].

Hence, the main premises behind the automation of radiosyntheses are outlined:

- Allowing a handling of high amounts of radioactivity for batch productions

  without manual intervening (maximum reduction of radiation exposure during syntheses)
- Allowing a reproducible and fast radiochemical synthesis
- Being flexible and versatile for many different reactions settings
- Including a preparative HPLC system for on-line purification
- Being easily programmable for new reactions set-ups
- Requiring only small space, inevitable for installation in hot cells
- Compatibility with international standards for production of pharmaceuticals (GMP, GLP, GRP,…)

The utmost obvious consequence of automated radiosyntheses is the reduction of the radiation burden for the radiochemists to a minimum extent. Moreover, the simplified, fully automated synthesis shrinks the possibility of potential human faults, and enlarges the availability of PET radiopharmaceuticals for routine applications.

A multitude of commercially available synthesizers is nowadays accessible, fulfilling most of the above mentioned criteria. Thereof, two modules were used within this thesis, and will be therefore included in a short discussion: TRACERlab FX C Pro and the Nuclear Interface® synthesizer (both GE Healthcare, Uppsala, Sweden).

For ^{11}C-radiosyntheses, the TRACERlab FXc Pro module was used. It is equipped with a methylation unit, where the ‘dry’ production method of [^{11}C]MeI is implemented. For direct use of [^{11}C]CO_2 in carboxylation reactions, a bypass of the methylation unit is embedded. It features several ascarite traps to provide an anhydrous environment for high yields. Moreover, cooling is supported by liquid nitrogen, which reduces the cool-down time tremendously in comparison to conventional syntheses. For purification of the respective tracer, it is connected to a semi-preparative HPLC system (equipped with UV and γ-detector), and features a solid-phase-extraction (SPE) based final purification. All steps are remotely controlled by a laptop with the dedicated software. For each molecule, a special commando-timeline can be programmed and the resulting macro can be provided for GMP-like syntheses. In figure 12, the flowscheme of the ^{11}C-synthesizer is presented. This module was used within this thesis for all

^{11}C-reactions (i.e. [^{11}C]Me@APPI, [^{11}C]Me@HAPTHI, [^{11}C]FAPPI:1).

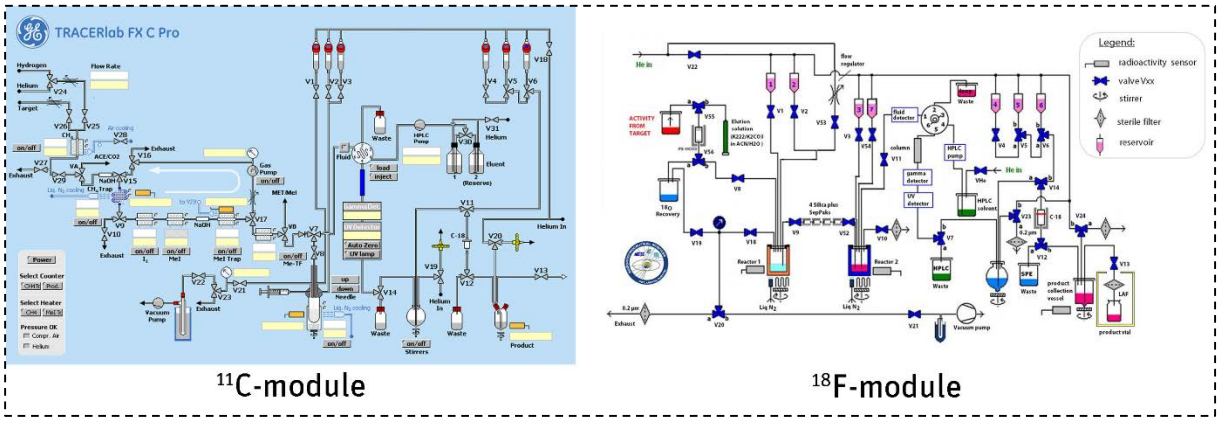

Figure 12: Flowscheme of the Tracerlab FxC Pro and Nuklear Interface synthesizers (GE Healthcare)

For fluorination reactions (nucleophilic substitutions and fluoroalkylations) the Nuclear Interface® synthesizer was used. It is additionally equipped with a second heatable/coolable reaction vessel, which allows a distillation purification between two reaction steps. Moreover, it features an extra vacuum pump to enable the ^{18}F-fluoride fixation and release, as well as to support the azeotropic drying procedure. This module was used for the preparation of all ^{18}F-labeled tracers in this thesis (i.e. [^{18}F]FE@APPI and [^{18}F]FMeNER-D2).

iv. Quality control of PET-tracers

The preparation of PET radiopharmaceuticals requires a strict quality control to guarantee highest purity and safety for animal or human application. In the European Pharmacopoeia, there are guidelines to be followed for each produced PET-tracer [1, 111]. Since there are yet no guidelines present for newly developed radiopharmaceuticals, the criteria of the already established tracers are used. In table 2, the main tested parameters are outlined.

For every produced PET-tracer, chemical and radiochemical purity and identity are tested and confirmed by analytical HPLC with UV and gamma-detection. Especially for CNS-tracers, specific activity ought to be high to ensure a reliable and feasible quantification of receptors or transporters. For metabolic tracers, it presents only a minor issue. For fluorinated ligands, the residual amount of amino-polyether is determined via a spot test, and should not exceed 50µg/mL of final product solution. Moreover, residual solvents from the reaction media or preparative HPLC purification should not exceed their respective safety limit and are tested by gas chromatography (GC). Since the PET-radiopharmaceuticals are applied intravenously, the final product solution needs to be in a physiological range. Therefore, pH and osmolality are tested for every batch produced. Last but not least, the sterility and absence of endotoxins is tested. The time for micro bacterial growth would exceed the timeframe of the short-lived PET-nuclides, therefore the sterility and microbiological safety is confirmed after release of the radiopharmaceutical as in-process control.

Table 2 : Radiopharmaceutical quality control criteria, test methods and applied thresholds [1]

CRITERIA	TEST METHOD	THRESHOLD
Chemical purity	HPLC: UV-detection	no side products, reasonable low precursor amounts, high specific activity
Kryptofix (only ^{18}F-tracer)	colour spot test	<50µg/mL
Radiochemical identity	HPLC: UV-detection & γ-detection	same retention time
Radiochemical purity	HPLC: γ-detection	<95%, a single impurity should not exceed 3%
Radionuclidic identity & purity	half-life & γ-spectrum	half-life ± 10%, y-spectrum: peak at 430-520keV
Residual solvents	GC (FID)	ACN <410ppm, DMF <880ppm, DMSO <5000ppm, MEK <5000ppm, EtOH <8.5%
pH	pH electrode	4.5-8
Osmolality	osmometer	200-400 mosm/kg
microbiological purity & sterility	LAL-test & sterility test	no endotoxins (<1 EU/mL) sterile
Particle contamination	visual inspection	free of particles
Sterile filter integrity	bubble point test	no bubbles <50psi

1.2. NEUROTRANSMISSION

In the central nervous system, neurons have developed exceptional abilities for signal transduction. These inter- or intracellular communication strategies are accomplished by the process of neurotransmission (latin: *transmitto* = send, let through, convey across). Intercellular signaling is thereby mediated by the release of so called neurotransmitters, small endogenous molecules that are released from the presynaptic neuron by exocytosis in response to a threshold action potential and Ca^{2+} influx [112]. Upon binding of these neurotransmitters on postsynaptic receptors, the signal is transduced to the adjacent neuron. This binding can elicit both excitatory and inhibitory effects on the postsynaptic neuron. Moreover, these effects can be either short term effects (such as changes in the postsynaptic membrane potential) or prompt longer term changes by activation of signaling cascades. The termination of signaling is triggered, besides degradation and diffusion, by the re-uptake of excess neurotransmitters from the synaptic cleft into back in the neuron using presynaptic reuptake transporters [113].

Besides amino acids and peptides, monoamine neuromodulators form the major neurotransmission systems in the human body. Amongst these, the dopaminergic, serotonergic and adrenergic systems are the key neurotransmitter pathways in the human brain [114, 115]. These monoamines are classified by their NH2-group linked via an ethyl group to an aromatic ring scaffold, and can by assorted into catecholamines (dopamine (DA) and noradrenalin (norepinephrine, NE)) and tryptamines (serotonin (5-hydroxytryptamine)) (figure 13).

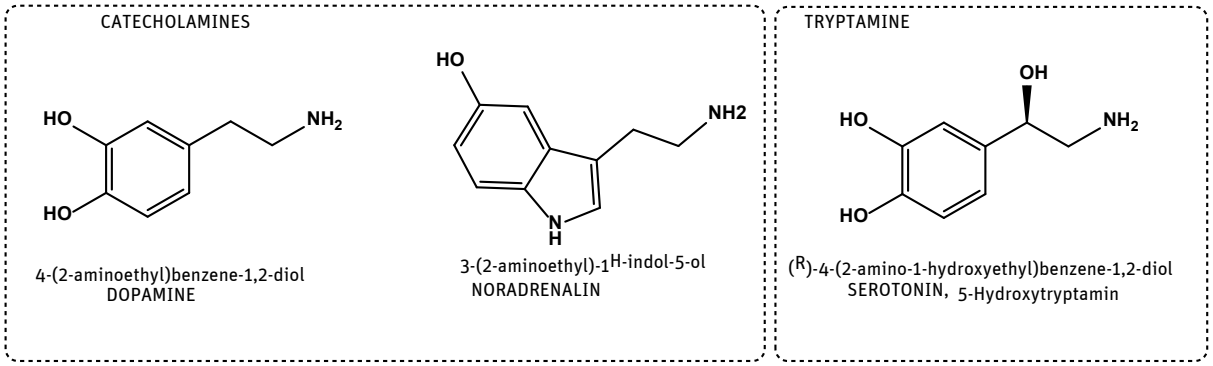

Figure 13: Three major monoamine neurotransmitter dopamine, noradrenalin and serotonin.

First evidence for the presence of catecholaminergic neurons in the human brain was found in the 1970s [116-124] in the cerebellum. The abundance of these neurons is not uniformly over the human brain. Dopaminergic neurons can be found most prominently in the ventral midbrain regions (i.e. substantia nigra and ventral tegmentum) and to a smaller extent also in the diencephalon [125, 126], also their projections are well-limited to the nigro-stratial regions. Serotonergic neurons are typically located in the hindbrain areas with the vast population in the raphe nuclei [126-128]. Noradrenergic neurons are peaking in their highest density in the locus coeruleus (LC), the major adrenergic nucleus in the metencephalon. In contrast, their projections are widely distributed and reaching from the LC axons virtually all brain regions [126, 127].

1.3. THE (NOR-)ADRENERGIC SYSTEM

Adrenergic receptors and transporters are expressed ubiquitously in the mammalian tissue, forming thereby one of the principal neurotransmitter systems in the sympathetic nervous system and the CNS. In figure 2, an (nor-)adrenergic synapse is shown. The presynaptic membrane comprises on the axonal terminal the norepinephrine transporters. Adrenergic receptors are located on the postsynaptic membrane. The natural ligands for both receptors and transporters are adrenalin and noradrenalin, mediating the fight-to-flight stress response via the sympatho-adrenomedullary sytem [129, 130]. Within the CNS, NE is involved in sleep and mood regulation, behavioral expression and exerts central control over the endocrine and autonomic nervous system. Furthermore, NE is located in sympathetic nerve endings [131, 132]. Although the LC–NE system is innervating virtually the entire central nervous system by efferent projections, the basal ganglia (striatum, globus pallidus) presents an exception, being nearly devoid of noradrenergic input [133].

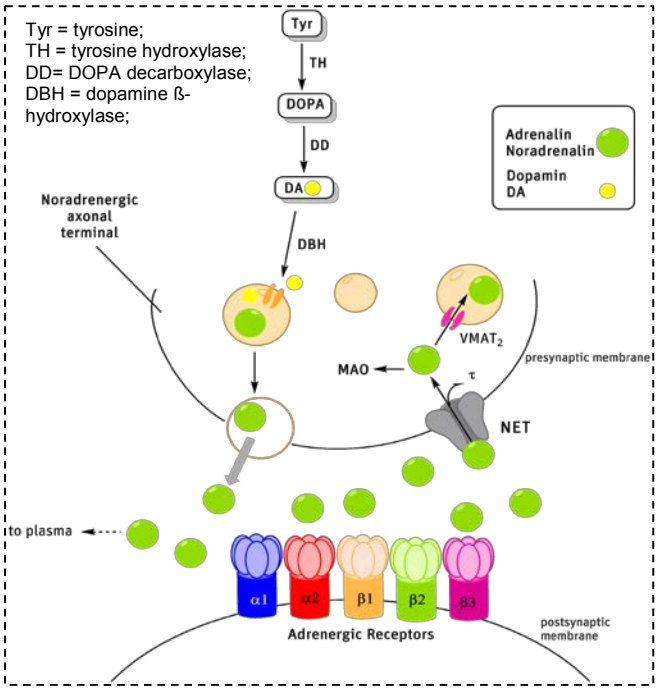

Figure 14: Noradrenergic Synapse

Besides their effect on cardiovascular response and endocrine processes, disturbed regulation in these neurotransmitter systems, and particularly in the NE-system, leads to severe neurological or psychiatric impairments, like major depression, schizophrenia, Alzheimer's dementia (AD), or Parkinson's disease (PD) [134-140]. For the understanding of the underlying (patho-)physiological mechanisms, a deeper insight on a molecular level is of high interest.

Norepinephrine is the primary neurotransmitter for postganglionic sympathetic adrenergic nerves [141]. NE is synthesized in the locus coeruleus and adrenal medulla within noradrenergic neurons (figure 14) starting from the amino acid tyrosine [142]. After enzymatic hydroxylation to DOPA and decarboxylation, the resulting neurotransmitter dopamine is converted intravesicularly into NE. Via Ca^{2+}-dependent exocytosis, NE is released into the junctional cleft. There, it can be bound either to postsynaptic adrenoreceptors stimulating effector organ response or taken back up into the presynaptic neuron via the norepinephrine transporter (NET) [132]. The distribution pattern of NE in the brain was first described in 1954 by Vogt [142]. Highest concentrations of NE were found in the hypothalamus, but also in metencephalon, medulla oblongata and striatum [132]. NE constitutes about 20% of total catecholamine content of the human adrenal medulla [141]. Present understanding of the disposition and metabolic fate of NE has evolved over the last 20 years, identifying a plethora of enzymes to which its metabolic clearance is attributed. The predominant enzymes involved in the NE-degradation are catechol-O-methyltransferase (COMT) and monoamine oxidase A and B (MAO). The latter metabolite is vanillyl mandelic acid (VMA), which is excreted hepato-biliary [130, 132, 143].

1.2.1 Adrenoreceptors

The postsynaptic key target for adrenalin or noradrenalin in the body are the adrenergic receptors. They form a crucial element in the sympathetic nervous system, thus being mainly responsible for maintenance of homeostasis, regulation of physiological processes and response to stress [144, 145]. The adrenoreceptors form a family of cell surface receptors, which carry out signal transduction via coupling to guanine nucleotide binding proteins (G-proteins). In the adrenergic receptor signaling cascade, an adrenergic receptor is activated by initial ligand binding. A heterodimeric G-protein is subsequently coupled, thereby activating signaling factors like G protein kinases and downstream effectors for signal amplification and propagation [144]. The adrenergic receptors (AR) consist of nine subtypes: α_1AR (α_{1A}AR, α_{1B}AR, α_{1D}AR), α_2AR (α_{2A}AR, α_{2B}AR, α_{2C}AR) and β_1AR, β_2AR and β_3AR [144, 145]. They differ by their G-protein coupling pathways (figure 15), α_1AR couple to G_q-proteins (stimulation of phospholipase C), α_2AR couple to G_i-proteins (inhibition of adenylyl cyclase) and βAR couple to G_s-proteins (stimulation of adenylyl cyclase) [144-147].

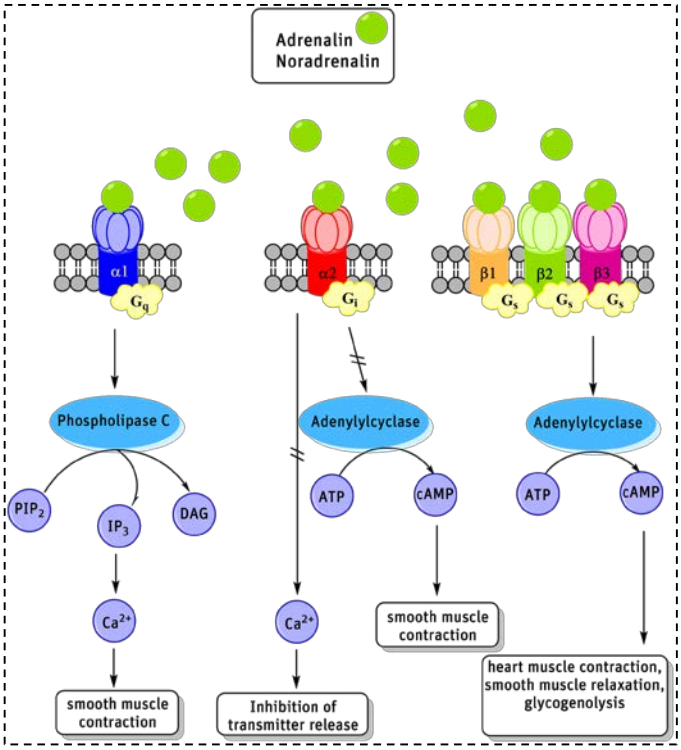

Figure 15: Adrenergic pathway

Thus, different response to (nor-)adrenalin binding to the different receptors is observed. Stimulation of αAR and thus activation of phospholipase and inhibition of adenylyl cyclase leads to vasoconstriction and smooth muscle contraction. Moreover, endocrine effects on insulin sequestration and glyogenesis are reported [143]. On the contrary, β-adrenergic activation drives heart muscle contraction and vasodilatation (e.g. increase of bronchial flow) [141]. The importance of these receptors is demonstrated clearly, when taking a look on the most frequently prescribed drugs. The class of β-adrenergic (ant-)agonists (so-called β-blockers) form one of the leading classes of prescription drugs in the last three decades (i.e. Statistic Austria: in 2006/07: 37.6% of drugs for hypertension, 14.1% other cardiac failures). Thus leading to a significantly reduced mortality rate in cardiac diseases [148, 149]. More recently, an impact of the β-adrenergic system in tumor progression and cancer therapy was reported, indicating towards a valuable new target for an anti-tumor treatment [129]. However, a deeper examination of the mechanisms in stress response and action of β-ARs in tumor blood vessel normalization has to be done.

1.2.2 Norepinephrine Transporter (NET)

The norepinephrine transporter (NET) is a monoamine transporter of the solute carrier chain protein 1 family. It consists of 617 amino acids and constitutes 12 hydrophobic transmembrane domains with cytoplasmatic C and N termini (figure 16) [150-152]. The NET is a Na^+/Cl^- co-transporter protein located on the presynaptic terminal of the glial membrane. It is involved in NE clearance from the synaptic cleft, driven by an ion concentration gradient generated by a Na^+/K^+ ATPase [153]. By facilitation of the re-uptake of the neuromodulator NE, it terminates the noradrenergic action on postsynaptic ARs, regulates thereby the NE concentration in the synaptic cleft and supports presynaptic homeostasis [150, 151, 153].

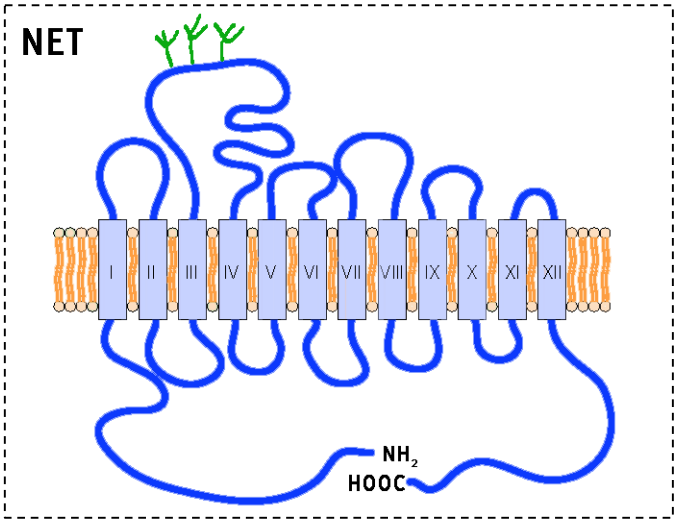

Figure 16 Schematic NET protein structure embedded in the membrane. Transmembrane domains (light blue; I-XII) of the NET are connected to intra- and extracellular loops (depicted blue). Glycosylation sites are colored green. (modified, Nature Rev.Neurosci.2003, 4, 13.)

The NET is located on the human chromosome 16 [151]. In 1961, Hertting and Axelrod discovered the NET as the first re-uptake transporter in the human body [154]. Until the 1990s understanding of the amino acid sequence of NET was limited by the lack of sufficiently purified proteins for sequencing. Profiting from the advances in molecular cloning techniques, Pacholczyk et al. managed to isolate in 1991 the cDNA of the human NET from brainstem tissue. They identified the 12 transmembrane domains and the relative molecular mass (Mr= 69K) using hydropathy analysis [152, 155]. Improved animal models and heterologous expression systems enabled from this time on the research on the monoamine transporter. Integration of pharmacological and neurobiological techniques has fostered a deeper understanding in the involved molecular processes [153].

Recent data also addresses the influence of tyrosine kinases, phosphatidylinositol-3-kinase (PI3K) and mitogen-activated protein (MAP) kinase in regulation of monoamine transporters [156]. However, the mechanisms are still largely unknown and explanations not entirely satisfactory. N-linked glycosylation is also claimed to influence transporter function. Large glycosylation areas were found on the extracellular loop between transmembrane III-IV (figure 16). Data seems to indicate so far, that glycosylation is essential for regular expression of the transporters and its protein stability, but not for substrate binding or recognition [153, 157, 158].

In 1983, Lee and coworkers presented for the first time a neurotransmitter-concentration-dependent alteration in NET expression, enabling a dynamic regulation in synaptic homeostasis [159, 160]. Ample support for this hypothesis was raised by the effects of reserpine, a selective blocker of the monoamine vesicular transporter (VMAT) and therefore leading to a depletion of tissue NE stocks [160]. Thereby suggesting that low NE concentrations lead to a down regulation of NETs and subsequently less

withdrawal of NE from the synaptic cleft [156].
This pioneer discovery enabled novel treatment options, since changes in the NE circuit were found in a plethora of neurological and psychiatric disorders, like Alzheimer's dementia, Parkinson's disease, attention deficit hyperactivity disorder (ADHD), major depression, anxiety and schizophrenia [134, 135, 137-139, 150, 161, 162]. Moreover an involvement of the NET in cardiovascular pathologies like hypertension, cardiomyopathy and heart failure was reported [163, 164]. Recently, a profound influence of NE and the NET in metabolic maladies, diabetes and adiposity was shown, mainly acting via activation of brown adipose tissue [165-169]. A first association of a human pathology (i.e. orthostatic intolerance and tachycardia) with a genetic variation in the NET coding region (amino acid 457: alanin residue change to prolin) was confirmed by Shannon et al. [170].

i. Involvement in neurological disorders

Noradrenergic neurons form efferent projections from the LC in nearly all brain areas. Therefore, the NET exerts a profound effect on neural pathways involved in arousal, attention and intricate behavior and is consequently playing a major role in affect, emotion and depression [134, 135, 137-139, 150, 152, 161, 162]. In ADHD, dysregulation of the noradrenergic system was reported [171], being responsible for regulation of attention, motor function, and execution of fronto-striatial and fronto-parietal network tasks [172-174]. The present understanding of the underlying mechanisms is limited, but current research seem to validate a contribution of genetic alterations in catecholamine pathways in the prefrontal cortex area [175, 176]. In a first meta-analysis of MRI structural findings in children with ADHD, large volumetric reductions were found in the posterior inferior cerebellar vermis, the splenium of the corpus callosum, the right caudate, and the total and right cerebral volume in juvenile ADHD [171]. Further evidence is corroborating the notion that these perturbations are modulated via the NE-system through dynamic adaption of tonic and phasic firing [133, 172].
Moreover, involvement in major depression and schizophrenia is intensively discussed [137, 177], pinpointing a supportive role of the concomitant inhibition of NET in addition to NMDA receptors, and increased overall therapeutic effectiveness of antipsychotics [178].
Additionally, NET function and abundance has received large interest in Parkinson's disease, where early stage NE-depletion, resulting from selective degeneration of neurons of the locus coeruleus and sympathetic ganglia, is portrayed as central issue for motor disturbances [139, 179-182].
The extent, to which deficiencies in NE-neurotransmission are implicated in the etiology of these cognitive/affective disorders is still unclear, however, actions of noradrenergic systems likely contribute to the efficacy of a variety of drugs used in the treatment of these conditions [133-140]. This may simply reflect the difficulty of quantification and visualization of CNS processes *in vivo* in humans and the limitations of indirect measures that are fundamentally needed to assess central NE-transmission in humans.

ii. Involvement in cocaine addiction

Abuse of common psychostimulants, like cocaine or amphetamines, is a worldwide mental and social problem. Generally, cocaine is predominantly associated with DAT occupancy, but recent findings are

drawing a firm conclusion on a NET involvement in long-term studies [183]. *In vitro* and *in vivo* investigation on NET response to cocaine revealed contradictory results: rodent NET and hNET cells (human embryonic kidney-293 (HEK-293) cells, transfected with human NET [151]) presented insensitive to cocaine exposure, whereas murine NET mRNA augmented in response to cocaine [184-187]. Further research on cocaine intake in non-human primates demonstrated alterations in the NE system, where NET binding sites in the forebrain projections of both the ventral and dorsal noradrenergic bundles were found affected [188].

In a human *post-mortem* study, Mash et al showed that chronic cocaine-exposure lead to an upregulation in NET protein expression and [^{3}H]nisoxetine binding in the insular cortex [135]. More recently, in a human *in vivo* PET study a significant up-regulation of NET in thalamus and dorsomedial thalamic nucleus was found in cocaine abusers [189]. Thus, an *in vivo* imaging of NET is indispensable to corroborate these *in vitro* findings on a molecular level and to foster an early stage diagnosis and treatment.

iii. NET in cardiovascular diseases

Given the importance of cardiovascular diseases in modern society, literature is rapidly growing on the factors influencing treatment options and patient outcome. Current research seems to validate a profound impact of the noradrenergic system, and more specifically the NET in cardiovascular maladies [164]. Changes in NET function prompt specific cardiovascular and metabolic reactions [163, 190-192]. In the periphery, the NET controls heart rate, contractility, vascular tone and renal Na^+ absorption, and therefore, NET alterations are able to provoke pivotal changes in cardiovascular regulation and even induce structural changes in the heart tissue [164]. Recently, also a hormonal influence on cardiovascular-NET function was reported [163]. Whether NET dysfunction is cause or merely the consequence of heart failure remains still unclear. To shed light on these dysregulations in terms of NE-turnover and sympathetic nervous function, a feasible *in vivo* visualization and quantification of NET might foster our present understanding of the pathophysiology and facilitate an improved preterm diagnosis.

iv. NET in BAT

The unique ability of brown adipose tissue (BAT), as major lipid-burning tissue, to regulate thermogenesis is apparently an evolutionary remnant, which permitted our ancestors to survive in nocturnal and hibernal cold. Since an involvement of NET in regulatory processes in BAT thermogenesis is intensely discussed, a fuller theroretical background on BAT is included in this thesis.

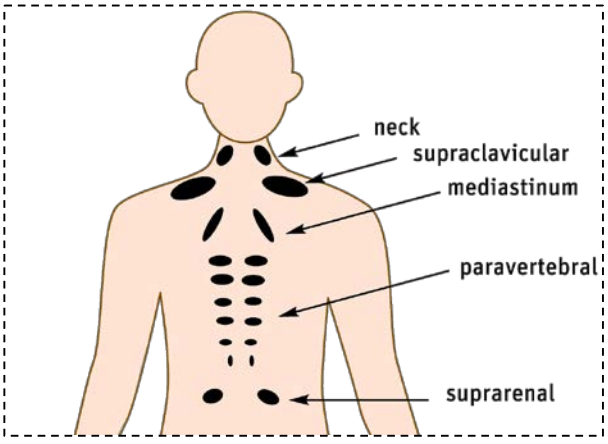

Figure 17 Schematic localization of brown adipose tissue in the human adult body

The existance of BAT in certain mammals was discovered almost five centuries ago by the swiss biologist Gessner (*Tigurine Historiae Animalium: Lib. I De Quadrupedibus viviparis*, 1551), but it

attracted more and more attention in the last century [193]. In the 1950s, it was found predominantly in non-hibernating but to a slight extent in all animals, but its existence and unique function was first elucidated in human adults and neonates in the 21st century [169, 194-197]. Brown adipose tissue is rich in mitochondria and capillaries and a highly innervated tissue, which in contrast to white adipose tissue (WAT), does not serve as energy storage [198].

BAT itself, is primary located in human adults in the supraclavicular area, in the neck, para-aortic in the mediastinum, paravertebral and to a small extent suprarenal (figure 17). As the major organ of glucose disposal it is responsible for glucose metabolism, upon transport into the BAT cell via the Glut-1 [199] or Glut-4 [200] transporters (figure 18). Subsequently, it is metabolized by production of heat in the mitochondria. As key-lipid burning tissue, triglycerides are enzymatically converted into the respective free fatty acids (FFA). The mitochondrial brown fat uncoupling protein 1 (UCP-1) creates H^+ leaks across the inner mitochondrial membrane, resulting in a separation of oxidative respiration from adenosine triphosphate (ATP) synthesis, the FFAs are β-oxidized and the resulting energy is dissipated as heat [198, 201-203]. This process can be stimulated by sympathetic activation via NE. As presented in figure 18, the NE sequestration from the noradrenergic neuron can activate the conversion of ATP to cyclic adenosine monophosphate (cAMP) by NE-binding to β3ARs, expressed on the BAT cell surface. Activation of the cAMP downstream cascade leads to an increased synthesis and translocation of Glut1 transporters and therefore an increased glucose uptake in the brown adipocytes. Moreover, it triggers a lipase catalyzed conversion of triglycerides into FFAs. Together, they are up-taken into the mitochondria via UCP-1 and consumed in the thermogenetic process. Thus, inhibition of NETs leads to an increase in the synaptic NE-concentration, and therefore activated β_3-adrenoreceptors resulting in BAT hypermetabolism.

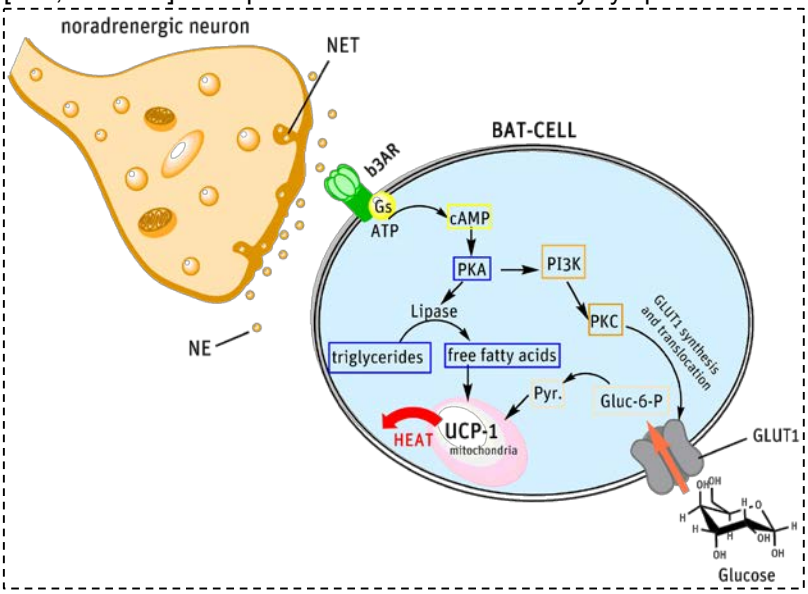

Figure 18 Schematic route of BAT activation and thermogenesis. Noradrenalin (NE) binds to the β3ARs on the BAT cell surface, activating thereby the cyclic adenosine monophosphate (cAMP) cascade. Triglycerides and glucose are transported in the cell, metabolized and activate the UCP-1. As a result, thermogenesis is induced.

Moreover, recent findings suggest a significant impact of the NE system in eating behaviors, obesity and obesity-related health conditions [165, 204-206]. Additional data from NET-inhibitors, used as antidepressants, revealed an altered food intake behavior and decreased body mass, and therefore may offer a new treatment and imaging option for adiposity and diabetes [137, 207, 208]. In late PET studies, the existence and activation of BAT via NET was proven using [^{18}F]FDG-PET or [^{11}C]MRB-PET [165, 209]. Nevertheless, further studies on the involvement of NET in BAT regulation and function are needed to corroborate these findings.

1.4. NET INHIBITORS AND RADIOPHARMACEUTICALS

So far, only a very limited number of NET-selective inhibitors are available. New potent and selective NET inhibitors (SNRIs, selective noradrenalin reuptake inhibitors) may find application in the treatment of mental disorders or in PET imaging. Thus, they may enhance our basic understanding of the underlying pathophysiology and molecular mechanisms of the above mentioned diseases.

1.4.1 NET inhibitors

Substances, known to inhibit NE reuptake can be classified depending on the number of joined aromatic rings present in their chemical structure. Tricyclic antidepressants represent the main subclass of commonly used antidepressants [210, 211], but there are also monocyclic [212-215], bicyclic [216] and tropane-based [217, 218] NET inhibitors available. Except the tropane derivatives, all substance classes are bearing two aryl moieties (labelled as A +B in figure 19) and a secondary amine function. An antiperiplanar geometric orientation of both aryl-rings towards the amine seems to be crucial for favorable NET binding behavior [216]. Moreover, an essential issue presents the steric orientation of an H-bond acceptor (aliphatic group, OH moiety, ether) in the candidate molecule [213, 214, 216, 219]. Thus, there are ample arguments for a high impact on NET-affinity. One example is presented in a study of Waldmeier et al., where the two enantiomers are showing a eudismic ratio of 8/1000 [211, 214]. Moreover, halides seem to be well tolerated on the aromatic rings, favorably in para-position on the B-aryl moiety [216, 220]. In recently published studies, the substitution pattern of the aryloxy-ring (A) was discussed. Thereby, a substitution in *ortho*-position proved to be indispensable for NET affinity, whilst a *para*-substitution leads to potent serotonin transporter reuptake inhibitors ([221, 222].

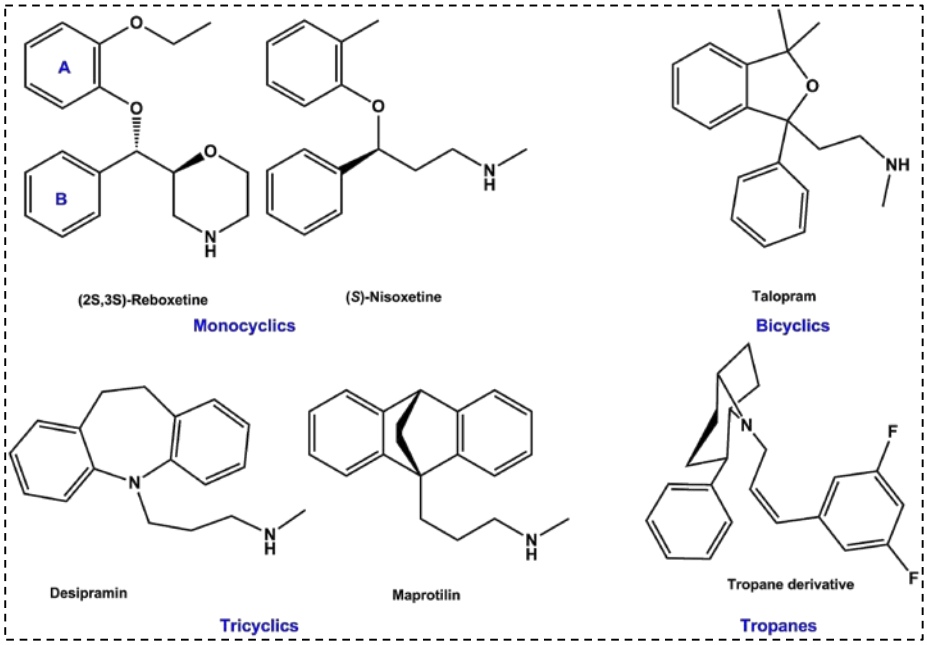

Figure 19 Overview on the chemical structure of NET inhibitors – the four main substance classes.

i. Reboxetine and aryloxy morpholine derivatives

The first NET ligand synthesized and evaluated was Reboxetine in 1984 by Melloni et al. [213], where its potential as first monocyclic antidepressant was assessed. As first commercially available, selective NE reuptake inhibitor (SNRI), it was used as first-line therapeutic in major depression [223-228]. Since 2007 Reboxetine (figure 20) is officially traded in Austria as racemic mixture of (2S,3S)- and (2R,3R)-2-[α-(2-ethoxyphenoxy)phenylmethyl]-morpholine under the name Edronax® [225], although the (2S,3S)-enantiomer showed over 23-fold higher affinity towards NET. Nevertheless, in recent meta-analytic data Reboxetine showed to be less effective than second-generation antidepressants [229].

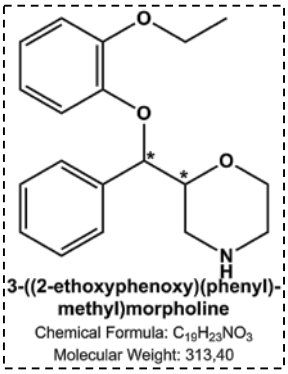

Figure 20 Chemical structure of Reboxetine (Edronax®)

However, Reboxetine was chosen as first lead structure for improved NET-inhibitors. Slight modifications were tolerated without significant deterioration of affinity. Au contraire, replacement of the ethoxy group in the Reboxetine structure with a methoxy moiety revealed an increase in potency [213]. In figure 21, the Reboxetine-derived, monocyclic NET inhibitors MeNER, FMeNER-D2, FERB, PBM and Atomoxetine are depicted.

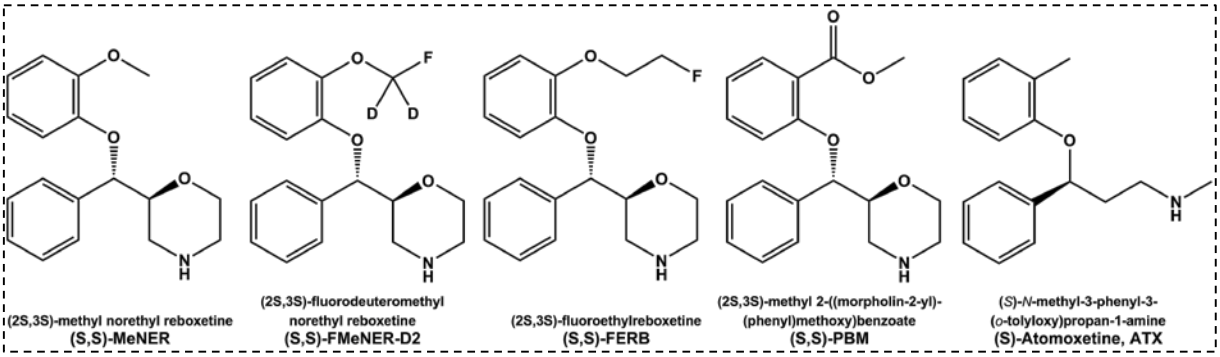

Figure 21 Chemical structure of the Reboxetine-derived NET inhibitors

Reboxetine and its derivatives display certain limitations regarding their *in vivo*/vitro stability, selectivity, complex (radio-)synthesis and late alignment of binding equilibrium [230-234]. Hence, several new, non-Reboxetine-based compounds have been developed recently.

ii. Benzo[d]imidazolone and indolyl-phenyl propanamine based NET inhibitors

In 2006, a novel class of NET inhibitors was published by Mahaney et al., who presented 3-(1*H*-indol-1-yl)-3-arylpropan-1-amines with an improved pharmacological profile (figure 22, substance **A**). However, these molecules were derived from Atomoxetine (figure 21), but comprise an indole ring as a substitute for the aryloxy moiety at the propane amine scaffold [222]. Unfortunately, these substances showed binding not only to NET alone, but also displayed high SERT-affinity (best compound: hSERT/hNET 0.03). Therefore, McComas et al. replaced the indole moiety with an indolyl-phenyl group (substance **D**), thus resulting in improved NET affinity, but unfortunately, for the majority of presented substances, also a significantly increased SERT binding affinity was observed [235, 236].

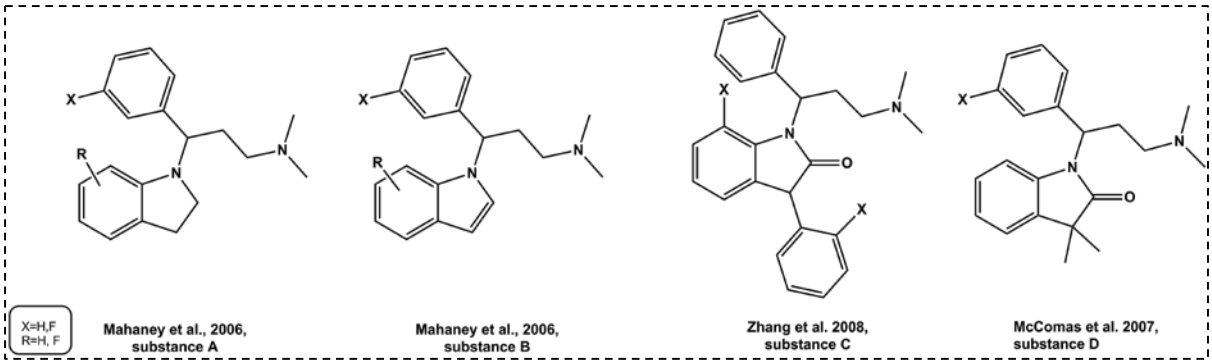

Figure 22 Chemical structure of the first non-reboxetine based NET ligands [221, 234-237]

On these grounds, Zhang and co-workers displaced the indole moiety with a benzoimidazolone group. Thereby, selectivity NET/SERT and NET/DAT was increased tremendously [237, 238]. Binding affinity was determined as half maximum inhibitory concentration (IC_{50}) on all three monoamine transporters. Thus, a binding affinity for the best substance (X=H, figure 22, substance **C**) was determined as 9nM on hNET and 3µm on hSERT, respectively. Exchanging of the 2'-substituents (X) to fluorine though resulted in slightly higher NET affinity, but also highly increased SERT binding was observed. Moreover, hDAT affinity proved to be reasonable low in all cases (4-36 hDAT% inhibition at 10µM) [238]. All over, selectivity of all presented compounds was 15-300 fold higher than for Reboxetine or Atomoxetine (ATX).

iii. Aryloxytetralines and aryloxyindanes as NET inhibitors

A further substance group as potential NET inhibitors was described by Wu and co workers. They presented a couple of aryloxy-tetralines and –indanes as novel potent NET ligands (figure 23, substance **E, F** and **G**)[239].

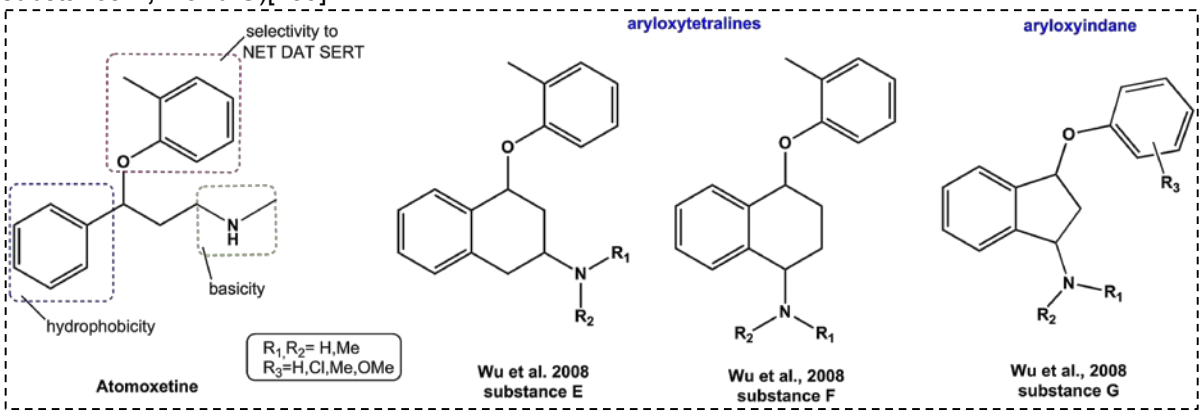

Figure 23 Chemical structure of the aryloxyindanes and -tetralines described by Wu et al. as novel NET ligands [238]. The pink area marks the scaffold responsible for selectivity, the blue one indicates the hydrophobic core and the green area depicts the basic amine function

These novel candidate structures were derived from Atomoxetine, but were designed to exhibit less metabolic degradation and clearance due to a more rigid and inflexible backbone [240-242]. However, the main structural features from ATX were still preserved, ensuring a reasonable NET binding behavior (figure 23). The pink-depicted aryloxy moiety proved to be responsible for NET-selectivity, favorably with an electron donating *ortho*-sustituent (e.g. methyl). The amine function, framed green in figure 23, is still preserved, but the hydrophobic scaffold (blue-framed) is designed to be less flexible as compared to

ATX. Thus, all novel compounds exhibited a 5-fold increased stability towards cytochrome-P-450 isoenzyme 2D6 (CYP2D6) in comparison to Atomoxetine. Unfortunately, the selectivity of these structurally rigid inhibitors did not improve with its stability. Generally, the aryloxytetralines (**E,F**) proved to be superior to the aryloxyindanes (**G**). Amongst the tetraline derivatives, the 2-amine (**E**) showed better results than the 1-amine (**F**). The best candidate compound (substance **E**, R_1=Me, R_2=H), revealed an affinity towards NET of 8nM, but to SERT 590nM and to DAT 8µM, respectively [239]. Nonetheless, these features appear to be still suitable for a low density target binding like NET.

iv. Phenoxyisochromane and phenoxychromane derived NET inhibitors

The preceeding discussion clearly demonstrated that enhanced stability is directly linked to a decreased flexibility of the aromatic scaffold. In this respect, Hudson et al recently presented a series of novel NET inhibitors with reduced flexibility thus providing an improved metabolic profile [243, 244].

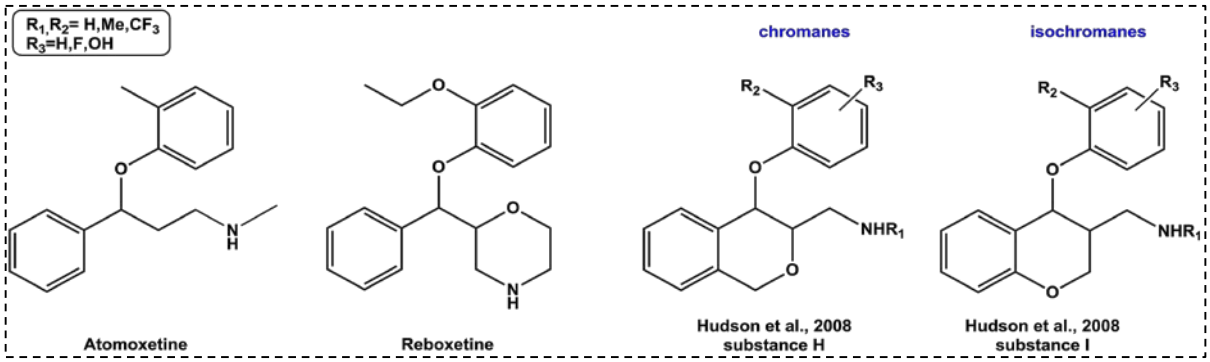

Figure 24 Chemical structure of the chromanes and isochromane-NET inhibitors described by Hudson et al. [242,243].

In figure 24, the chemical structures of these new substance classes are outlined. The data suggests a higher selectivity for these substances in comparison to Atomoxetine and all other previously published compounds by Wu et al. Highest NET-affinity and selectivity was found for R2 substituted compounds (**R_2**=Me, OMe, CF_3). In contrast to the previously published NET ligands, a second substitution of the **R_3** moiety at the aryloxy scaffold by a halide in any position resulted in significantly higher NET affinity and a vast increase in NET-selectivity. Generally, all isochromane derivatives **I** exhibited higher potency than the chromane ligands **H**. Therefore, data suggest that the oxygen-moiety is highly involved in NET-binding, and the isochromane structure favors the ligand-target-interactions [243, 244]. In a molecular modeling approach, Hudson and co-workers showed that the orientation of the isochromane scaffold equals the morpholine structure of Reboxetine in respect to their 3D orientation. Furthermore, all *cis*-oriented ligands exhibited higher NET-potency and selectivity than their *trans*-diastereomers. Therefore, a pseudo-axial orientation of either the NHR_1-group or the aryloxy moiety seems to be crucial for an appropriate NET binding behavior [243, 244].

Moreover, their increased rigidity due to the (iso-)chromane scaffold is resulting in slightly higher stability against CYP2D6 and CYP3A4 than reported for the previously presented NET ligands [243]. However, still higher metabolic degradation than for ATX is observed, which could be attributed to the higher lipophilicity of the presented compounds. Therefore, future NET inhibitors should elicit reasonable polarity in the core to prevent inhibition of CYP2D6.

v. Phenylbenzothiadiazole based NET inhibitors

Recently, O'Neill and co-workers presented a novel substance class as potent NET inhibitors. Derived from the benzoimidazolones structures, a series of phenylbenzothiazoles was prepared (figure 25, substance **J,K**) [245, 246]. The structures generated showed a clear trend towards excellent affinity and selectivity, and slightly reduced flexibility. Overall, better affinity was observed for the R-enantiomers, as well as the open-chained structures **J** revealed higher NET potency than the tethered alkylmorpholinethiadiazoles **K**. The most persuasive compound of the open-chained substances **J** was the 2-hydroxy-3-methylamino-propane substituted, not fluorinated phenylbenzothiadiazole dioxide.

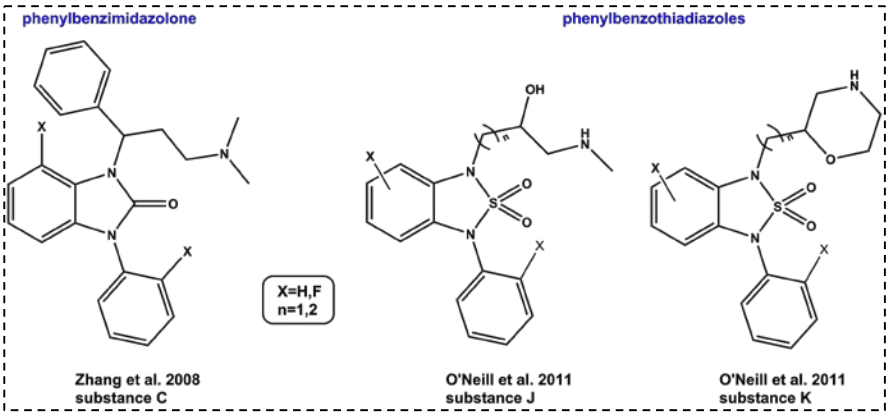

Figure 25 Chemical structure of the phenylbenzothiadiazoles derived from the compounds presented by Zhang in 2008. [244,245]

Moreover, a shorter length of the side chain was beneficial for NET affinity. Conversion of the alcohol to the respective ketone resulted in equal NET potency; however, a decreased metabolic stability was observed [246]. Furthermore, a methylation of the alcohol to the respective ether resulted in a decrease in NET affinity of **K**, but interestingly this observed drop in affinity was 5-fold more for the S-enantiomer [245]. Thus indicating that the oxygen moiety is involved in NET-binding interactions and should be sterically unconstrained. Halogenation of the pendent aryl ring moiety resulted in increased metabolic stability, but decreased NET potency except for the single ortho-fluorinated subtance **K.** Also multiple fluorinations showed deteriorated properties. Moreover, fluorination of the benzothiadiazole scaffold showed tolerable results for both 4- or 7-substituted ligands. In general, all presented substances J and K presented moderate stability against rat multienzyme complexes. Best metabolic stability and NET potency was observed for the 1-(2-fluorophenyl)-3-(2-(morpholin-2-yl)ethyl)-1,3-dihydrobenzo[c][1,2,5]thiadiazole 2,2-dioxide (figure 25: **K,** X_{Phenyl}=F, n=1), as well as for the corresponding open-chained compound **J** [245, 246].

Hence, these substances offer an optimal basis for the constitution of NET-inhibitors for PET imaging.

1.4.2 NET radiopharmaceuticals

Due to the low abundance of NET in the human brain, *in vivo* neuroimaging presents a large challenge. This becomes clear when considering the first accessibility of NET PET tracers. Until the beginning of the 21st century no suitable PET tracer for NET imaging was available. Early attempts were made in 1989 by radiolabeling of Nisoxetine with carbon-11 instead of tritium [247], frequently used for autoradiographic studies [135, 188, 248]. However, the ^{11}C-labeled isotopomer revealed high lipophilicity and therefore high non-specific binding [247]. In 2004, a further carbon-11 labeled NET PET tracer was presented by McConathy et al. The outlined benzo[*c*]thiophene and benzo[*c*]furan derivatives talopram and talsulopram [249, 250], two frequently used antidepressants, did unfortunately show *in vivo* in rodents only a very poor brain uptake [251-253]. The lack of cerebral penetration (only 0.05-0.07% injected dose (% I.D.) per gram) could not be attributed to their lipophilicity, since logD proved to be in a proper range. One tentative explanation might be, that both substances present efflux transporter substrates. However, their suitability as cerebral NET PET tracers might be disputed. Further attempts in radiolabeling of well-established SNRIs were made (e.g. ^{11}C-labeled lortalamin, oxaprotilin, desipramin), but failed due to either lack of selective binding or high non-specific binding [233, 252, 254, 255].

In general, all NET-PET tracers in preclinical and clinical use so far are based on the aryloxy morpholine scaffold from reboxetine (figure 26) and will be addressed in detail in the next sections.

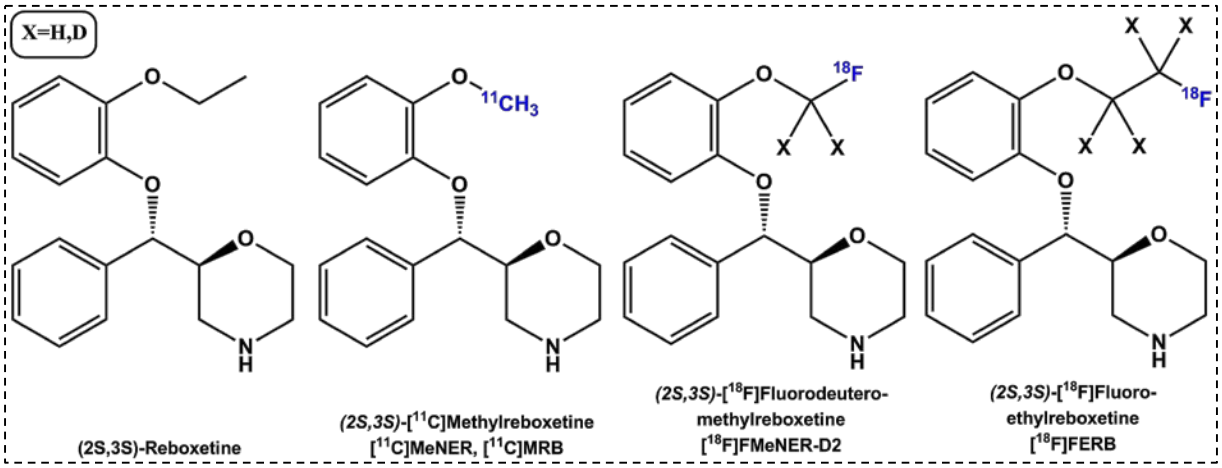

Figure 26 Chemical structures of the aryloxy morpholine based NET PET tracers. [188,229,231,255-258]

i. [^{11}C]MeNER

In 2003, two working groups presented a first Reboxetine derived carbon-11 labelled NET-PET-ligand: [^{11}C](S,S)-2-(α-2-methoxyphenoxy)phenyl)methylmorpholine ([^{11}C]MeNER, [^{11}C]MRB) [189, 230, 232, 256-258]. This tracer seemed to be promising since the radiosynthesis can be accomplished straightforwardly by automated *O*-[^{11}C]-methylation. Moreover its affinity and selectivity evinced favorable properties in an *in vitro* setting [230, 252]. However, there are major drawbacks of this NET-PET tracer. One of the prime failings is, that its binding equilibrium was not reached within the PET-scan time of 93 minutes (4 ½ half lifes, $T_{½}$=20 min) in initial PET-scans of non-human primates [232]. Moreover, a serious drawback of this candidate tracer is its weak metabolic stability. After 30 min post

injection, only 50% of the [^{11}C]MeNER remained intact and stability decreased further over time to 20 % intact tracer after 1h in rat plasma [230]. Interestingly, a plasma metabolite study in monkeys evinced 75% intact tracer after 1h. Thus, a high interspecies difference is observed for this tracer [232]. Moreover, an *in-vivo* baboon NET-PET study was performed by Severance at al., demonstrating a low signal-to-noise ratio (S/R ratio) and a lack of sensitivity and reliability of [^{11}C]MeNER [258]. The extent to which these results from animal studies reflect the human situation is still unclear. However, [^{11}C]MeNER was used recently for NET-PET-scans in clinical trials [167, 232, 256].

ii. [^{18}F]FMeNER-D2

Along with the above listed methylated aryloxy morpholine, also radio-fluorinated Reboxetine analogues were designed (figure 26), to permit the attainment of the equilibrium state within a reasonable timeframe regardless of the required long timespan. Although the half-life of the fluorinated ligands ($T_{1/2}$(^{18}F) =110 min) is long enough to reach binding equilibrium *in vivo*, the S/R-ratio is described slightly lower than for the ^{11}C-methylated Reboxetine derivative [61, 259].

For both [^{18}F]fluoromethylated and –ethylated tracers, a high metabolic instability (leading to defluorination) was observed *in vitro* and *in vivo* [255, 260, 261]. Hence, a replacement of the hydrogen atoms by deuterons (X, in figure 26) lead to a significant decrease in fluoride-cleavage and therefore an substantial increase in metabolic stability [260]. Moreover, the inevitably complex radiosyntheses of these fluoroalkylated PET-tracers put certain restraints on the availability of these PET tracers for clinical routine (see section 1.1.2.i).

In 2005, Schou et al claimed that the so far best NET-PET tracer '(S,S)-[^{18}F]FMeNER-D2 is a useful radioligand for imaging of NET within the locus coeruleus of the postmortem human brain. However, the signal to noise ratio is significantly lower outside the LC, reflecting the lower densities of NET. It therefore seems crucial to develop a selective radioligand with higher affinity for NET to enable *in vitro* visualization and quantification of NET in regions external to LC.'[231] Nonetheless, PET studies in higher primates and humans, as well as biodistribution and dosimetry studies in humans were conducted using [^{18}F]FMeNER-D2 [172, 231, 262-264].

The synthesis, automation and preclinical evaluation of the NET-PET tracer [^{18}F]FMeNER-D2 is addressed within this thesis.

iii. [^{11}C]Me@APPI and [^{11}C]Me@HAPTHI

Recently, first non-reboxetine based NET-PET tracers were presented: [^{11}C]Me@APPI and [^{11}C]Me@HAPTHI (figure 27) [265],manuscript #6. The development, automation of radiosynthesis and the first preclinical evaluation of these novel NET radiopharmaceutical will be in the central focus of this PhD thesis.

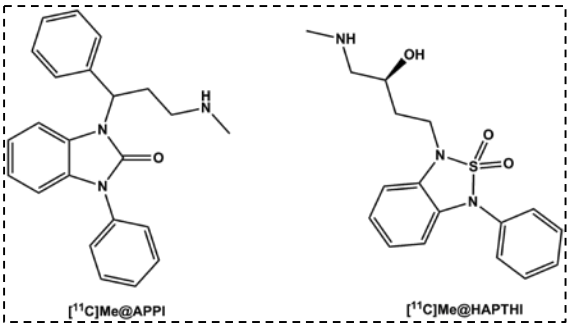

Figure 27 Chemical structures of the novel non-reboxetine based NET PET tracers. [246, manuscript 6]

1.5. PRECLINICAL EVALUATION OF PET-TRACERS

In the development of novel PET radiopharmaceuticals for neuroimaging, several criteria need to be met prior to a possible application. Thus, they ought to:

- Show selective target binding
- reach the specific binding equilibrium
- within the study interval
- at a commensurate signal-to-noise ratio

Hence, suitable cerebral PET tracers must display high affinity and high selectivity towards their target (low nM to *sub*-nM range), particularly when the abundance of the target is low compared to kindred receptors or transporters. Furthermore, the candidate ligands should demonstrate reasonable binding kinetics. Substances with too high affinity tend to display slow on-/off-kinetics, and therefore, they are not able to reach the binding equilibrium within a reasonable timespan due to blood flow dependent brain uptake. In contrast, too low affinity prompts insufficient signal in the target region [266]. Moreover, for cerebral PET-tracers an efficient crossing of the blood-brain-barrier (BBB) is mandatory without being a substrate for an efflux transporter (e.g. P-glycoprotein, BCRP1,…) [267-269]. Therefore, lipophilicity needs to be reasonably high to enable passive diffusion through the BBB, but also concomitantly low to avoid excessive non-specific binding (logD < 3.5) [270]. Furthermore, all (CNS-)PET-tracers aim at high *in vivo* stability against metabolism and considerably fast blood clearance for optimum PET quantifications.

Hence, the entire criteria portfolio (figure 28) needs to be assessed and comprehensively evaluated for each candidate compound *in silico, in vitro* and, if promising, also *in vivo (*in small animal models), before a human application can be possibly striven.

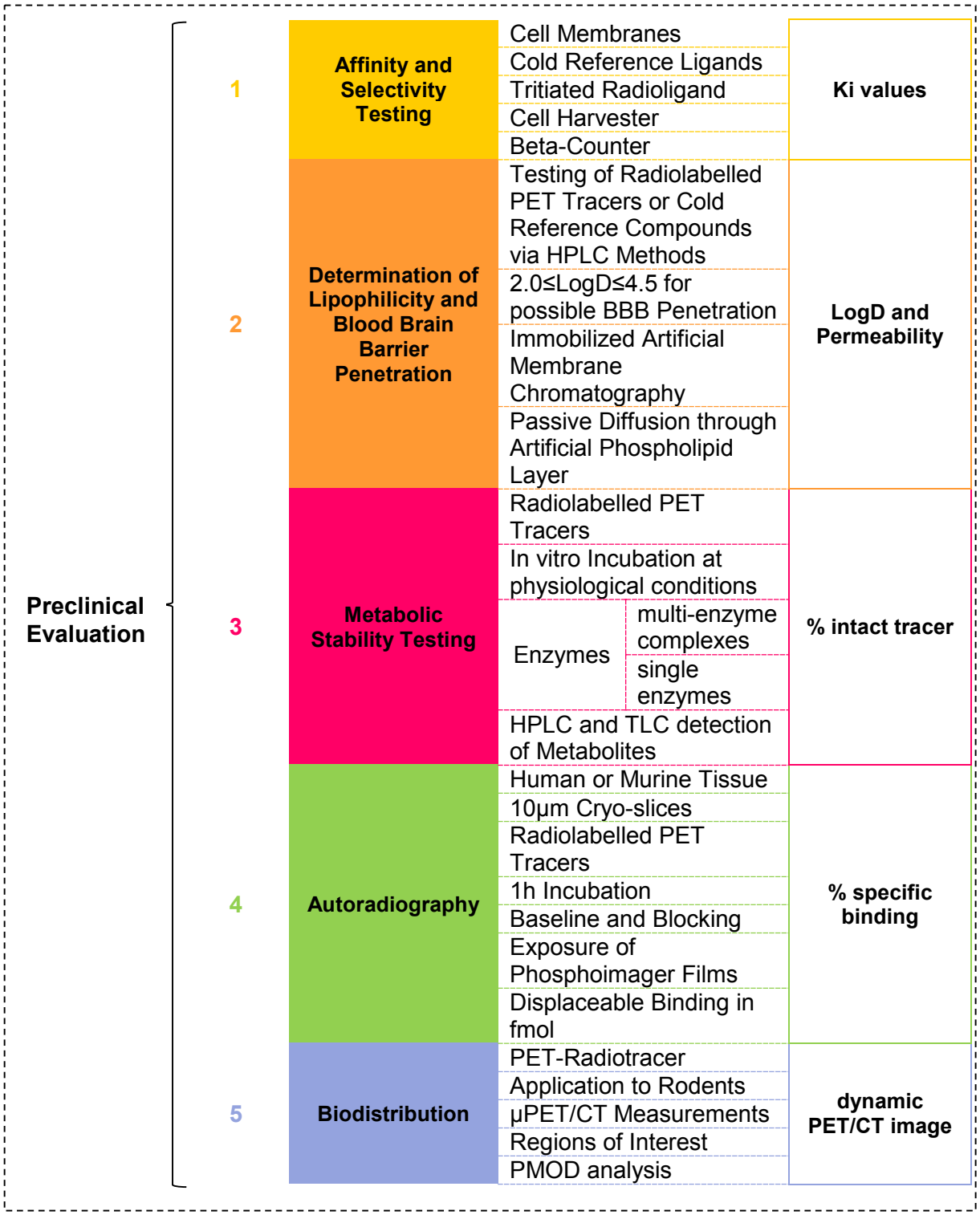

Figure 28 Schematic overview on the preclinical evaluation of PET tracers. In the framed boxes on the right side, the main outcome parameters are given.

1.5.1 Affinity and Selectivity

The binding affinity is a property of a drug that reflects its interaction with the binding site (e.g. receptor or transporter), or the chance that the drug will bind to an adjacent target [271]. In general, the interaction of a molecule with the binding site of the target is described by its binding affinity as K_d or K_i value (equilibrium dissociation or inhibition constant) [272]. The K_d value of a substance represents the reciprocal of its affinity, and is determined as the ratio of the ligand-receptor complex dissociation rate and the rate of product formation at the equilibrium state (L=ligand, R=target) [273]:

$$K_d = {k_{off}}/{k_{on}} = {[L][R]}/{[LR]}$$

In general, the K_d value is attained in saturation experiments using radioligands. Hereby, increasing concentration of the radioactive ligand are added repeatedly to a stationary concentration of target protein. In contrast, the equilibrium inhibition constant K_i is obtained in competition experiments. Hereby, a displacement of the reference radioligand (with known affinity and molarity) is done using varying concentrations of the non-radioactive substance of interest. The K_i value is subsequently calculated by the Cheng-Prusoff-equation [274]:

$$K_i = \frac{IC_{50}}{1+\frac{[L]}{K_d}}$$

The half maximum inhibitory concentration (IC_{50}) is a direct measure for the specific binding of the candidate ligand. The Ki is subsequently calculated by division of the IC_{50} value by the concentration of employed radioligand [L] and its known K_d at the respective target.

The candidate substances evaluated within this thesis were tested for their affinity in a competition experiment using a cell harvester (semi-automated vacuum filtration device which enables a uniform washing and filtration of the cell membranes; schematic procedure in figure 29). Thereby, different concentrations of the candidate ligands (competitors) are incubated with cell membranes (expressing the respective target) and an established radioligand in known concentration. After filtration over a glass fiber filter using a cell harvester, the filter discs are transferred to scintillation vials and a liquid scintillation cocktail is added. Data from the competition plots obtained from the β-counter was analyzed and IC_{50} and K_i values were calculated.

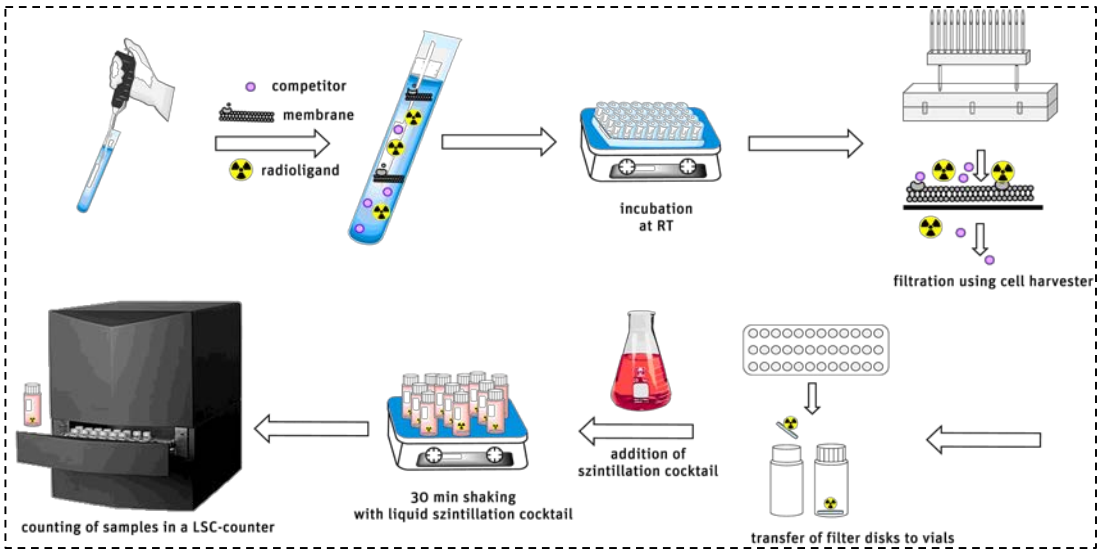

Figure 29 Schematic procedure of the radioligand binding assay using a cell harvester.

1.5.2 Lipophilicity and Blood Brain Barrier Penetration

The lipophilicity presents a central characteristic of a compound determining its pharmacodynamics and -kinetics. The lipophilicity itself is described as the logarithm of the partition coefficient P (or distribution coefficient D) of a substance in an aqueous buffer at neutral pH and an immiscible organic solvent (i.e. *n*-octanol) [275, 276]: $\log D_{oct}^{7.4} = \log P_{oct} + \log[1/(1 + 10^{pKa-pH})$

Thus, the lipophilicity of a substance has been revealed to elicit paramount influence on its adsorption, distribution, metabolism and excretion (ADME) [275, 277]. Despite the influence on the solubility of a compound, the lipophilicity portrays one key feature influencing the passive blood brain barrier (BBB) penetration. Moreover, high lipophilicity of a molecule leads to increased metabolic clearance and high plasma protein binding [275, 276, 278, 279]. Thus, lower amounts of the free drug are available for target binding and visualization.

Lipinski et al. stated in 2001 the 'rule of five', which aims at a prediction of the capability of candidate substances to penetrate the BBB and the solubility of potential drugs. More recently, a restriction of these thresholds was presented in a meta-review by Pike et al. Hence, all candidate compounds must be within the following parameter cutoffs to ensure appropriate pharmacokinetic behavior and efficient passive brain entry [270, 277, 280, 281]:

- ≤ 5 H-bond donors
- ≤ 10 H-bond acceptors
- molecular weight ≤ 500 (optimum <300)
- logP or log D ≤ 5 (optimum 1<pH<3.5) or Moriguchi MLogP <4.15
- small cross-sectional area (< 80 Å^2)
- no formal charge

This point is particularly relevant to PET tracers for cerebral applications, since it's an inevitable prerequisite that they are capable to efficiently penetrate the blood brain barrier. All compounds, which are conveyed actively into the brain by transporters present exceptions to the above mentioned criteria. However, meta-analytic data suggests that logP or logD values alone are beyond doubt insufficient for a prediction of BBB-penetration. Therefore, improved *in vitro* high throughput methods have been established for quantification of passive diffusion through the BBB. Amongst these, immobilized artificial membrane (IAM) chromatography displayed encouraging results. The principle of IAM method is outlined in figure 30. The chemical structure of the lipid double layer of the biomembrane is mimicked within an HPLC column. Hereby, artificial phosphatidyl choline esters are linked to the silica gel. The time, which the analyte is retained on the matrix, is proportional to the K_{IAM} value (IAM partition coefficient) and the permeability P_m of the tested substance [282, 283].

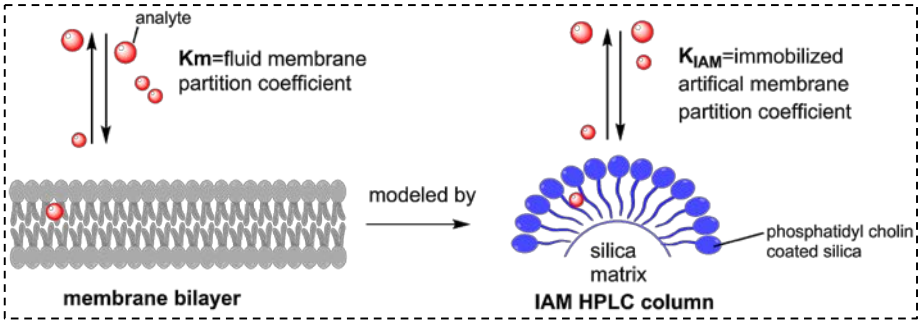

Figure 30: Transformation of the membrane bilayer into an IAM HPLC column for the prediction of BBB permeability [modified from registech, IAM chromatography]

1.5.3 Metabolic Stability Testing

The metabolic fate of a substance presents sometimes an insurmountable obstacle in the drug development process. Particularly in cerebral PET imaging, impeding radiometabolites may sully the nature of the PET signal being recorded, due to the lack of PET in signal discrimination between the sources of detected radioactivity [270]. Even though these metabolites are more hydrophilic than the parent compound, and therefore, elicit reduced propensity to enter brain, they are not all satisfactorily discharged from brain. Moreover, also within the brain a metabolic cleavage of the radiotracer can occur and therefore blur the PET signal.

Hence, the *in vitro* evaluation of the metabolism of a potential (radio-)pharmaceutical is inevitable prior to first *in vivo* testing. A plethora of human and small animal enzymes and multi enzyme complexes is available for the examination of the metabolic fate. The vast majority of enzymes involved in metablic degradation of endogeneous chemical substances and xenobiotics present the cytochrome P450 membrane associated proteins (CYP) [284-287]. These oxido-reductases are involved in the phase I metabolism under the use of NADP+/NADPH-reductase as co-substrate [285, 288] and account for approximately 3/4 of total metabolism occurring within the human or animal body [289]. The CYPs are located in the endoplasmic reticuli or the mitochondrial membranes of the cells, but being predominantly expressed within the liver. In table 4, an exemplary overview on different CYP single enzymes is presented.

Table 4 : Selected CYP P450 enzymes involved in phase I metabolism [286-294]

ENZYME	GENERIC NAME	SUBSTRATE	REACTION
CYP1A1	ethoxyresorufin-O-deethylase	7-ethoxyresorufin, aryl-hydrocarbon receptor ligands	Hydroxylation, oxidative deethylation
CYP1A2	phenacetin deethylase	Phenacetin,	hydroxylation
CYP2A1	Steroid hormones 7-alpha-hydroxylase	Coumarin	epoxidations
CYP2B6	1,4-cineole 2-exo-monooxygenase	cineole	hydroxylation
CYP2C9	limonene monooxygenase	Limonene, phenytoin, monoterpenoids	phenytoin 4-hydroxylation
CYP2C19	limonene monooxygenase	Limonene, monoterpenoids	hydroxylations, oxidative demethylation
CYP3A4	testosterone 6-β-hydroxylase	cholesterol, steroids and lipids	hydroxylation, oxidative demethylation, N-demethylations

CYP 2D6	Debrisoquine 4-hydroxylase	Debrisoquine, hydroxytryptamines, neurosteroids	hydroxylations, oxidative demethylation

The major metabolizing CYP isoenzymes involved in xenobiotic degradation present the CYP3A4 and CYP2D6. Interestingly, the CYP2D6 accounts only for 2% of all hepatic CYPs in the human body, but substantially degrades over 25% of all clinically applied drugs [295]. Only the CYP3A4 is capable to metabolize an even greater percentage of drugs and xenobiotics (appr. 50%) [286]. Together, these two cytochrome P450 enzymes constitute an effective barrier for many exogeneous and endogeneous compounds.

Along with the CYPs, carboxylic ester hydrolases (CES) are mainly involved in enzymatic degradation processes in the human body. In humans, five different serine esterases are present (CES 1-5) and are classified according to their homology but highly diverse substrate specificity [296, 297]. Their vast control on metabolism and activation of endobiotics and xenobiotics is attributed predominantly to hCES1 and hCES2 in the liver and small intestines [296]. The resulting CES-metabolites are displaying increased polarity which leads to a facilitated renal elimination.

Moreover, the extent of plasma protein binding presents an important characteristic of the candidate compounds, since only the unbound fraction of the radiotracer is accessible for the desired target binding. Thus, the free fraction of a PET tracer (and any other pharmaceutical) is aimed to be high for favorable binding behavior.

Given the centrality of the metabolic stability of newly developed compounds for PET imaging, their stability against the enzymes principally involved in metabolic clearance should be attained *in vitro* prior to *in vivo* applications. Therefore, all compounds included in this thesis were incubated with the respective enzyme preparations and plasma and the percentage of intact tracer determined.

1.5.4 Autoradiography

The autoradiography was initially developed more than 60 years ago as first tool for *in vitro* imaging [298-300]. Since the 1950s the autoradiography techniques have flourished more and more, being a versatile method for *in vitro* characterization of binding behavior of radioligands in toxicology and pharmacology [301]. Especially in the field of neurosciences, the data obtained from autoradiographic studies has significantly contributed to the understanding of the (patho-)physiology and etiology of the neurodegenerative maladies [301]. The recorded spatial distribution of the applied radioactive compound offers a first image of the binding characteristics *in vivo*. Since the 1970s, receptor ligands were increasingly investigated in autoradiographic experiments on human or rodent specimen material - opening the field for today's neuroimaging [301-312]. The significant impact of the resulting understanding of distribution and function of receptors and transporters on the development of novel

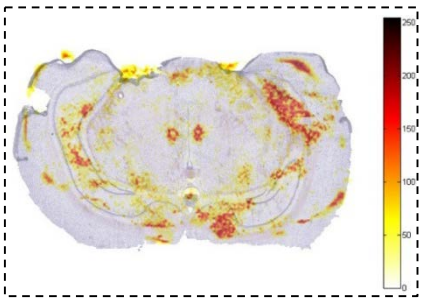

Figure 31: NET-autoradiography on a coronal rat cryo-slice superimposed on a Nissl staining of the identical tissue slice

therapeutic and diagnostic methods is evident.
Plotting of different competitor concentrations can elucidate binding kinetics of the desired radioligand. Moreover, morphological assignment of the high-uptake areas can be done by co-registration of immunohistochemical staining or Nissl staining (figure 31) [313, 314].

Thus, the radioactive labeled compounds within this thesis were investigated also with this important *in vitro* method. Therefore, the respective tissue slices (20µm, cryo-slices) were incubated with the radiotracer in physiological buffer [315]. After a certain time-point, the solution was removed, and the rinsed slices are placed on phosphor-imager autoradiography films. Exposure of the high-contrast films and subsequent processing of the imprints, leads to a qualitative and quantitative autoradiographic image. The use of a radioactive calibration curve, used during each exposure, enabled a quantification of registered digital light units [299]. Moreover, specificity of binding could be tested by blocking experiments using dedicated 'cold' competitor ligands [316, 317].

Another issue presents the *ex vivo* autoradiography, where the radiotracer is applied to the living small animal model [168, 315, 318]. Upon distribution of the radiotracer, the animal specimen is sacrificed and the organs of interest removed. Present methods urge a quick-freezing in i-pentane to preserve the morphological structure of the tissue until cryo-slicing [319-322]. The slices are subsequently placed on phosphor-imager films and treated as stated above for the *in vitro* autoradiography.

1.5.5 Biodistribution

Since the end of the 1980s, biodistribution experiments are used to quantify the *in vivo* distribution of the respective radioligand in a small animal model [323-326]. Moreover, the pharmacokinetic elimination of the tracer and the highest organ doses can be predicted.
For biodistribution experiments, the radiotracer is injected in a small animal model, which is after a certain time-point euthanized (minutes or hours, dependent on density of the target and T1/2 of the radiotracer) and subsequently dissected. The organs of interest are removed and counted in the corresponding counting device (i.e. γ-counter, β-counter). The measured activity is subsequently related to the weight of the respective organ for a first assessment of radiation dosimetry (figure 32).

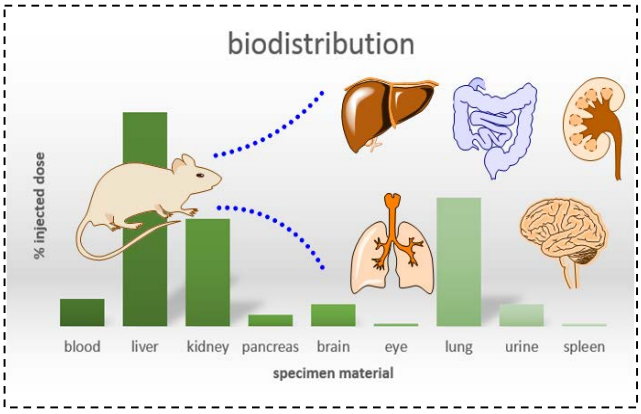

Figure 32: schematic procedure of a biodistribution experiment

1.5.6 µPET – *in vivo* imaging

Along with *in vitro* autoradiography, also *in vivo* preclinical imaging of small animals can be performed. Since it's origin in the 1990s [327, 328], this non-invasive small animal imaging method offers a three-dimensional PET image [329-331]. Therefore, it gives great insight in tracer binding kinetics, distribution

and elimination in a reasonably fast time-frame. Moreover, a co-registration of a CT or MRI offers the possibility to map and allocate areas of higher radiotracer-uptake. Only the restricted spatial resolution of ~1 mm sets limits to this *in vivo* imaging technique [330, 332], hampering a quantification of miniscule areas. The sensitivity of μPET scanners is higher than for clinically used detectors. However, due to statistic reasons, an application of disproportional high doses of radiotracers is required for optimal registration of the μPET scan, thus leading to excess injected (non-radioactive) mass and therefore an inferior signal-to-noise ratio, dependent on the specific radioactivity of the compounds.

The signal from the PET scanner is processed and the regions of interest (ROI) are aligned manually. From these regions also 3D-volumes of interest (VOI) can be delineated. To facilitate an inter-individual comparison, these ROIs or VOIs are converted into standardized uptake values (SUV), where the administered dose and the body weight of the respective animal are considered as well.

Previous studies have corroborated that best results to predict the performance of the novel PET-radiopharmaceutical in humans are furnished by small animal PET studies. Still, inter-species differences can hamper a direct translation and validation of data [329]. Apparently, human studies would be ideal to explore the underlying pathophysiological mechanism *in vivo*. However, these trials are mostly unfeasible due to ethical concerns [330]. Therefore, these *in vivo* studies can be only accomplished in small animal models using μPET, elucidating the pathophysiological principles in various neurological, psychiatric and oncological diseases. Moreover, the visualization of molecular abnormalities, treatment response and detrimental effects is possible in the same individual, vastly fostering thereby medical and biological research on a molecular level.

2. AIM OF THE THESIS

Aim of the presented thesis was to develop novel compounds for PET imaging of the norepinephrine transporter. Given the intense influence of the NET in a multitude of psychiatric and neurodegenerative diseases as well as cardiovascular maladies, the centrality of non-invasive NET imaging is evident. Therefore, on the one hand novel candidate tracers are needed, aiming at high NET affinity and selectivity, a high signal/noise ratio, enhanced metabolic stability, as well as facile radiolabeling strategies. Apart from that, also the availability of already existing NET-PET tracer should be enhanced and further preclinical and clinical evaluations are needed. The knowledge on NET-function and distribution is, so far, well-limited; therefore it seemed fair to gain additional information on a molecular level.

The first aim of the presented thesis was concerned with the rational design of novel ligands for the norepinephrine transporter. Therefore, this thesis comprises not merely the synthesis of novel ligands but rather the design and preparation of suitable labeling progenitors for radiosyntheses.
Along with the design of APPI-derivatives bearing an *ortho*-fluoro-substituent (**manuscript #4**), also unpublished data (in **chapters 3.2.1 and 3.2.3**) regarding a database for potential NET ligands is included within this thesis.

The second objective was the radiolabeling of the newly developed and already existing NET-PET tracers, [^{11}C]Me@APPI, [^{11}C]Me@HAPTHI, [^{11}C]FAPPI, [^{18}F]FE@APPI and [^{18}F]FMeNER-D2. Therefore, the radiosyntheses were evaluated in small scale experiment, the optimum conditions transferred to an automated synthesizer and up-scaled for routine (pre-)clinical applications (**manuscript #1, #2 and #6** as well as unpublished data chapter).

The third aim was the preclinical evaluation of the produced NET-PET-ligands *in silico* and *in vitro*, which included the assessment of their NET- affinity and selectivity, metabolic stability as well as lipophilicity and BBB penetration. Within the context of this thesis, these findings are outlined in **manuscript #1, #4, #5** and **#6**. Moreover *in vitro* autoradiography was performed to evaluate the binding behavior on brain and peripheral tissue of human and rodent origin (included in **manuscript #5** and **#6**).

The fourth objective presents the *in vivo* evaluation of the prepared NET radiopharmaceuticals in biodistribution and (micro-)PET experiments. Within this thesis, the preclinical imaging is included in the **manuscript #6** as well as in the unpublished data section. Moreover, through a fully automated production of [^{18}F]FMeNER-D2, a clinical NET-PET-study was enabled. Thus allowing the investigation of NET influence on human healthy volunteers compared to patients suffering from attention deficient hyperactivity disease (**manuscript #3**).

3. SCIENTIFIC PART

3.1 PUBLISHED DATA

3.1.1 Authors contribution

I herewith affirm that I contributed significantly to all peer-reviewed articles comprised in this thesis. All included publications are in the format as submitted to the journal and the references follow the citation style of the respective journals. Following responsibilities were taken for each publication:

- **MANUSCRIPT #1**: 'Development and automation of a novel NET-PET tracer [11C]Me@APPI'
  Christina Mark, Birgit Bornatowicz, Markus Mitterhauser, Matthias Hendl, Lukas Nics, Daniela Haeusler, Rupert Lanzenberger, Michael Berger, Helmut Spreitzer, Wolfgang Wadsak.
  Nucl Med Biol., 2013, 40, 2, 295-303.

  I developed and automated the radiosynthesis and affinity testings, and performed all radiosynthetic experiments and binding studies at the NET. Furthermore I participated in metabolic stability testings and immobilized artificial membrane testings and logP determinations. I carried out the data analysis and wrote the manuscript.

- **MANUSCRIPT #2**: '[^{18}F]FMeNER-D2 : Reliable fully-automated synthesis for visualization of the norepinephrine transporter'
  Christina Rami-Mark, Ming-Rong Zhang, Markus Mitterhauser, Rupert Lanzenberger, Markus Hacker, Wolfgang Wadsak.
  Nucl Med Biol., 2013, 40, 1049-1054.

  I optimized the radiosynthesis and performed the first automation of synthesis of this radiotracer and subsequently all radiosyntheses. Moreover, I collected all data, performed the analyses and wrote the manuscript.

- **MANUSCRIPT #3**: 'The Norepinephrine Transporter in Attention-Deficit/Hyperactivity Disorder Investigated With Positron Emission Tomography'
  Thomas Vanicek, Marie Spies, Christina Rami-Mark, Markus Savli, Anna Höflich, Georg Kranz, Andreas Hahn, Alexandra Kutzelnigg, Tatjana Traub-Weidinger, Marcus Mitterhauser, Wolfgang Wadsak, Marcus Hacker, Nora Volkow, Siegfried Kasper, Rupert Lanzenberger.
  JAMA Psychiatry, 2014, 71, 1340-1349

  I performed all radiosyntheses and participated in the analysis and interpretation of the data. Moreover I was involved in the revision of the manuscript.

- **MANUSCRIPT #4:** 'Synthesis and in silico evaluation of novel reference compounds for PET based investigations of the norepinephrine transporter'
  Catharina Neudorfer, Amir Seddik, Karem Shanab, Andreas Jurik, Christina Rami-Mark, Wolfgang Holzer, Gerhard Ecker, Markus Mitterhauser, Wolfgang Wadsak, Helmut Spreitzer.
  Molecules 2015, 20, 1712-1730.

  I participated in the conception of the study, design of the molecules. Aditionally I performed data analysis and was involved in drafting of the manuscript.

- **MANUSCRIPT #5:** 'Comparative Preclinical Evaluation of the Norepinephrine Transporter PET-ligands [11C]Me@APPI and [18F]FMeNER-D2'
  Christina Rami-Mark, Cecile Philippe, Chrysoula Vraka, Lukas Nics, Monika Dumanic, Helmut Spreitzer, Rupert Lanzenberger, Marcus Hacker, Wolfgang Wadsak and Markus Mitterhauser.
  Journal of Nuclear Medicine, 2015, in review.

  I performed all radiosyntheses and binding studies, and I carried out all autoradiographic and immunohistochemical experiments. I participated in the assessment of metabolic stability and immobilized artificial membrane testings and logP determinations. I performed the data analysis and wrote the manuscript.

- **MANUSCRIPT #6:** 'Radiosynthesis and first preclinical evaluation of the Novel Norepinephrine Transporter PET-ligands [^{11}C]Me@HAPTHI'
  Christina Rami-Mark, Neydher Berroteran, Cecile Philippe, Stefanie Foltin, Chrysoula Vraka, Alexander Hoepping, Rupert Lanzenberger, Marcus Hacker, Markus Mitterhauser and Wolfgang Wadsak.
  European Journal of Nuclear Medicine and Molecular Imaging Research, 2015, in review.

  I performed all radiosyntheses, all preclinical evaluations as well as the autoradiographic experiments. Moreover, I performed the analysis of all resulting data and wrote the manuscript.

3.1.2 Manuscript #1

DEVELOPMENT AND AUTOMATION OF A NOVEL NET-PET TRACER: [^{11}C]ME@APPI

Nucl. Med. Biol., 2013, 40, 2, 295-303

Christina Mark[a,b], Birgit Bornatowicz[c], Markus Mitterhauser[a,d], Matthias Hendl[a], Lukas Nics[a,f], Daniela Haeusler[a], Rupert Lanzenberger[g], Michael L. Berger[h], Helmut Spreitzer[c], Wolfgang Wadsak[a,b*]

[a]*Radiochemistry and Biomarker Development Unit, Department of Nuclear Medicine, Medical University of Vienna, Austria*
[b]*Department of Inorganic Chemistry, University of Vienna, Austria*
[c]*Department of Drug and Natural Product Synthesis, University of Vienna, Austria*
[d]*Hospital Pharmacy of the General Hospital of Vienna, Austria*
[f]*Department of Nutritional Sciences, University of Vienna, Austria*
[g]*Department of Psychiatry and Psychotherapy, Medical University of Vienna, Austria*
[h]*Center for Brain Research, Department of Biochemistry and Molecular Biology, Medical University of Vienna, Austria*

Short title: **[^{11}C]Me@APPI – a novel NET-PET tracer**

Keywords**:** transporter, noradrenaline, PET, Me@APPI, Carbon-11, radiosynthesis

**** Corresponding author:***
Prof. Dr. Wolfgang Wadsak
Medical University of Vienna - Department of Nuclear Medicine
Radiochemistry and Biomarker Development Unit
Waehringer Guertel 18-20
A-1090 Vienna - Austria
Tel.: +43 1 40400 5255
fax: +43 1 40400 1559
E-mail address: wolfgang.wadsak@meduniwien.ac.at

Nucl Med Biol [IF: 2.408]

Abstract:

Introduction: The norepinephrine transporter (NET) is an important target for research in neurology and psychology and is involved in the pathophysiology of many neurodegenerative diseases such as Alzheimer's disease and attention deficient hyperactivity disorder. For visualization of NET abundance and deregulation, a novel PET tracer - [^{11}C]Me@APPI - has been developed.

Methods: For precursor synthesis, a 4-step synthesis starting from N-phenyl-o-phenylenediamine was set up. Radiosynthesis was established and optimized using standard methods and subsequently automated in a GE TRACERlab Fx C Pro synthesizer. Preclinical testing was performed comprising affinity and selectivity testing on human membranes as well as stability and blood-brain-barrier-penetration using *in-vitro* models.

Results: Precursor molecule (APPI:0) and reference compound (Me@APPI) were synthesized with 26.5% and 21.4% overall yield, respectively. So far, 1.25 ± 0.72 GBq [^{11}C]Me@APPI with 54.35 ± 7.80 GBq/µmol specific activity were produced (n=11). Affinity of reference compounds was determined as 8.08 ± 1.75 nM for Me@APPI and 19.31 ± 2.91 nM for APPI:0, respectively (n≥9). IAM-chromatography experiments (n=3) revealed a P_m value of 1.51 ± 0.34 for Me@APPI. Stability testing using human liver microsomes revealed that 99.5% of the tracer was found to be still intact after 60 minutes (n=4).

Conclusion: Present data indicate that [^{11}C]Me@APPI has promising properties to become a clinically useful NET-PET-tracer. Further in-vitro and in-vivo evaluations are currently under way.

INTRODUCTION

In the central nervous system monoamines such as norepinephrine (NE, noradrenaline), dopamine (DA) and serotonin (5-HT) play an important modulatory role in neurotransmission, and are involved in various (patho-)physiological functions and processes; including depression, attention deficient hyperactivity disorder (ADHD), anxiety and personality disorders, Alzheimer's Disease (AD) and substance abuse. [1] Specifically, dysregulation of NE – and, therefore, also of the norepinephrine transporter (NET) - plays a pivotal role in mood and affective disorders. Thus many selective monoamine transporter inhibitors have been developed for specific treatment. In major depression, perturbated regulation/expression of NET has been reported. [2] The most significant evidence for an increase in synaptic NE concentration in the treatment of depression originates from data gained using reboxetine, a selective NET-inhibitor. [3] In autoradiographic studies (using [^{3}H]-nisoxetine) high levels of NET were found in locus ceruleus (LC), while there was a significant decrease in NET availability in LC in major depressed patients. [4],[5]

To understand this dysregulation of the NE system and its role in depression and other (psychiatric) disorders, it is crucial to gain information about the receptor abundance and density in healthy and pathological brains *in-vivo*. For that purpose, non-invasive molecular imaging using specific radioligands is the method of choice. Moreover, imaging of receptor and transporter dynamics before and after treatment of depression would be important to visualize and quantify molecular changes in the human brain and measure therapeutic outcome. Hence, the availability of suitable radioligands for positron emission tomography (PET) is crucial for gaining insight in molecular changes in the noradrenergic system. As a consequence selective NET-PET-ligands must be developed and evaluated.

Considering a B_{max} value of 4.4 nM for NET in human insular cortex, the affinity of a candidate NET-

PET ligand must be high enough for a suitable visualization of NET in that brain region. [6] Other regions, such as the LC are 4-8 fold richer in NET, therefore imaging of these regions will be possible also for lower affinity NET-PET-ligands. [7-9]

Furthermore, the affinity of the radioligand will have an impact on its binding kinetics, e.g. longer equilibration times for higher affinity ligands in regions with high NET-density. [10] Also the selectivity of tracers targeting the NET is of great importance for their suitability. Dopamine transporters (DAT) and serotonin transporters (SERT) are highly abundant in human brain and most NET ligands tend to bind to a certain extent also to these other monoamine transporters. [11-14]

So far, radiolabeled reboxetine analogs [^{11}C]MeNER ([^{11}C]MRB, ((S,S)-2-(α-(2-[^{11}C]methoxyphenoxy)benzyl)morpholine) and [^{18}F]FMeNER-D$_2$ ((*S,S*)-2-(α-(2-[^{18}F]Fluoro[^{2}H$_2$] methoxyphenoxy)benzyl) morpholine) have been described [5, 15-17]. Since both compounds display certain limitations (e.g. metabolic stability, late equilibrium, complex radiosynthesis) [15, 18], which put some constraints on their applicability in clinical trials, better suitable NET-PET ligands are still of interest.

Thus, the rationale of this and future work is the use of the recently described lead structure 1-(3-(methylamino)-1-phenylpropyl)-3-phenyl-1H-benzo[d]imidazol-2(3H)-one (=Me@APPI, figure 1) as starting point for novel NET-PET ligands.[19] The authors evaluated Me@APPI, which is not derived from reboxetine, *in-vitro* and found very promising affinity (hNET IC50= 9 nM) and selectivity towards NET (hSERT /hNET = 333; hDAT= 33 % inh. at 10 µM Mazindol).[19]

Hence, main objectives of the presented investigations were:

- the preparation and characterization of a suitable labelling precursor, APPI:0 (1-(3-amino-1-phenylpropyl)-3-phenyl-1H-benzo[d]imidazol-2(3H)-one);
- the establishment of a radiosynthetic procedure for the preparation of the carbon-11 labelled analogue, [^{11}C]Me@APPI and its optimization;
- up-scaling and set-up of a fully automated preparation of [^{11}C]Me@APPI, including purification and formulation;
- set-up of a suitable quality control and;
- *in-vitro* evaluation, including binding studies for determination of affinity and selectivity of both Me@APPI and APPI:0 towards NET using NET, SERT and DAT expressing membranes; metabolic stability testing *in-vitro* against selective enzymes; logP analysis and IAM chromatography for indirect measurement of blood-brain-barrier penetration.

MATERIALS AND METHODS

Materials

Precursor, 1-(3-amino-1-phenylpropyl)-3-phenyl-1H-benzo[d]imidazol-2(3H)-one (APPI:0), and cold reference compound 1-(3-(methylamino)-1-phenylpropyl)-3-phenyl-1H-benzo[d]imidazol-2(3H)-one (Me@APPI) were synthesized at the Department of Drug and Natural Product Synthesis, Faculty of Life Sciences, University of Vienna (for details see 'Methods' section).

Acetonitrile (ACN for synthesis of DNA, ≥99.9% (GC) and ACN HPLC grade), tetrabutylammonium hydroxide 30-hydrate (TBAH), methanol (MeOH, CHROMASOLV®, for HPLC, ≥99.9%), ammonium formate, and ethanol (absolute) were purchased from Sigma Aldrich (Vienna, Austria). Iodine

(sublimated grade for analysis; ACS, Pharm.Eur.) was obtained from Merck (Darmstadt, Germany). Silver triflate impregnated carbon was prepared by dissolving 1 g of silver trifluoromethanesulfonate (Sigma Aldrich, Vienna, Austria) in 20 mL ACN and adding 3 g of Graphpac-GC (80/100 mesh, Alltech, Deerfield, USA). The suspension was stirred under protection from light for 30 min, the solvent was removed and the powder was dried for further 2 h under reduced pressure and protection from light.

For formulation of the product 0.9% saline solution from B. Braun (Melsungen, Germany), 3% saline solution (Landesapotheke Salzburg, Austria) and sodium dihydrogenphosphate-monohydrate and disodiumhydrogenphosphate-dihydrate (both from Merck, Darmstadt, Germany) were used. Sterile water was purchased from Meditrade Medicare Medizinprodukte (Kufstein, Austria). Phosphate buffer (125 mM) was prepared by dissolving 0.224 g sodium dihydrogenphosphate-monohydrate and 1.935 g disodiumhydrogenphosphate-dihydrate in 100 mL sterile water. For solid phase extraction C8 plus SepPak® cartridges were purchased from Waters (Waters® Associates Milford, USA). Low-protein binding Millex® GS 0.22 µm sterile filters were obtained from Millipore (Bedford, USA).

All other chemicals and solvents for the radiosyntheses were obtained from Merck (Darmstadt, Germany) and Sigma-Aldrich (Vienna, Austria) with at least analytical grade and used without further purification.

Instrumentation

^{1}H- and ^{13}C-NMR spectra were recorded on a Bruker Avance DPX-200 spectrometer at 27°C (200.13 MHz for ^{1}H, 50.32 MHz for ^{13}C). Mass spectra were obtained using a SHIMADZU mass spectrometer (GC/MS-Q95050 GC-17A SHIMADZU), high resolution mass spectra were recorded on a Finnigan MAT 8230 using EI at 70 eV and on a Finnigan MAT 900 S using ESI at 4 kV (3 µA CH_3CN/MeOH). Chemical shifts δ are given in ppm relative to the residual peaks of the deuterated solvent used. Spectra measured in $CDCl_3$ are referenced to 7.24 ppm (^{1}H) and 77.00 ppm (^{13}C). Coupling patterns are designated as s (singlet), d (doublet), m (multiplet) and b (broad). The ^{13}C spectra were recorded in a j-modulated mode. Signals are assigned as C, CH, CH_2 and CH_3. Coupling constants J are given in Hz.

$[^{11}C]CO_2$ was produced within a GE PET trace cyclotron (General Electric Medical System, Uppsala, Sweden) by a $^{14}N(p,\alpha)^{11}C$ nuclear reaction under irradiation of a gas target (Aluminium) filled with N_2 (+1% O_2) (Messer Gases, Vienna, Austria). The production of $[^{11}C]CH_3I$ and $[^{11}C]CH_3OTf$ was performed within a TRACERlab™ FX C Pro synthesizer (GE Healthcare, Uppsala, Sweden). Evaluation of reaction conditions was performed manually in a lead-shielded hood with small quantities of radioactivity (<1 GBq). After optimization, [^{11}C]Me@APPI-synthesis was automated in the TRACERlab™ FX C Pro synthesizer, remotely controlled by a standard laptop with suitable processing software.

[^{11}C]Me@APPI was purified by semi-preparative reversed phase HPLC using the built-in semi-preparative HPLC system equipped with a radioactivity and a UV detector (Linear Instruments Model 200 Detector UV/VIS) and a LaPrep HPLC pump (VWR International, Radnor, USA). A Phenomenex® Gemini, C-18 with TMS endcapping, 10 µm, 250x10 mm (Phenomenex®, Aschaffenburg, Germany) column with a mobile phase of MeOH/0.1 M ammonium formate 70/30 v/v% +1 % NEt_3 at a flow rate of 8 mL/min was used for purification.

Analytical HPLC was performed on Merck-Hitachi LaChrom HPLC system (L-7100 pump; LaChrom L-7400 UV detector at 254 nm) and a NaI radio-detector (Bertholdt Technologies, Bad Wildbach, Germany) using Raytest software (Raytest, Straubenhardt, Germany). A Phenomenex® Prodigy,

Phenyl-3(PH-3), 5 µm, 250x4.6 mm (Phenomenex®, Aschaffenburg, Germany) column with a mobile phase consisting of ACN/0.1 M ammonium formate 50/50 v/v% at a flow rate of 2 mL/min was used.
The osmolality was measured with a Wescor osmometer Vapro® 5600 (Sanova Medical Systems, Vienna, Austria) and pH was measured using a WTW inoLab 740 pH meter (WTW, Weilheim, Germany).

Methods

Precursor chemistry (APPI:0) and reference standard (Me@APPI)

The synthesis scheme of APPI:0 is outlined in figure 2 based on Zhang et al.[19]

A solution of 3-chloro-1-phenylpropan-1-one (**1**, 5.00 g, 29.65 mmol) in 25 mL THF and 35 mL EtOH was cooled to -10°C and sodium borohydride (1.17 g, 31.12 mmol) was slowly added. After stirring at -5°C for 10 min, the solution was poured into a mixture of 80 mL saturated aqueous ammonium chloride and 40 g of ice. After extraction with diethylether, the organic layers were separated, dried over sodium sulfate and evaporated to give 4.78 g (94.45%) of a pale yellow oil **2**. After addition of 40 mL of 48% aqueous hydrobromic acid to chloride **2** (2.09 g, 12.24 mmol), the mixture was stirred at room temperature for 3 h and then carefully poured into a mixture of 11 g potassium carbonate in 70 g ice. After neutralization, the product was extracted with diethylether. The combined organic extracts were dried ($MgSO_4$) and evaporated to give 1.74 g (60.84%) of **3** as a pale yellow oil.[20]

N-phenyl-*o*-phenylenediamine (1.00 g, 5.43 mmol) and 1,1-carbonyldiimidazol (CDI) (1.23 g, 7.60 mmol) were stirred in THF over night at room temperature. After evaporation of the solvent the crude mixture was purified by chromatography (ligroin/ethylacetate 1/1) yielding 845 mg (74.05%) of pink crystals **5**.[19] Subsequently, 0.84 g (4.00 mmol) of intermediate **5** and 1.04 g (8.00 mmol) potassium carbonate were suspended in DMF. After stirring for 30 min at room temperature, synthon **3** (1.03 g, 6.00 mmol) was added and the mixture stirred overnight. The mixture was poured into ethylacetate and H_2O, extracted with ethylacetate and the combined organic layers were dried over $MgSO_4$. After evaporation and silica gel chromatography (ligroin/ethylacetate 9/1) of the residue 1.15 g (79.38%) of chloride **6** were obtained as colorless solid.[21]

A solution of chloride **6** (2.30 g, 6.34 mmol) and sodium iodide (1.90 g, 12.69 mmol) in acetone was refluxed for 24 h. The crude product was filtered and dried under reduced pressure to give 2.74 g (95.08%) of **7** as a yellow solid. After heating iodide **7** (0.20 g, 0.44 mmol) and 22 mL of 2 M ammonia in isopropanol to 80°C for 3 h in a sealed tube, the solvent was removed under reduced pressure and the crude product purified by chromatography (dichloromethane/methanol 9/1). After recrystallization (dichloromethane/hexane) 72 mg (47.62%) of APPI:0 (**8**) were obtained as white solid.

NMR analysis (^1H and ^{13}C) of intermediates were in full accordance with the literature.

6: **^{1}H-NMR** (200 MHz, $CDCl_3$): δ (ppm) 7.54 (m, 6 H), 7.38 (m, 4H), 7.07 (m, 4H), 5.78 (m, 1H), 3.65 (m, 2H), 3.09 (dm, 2H); **^{13}C-NMR** (50 MHz, $CDCl_3$): δ (ppm) 153.1, 138.4, 134.3, 129.3, 128.7, 128.6, 127.9, 127.5, 127.3, 125.9, 121.8, 121.4, 108.8, 108.7, 54.3, 41.9, 34.1; **MS**: m/z (%): 362 (M^+18%), 211 (19), 210 (100), 181 (15), 167 (20), 115 (10), 91 (58), 77 (18), 51 (9); **HRMS**: m/z calculated for $C_{22}H_{19}ClN_2O$ Na (M^+ + Na): 385.1084. Found: 385.1077.

7: ^{1}H-NMR (200 MHz, $CDCl_3$): δ (ppm) 7.55 (m, 6H), 7.36 (m, 4H), 7.07 (m, 4 H), 5.72 (m, 1H), 3.64 (m, 1H), 3.22 (m, 2H), 2.86 (m, 1H); **^{13}C-NMR** (50 MHz, $CDCl_3$) : δ (ppm) 153.3, 138.3, 134.4, 129.5, 128.9, 128.6, 128.1, 127.7, 127.4, 126.0, 122.0, 121.5, 109.1, 108.9, 57.5, 35.3, 2.5; **MS**: m/z (%): 454 (M^+13%), 211 (16), 210 (100), 167 (22), 117 (45), 115 (17), 91 (48), 77 (27), 51 (15); **HRMS**: m/z

calculated for $C_{22}H_{19}IN_2O$ Na (M^+ + Na): 477.0440. Found: 477.0457.

8: ^{1}H-NMR (200 MHz, $CDCl_3$): δ (ppm) 7.51 (m, 6H), 7.30 (m, 4H), 6.95 (m, 4H), 5.82 (m, 1H,), 5.15 (s, 2H), 2.84 (m, 2H), 2.73 (m, 2H); **^{13}C-NMR** (50 MHz, $CDCl_3$): δ (ppm) 154.0, 137.5, 134.0, 129.7, 129.5, 128.9, 128.1, 127.6, 127.3, 126.4, 122.2, 121.9, 110.2, 109.1, 53.1, 37.9, 30.6; **MS**: m/z (%): 343 (M^+20 %), 313 (11), 300 (12), 210 (84), 181 (24), 126 (29), 77 (31), 60 (38), 58 (31), 45 (91), 43 (100), 42 (34), 41 (31); **HRMS**: m/z calculated for $C_{22}H_{21}N_3O$ (M^+ + 1): 344.1685. Found: 344.1755.

Reference standard:

A mixture of iodide **7** (1.026 g, 2.26 mmol) and 28.25 ml 8 M methylamine in ethanol was heated at 80°C for 3 h in a sealed tube. Evaporation of the solvent and subsequent column chromatography (dichloromethane/methanol 9/1) yielded 311 mg (38.52%) of Me@APPI **9** as yellow solid.

9: ^{1}H-NMR (200 MHz, $CDCl_3$): δ (ppm) 7.52 (m, 6H), 7.35 (m, 4H), 7.03 (m, 3H), 6.73 (d, *J*= 7.46 Hz), 5.79 (m, 1H), 3.26 (m, 2H), 2.93 (m, 2H), 2.59 (s, 3H); **^{13}C-NMR** (50 MHz, $CDCl_3$): δ (ppm) 153.6, 138.3, 134.4, 129.5, 128.8, 128.0, 127.9, 127.8, 127.3, 126.1, 122.0, 121.5, 109.8, 108.9, 53.8, 48.0, 35.2, 29.6; **MS:** m/z (%): 357 (M^+ 8%), 210 (20), 97 (26), 81 (22), 71 (44), 69 (56), 67 (27), 57 (100), 55 (72), 44 (58), 43 (89), 41 (37). **HRMS**: m/z calculated for $C_{23}H_{23}N_3O$ (M^+ +1): 358.1841. Found: 358.1930.

Radiochemistry

Production of [^{11}C]CH_3I and [^{11}C]CH_3OTf

[^{11}C]CO_2 production was stopped as soon as the desired activity (40-50 GBq) at currents between 45 and 54 µA was achieved (10-15 min). [^{11}C]CH_3I was produced using a gas phase conversion described by Larsen et al. [22] within the GE TRACERlab™ FX C Pro synthesizer adopting modifications described by Kniess et al. [23] Briefly, [^{11}C]CO_2 was trapped on a molecular sieve (4 Å) within the module and subsequently converted into [^{11}C]CH_4 by a Ni-catalysed reduction with H_2 at 400°C. The resulting [^{11}C]CH_4 was reacted in a recirculating process for 4 min with sublimated iodine at 720°C to give [^{11}C]CH_3I. The produced [^{11}C]CH_3I was trapped on-line on a Porapak® N column and finally released by heating the trap to 190°C. [^{11}C]CH_3OTf was prepared on-line at the passage of [^{11}C]CH_3I through a pre-heated (220°C) column containing 300 mg silver-triflate impregnated graphitized carbon. [24]

Set up of small-scale reaction and optimization

For small-scale examinations [^{11}C]CH_3I or [^{11}C]CH_3OTf, respectively, was trapped in 500 µL of ACN and divided for further experiments. If not stated otherwise all experiments were performed in triplicates. All evaluation reactions were performed manually (shielded hood; starting activity <1 GBq). The influence of reaction time (1, 2, 5 and 10 min), reaction temperature (RT, 50°C, 75°C), base (triethylamine and TBAH) and precursor concentration was investigated. Finale reaction volumes of small-scale reactions were 100 - 200 µL. In figure 3 the reaction scheme is presented.

Automation of radiosynthesis

The automation of the radiosynthesis was done on the TRACERlab™ FX C Pro (GE Healthcare) [25], a schematic flowchart is depicted in figure 4.

Produced CH_3OTf was trapped at RT within the glass reactor (2 mL) containing APPI:0 (1 mg, 2,9 µmol) and 1 µL of an aqueous TBAH-solution (2 mg/µL) in 500 µL ACN. After heating the sealed reaction vessel to 75°C for 5 min, the mixture was cooled to 25°, the reaction was quenched and diluted by addition of 1 mL HPLC eluent (V2) and the whole volume was transferred to the injection loop. The

crude mixture was automatically (fluid detector controlled) injected onto the semi-preparative HPLC column. The [^{11}C]Me@APPI peak was cut into a bulb, and subsequently diluted with 80 mL water. The aqueous product solution was subjected to solid phase extraction by transferring over a preconditioned (10 mL EtOH, air, 20 mL water, air) C8 SPE cartridge. After rinsing the C8 SepPak® with water (V6), the pure product was eluted with 1.5 mL EtOH (V5) and the cartridge and transfer lines washed with 5 mL 0.9% saline. After formulation with further 4 mL 0.9% saline, 1 mL 3% saline and 1 mL 125 mM phosphate buffer, sterile filtration (0.22 µm) was performed under aseptic conditions (laminar air flow hot cell, class A) to avoid microbial contamination.

Quality control

Chemical and radiochemical impurities were identified using radio-HPLC according to the monograph in the European Pharmacopoeia. [26] Osmolality and pH were tested with designated equipment. Radiochemical identity and purity were assessed via analytical radio-HPLC by comparison of retention times with authentic samples. Radiochemical purity always exceeded 98%. Specific radioactivity was determined by quantification of the non-radioactive product (HPLC UV channel at 254 nm) and determination of overall radiochemical yield (GBq at end of synthesis). Sterility, presence of endotoxins, pH, osmolality and residual solvents were determined by standard procedures routinely performed at the PET Centre of the Vienna General Hospital/ Medical University of Vienna.

Statistical analysis

All quantitative data (both in text and figures) are given as arithmetic mean ± standard deviation. A student t-test (two-tailed) with α=0.95 was performed for determination of significance; i.e. P values of < 0.05 were considered to be significant.

NET-expressing membrane binding studies

The affinity of new radiolabeled ligands was tested in a NET-expressing membrane binding protocol. [13, 27] Effects of sodium concentration, temperature and incubation times were investigated. The competitive binding experiments were performed in glass test tubes, filled with 350 µL of the new 'cold' (=non-radioactive) reference compounds, 100 µL of the membrane suspension (in assay buffer; 3 µg protein/unit, human Norepinephrine Transporter RBHNETM400AU, Perkin Elmer) and 50 µL of a 2 nM ^{3}H-nisoxetine*HCl solution (in assay buffer, 70-87 Ci/mmol, NET1084; Perkin Elmer). For non-specific binding 10 µM reboxetine (Sigma-Aldrich, Vienna, Austria) was used; and for total binding (control) only ^{3}H-nisoxetine*HCl, buffer and membrane suspension were incubated. After incubation time, binding was quenched with ice cold buffer, and membrane bound radioactivity was recovered by rapid vacuum filtration through GF/C glass fiber filters (Whatman® Inc., Clifton, USA) presoaked in assay buffer containing 0.3% polyethylene imine (PEI). Filters were washed with 3 times with 4 mL assay buffer and transferred into β-counting vials. After addition of a β-scintillation cocktail (2 mL Ultima Gold™, biodegradeable, Perkin Elmer), the tubes were shaken for 20 min and then counted. Data from the competition plots was analyzed; IC_{50} and K_i values were calculated using GraphPad Prism® software (San Diego, USA). (Arithmetic means of values derived from three different assays, each in triplicate for each compound.)

To determine the selectivity of the tested compounds towards NET in comparison to DAT and SERT, respectively, assays similar to those described for NET were performed. DAT and SERT expressing membranes were used instead of NET-membranes (hSERT: 9 µg protein/unit, RBHSTM400UA, Perkin

Elmer and hDAT: 12.7 µg protein/unit, RBHDATM400UA, Perkin Elmer, Waltham, USA).
IC_{50} and K_i values were obtained in analogy to NET experiments. Ratios DAT/NET and SERT/NET were determined.

LogD analysis, IAM chromatography and blood-brain-barrier-penetration

LogD values were determined using a HPLC based assay according to Donovan and Pescatore. [28] All compounds (as cold references) were injected in a mix of two known compounds with known logD and k' values according to a standard protocol. A short polymeric ODP-50 column (Shodex®, Showa Denko Europe GmbH, Munich, Germany) was used; a linear gradient from 10% MeOH 90% 25 mM Phosphate buffer to 100% methanol within 9.4 min at a flow-rate of 2 mL/min was applied. Internal standards were triphenylene and toluene; detection was performed at 260 nm and 285 nm.
Since logP or logD values were shown to be poor predictors for BBB-penetration other *in-vitro* methods have been described [29, 30], such as immobilized artificial membrane (IAM) chromatography and parallel artificial membrane permeability assays. IAM chromatography was performed using a Redistech IAM.PC.DD2 (Regis Technologies Inc., Morton Grove, USA) column (15 cm x 4.6 mm) according to Tavares et al. [31] For analysis, 0.01 M phosphate buffer (pH 7.4) and ACN (in different ratios) were used as mobile phase at a flow rates of 1 mL/min isocratically. Resulting K_m (membrane partition coefficient) and P_m (permeability) were obtained after data analysis and compared with known BBB penetrating compounds. The data were compared with those derived from DASB (3-amino-4-[2-[(di(methyl)amino) methyl]phenyl]sulfanylbenzonitrile) , a compound known to penetrate BBB, as external standard.

Metabolic stability testing

Pooled human liver microsomes (BD Biosciences, Woburn, 20 mg/mL in sucrose) are subcellular fractions (mainly endoplasmatic reticulum) that contain many drug-metabolizing enzymes, e.g. cytochrome P450s, flavinmonooxygenases and epoxide hydrolase. To investigate the metabolic fate of [^{11}C]Me@APPI, i.e. the metabolic stability and *in vitro* intrinsic clearance [V_{max}/K_m], microsomal incubations were performed. Briefly, microsome solution (in sucrose) were pre-incubated under physiological conditions (phosphate buffer, pH 7.4, 37°C) with a NADPH-generating system (solution-A: $NADP^+$, Glucose-6-phosphate and magnesium-chloride in H_2O and solution-B: Glucose-6-phosphate dehydrogenase in sodium citrate) for 5 min. After adding 6 µL of [^{11}C]Me@APPI, the final volume of the mixture was 300 µL. [32] Enzymatic reactions were stopped by adding one volume of an ice-cold methanol/ACN mixture (10/1 v/v). The mixtures were vortexed, followed by a centrifugation step (23.000g, 5 min, RT). Aliquots of the obtained supernatant were analysed by HPLC (pH 7.4, 37°C). As results, both the percentage of test compound metabolized after a certain time and the biological half-life were determined.

RESULTS

Chemistry

Successful preparation of precursor APPI:0 and reference compound Me@APPI was achieved. APPI:0 was prepared in a 4-step synthesis starting from N-phenyl-o-phenylenediamine (**4**) in 26.5% overall yield. Reference compound Me@APPI was synthezised likewise in 21.4% overall yield.

Radiochemistry:

Radiochemical incorporation yields (RCIY) of [^{11}C]Me@APPI were below 0.5% for all examined conditions using [^{11}C]CH_3I as methylation agent. Using [^{11}C]CH_3OTf for methylation, the influence of precursor concentration, reaction time and temperature as well as amount of base were investigated (figure 5a-c). RCIYs ranged from 9.04 ± 0.23% for low precursor concentrations (0.25 µg/mL) at RT up to 32.81 ± 1.8% for reaction with 1 mg/mL precursor concentration. Addition of triethylamine instead of aqueous TBAH solution lead to formation of an unknown side product in high amounts. Increasing reaction temperature from RT to 75°C lead to increased RCIYs.

Optimum conditions were used for large scale preparations within a fully automated procedure. In table 1, synthesis steps, conversion and yields are outlined. For SPE procedure C-18 plus, C-18 light and C-8 plus cartridges were evaluated. Using the frequently used C-18 plus SPE cartridge 35.9% of the pure product was lost on the SepPak® after elution of the product. Changing to a C-18 light SepPak® revealed 32.0% of product bound to the cartridge; moreover addition of another 2 mL of EtOH could not achieve quantitative elution of the product, either. Therefore, a C-8 plus SPE cartridge was used; hereby only 6.3% of the product was lost due to retention on the cartridge.

So far, 11 large scale radio-syntheses have been performed, yielding 1.25 ± 0.72 GBq (8.79 ± 4.34% EOB, corrected for decay) of formulated [^{11}C]Me@APPI within less than 40 min. Specific activity (SA) was found to be 54.35 ± 7.80 GBq/µmol.

Purification of [^{11}C]Me@APPI

A typical semi-preparative radio-RP-HPLC chromatogram is shown in figure 6. The retention times were 1.9-2.1 min (*k'*=0-0.1) for [^{11}C]CH_3OTf, 3.5-3.8 min (*k'*=0.84-1.0) for [^{11}C]CH_3I, 4.5-5.2 min (*k'*=1.4-1.7) for precursor APPI:0 and 6.5-7.5 min (*k'*=2.4-2.9) for [^{11}C]Me@APPI.

Quality control

Quality control was performed directly after synthesis within 7 min. In figure 7 a typical analytical HPLC chromatogram is shown. The retention times in the analytical HPLC assay were 6.0-6.3 min (*k'*=4-4.3) for precursor (APPI:0), 1.7-1.9 min (*k'*=0.4-0.6) for [^{11}C]MeOH, 2.7-2.8 min (*k'*=1.2-1.3) for [^{11}C]CH_3OTf and 3.1-3.2 min (*k'*=1.6-1.7) for [^{11}C]CH_3I, respectively. The product [^{11}C]Me@APPI was eluted at a retention time of 7.6-8.1 min (*k'*=5.3-5.8). Osmolality and pH values were found to be in a physiological range. Residual solvent analysis revealed ACN <5 ppm and methanol <20 ppm, besides 8.5% ethanol present in the formulation (total product volume: 17.5 mL).

Affinity and Selectivity

Modification of testing conditions had a high impact on the feasibility of the experiments in terms of determined B_{max}, binding equilibrium and non-specific binding. The tested conditions for the NET-membranes were: 1) influence of Na^+ and Cl^- concentration: 120 mM and 300 mM; 2) temperature: 4°C and 25°C; 3) incubation time: 1 h, 2 h and 4 h. Testing at 4°C lead to low B_{max} values, therefore incubation time was elongated from 1 h to 4 h. Thereby, an increase in B_{max} and a decrease of non-specific binding was observed. Generally, binding was rather low at 4°C, as compared to experiments at 25°C, where binding equilibrium was reached, resulting in higher B_{max} values and low non-specific binding. Moreover, experiments at higher temperature (25°C) better represent the *in-vivo* situation (37°C). Hence, optimum conditions were obtained using incubation at 25°C for 1 h in a buffer containing 300 mM NaCl, 50 mM TRIS and 5 mM KCl.

Affinity of reference compounds (Me@APPI, APPI:0 and reboxetine) was determined using the optimum

conditions as 8.08 ± 1.75 nM for Me@APPI, 19.31 ± 2.91 nM for APPI:0 and 3.29 ± 0.43 nM for reboxetine, respectively (n≥9).

For determination of selectivity, the affinity of Me@APPI and APPI:0 towards DAT and SERT was assessed and revealed >5 µM for both compounds for DAT and 670 ± 210 nM (Me@APPI) and 485 ± 105 nM (APPI:0) towards SERT, respectively, (n≥6). Therefore, Me@APPI was found to display 83-fold affinity towards NET as compared to SERT.

LogD and BBB-penetration

LogD values were 3.08 ± 0.01 for APPI:0 and 3.14 ± 0.01 for Me@APPI, respectively. BBB-penetration experiments revealed that Me@APPI shows a similar behavior to DASB, a SERT-PET-tracer known to be able to penetrate BBB sufficiently for *in-vivo* imaging. IAM-chromatography experiments (n=4) revealed K_m values of 540 ± 120 for Me@APPI. The permeability P_m of Me@APPI was calculated as 1.51 ± 0.34 and 1.23 ± 0.13 for DASB.

Metabolic stability

Stability testing using human liver microsomes (n=4), revealed no significant metabolism of [^{11}C]Me@APPI so far. After 1 h, 99.5% of the tracer was found to be still intact.

DISCUSSION

Synthesis of precursor APPI:0 and of cold reference compound Me@APPI were successfully established. Satisfactory preparation of [^{11}C]Me@APPI was achieved in small-scale reactions, hereby determining the ideal reaction conditions. Furthermore, up-scaling and automation of radiosynthesis was accomplished, and also purification via semi-preparative HPLC and subsequent SPE succeeded. The proposed assay guarantees the (almost) quantitative separation of APPI:0 from the product peak which is essential since the precursor molecule also displays considerable binding towards NET.

Methylation attempts of APPI:0 with [^{11}C]methyliodide showed only poor radiochemical incorporation yields (<0.5%), whereas [^{11}C]methylation with [^{11}C]MeOTf yielded 32.8% in optimum conditions. The use of triethylamine as base lead predominantly to the formation of an unknown by-product, hence only small amounts of product were obtained. Using TBAH, satisfying amounts of [^{11}C]Me@APPI were achieved and no undesired by-product formation occurred.

Interestingly, we found when using a C-18 plus SPE cartridge for final product purification more than a third of the product was retained on the column irreversibly. Changing to a C-18 light cartridge, the amount of product bound after elution was decreased by 11%, but still unsatisfactory high amounts of irreversibly bound radioactivity were observed. Fortunately, the product could be eluted almost quantitatively using a C-8 plus cartridge. After sterile filtration, satisfying amounts of radioactivity with acceptable specific activity were obtained. Strict radiopharmaceutical quality control was passed for all produced batches allowing for preclinical testing and future in-vivo-applications.

When determining affinity and selectivity using membranes expressing the respective human transporter we found K_i-values of 8.08 ± 1.75 nM for Me@APPI, 19.31 ± 2.91 nM for APPI:0 and 3.29 ± 0.43 nM for reboxetine, respectively, towards hNET. The value for Me@APPI is well in line with the one already published by Zhang et al. (hNET IC_{50}= 9 nM). [19] Although the affinity of the title compound is “only” around 8 nM previous data indicate that the density of NET especially in LC should be sufficiently high to enable *in-vivo* visualization. [7-9]

For determination of metabolic stability human liver microsomes were used. These experiments revealed excellent stability of the title compound, showing no significant degradation after 1 h incubation time for [^{11}C]Me@APPI (<0.05%). Setup of further tests to examine also phase-two-metabolism is currently in progress. In contrast, other widely used brain-PET tracers, e.g. [^{11}C-*carbonyl*]WAY-100635 [33], [^{11}C]DASB [34, 35] and [^{11}C]MeNER [18], display significant metabolic degradation . This highlights the outstanding stability of this novel PET-ligand.

In consideration of a possible application of [^{11}C]Me@APPI as NET-PET-tracer in human brain, BBB-penetration was tested as well. In IAM-chromatography experiments Me@APPI showed comparable behaviour to DASB. Since all preliminary data indicate [^{11}C]Me@APPI's suitability for clinical use, further *in-vitro* and *in-vivo* experiments including autoradiography and small-animal-PET examinations are planned.

CONCLUSION

Automated radiosynthesis of the novel NET-PET-tracer, [^{11}C]Me@APPI, was established, leading to satisfying yields and specific radioactivities. So far, 1.25 ± 0.72 GBq with 54.35 ± 7.80 GBq/µmol SA were produced (n=11). Furthermore, all tested preclinical parameters such as selectivity, affinity, metabolic degradation, BBB-penetration and lipophilicity clearly indicate the suitability of [^{11}C]Me@APPI to become a NET-PET-tracer in clinical application. Further *in-vitro* and *in-vivo* tests will be performed to strengthen the presented findings.

REFERENCES

[1] Zhou J. Norepinephrine transporter inhibitors and their therapeutic potential. Drugs Future 2004;29:1235–44.

[2] Klimek V, Stockmeier CA, Overholser J, Meltzer HY, Kalka S, Dilley G, et al. Reduced Levels of Norepinephrine Transporters in the Locus Coeruleus in Major Depression The Journal of Neuroscience 1997;17:8451-8.

[3] Ressler KJ and Nemeroff CB. Role of Norepinephrine in the Pathophysiology and Treatment of Mood Disorders. BIOL PSYCHIATRY 1999;46:1219–33.

[4] Ordway GA, Stockmeier CA, Cason GW, and Klimek V. Pharmacology and Distribution of Norepinephrine Transporters in the Human Locus Coeruleus and Raphe Nuclei. The Journal of Neuroscience 1997;17:1710-9.

[5] Gulyás B, Brockschnieder D, Nag S, Pavlova E, Kása P, Beliczai Z, et al. The norepinephrine transporter (NET) radioligand (S,S)-[18F]FMeNER-D2 shows significant decreases in NET density in the human brain in Alzheimer's disease: A post-mortem autoradiographic study. Neurochemistry International;56:789-98.

[6] Mash DC, Ouyang Q, Qin Y, and Pablo J. Norepinephrine transporter immunoblotting and radioligand binding in cocaine abusers. Journal of Neuroscience Methods 2005;143:79-85.

[7] Smith HR, Beveridge TJR, and Porrino LJ. Distribution of norepinephrine transporters in the non-human primate brain. Neuroscience 2006;138:703-14.

[8] Logan J, Wang G-j, Telang F, Fowler JS, Alexoff D, Zabroski J, et al. Imaging the norepinephrine transporter in humans with (S,S)-[11C]O-methyl reboxetine and PET: problems and progress. Nuclear Medicine and Biology 2007;34:667-79.

[9] Donnan GA, Kaczmarczyk SJ, Paxinos G, Chilco PJ, Kalnins RM, Woodhouse DG, et al. Distribution of catecholamine uptake sites in human brain as determined by quantitative [3H] mazindol autoradiography. The Journal of Comparative Neurology 1991;304:419-34.

[10] Halldin C, Farde L, Högberg T, Mohell N, Hall H, Suhara T, et al. Carbon-11-FLB 457: A Radioligand for Extrastriatal D2 Dopamine Receptors. Journal of Nuclear Medicine 1995;36:1275-81.

[11] Fowler JS, Volkow ND, Wang GJ, Gatley SJ, and Logan J. [11C]Cocaine: PET studies of cocaine pharmacokinetics, dopamine transporter availability and dopamine transporter occupancy. Nucl. Med. Biol. 2001;28:561-72.

[12] Pristupa ZB, Wilson JM, Hoffman BJ, Kish SJ, and Niznik HB. Pharmacological heterogeneity of the cloned and native human dopamine transporter: disassociation of [3H]WIN 35,428 and [3H]GBR 12,935 binding. Molecular Pharmacology 1994;45:125-35.

[13] Tejani-Butt SM. [3H]nisoxetine: a radioligand for quantitation of norepinephrine uptake sites by autoradiography or by homogenate binding. Journal of Pharmacology and Experimental Therapeutics 1992;260:427-36.

[14] Bock N, Quentin DJ, Hüther G, Moll GH, Banaschewski T, and Rothenberger A. Very early treatment with fluoxetine and reboxetine causing long-lasting change of the serotonin but not the noradrenaline transporter in the frontal cortex of rats. World Journal of Biological Psychiatry 2005;6:107-12.

[15] Wilson AA, Patrick Johnson D, Mozley D, Hussey D, Ginovart N, Nobrega J, et al. Synthesis and *in vivo* evaluation of novel radiotracers for the *in vivo* imaging of the norepinephrine transporter. Nuclear Medicine and Biology 2003;30:85-92.

[16] Takano A, Gulyás B, Varrone A, and Halldin C. Comparative evaluations of norepinephrine transporter radioligands with reference tissue models in rhesus monkeys: (S,S)-[18F]FMeNER-D2; and (S,S)-[11C]MeNER. European Journal of Nuclear Medicine and Molecular Imaging 2009;36:1885-91.
[17] Schou M, Halldin C, Sóvágó J, Pike VW, Hall H, Gulyás B, et al. PET evaluation of novel radiofluorinated reboxetine analogs as norepinephrine transporter probes in the monkey brain. Synapse 2004;53:57-67.
[18] Schou M, Zoghbi S, Shetty H, Shchukin E, Liow J-S, Hong J, et al. Investigation of the Metabolites of (S,S)-[11C]MeNER in Humans, Monkeys and Rats. Molecular Imaging and Biology 2009;11:23-30.
[19] Zhang P, Terefenko EA, McComas CC, Mahaney PE, Vu A, Trybulski E, et al. Synthesis and activity of novel 1- or 3-(3-amino-1-phenyl propyl)-1,3-dihydro-2H-benzimidazol-2-ones as selective norepinephrine reuptake inhibitors. Bioorg. Med. Chem. Lett. 2008;18:6067-70.
[20] Varney M, Romines W, Boritzki T, Margosiak S, Bartlett C, and Howland E. Syntheses and biological evaluation of N-[4-(2-trans-[([2,6-diamino-4(3H)-oxopyrimidin-5-YL]methyl)thio]cyclobutyl)benzoyl]-L-glutamatic acid a novel 5-thiapyrimidone inhibitor of dihadrofolate-reductase. Journal of Heterocyclic Chemistry 1995;32:1493-8.
[21] Jona H, Shibata J, Asai M, Goto Y, Arai S, Nakajima S, et al. Efficient and practical asymmetric synthesis of 1-tert-butyl 3-methyl (3R,4R)-4-(2-oxo-2,3-dihydro-1H-benzimidazol-1-yl)piperidine-1,3-dicarboxylate, a useful intermediate for the synthesis of nociceptin antagonists. Tetrahedron-Asymmetry 2009;20:2439-46.
[22] Larsen P, Ulin J, Dahlstrøm K, and Jensen M. Synthesis of [11C]iodomethane by iodination of [11C]methane. Applied Radiation and Isotopes 1997;48:153-7.
[23] Kniess T, Rode K, and Wuest F. Practical experiences with the synthesis of [11C]CH3I through gas phase iodination reaction using a TRACERlabFXC synthesis module. Applied Radiation and Isotopes 2008;66:482-8.
[24] Jewett DM. A simple synthesis of [11C]methyl triflate. International Journal of Radiation Applications and Instrumentation. Part A. Applied Radiation and Isotopes 1992;43:1383-5.
[25] GE Healthcare U, Sweden.
[26] Radioactive pharmaceuticals (Radiopharmaceutica, 6.0/0125), . European Pharmacopoeia (Europäisches Arzneibuch): Verlag Österreich GmbH; 2008, p. 995 ff.
[27] Zeng F, Jarkas N, Owens MJ, Kilts CD, Nemeroff CB, and Goodman MM. Synthesis and monoamine transporter affinity of front bridged tricyclic 3β-(4'-halo or 4'-methyl)phenyltropanes bearing methylene or carbomethoxymethylene on the bridge to the 2β-position. Bioorganic & Medicinal Chemistry Letters 2006;16:4661-3.
[28] Donovan SF and Pescatore MC. Method for measuring the logarithm of the octanol–water partition coefficient by using short octadecyl–poly(vinyl alcohol) high-performance liquid chromatography columns. Journal of Chromatography A 2002;952:47-61.
[29] Naik P and Cucullo L. *In vitro* blood–brain barrier models: Current and perspective technologies. Journal of Pharmaceutical Sciences 2012;101:1337-54.
[30] Neuhaus W, Freidl M, Szkokan P, Berger M, Wirth M, Winkler J, et al. Effects of NMDA receptor modulators on a blood–brain barrier *in vitro* model. Brain Research 2011;1394:49-61.
[31] Tavares AA, Lewsey J, Dewar D, and Pimlott SL. Radiotracer properties determined by high performance liquid chromatography: a potential tool for brain radiotracer discovery. Nucl Med Biol 2012;39:127-35.

[32] Nics L, Vraka C, Hendl M, Haeusler D, Wagner K-H, Shanab K, et al. In-vitro stability of [18F]FE@SUPPY and [18F]FE@SUPPY:2 against human liver-microsomes and human plasma. Nuklearmed-Nucl Med 2011;50, A176.
[33] Någren K, Halldin C, Pike VW, Allonen T, Hietala J, Swahn CG, et al. Radioactive metabolites of the 5-HT1A receptor pet radioligand, [carbonyl-11C]way-100635, measured in human plasma samples. Journal of Labelled Compounds and Radiopharmaceuticals 2001;44:S472-S4.
[34] Parsey RV, Ojha A, Ogden RT, Erlandsson K, Kumar D, Landgrebe M, et al. Metabolite Considerations in the *In vivo* Quantification of Serotonin Transporters Using 11C-DASB and PET in Humans. Journal of Nuclear Medicine 2006;47:1796-802.
[35] Ginovart N, Wilson AA, Meyer JH, Hussey D, and Houle S. Positron Emission Tomography Quantification of [11C]-DASB Binding to the Human Serotonin Transporter[colon] Modeling Strategies. J Cereb Blood Flow Metab 2001;21:1342-53.

CAPTIONS:

TABLE 1 Fully automated preparation of [^{11}C]Me@APPI with n≥5 (*at end of synthesis)

FIGURE 1 Structure of noradrenaline (NE), reboxetine, precursor APPI:0 and Me@APPI

FIGURE 2 Synthesis of precursor molecule and cold reference compound

a) $NaBH_4$, 5 min, -10°C; b) HBr, 3 h, RT; c) CDI, overnight, RT; d) K_2CO_3, overnight, 65°C; e) NaI, 24 h, reflux; f) NH_3/$MeNH_2$, 80°C, 3 h;

FIGURE 3 Radio-synthesis of [^{11}C]Me@APPI

FIGURE 4 Scheme of the synthesizer for the radiosynthesis and purification of [^{11}C]Me@APPI

FIGURE 5 Dependence of the radiochemical incorporation yield of [^{11}C]Me@APPI (n ≥ 2) on (a) amount of precursor (RT, 5 min), (b) reaction temperature (1 mg/mL, 5 min) (c) base (75°C, 5 min). All reactions for a) and b) were done with TBAH as base. If not visible, error bars are within the margin of the symbols.

FIGURE 6 Semi-preparative radio-HPLC chromatogram

FIGURE 7 Analytical HPLC chromatogram

TABLE:

n≥5	**GBq**	**% of initial activity (corr. for decay)**	**time from EOB [min]**
[^{11}C]CO_2,target activity	46.7 ± 7.4	100	0
[^{11}C]CH_4 trapped on mol.sieve	35.6 ± 6.2	95.0 ± 17.9	6 ± 1
[^{11}C]CH_3I trapped on porapak	26.3 ± 5.2	79.89 ± 12.3	10 ± 1
[^{11}C]CH_3OTf trapped in reactor	16.6 ± 7.8	57.0 ± 23.3	14 ± 1
residual in reactor (after transfer to HPLC)	1.0 ± 0.5	4.6 ± 1.9	22 ± 1
residual in HPLC injection loop waste	0.3 ± 0.2	1.1 ± 0.6	23 ± 1
[^{11}C]Me@APPI final product yield	**1.25 ± 0.7**	**8.8 ± 4.3**	37 ± 2
specific activity *	**54.35 ± 7.8 GBq/µmol**		

TABLE 2 Fully automated preparation of [^{11}C]Me@APPI with n≥5 (*at end of synthesis)

FIGURES

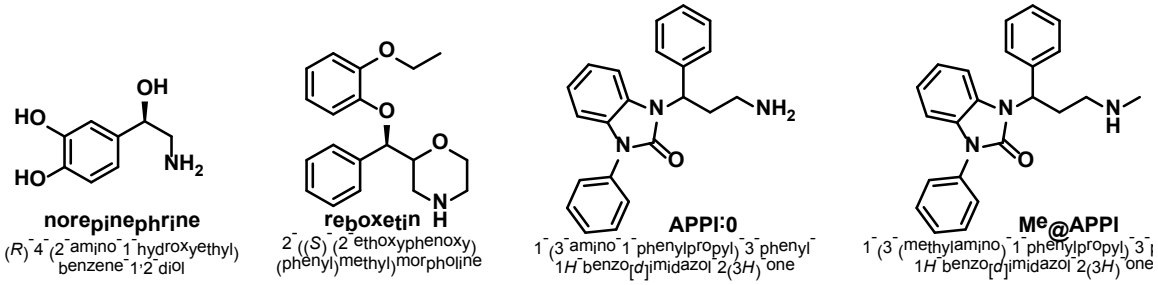

FIGURE 1 Structure of noradrenaline (NE), reboxetine, precursor APPI:0 and Me@APPI

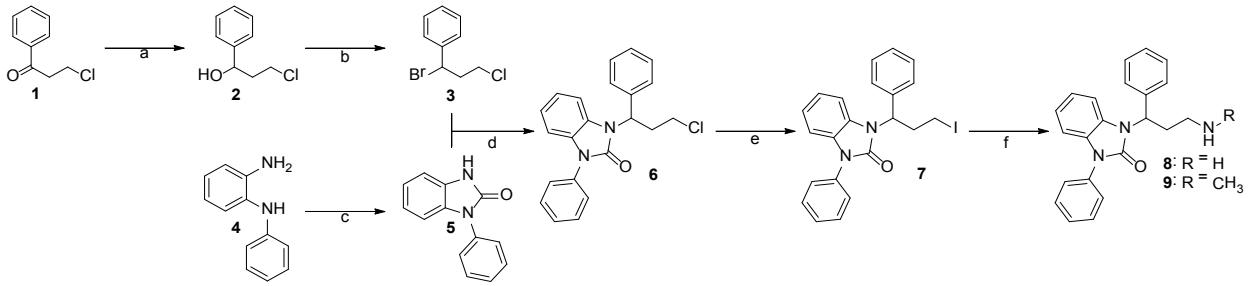

FIGURE 2: Synthesis of precursor molecule and cold reference compound

a) $NaBH_4$, 5 min, -10°C; b) HBr, 3 h, RT; c) CDI, overnight, RT; d) K_2CO_3, overnight, 65°C; e) NaI, 24 h, reflux;

f) $NH_3/MeNH_2$, 80°C, 3 h;

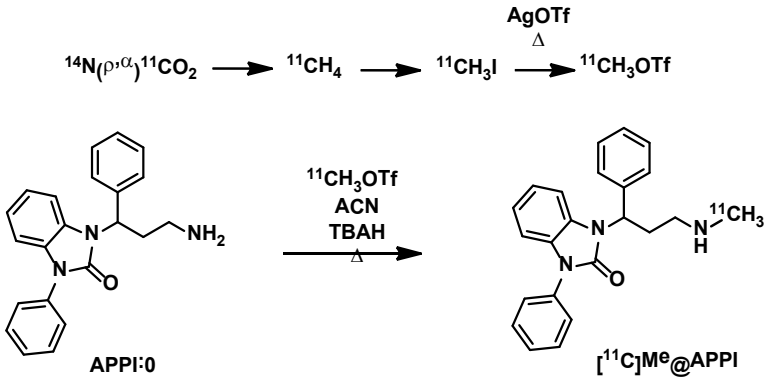

FIGURE 3 Radio-synthesis of [^{11}C]Me@APPI

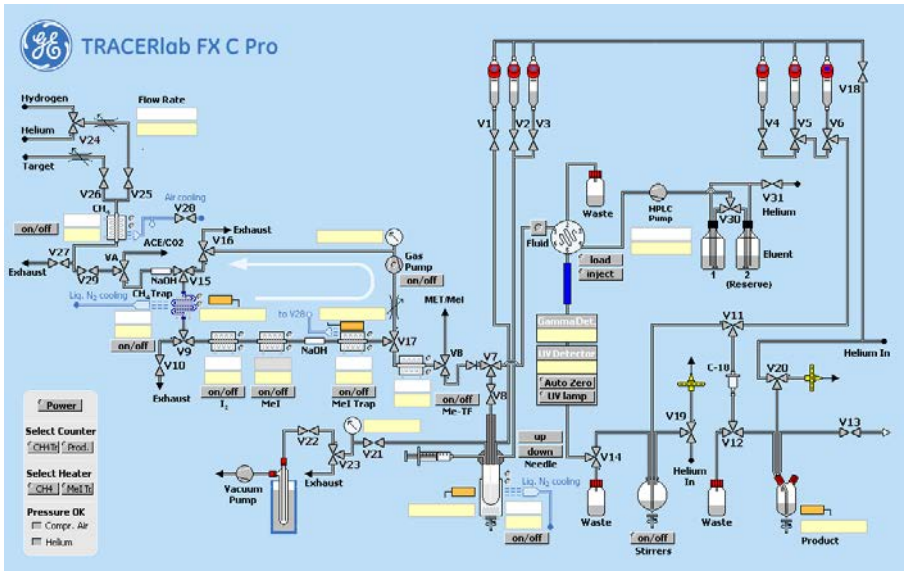

FIGURE 4 Scheme of the synthesizer for the radiosynthesis and purification of [^{11}C]Me@APPI

a)

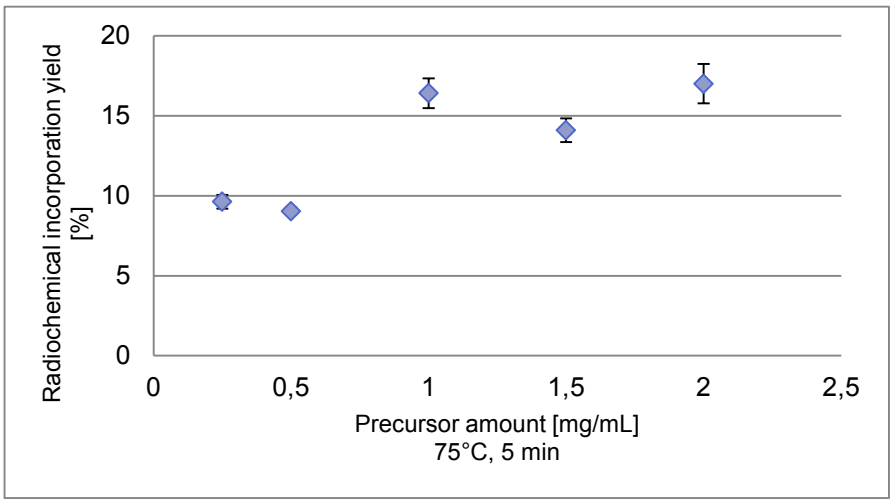

b)

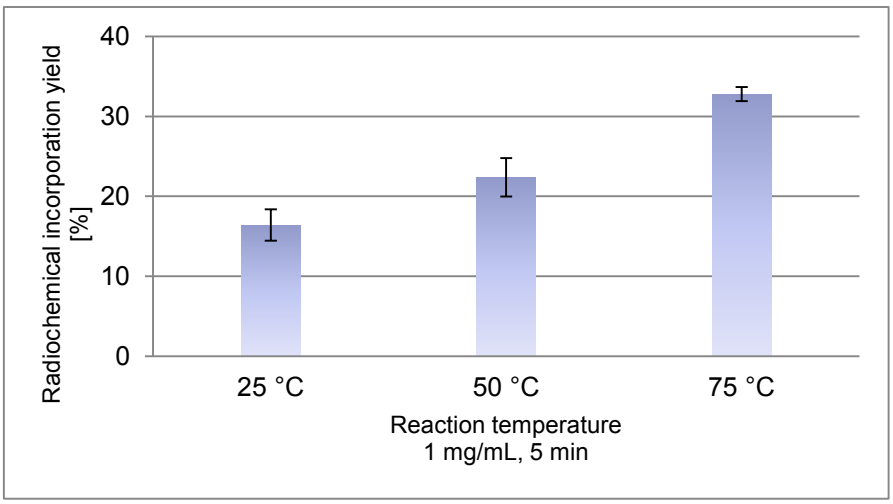

c)

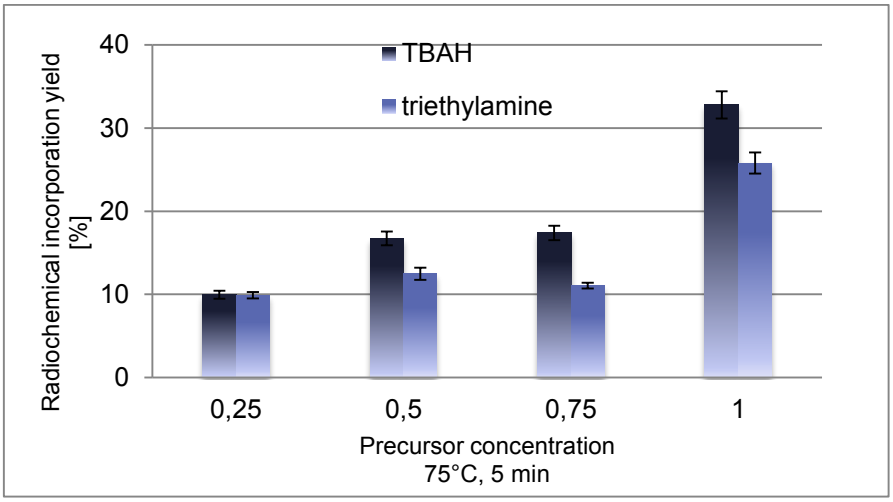

FIGURE 5 Dependence of the radiochemical incorporation yield of [^{11}C]Me@APPI (n ≥ 2) on (a) amount of precursor (RT, 5 min), (b) reaction temperature (1 mg/mL, 5 min) (c) base (75°C, 5 min). All reactions for a) and b) were done with TBAH as base. If not visible, error bars are within the margin of the symbols.

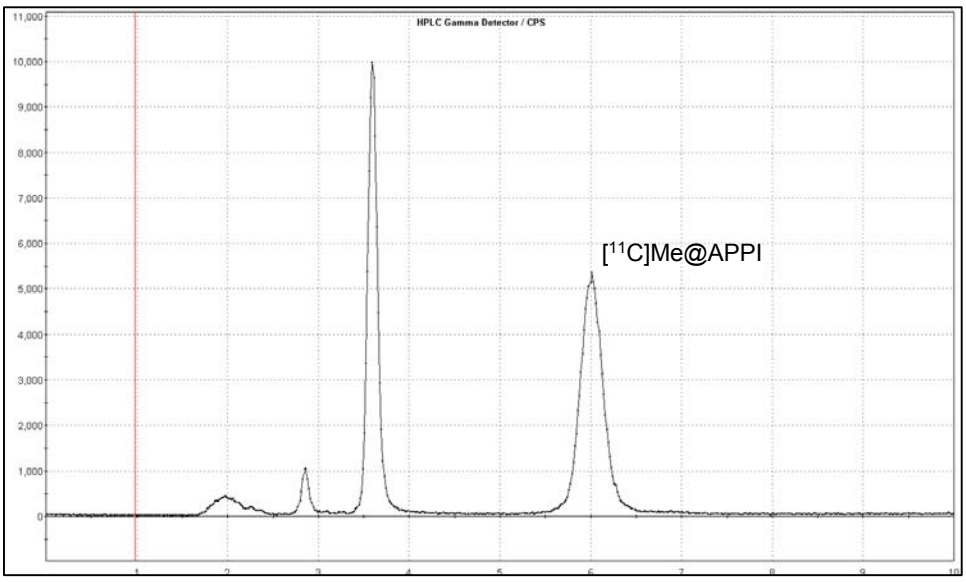

FIGURE 6 Semi-preparative radio-HPLC chromatogram

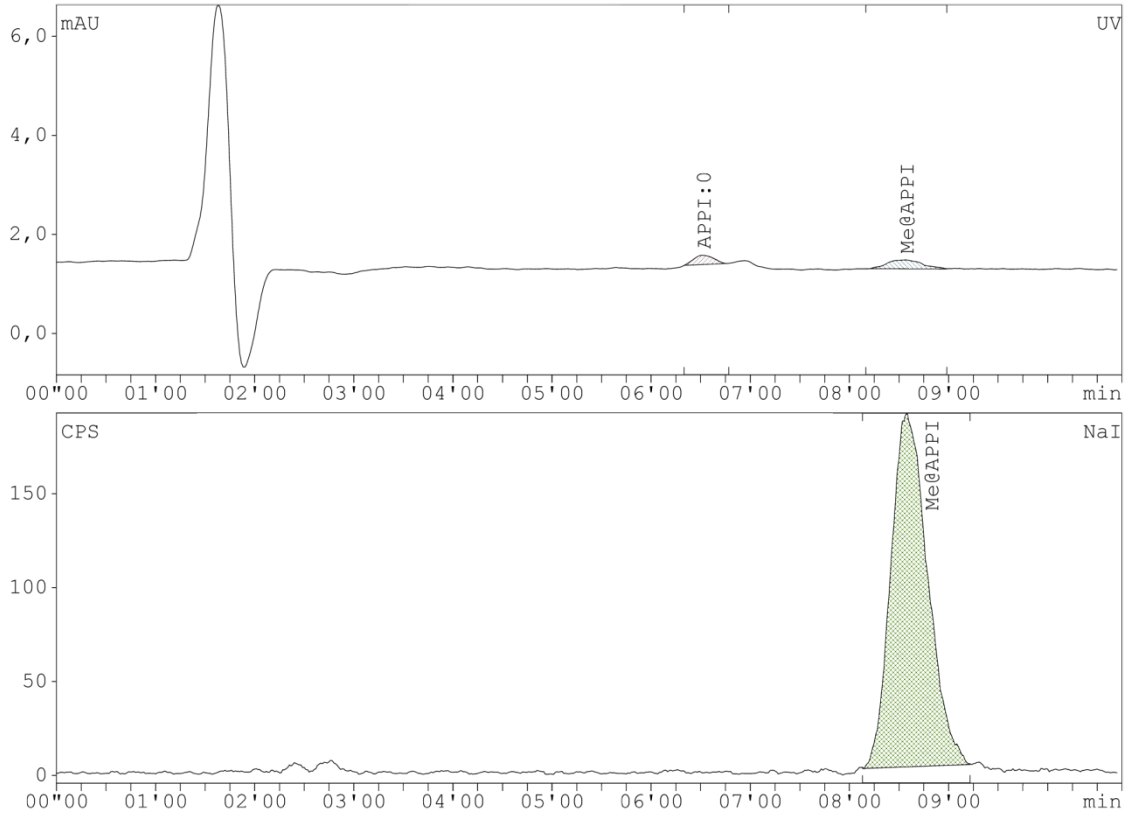

FIGURE 7 Analytical HPLC chromatogram

3.1.3 Manuscript #2

[^{18}F]FMENER-D2 : RELIABLE FULLY-AUTOMATED SYNTHESIS FOR VISUALIZATION OF THE NOREPINEPHRINE TRANSPORTER

Nucl. Med. Biol., 2013, 40, 8, 1049-1054.

Rami-Mark, Christina [1,2]; Zhang, Ming-Rong[3]; Mitterhauser, Markus [1,4]; Lanzenberger, Rupert[5]; Wadsak, Wolfgang [1,2]

1 Radiochemistry and Biomarker Development Unit, Department of Nuclear Medicine, Medical University of Vienna, A-1090 Vienna, Austria

2 Department of Inorganic Chemistry, University of Vienna, Austria

3 Molecular Imaging Center, National Institute of Radiological Sciences, Chiba, Japan

4 Hospital Pharmacy of the General Hospital of Vienna, Austria

5 Department of Psychiatry and Psychotherapy, Medical University of Vienna, Austria

Short title: [^{18}F]FMeNER-D2: automated synthesis

Keywords: norepinephrine transporter, PET, radiosynthesis, fluorine-18, FMeNER, FMeNER-D2, automation

Manuscript category: ARTICLE

** Corresponding author:*

Prof. Dr. Wolfgang Wadsak

Medical University of Vienna - Department of Nuclear Medicine

Radiochemistry and Biomarker Development Unit

Waehringer Guertel 18-20

A-1090 Vienna - Austria

Tel.: +43 1 40400 5255

Fax: +43 1 40400 1559

E-mail address: wolfgang.wadsak@meduniwien.ac.at

Nucl Med Biol [IF: 2.408]

Abstract

Purpose: In neurodegenerative diseases and neuropsychiatric disorders dysregulation of the norepinephrine transporter (NET) has been reported. For visualization of NET availability and occupancy in the human brain PET imaging can be used. Therefore, selective NET-PET tracers with high affinity are required. Amongst these, [^{18}F]FMeNER-D2 is showing best results so far. Furthermore, a reliable fully automated radiosynthesis is a prerequisite for successful application of PET-tracers.

The aim of this work was the automation of [^{18}F]FMeNER-D2 radiolabelling for subsequent clinical use. The presented study comprises 25 automated large-scale syntheses, which were directly applied to healthy volunteers and adult patients suffering from attention deficit hyperactivity disorder (ADHD).

Procedures: Synthesis of [^{18}F]FMeNER-D2 was automated within a Nuclear Interface Module. Starting from 20-30 GBq [^{18}F]fluoride, azeotropic drying, reaction with Br_2CD_2, distillation of 1-bromo-2-[^{18}F]fluoromethane-D2 ([^{18}F]BFM) and reaction of the pure [^{18}F]BFM with unprotected precursor NER was optimized and completely automated. HPLC purification and SPE procedure were completed, formulation and sterile filtration were achieved on-line and full quality control was performed.

Results: Purified product was obtained in a fully automated synthesis in clinical scale allowing maximum radiation safety and routine production under GMP-like manner. So far, more than 25 fully automated syntheses were successfully performed, yielding 1.0-2.5 GBq of formulated [^{18}F]FMeNER-D2 with specific activities between 430-1707 GBq/µmol within 95 min total preparation time.

Conclusions: A first fully automated [^{18}F]FMeNER-D2 synthesis was established, allowing routine production of this NET-PET tracer under maximum radiation safety and standardization.

Introduction:

The norepinephrine transporter (NET) is one of the major targets in neuropsychiatric and neurodegenerative diseases like attention deficit hyperactivity disorder (ADHD), depression, Alzheimer's disease (AD), Parkinson's disease (PD) and substance abuse [1]. For treatment of these diseases, selective norepinephrine (NE) reuptake inhibitors (SNRI) are commonly used, which are typically based on reboxetine. The NET itself facilitates the synaptic reuptake of NE from the synaptic cleft at the presynaptical terminals. Blocking of this transporter prolongs the NE action in the synapse, due to an increase in the concentration of NE in the cleft. Perturbation of the noradrenergic system (and the NET-expression) has been reported to trigger many neuropsychiatric disorders and neurodegenerative diseases. Especially, in the locus coeruleus (LC) a reduction of NET levels has been shown in major depression, AD and PD.[1-3] Furthermore, also in ADHD a dysregulation of the NE system was reported.[2]

For gaining insight in NET availability and dynamics in both healthy and diseased human brains, a non-invasive molecular imaging protocol has been developed using positron emission tomography (PET). Thus, specific and selective NET-PET radioligands are needed. One of the major prerequisites on these candidate tracers is their affinity towards NET, especially when considering the very low density of NET in cerebellum, striatum and human insular cortex.[3-8] Visualization of NET-rich regions like LC, where NET density is 4-8-fold higher, can be also achieved using ligands with slightly lower affinity.[4, 7, 9] Besides, affinity of the candidate ligands correlates with their binding kinetics, i.e. longer equilibration times for high-affinity substances (e.g. [^{125}I]iodo-nisoxetine (Ki=0.7 nM) reaches its binding equilibrium 3 h post injection).[10, 11] Moreover, selectivity of the tracers towards NET is required for feasible NET-PET imaging, since NET displays a high similarity to dopamine transporter (DAT) and serotonin transporter (SERT), but shows a significantly lower density in the human brain.[5, 12, 13]

Most described NET-PET tracers used in clinical studies are derived from reboxetine as known NET-selective compound. Both ^{11}C-methylated and ^{18}F-fluoroethylated tracers were proposed.[9, 14-20] Thereof, [^{18}F]FMeNER-D2 ((*S,S*)-2-(α-(2-[^{18}F]fluoro[$^{2}H_2$]methoxyphenoxy) benzyl)morpholine) is so far displaying best properties regarding affinity, selectivity and stability. [^{18}F]FMeNER-D2 was developed at the Karolinska Institute (Sweden) in 2004 by Schou and co-workers (figure 1).[21-23]

Major drawbacks of this NET-PET tracer were the complexity of the radiosynthesis and lack of an automated preparation sequence. Thus the aim of this work was the set-up of a reliable automated production of [^{18}F]FMeNER-D2 allowing for human NET-PET studies. With this computer-controlled fully-automated synthesis, more than 25 patients were injected with the so-produced [^{18}F]FMeNER-D2 at a dose of 4.7 MBq/kg body weight and, so far, subsequent NET PET scans were successfully acquired.

Materials and Methods:

Materials

Precursor (*S,S*)-NER (=(*S,S*)-norethyl-reboxetine, =(2*S,*□□*S*)-2-[□(2-hydroxyphenoxy) benzyl]morpholine) and reference standard (*S,S*)-FMeNER-D2*TFA ((*S,S*)-2-[a-(2-(dideutero fluoromethoxy)phenoxy)benzyl]morpholine trifluoroacetate) were obtained from PharmaSynth AS (Tartu, Estonia).

Acetonitrile (ACN for synthesis of DNA, ≥99.9% (GC) and ACN HPLC grade), dimethylformamide (DMF,

p.a, dried over molecular sieves (4 Å)), dibromomethane-d2 (99 atom% D, copper stabilized), sodium hydroxide, methanol (MeOH, CHROMASOLV®, for HPLC, ≥99.9%), ammonium formate, Kryptofix K2.2.2 (4,7,13,16,21,24-hexaoxa-1,10-diazabicyclo[8.8.8]hexacosane) and ethanol (absolute) were purchased from Sigma-Aldrich (Vienna, Austria). Anion-exchange cartridges (PS-HCO_3) for [^{18}F]fluoride fixation were purchased from Macherey-Nagel (Dueren, Germany). Sterile water was purchased from Meditrade Medicare Medizinprodukte (Kufstein, Austria). Phosphate buffer (125 mM) was prepared by dissolving 0.224 g sodium dihydrogenphosphate-monohydrate and 1.935 g disodiumhydrogenphosphate-dihydrate (both from Merck, Darmstadt, Germany) in 100 mL sterile water. For solid phase extraction C18 plus SepPak® cartridges and Silica plus long SepPak® cartridges were purchased from Waters (Waters® Associates Milford, USA). For formulation of the product 0.9% saline solution from B. Braun (Melsungen, Germany), 3% saline solution (Landesapotheke Salzburg, Austria) and 125 mM Phosphate buffer) were used. Low-protein binding Millex® GS 0.22 µm sterile filters were obtained from Millipore (Bedford, USA). All other chemicals and solvents for the syntheses and radiosyntheses were obtained from Merck (Darmstadt, Germany) and Sigma-Aldrich with at least analytical grade and used without further purification.

Instrumentation

[^{18}F]Fluoride was produced within a GE PETtrace cyclotron via ^{18}O(p,n)^{18}F reaction (16.5-MeV protons; GE Medical Systems, Uppsala, Sweden). $H_2{}^{18}O$ (HYOX18; > 98%) was obtained from Rotem Europe (Leipzig, Germany).

Evaluation of reaction conditions was performed manually in a lead-shielded hood with small quantities of initial radioactivity (<1 GBq). After optimization, [^{18}F]FMeNER-D2 synthesis was automated within a Nuclear Interface synthesizer (GE Healthcare, Sweden), remotely controlled by a standard laptop with dedicated processing software (figure 3).

Purification of [^{18}F]FMeNER was performed by semi-preparative reversed phase HPLC using the built-in semi-preparative HPLC system equipped with a radioactivity-, a UV-detector (Linear Instruments Model 200 Detector UV/VIS) and a LaPrep HPLC pump (VWR International, Radnor, USA). A Phenomenex® Gemini, C-18 column with TMS endcapping, 10 µm, 250x10 mm (Phenomenex®, Aschaffenburg, Germany) and a mobile phase of MeOH/0.1 M ammonium formate (AMF) in water 50/50v/v% at a flow rate of 12 mL/min was used for purification.

Analytical HPLC was performed on Merck-Hitachi LaChrom HPLC system (L-7100 pump; LaChrom L-7400 UV detector at 254 nm) and a NaI radio-detector (Bertholdt Technologies, Bad Wildbach, Germany) using Raytest software (Raytest, Straubenhardt, Germany). A Phenomenex Prodigy Phenyl-PH3 column; 250x4.6 mm, 5 µm (Phenomenex®, Aschaffenburg, Germany) and a mobile phase consisting of ACN/0.1M AMF in water 50/50 %v/v at a flow rate of 2 mL/min was used. The osmolality was measured with a Wescor osmometer Vapro® 5600 (Sanova Medical Systems, Vienna, Austria) and pH was measured using a WTW inoLab 740 pH meter (WTW, Weilheim, Germany). GC-Analysis was performed with a Bruker Gas Chromatography System 430-GC. Radio-TLC Analysis was performed using silica gel 60 RP-18 $F_{254}S$ plates from Merck (Darmstadt, Germany) with a mobile phase consisting of ACN/water 70/30 %v/v. Analyses of radio-TLC plates were done using a Canberra-Packard Instant Imager (Perkin Elmer, Watford, UK).

PET scans were performed in the Department of Nuclear Medicine, Medical University Vienna, using a

GE Advance PET-scanner and kinetic model was done with PMOD 3.0 using a two compartment model.

Methods:

Preparation of 1-bromo-2-[^{18}F]fluoromethane-d2 ([^{18}F]BFM)

In figure 2 the reaction scheme for the synthesis of [^{18}F]BFM and [^{18}F]FMeNER-D2 is outlined.

[^{18}F]Fluoride was produced within the cyclotron via ^{18}O(p,n)^{18}F reaction and trapped on an anion exchange cartridge (PS-HCO_3). It was eluted from the cartridge using 0.8 mL of solution containing (20 mg/mL, 53.2 µmol/mL) Kryptofix 2.2.2 and (4.5 mg/mL, 33.2 µmol/mL) K_2CO_3 in ACN/water 80/20% v/v. To test the influence of the quality of the water used on the specific activity 'trace select water' was compared with compared with 'aqua ad injectabilia'.

After complete evaporation, azeotropic drying was performed iteratively by twofold addition of 0.8 mL ACN. For optimization of [^{18}F]BFM synthesis, the dried fluoride was split and cooled to 20°C and 50 µL dibromomethane-d2 in 500 µL ACN, DMF or *o*-dichlorobenzene was added. The vessel was sealed tightly and the mixture heated (90°C, 100°C) for 5 minutes. The crude solution containing [^{18}F]fluoride, dibromomethane-d2 and [^{18}F]BFM was cooled to RT and distilled under different conditions for optimization purpose: a smooth He stream (10 ml/min, 30 mL/min and 40 mL/min) was applied over *(a)* an empty, sealed 2 mL glass vial; *(b)* 2 omnifit cartridges filled with silica in sequence; and *(c)* 4 silica plus SepPak® cartridges linked in series. The volatile [^{18}F]BFM was trapped in a second vessel containing 400 µL DMF (at RT or cooled at -20°C in advance). The chemical and radiochemical purity of the product was assessed by analytical HPLC. The [^{18}F]BFM solution was directly used for the next step of synthesis.

Synthesis of [^{18}F]FMeNER-D2

Synthesis was performed according to Schou et al.[22] Precursor NER (1 mg; 3.5 nmol) was dissolved in 200 µL DMF and 6 µL of aqueous 5 M NaOH were added. After addition of 400 µL of the freshly produced [^{18}F]BFM in DMF, the reaction vessel was sealed and the mixture heated to 90°C for 5 minutes. The crude reaction mixture was analyzed by analytical HPLC and TLC.

Automation of radiosynthesis

Automation of synthesis was done within a Nuclear Interface module using the optimized conditions.

[^{18}F]Fluoride (20-30 GBq) was transferred into a lead shielded hot cell and connected to the V55 target water line (figure 3). [^{18}F]F^- was sucked over the anion exchange cartridge using a vacuum pump (**V55 →a, V56 →a, V19, V20, V21→b**, vacuum pump) and the ^{18}O enriched water recovered. [^{18}F]Fluoride was eluted from the PS-HCO3 cartridge into the **reactor 1** by priming (via **V55→b, V56→b, V8, V18, V20→b, V21** and vacuum pump) of 0.8 mL elution solution containing K 2.2.2 and potassium carbonate in ACN/ trace select water 80/20). Then, [^{18}F]fluoride was azeotropically dried by heating to 100°C for 5 min. Drying was completed by elevation of temperature to 120°C for 2 min. Then, the vessel was cooled to 40°C and 0.8 mL ACN were added over the same lines as the elution solution. After drying, another portion of ACN was added from **vial 1** (using Helium from **V22**) and evaporated to complete dryness. The thoroughly dried fluoride was cooled to 20°C and dibromomethane-d2 (50 µL) in 500 µL ACN was added via **vial 2**. The vessel was sealed tightly and the mixture heated to 100°C for 5 minutes. After cooling **reactor 1** to 28°C, the second reactor containing 400 µL DMF was cooled to -20°C. Purification by distillation was performed over 4 silica plus SepPak® cartridges using a smooth He stream (1 min with 10 mL/min; then 40 mL/min for 10-15 min) and the pure [^{18}F]BFM trapped in **reactor 2** (by bubbling

inside the DMF through a peek tubing (**V52**)). After a plateau of activity in the second reactor was reached, distillation was stopped and precursor NER (1 mg in 200 µL DMF + 6 µL 5 M NaOH) was transferred into **reactor 2** via **vial 3**. The reaction mixture was sealed and alkylation was performed for 5 min at 90°C. The reaction was cooled to RT and quenched by addition of 1 mL water (**vial 7**). The crude product solution was transferred to the prep HPLC injection loop and automatically injected onto the column (Phenomenex Gemini, MeOH/ 0.1 M AMF 50/50% v/v; 12 mL flow rate) using a fluid detector. The product fraction was cut into a 100 mL bulb and diluted with 80 mL water. After removal of solvents by reversed-phase SPE (C-18 plus SepPak) [24], the product was washed with 10 mL water (**vial 6**) and eluted with 1.5 mL EtOH (**vial 5**) into the product collection vessel containing 4 mL 0.9% saline, 1 mL 125 mM phosphate buffer (pH 7.4) and 1 mL 3% saline. The tubings were washed with another 5 mL saline (**vial 4**) and the formulated product was passed over a 0.22 µm sterile filter into an evacuated sterile vial containing a further 5 mL 0.9% saline. Final volume was 17.5 mL, containing 8.5% ethanol. Purified [^{18}F]FMeNER-D2 was analyzed by analytical HPLC, GC and TLC; pH and osmolality were measured and a y-spectrum was recorded. Testing for endotoxins and sterility was performed retrospectively. Total quality control was performed according to the guidelines presented in the European Pharmacopoeia and using routine procedures at the PET Centre of the Vienna General Hospital, Medical University of Vienna. Specific radioactivity was assessed by quantification of the non-radioactive product (HPLC UV channel at 254 nm) and determination of overall radiochemical yield (GBq at end of synthesis).

Results:

Preparation of 1-bromo-2-[^{18}F]fluoromethane-d2 ([^{18}F]BFM)

Small scale reactions evinced that reaction of [^{18}F]fluoride with dibromomethane-d2 was highly dependent on the solvent used. Using DMF as solvent did only result in 5-25% [^{18}F]BFM, even at elevated temperatures (90-150°C) only 75-95% of [^{18}F]fluoride were recovered. Nucleophilic substitution in o-DCB at 100°C, commonly used for synthesis of 1-bromo2-[^{18}F]fluoroethane [25-27], evinced 52±5% radiochemical incorporation. Interestingly, a second radioactive byproduct was formed, eluting from the HPLC at almost the same retention time as the later formed [^{18}F]FMeNER-D2. Synthesis of [^{18}F]BFM in ACN for 5 min at 100°C showed best results; 56±4% radiochemical incorporation was found without by-product formation.

Purification of the crude [^{18}F]BFM is mandatory, and was performed by distillation. For the removal of ACN and dibromomethane-d2 three different approaches were tested. At first, an empty 2 mL glass vial was linked in between the crude (**reactor 1**) and the DMF trap (**reactor 2**). Unfortunately, almost all of the product was retained within this trap, and only very small amounts of [^{18}F]BFM could be obtained in the DMF distillate. Also elevation of temperature from RT to 50°C did not result in much higher activity in the distillate; on the contrary, larger quantities of ACN were spilled into the product trap. Since it was crucial to remove ACN for the next reaction step, this set-up was discarded.
Next, two omnifit cartridges (3 mm/25 mm each) were filled with silica (80-100 mesh, each 300 mg) and secured with glass wool and frits. These were linked in series and inserted between the crude product vial and the DMF trap. Hereby, all ACN and dibromomethane was trapped on the columns, but also almost the entire product was retained on the column. The quantities of product within the DMF trap were too small for further reactions. Therefore, a third approach of purification was tried: linking 4 silica

plus SepPak® cartridges in series. Using this setup, the removal of ACN and dibromomethane-d2 could be achieved at RT, and also the amounts of trapped [^{18}F]BFM (>97% radiochemical purity) were sufficient for further syntheses. After 10-15 minutes, no further product was distilled using 40 mL/min He.

Synthesis of FMeNER-D2

The distilled [^{18}F]BFM (in 400 µL DMF) was reacted with 1 mg NER in 200 µL DMF and 6 µL 5 M NaOH yielding 95-99% radiochemical incorporation after 5 minutes at 90°C. For purification, a preparative HPLC assay was developed and allowed the separation of all compounds. The retention times were 1.62 min (k'=0) for [^{18}F]fluoride, 2.50 min (k'= 0.55) for precursor NER, 2.97 min (k'=0.84) for [^{18}F]BFM, 6.77 min (k'=3.19) for Br_2CD_2 and 8.83 min (k'=4.46) for [^{18}F]FMeNER-D2. Less than 5% of radioactive impurities were detected in all [^{18}F]FMeNER-D2 syntheses, so far. After dilution of the product fraction (8-9.5 min) with 80 mL water, SPE was performed using a C18 plus SepPak®. The product was formulated (8.5% EtOH), sterile filtered and analyzed by analytical HPLC. The retention times were 1.49 min (k'=0) for [^{18}F]fluoride, 3.03 min (k'=0.66) for [^{18}F]BFM, 3.62 min (k'=0.99) for Br_2CD_2, 4.03 min (k'=1.21) for precursor NER and 5.42 min (k'=1.98) for product [^{18}F]FMeNER-D2, respectively. In figure 4, exemplary HPLC chromatograms (both preparative and analytical) are shown.

Automation of synthesis

Fully automation of [^{18}F]FMeNER-D2 synthesis was achieved successfully. [^{18}F]Fluoride fixation, azeotropic drying and reaction with Br_2CD_2 were performed with high yields and purity. Automation of distillation of [^{18}F]BFM remained the crucial step within the synthesis, where the major loss of activity occurred. About half of the formed [^{18}F]BFM was found to be retained on the Silica plus cartridges when distilling with 40 mL/min He stream. However, amount of [^{18}F]BFM trapped using 40 mL/min was sufficient for the following reaction and purification. Increasing the flow to 50 mL/min and higher, did on the one hand result in higher activity trapped in the second reactor, but separation from dibromomethane-d2 and ACN could no longer be achieved quantitatively. Subsequently, almost quantitative conversion of [^{18}F]BFM to FMeNER-D2 was observed for the automated large scale preparations.

So far, more than 25 fully automated radiosyntheses have been performed, yielding 1.53 ± 0.6 GBq [^{18}F]FMeNER-D2 (12.0 ± 5.2%, not corrected for decay) within 100 minutes from the end of bombardment (for details see table 1). Specific radioactivities ranged from 430-1707 GBq/µmol. Radiochemical and chemical purity were always ≥ 98%, osmolality and pH were found to be in a physiological range. GC analysis evinced ACN <10 ppm and methanol <20 ppm for each batch. In TLC and analytical radio-HPLC presence of [^{18}F]fluoride and [^{18}F]BFE was quantified, and found to be <1%. For the ongoing clinical study, the product was injected directly after release (4.7 MBq/kg body weight) to healthy volunteers and ADHD patients. 120 min post injection, dynamic PET scans were performed for 60 min. In figure 5, exemplary NET distribution maps measured with PET and FMeNER-D2 in a health male subject are shown (for details, see figure`s legend).

Discussion

Since so far only [^{18}F]FMeNER-D2 is used as a feasible NET-PET tracer in clinical trials, an automated radiosynthesis is of great benefit in terms of routine availability, reproducibility and radiation safety.

For evaluation of optimum parameters, small scale experiments were performed. During the examinations, the purification step of [^{18}F]BFM turned out to be the chokepoint of the synthesis. Within the first experiments, it rapidly turned out that distillation at 70°C as described by Schou et al was not the method of choice. Thus, huge amounts of ACN were found to be present in the DMF trap even when very weak adjuvant gas flow was applied and no matter which trap was used (glass vial, Silca plus SepPak® and omnifit cartridges). The presence of ACN, even in trace amounts, seems to impede the reaction between NER and [^{18}F]BFM, possibly due to the insolubility of NER in ACN. Moreover, large quantities of Br_2CD_2 were found in the DMF trap as well, leading to cold side product formation (BrMeNER) with unknown, but expected high affinity towards NET. Therefore, a milder distillation procedure needed to be established, and was met when applying 28°C. This temperature seems to be high enough for the highly volatile synthon [^{18}F]BFM to be drawn by distillation, but low enough to prevent evaporation of Br_2CD_2 and ACN. Thereby an auxilary gas stream of 40 mL/min was found to be optimal. Best results were obtained when using 4 Silica plus SepPak® cartridges linked in series.

Upon complete separation of ACN from the pure [^{18}F]BFM solution, reaction with precursor NER yielded >95% radiochemical incorporation of [^{18}F]FMeNER-D2 in crude mixture. The purification of the product from [^{18}F]BFM and NER was performed quantitatively using the proposed preparative HPLC assay with a retention time of 8-9 min for [^{18}F]FMeNER-D2. After SPE (using a C18 plus SepPak), pure [^{18}F]FMeNER-D2 was eluted almost quantitatively from the cartridge, hence only 0.5-2% of the pure product were bound irreversibly. Satisfying amounts of product were achieved after formulation and sterile filtration. Strict radiopharmaceutical quality control was passed for all synthesized batches allowing for preclinical testing and *in-vivo* applications. Analytical HPLC evinced high specific acitivities (SA) for all lots of [^{18}F]FMeNER-D2 produced. High variation (430-1707 GBq/µmol) in SA was observed but can be explained likewise: The amount of non-radioactive FMeNER-D2 present in the product was so small that it was below the limit of detection. Therefore, the SA was only dependent on the product yield. Hence, the given values represented the lower limits in achieved SA, leading to the observed variances.

Furthermore, we examined the influence of the quality of water used for the fluoride elution solution in preliminary tests. We compared elution solution with ‘aqua ad injectabilia’, commonly used for other tracer preparations, with the one made with ‘trace select water’. Specific activitiy was found to be much lower (139.9 ± 69 GBq/µmol; range: 57.8-231 GBq/µmol, n≥8) for ‘aqua ad inj.’ as compared to the experiments with elution solutions containing ‘trace select water’ (SA=598.9 ± 352 GBq/µmol; range: 432.7-1707 GBq/µmol n≥15).

Conclusion

Automation of [^{18}F]FMeNER-D2 synthesis was set-up successfully, enabling a reliable and routine preparation of this NET-PET tracer for clinical use. More than 25 fully automated syntheses were performed yielding 1.53 ± 0.6 GBq [^{18}F]FMeNER-D2 with high purity and excellent specific radioactivites ready to use for animal or human application. Enhancing the routine availability of [^{18}F]FMeNER-D2 will lead to an increased interest in clinical trials regarding the norepinephrine transporter using PET.

Acknowledgements

We thank Markus Savli,PhD and Andreas Hahn,PhD for analyzing the PET data and providing figure 5.

REFERENCES:

[1] Zhou J. Norepinephrine transporter inhibitors and their therapeutic potential. Drugs Future 2004;29:1235–44.

[2] Curatolo P, D'Agati E, and Moavero R. The neurobiological basis of ADHD. Italian Journal of Pediatrics 2010;36:79.

[3] Mash DC, Ouyang Q, Qin Y, and Pablo J. Norepinephrine transporter immunoblotting and radioligand binding in cocaine abusers. Journal of Neuroscience Methods 2005;143:79-85.

[4] Smith HR, Beveridge TJR, and Porrino LJ. Distribution of norepinephrine transporters in the non-human primate brain. Neuroscience 2006;138:703-14.

[5] Tejani-Butt SM. [3H]nisoxetine: a radioligand for quantitation of norepinephrine uptake sites by autoradiography or by homogenate binding. Journal of Pharmacology and Experimental Therapeutics 1992;260:427-36.

[6] Ordway GA, Stockmeier CA, Cason GW, and Klimek V. Pharmacology and Distribution of Norepinephrine Transporters in the Human Locus Coeruleus and Raphe Nuclei. The Journal of Neuroscience 1997;17:1710-9.

[7] Donnan GA, Kaczmarczyk SJ, Paxinos G, Chilco PJ, Kalnins RM, Woodhouse DG, et al. Distribution of catecholamine uptake sites in human brain as determined by quantitative [3H] mazindol autoradiography. The Journal of Comparative Neurology 1991;304:419-34.

[8] Bäckström IT and Marcusson JO. High- and Low-Affinity [³H]Desipramine-Binding Sites in Human Postmortem Brain Tissue. Neuropsychobiology 1990;23:68-73.

[9] Logan J, Wang G-j, Telang F, Fowler JS, Alexoff D, Zabroski J, et al. Imaging the norepinephrine transporter in humans with (S,S)-[11C]O-methyl reboxetine and PET: problems and progress. Nuclear Medicine and Biology 2007;34:667-79.

[10] Kung M-P, Choi S-R, Hou C, Zhuang Z-P, Foulon C, and Kung HF. Selective binding of 2-[125I]iodo-nisoxetine to norepinephrine transporters in the brain. Nuclear Medicine and Biology 2004;31:533-41.

[11] Halldin C, Farde L, Högberg T, Mohell N, Hall H, Suhara T, et al. Carbon-11-FLB 457: A Radioligand for Extrastriatal D2 Dopamine Receptors. Journal of Nuclear Medicine 1995;36:1275-81.

[12] Fowler JS, Volkow ND, Wang G-J, Gatley SJ, and Logan J. [11]Cocaine: PET studies of cocaine pharmacokinetics, dopamine transporter availability and dopamine transporter occupancy. Nuclear Medicine and Biology 2001;28:561-72.

[13] Pristupa ZB, Wilson JM, Hoffman BJ, Kish SJ, and Niznik HB. Pharmacological heterogeneity of the cloned and native human dopamine transporter: disassociation of [3H]WIN 35,428 and [3H]GBR 12,935 binding. Molecular Pharmacology 1994;45:125-35.

[14] Ding Y-S, Lin K-S, Logan J, Benveniste H, and Carter P. Comparative evaluation of positron emission tomography radiotracers for imaging the norepinephrine transporter: (S,S) and (R,R) enantiomers of reboxetine analogs ([11C]methylreboxetine, 3-Cl-[11C]methylreboxetine and [18F]fluororeboxetine), (R)-[11C]nisoxetine, [11C]oxaprotiline and [11C]lortalamine. Journal of Neurochemistry 2005;94:337-51.

[15] Ding Y-S, Lin K-S, Garza V, Carter P, Alexoff D, Logan J, et al. Evaluation of a new norepinephrine transporter PET ligand in baboons, both in brain and peripheral organs. Synapse

2003;50:345-52.
[16] Ding Y-S, Singhal T, Planeta-Wilson B, Gallezot J-D, Nabulsi N, Labaree D, et al. PET imaging of the effects of age and cocaine on the norepinephrine transporter in the human brain using (S,S)-[11C]O-methylreboxetine and HRRT. Synapse 2010;64:30-8.
[17] Lin K-S and Ding Y-S. Synthesis and C-11 labeling of three potent norepinephrine transporter selective ligands ((R)-nisoxetine, lortalamine, and oxaprotiline) for comparative PET studies in baboons. Bioorganic & Medicinal Chemistry 2005;13:4658-66.
[18] Lin K-S, Ding Y-S, Kim S-W, and Kil K-E. Synthesis, enantiomeric resolution, F-18 labeling and biodistribution of reboxetine analogs: promising radioligands for imaging the norepinephrine transporter with positron emission tomography. Nuclear Medicine and Biology 2005;32:415-22.
[19] Wilson AA, Patrick Johnson D, Mozley D, Hussey D, Ginovart N, Nobrega J, et al. Synthesis and *in vivo* evaluation of novel radiotracers for the *in vivo* imaging of the norepinephrine transporter. Nuclear Medicine and Biology 2003;30:85-92.
[20] Nguyen VL, Pichika R, Bhakta PH, Kant R, and Mukherjee J. (R)-N-Methyl-3-(3′-[18F]fluoropropyl)phenoxy-3- phenylpropanamine (18F-MFP3) as a potential PET imaging agent for norepinephrine transporter. Journal of Labelled Compounds and Radiopharmaceuticals 2010;53:172-7.
[21] Schou M, Halldin C, Sóvágó J, Pike VW, Hall H, Gulyás B, et al. PET evaluation of novel radiofluorinated reboxetine analogs as norepinephrine transporter probes in the monkey brain. Synapse 2004;53:57-67.
[22] Schou M, Halldin C, Pike VW, Mozley PD, Dobson D, Innis RB, et al. Post-mortem human brain autoradiography of the norepinephrine transporter using (S,S)-[18F]FMeNER-D2. European Neuropsychopharmacology 2005;15:517-20.
[23] Gulyás B, Brockschnieder D, Nag S, Pavlova E, Kása P, Beliczai Z, et al. The norepinephrine transporter (NET) radioligand (S,S)-[18F]FMeNER-D2 shows significant decreases in NET density in the human brain in Alzheimer's disease: A post-mortem autoradiographic study. Neurochemistry International 2010;56:789-98.
[24] Lemaire C, Plenevaux A, Aerts J, Del Fiore G, Brihaye C, Le Bars D, et al. Solid phase extraction—an alternative to the use of rotary evaporators for solvent removal in the rapid formulation of PET radiopharmaceuticals. Journal of Labelled Compounds and Radiopharmaceuticals 1999;42:63-75.
[25] Gomzina NA, Vasil'ev DA, and Krasikova RN. Use of 2-[18F]fluoroethyl bromide in synthesis of O-(2'-[18F]fluoroethyl)-L-tyrosine, a radiotracer for PET diagnostics of brain tumors. Radiochemistry (N. Y., NY, U. S.) 2007;49:299-304.
[26] Murali D, Vandehey N, Christian B, Nickles J, Houser E, Converse A, et al. An efficient synthesis of F18-FECNT, a PET tracer for dopamine transporter. J NUCL MED MEETING ABSTRACTS 2008;49:288P-a-.
[27] Philippe C, Ungersboeck J, Schirmer E, Zdravkovic M, Nics L, Zeilinger M, et al. [18F]FE@SNAP—A new PET tracer for the melanin concentrating hormone receptor 1 (MCHR1): Microfluidic and vessel-based approaches. Bioorganic & Medicinal Chemistry 2012;20:5936-40.

TABLES:

n≥15	GBq	% of initial activity (corr. for decay)	Δt to start of synthesis [min]
[^{18}F]fluoride starting activity in reactor 1	25.2 ± 4.3	100	0
pure [^{18}F]BFM after distillation trapped in reactor 2	3.6 ± 1.1	23.6 ± 6.9	59 ± 4
residual after HPLC injection in reactor and loop waste	1.2 ± 0.3	7.7 ± 1.9	76 ± 1
[^{18}F]FMeNER-D2 final product yield	**1.53 ± 0.6**	12.0 ± 5.2	95 ± 6
Specific activity [GBq/µmol]	**598.8 ± 352** (range 432.7 – 1707.4)		

table 1: fully automated preparation of [^{18}F]FMeNER-D2 :
Yields, loss of radioactivity and required time.

FIGURES:

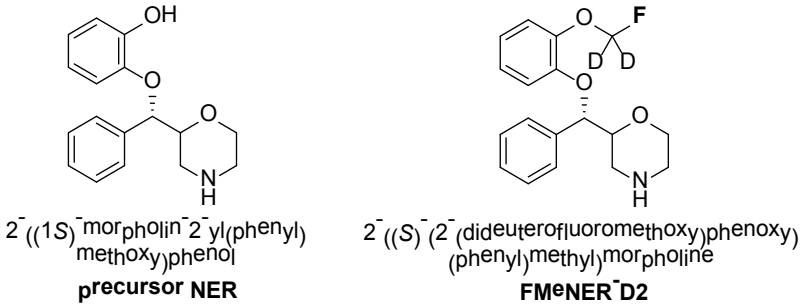

2-((1S)-morpholin-2-yl(phenyl)methoxy)phenol
precursor NER

2-((S)-(2-(dideuterofluoromethoxy)phenoxy)(phenyl)methyl)morpholine
FMeNER-D2

figure 1: structures of NER and FMeNER-D2

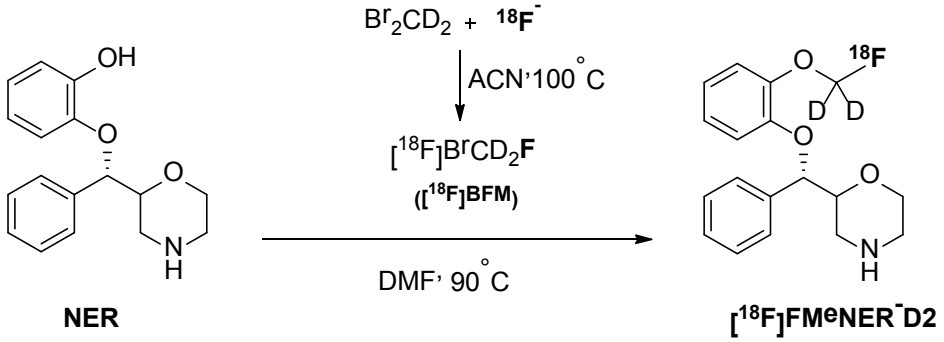

NER

[^{18}F]FMeNER-D2

figure 2: reaction scheme for [^{18}F]FMeNER-D2

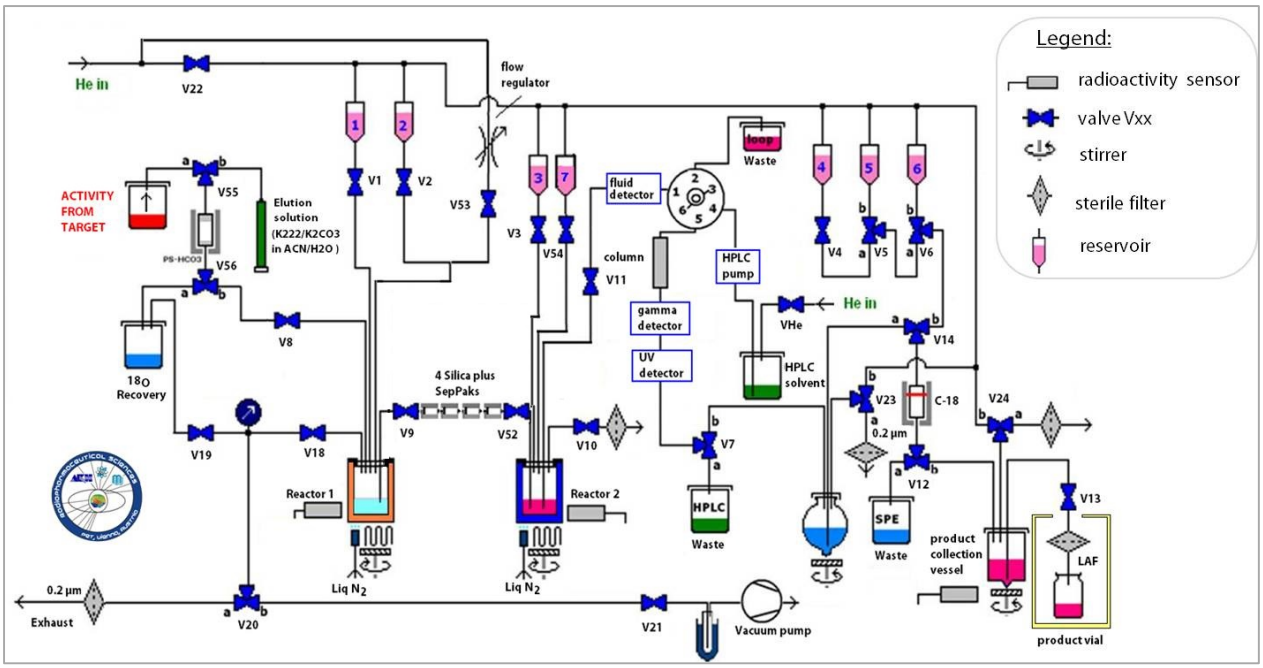

figure 3: set-up of the automated process of [^{18}F]FMeNER-D2 synthesis

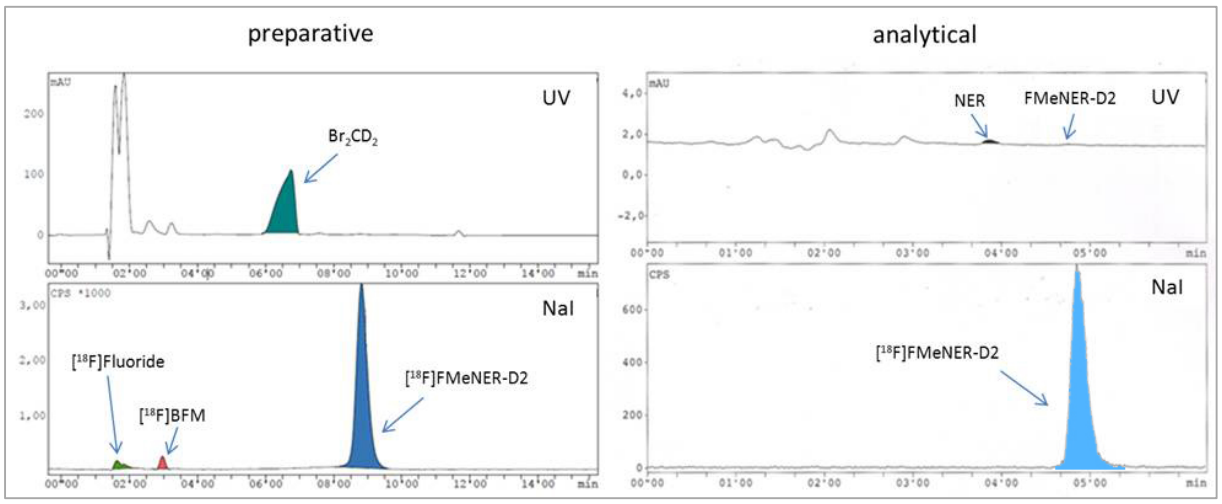

figure 4: preparative and analytical HPLC chromatogram of [^{18}F]FMeNER-D2

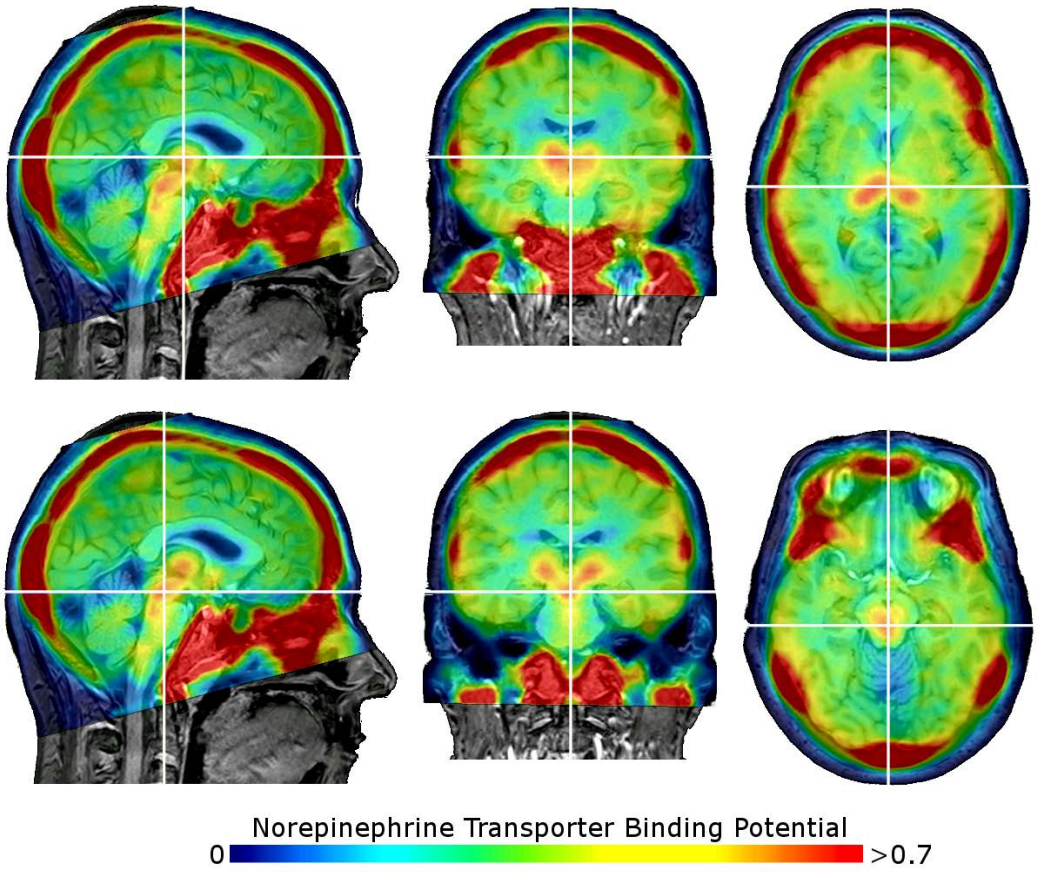

figure 5: parametric voxel-wise binding potential (BP_{ND}) maps of the norepinephrine transporter superimposed on structural magnetic resonance images in a healthy subject (male, age 21 years) using [^{18}F]FMeNER-D_2. The white cross in the triplanar view indicates the thalamus (upper column) and the locus coeruleus (lower column), the colour bar indicates the norepinephrine transporter binding potential. The BP_{ND} has been calculated using a 2-tissue compartment model with the caudate as reference region and the software PMOD 3.0. The injected dose was 416.6 MBq, the specific activity was 520.6 GBq/µmol (corrected for application time). Note also the high uptake in extracerebral areas.

FIGURE and TABLE CAPTIONS:

Tables:

table 1: Fully automated preparation of [^{18}F]FMeNER-D2: Yields, loss of radioactivity and required time.

Figures:

figure 1: structures of NER and FMeNER-D2

figure 2: reaction scheme for [^{18}F]FMeNER-D2

figure 3: set-up of the automated process of [^{18}F]FMeNER-D2 synthesis

figure 4: preparative and analytical HPLC chromatogram of FMeNER-D2

figure 5: parametric voxel-wise binding potential (BP_{ND}) maps of the norepinephrine transporter superimposed on structural magnetic resonance images in a healthy subject (male, age 21 years) using [^{18}F]FMeNER-D_2. The white cross in the triplanar view indicates the thalamus (upper column) and the locus coeruleus (lower column), the colour bar indicates the norepinephrine transporter binding potential. The BP_{ND} has been calculated using a 2-tissue compartment model with the caudate as reference region and the software PMOD 3.0. The injected dose was 416.6 MBq, the specific activity was 520.6 GBq/µmol (corrected for application time). Note also the high uptake in extracerebral areas.

3.1.4 Manuscript #3

THE NOREPINEPHRINE TRANSPORTER IN ATTENTION DEFICIT AND HYPERACTIVITY DISORDER INVESTIGATED WITH *(S,S)*-[^{18}F]FMENER-D_2

JAMA Psychiatry, 2014, 71, 1340-1349

Thomas Vanicek[1]*, Marie Spies[1]*, **Christina Rami-Mark**[2], Markus Savli[1], Anna Höflich[1], Georg S Kranz[1], Andreas Hahn[1], Alexandra Kutzelnigg[1], Tatjana Traub-Weidinger[2], Markus Mitterhauser[2], Wolfgang Wadsak[2], Marcus Hacker[2], Nora D. Volkow[3], Siegfried Kasper[1], Rupert Lanzenberger[1]**

[1]Department of Psychiatry and Psychotherapy, Medical University of Vienna, Austria
[2]Department of Biomedical Imaging and Image-guided Therapy, Division of Nuclear Medicine, Medical University of Vienna, Austria
[3]National Institute on Alcohol Abuse and Alcoholism (NIAAA), National Institutes of Health, Bethesda, MD, U.S.A.

** contributed equally*

JAMA Psychiatry [IF: 14.721]

Word count	
Main text	3570
#2 Tables, #3 Figures	

**Correspondence to: Assoc. Prof. Rupert Lanzenberger, MD
Department of Psychiatry and Psychotherapy
Functional, Molecular & Translational Neuroimaging Lab
Medical University of Vienna
Waehringer Guertel 18-20
1090 Vienna, Austria
Ph.: +43.1.40400.3576
Fax: +43.1.40400.3099
Email: rupert.lanzenberger@meduniwien.ac.at
Web: http://www.meduniwien.ac.at/neuroimaging/

Abstract

IMPORTANCE: ADHD research has long focused on dopaminergic contribution to pathophysiology, though results have been inconclusive. However, a case has been made fort the noradrenergic system, which has been associated with the modulation of cognitive processes such as arousal, working memory and response inhibition, all of which are typically affected in ADHD. Furthermore, the norepinephrine transporter (NET) is an important target for frequently prescribed medications in ADHD. Therefore, the NET is suggested to play a critical role in ADHD pathophysiology.

OBJECTIVE: To explore differences in NET binding potential (NET BP_{ND}) using positron emission tomography and the highly selective radio ligand *(S,S)*-[^{18}F]FMeNER-D_2 between adult ADHD patients and healthy subjects.

DESIGN; SETTING AND PARTICIPANTS: 22 medication-free ADHD patients (age: 30.7 ±10.1, mean ±SD, 15males) without psychiatric comorbidities and 22 age and sex matched healthy controls (HC; age: 30.9 ±10.4) underwent PET scanning once. A linear mixed model was used to compare NET BP_{ND} between groups.

INTERVENTION: Positron emission tomography.

MAIN OUTCOMES AND MEASURES: NET BP_{ND} in selected regions of interest (ROI) relevant for ADHD, including hippocampus, putamen, pallidum, thalamus, midbrain with pons (stating a ROI which includes the locus coeruleus) and cerebellum. In addition, NET BP_{ND} in thalamic sub-nuclei (13 atlas-based ROIs) was evaluated.

RESULTS: We show no differences in NET availability or regional distribution between ADHD patients and HC in all investigated brain regions ($F_{1,41}$<0.01, p=0.96). Further, we reveal no significant association between ADHD symptoms severity and regional NET availability. Neither sex nor smoking status influenced NET availability. Interestingly we show a significant negative correlation between NET availability and age (p>0.05, corrected), which corroborates prior findings of a decrease in NET availability with aging in the human brain.

CONCLUSION AND RELEVANCE: Our results do not find involvement of changes in brain NET availability or distribution in the pathogenesis of ADHD. However, the noradrenaergic transmitter system might be affected on a different level, such as cortical regions, which cannot be reliably quantified with this radioligand, or different key proteins of noradrenergic neurotransmission.

Introduction

Attention deficit hyperactivity disorder (ADHD), which is characterized by inattention, impulsivity and hyperactivity (1), affects up to 8-12% of children (2), persists into adulthood in approximately 30% of cases (3) and exhibits rising prevalence rates (4). ADHD is often associated with detrimental comorbidities (5-7), as well as with a large personal and social burden (7). As a result, a vast group of ADHD patients routinely undergoes psychopharmacologic treatment.

ADHD patients are commonly treated with methylphenidate (MPH) and amphetamine (AMPH), which are stimulant medications that enhance dopaminergic and noradrenergic signaling. Alternatively, atomoxetine (ATX), which is a non-stimulant drug that blocks the norepinephrine transporter (NET) thus effecting noradrenergic and, particularly in brain regions lacking the dopamine transporter (DAT), dopaminergic transmission (8, 9), is used. Treatment with MPH, AMPH and ATX is associated with improvement of clinical symptoms and performance in controlled tasks eliciting executive functions such as inhibitory control and of cognitive functions such as working memory and attention (10, 11).

While AMPH and MPH have been suggested to exert therapeutic efficacy via an increase in extracellular dopamine (DA) (12, 13), they have also been shown to modulate noradrenergic (NA) neurotransmission, which may also be therapeutically relevant (14, 15). MPH may dose-dependently block (NET), hereby regulating NA and DA reuptake (16, 17). Similarly, ATX has also been shown to facilitate therapeutic response by binding the NET (18). In addition, quetiapine, which is not applied as ADHD medication but has been shown to improve cognitive function in psychotic patients (19), was shown to bind to the NET (20). Ultimately, facilitation of therapeutic response by catecholamines in general and the NET in particular, suggests that these systems may be relevant to the pathophysiology of ADHD.

Further, ADHD symptomology has long been attributed to abnormalities within fronto-striatal and fronto-parietal networks implicated in executive functions (21) modulated by catecholaminergic systems (22, 23). The noradrenergic system, which originates in the locus coeruleus (LC) and exerts virtually ubiquitous influence within the brain, modulates, among other cortical regions, the prefrontal cortex through dynamic adaption of tonic- and phasic firing (24). In addition, studies displaying improvement of such symptoms by application of alpha-2 agonists further link noradrenergic influence on prefrontal cortex mediated cognitive functions to ADHD pathophysiology (25, 26).

More assertive investigation of underlying neurobiological pathophysiology is made possible through PET imaging studies, which have long focused on ADHD related changes in the dopaminergic system. While changes in DAT (27-29) and D2/D3-receptor levels and distribution (27, 30, 31) as well as DA release (27) have been investigated, results currently remain inconclusive. However, the proposition that MPH, AMPH and ATX may induce therapeutic response via NET modulation suggests that noradrenergic factors, and more specifically changes in NET, may play a role ADHD pathophysiology.

Therefore, we propose a thorough investigation of ADHD related NET distribution, as has been performed for the SERT and DAT. To address this issue, we used the recently developed NET-specific radio tracer *(S,S)*-[^{18}F]FMeNER-D$_2$, which has been successfully applied in healthy control subjects (32). To investigate the role of noradrenergic changes within ADHD pathophysiology, NET imaging was carried out in a regions of interest (ROI) approach focusing on brain areas integral to the noradrenergic system.

Methods

Subjects

22 adult ADHD patients (age: 30.7 ±10.1, mean ±SD, 15 males) and 22 age and sex matched healthy controls (HC) (age: 30.9 ±10.4, mean ±SD, 15 males; Table 1) were recruited through an ADHD outpatient clinic at the Department of Psychiatry and Psychotherapy, Medical University of Vienna and from the local community via advertisement, respectively. Patients were free from psychopharmacologic treatment for at least 6 months prior to the screening visit while HC were naïve to all psychopharmacologic treatment. Of the original 51 study participants, two were excluded due to substance abuse, two due to somatic disorders and three because of radiosynthesis difficulties. Written informed consent was obtained from all participants after detailed explanation of the study protocol and subjects received financial reimbursement for their participation. This study was approved by the Ethics Committee of the Medical University of Vienna and the General Hospital of Vienna (EK 552/2010).

Medical examination and clinical exploration

Subjects underwent standard medical examination including a general physical and neurological status, electrocardiography and routine laboratory tests at the screening- and final visit in order to ensure physical health. Female participants underwent a urine-pregnancy test at the screening visit and prior to PET measurement. A multidrug-urine test was performed at the screening visit in order to exclude current substance abuse. Participants were interviewed by experienced psychiatrists using Conners' Adult ADHD Diagnostic Interview for DSM IV (CAADID, Conners 1999) to evaluate current and childhood attentional and hyperactivity/impulsivity symptoms and to attest ADHD diagnosis. Conners Adult ADHD Rating Scale (Investigator- Screen Version; CAARS-Inv:SV; Table 1) was applied to assess presence and severity of ADHD, while third party- and self-report were acquired with Conners' Adult ADHD Rating Scale: Observer-Screen Version (CAARS-O:SV) and Conners' Adult ADHD Rating Scale: The self-report screening Version (CAARS-S:SV). Structured Clinical Interview for DSM IV Axis I and Axis II disorders (SCID-I, SCID-II) was performed to exclude comorbid psychiatric disorders. Handedness was evaluated with the Edinburgh Inventory (33, 34) and IQ with the Viennese Matrice Test-2 (WMT-2) (35). ADHD patients did not differ significantly from healthy controls in IQ (ADHD patients: 92.86 ±15.22; HC: 98.77 ±12.89; mean ±SD; $p>0.05$, t-test). Smoking status was recorded and subjects were subdivided into groups best describing their smoking status according to quantity of consumption (non-smokers, five cigarettes/week, five cigarettes/day, five to ten cigarettes/day, ten cigarettes/day, ten to 15 cigarettes/day, 15 cigarettes/day and 20 cigarettes/day; ranks 1-8, respectively). ADHD patients did not significantly differ in smoking status compared to healthy controls (ADHD patients: 0.00; healthy controls: 0.50; median; $Z=-0.481$, $p=0.630$; Mann-Whitney U Test). Subjects with PET- or MRI-incompatible implants or in pregnancy or breastfeeding were also excluded.

Data acquisition

All PET scans were carried out at the Department of Biomedical Imaging and Image-guided Therapy, Division of Nuclear Medicine, Medical University of Vienna using a full-ring scanner (General Electric Medical Systems, Milwaukee, WI, USA) in 3D acquisition mode. We applied *(S,S)*-[^{18}F]FMeNER-D$_2$, which is currently among the most suitable PET tracers for *in vivo* NET quantification (36, 37) as

prepared previously in detail (38) and for the following reasons, 1) Fluorine-18 labelled reboxetine analogues enable specific binding equilibrium to be reached within a reasonable time-frame for PET measurement, due to their five-fold higher half-life (39), 2) *in vivo* de-fluorination can be reduced considerably, and interpretability of bone near regions hereby increased, through the use of deuterated homologues (40) and lastly, 3) *(S,S)*-[^{18}F]FMeNER-D_2 shows both high affinity and selectivity to the NET (40). A 5min transmission scan using retractable ^{68}Ge rod sources for tissue attenuation correction was performed prior to the emission scan. Data acquisition started 120min after a bolus i.v. injection of 4.7 MBq/kg body weight (ADHD patients: 395.1±98.7 MBq, healthy controls: 379.0±62.2 MBq,; p>0.05) of *(S,S)*-[^{18}F]FMeNER-D_2. Mean specific radioactivity of *(S,S)*-[^{18}F]FMeNER-D_2 was 589.4±399.7 GBq/µmol (ADHD patients) and 440.4±233.7 GBq/µmol (healthy controls), (p>0.05, t-test). Brain radioactivity was measured in a series of 6 consecutive time frames lasting 10min each in the interval of 120 min. to 180 min. after bolus. Acquired data were reconstructed in volumes consisting of 35 transaxial sections (128x128 matrix) using an iterative filtered back-projection algorithm (FORE-ITER) with a spatial resolution of 4.36 mm. full-width at half maximum 1 cm. next to the center of the field of view. For coregistration, magnetic resonance (MR) images were acquired from all participants on a 3 Tesla (T) Philips scanner (Achieva) using a 3D T1 FFE weighted sequence, yielding 0.88 mm. slice thickness and inplane resolution of 0.8 x 0.8 mm.

Data quantification

Each time frame of the dynamic PET scan was realigned to the mean of frames with no head motion, identified by visual inspection. Subsequently, each summed image (PET integral image from realigned data) was coregistered (rigid body transformation) to each subject's MRI using a mutual information algorithm implemented in SPM8 (Wellcome Trust Centre for Neuroimaging, London, UK; http://www.fil.ion.ucl.ac.uk/spm/). Parametric images of binding potential non-displaceable (BP_{ND}) values were calculated using the caudate as the reference region because it was devoid of NET (39). According to nomenclature (41), the BP_{ND} were defined as (32):

$$BP_{ND} = \frac{\int_{120}^{180} C_{target}}{\int_{120}^{180} C_{reference}} - 1$$

Caudate ROIs were delineated on MR images in individual subject space by a neuro-anatomist using PMOD image analysis software, version 3.1 (PMOD Technologies Ltd, Zurich, Switzerland, www.pmod.com) which were subsequently transferred to coregistered summed PET images. Individual MRIs were spatially normalized to the T1-weighted MRI template provided in SPM. Resulting transformation matrices were applied to the coregistered parametric images warping them into MNI standard space.

Regions of Interests (ROIs)

ROIs selected included NET rich regions, based on post mortem and *in vivo* human brain studies (32, 39) and took good signal-to-noise-ratio and acceptable bone spill-over due to *(S,S)*-[^{18}F]FMeNER-D_2 defluorination into account (42). Binding potential values were extracted from parametric maps from either atlas based ROIs or manually delineated ROIs. Atlas generated ROIs were identified from the Hammers Maximum Probability Atlas (43) including six regions, namely the hippocampus, the putamen,

the pallidum, the thalamus, the midbrain with pons (stating a ROI which includes the LC), and the cerebellum. Since NET concentration in the thalamus is not homogenous (36), thirteen thalamic sub-nuclei were generated with the WFU Pickatlas Tool (listed in Tab. 2) (44). To verify atlas derived ROIs, four atlas ROIs were delineated on the MNI T1 single subject brain: midbrain (dorsally located including raphe nuclei, excluding pons), the LC located according to Keren et al. (45), the claustrum and the hypothalamus. As well as the above mentioned atlas ROIs, i.e. constant ROI dimension, the LC and thalamus, brain regions highest in NET concentration (36), were delineated manually for each subject for confirmatory purposes. Atlas ROIs match the MNI standard space.

Statistical analysis

Data were analysed using linear mixed models for the outcome measure NET BP_{ND} with ROI as repeated factor, subject groups, sex, and ROI as fixed factors and subjects and matched subject-pairs as random factors. A separate model was calculated for the six ROIs based on Hammers Maximum Probability Atlas and for the 13 thalamic sub-nuclei. Likewise, manually delineated ROIs were assessed in two further models, one using the four atlas based and one using the two individual-based ROIs. Fixed effects were included in the model in a multifactorial approach whereas interaction effects were dropped in case of non-significance. In case of significant interactions or main effects, post-hoc pairwise comparisons were computed and Bonferroni corrected for multiple comparisons. In a second exploratory approach to examine the effects of handedness, smoking status and age, a mixed model was calculated using a stepwise procedure with backward elimination, i.e., starting with all candidate variables (including subject groups and ROI) followed by a stepwise deletion of interactions and variables with largest p-values. Finally, mixed models using the same procedure were applied to investigate the effects of clinical variables CAARS-Inattentiveness and CAARS-Hyperactivity/ Impulsivity. According to Akaike's information criterion (46), repeated measurements were modelled using a compound symmetric covariance structure. As exploratory analysis we also compared the NET binding on the BP_{ND} images between patients and HC at the voxel level using SPM8 (paired t-test). SPSS version 19.0 for Windows was used for statistical computations. The 2-tailed significance level was set at 0.05. ROI and voxel-wise analysis results were corrected for multiple comparisons using Bonferroni and false discovery rate (FDR), respectively.

Results

Linear mixed models analysis revealed an expected main effect of ROI ($F_{5,215}$=117.71, p<0.001) but no main effects of subject group ($F_{1,41}$<0.01, p=0.96; Table 2; Fig. 1) or sex ($F_{1,41}$<0.01, p=0.98) and no interaction effects (all p>0.1). Post-hoc pairwise comparisons revealed significant NET BP_{ND} differences between the five tested brain regions (p<0.05, corrected) except for the comparisons of midbrain with pallidum and putamen with cerebellum, which had similar binding values (Table 2, Fig. 2). Analogous results were obtained from the two mixed models for the manually delineated ROIs, showing main effects of ROI, but no main effects of group and sex and no interaction effects. Similarly, the linear mixed model for NET binding within the thalamic sub-nuclei revealed a main effect of ROI ($F_{12,516}$=105.53, p<0.001), but no main effect of group ($F_{1,41}$=0.08, p=0.78) or sex ($F_{1,41}$=0.39, p=0.54) and no interaction effects (all p>0.1). There was also no significant difference in NET binding between ADHD patients and

HC in any brain region at the voxel level (p>0.05, corrected).

When investigating the potential effects of handedness, smoking status and age, mixed models analysis for ROI NET BP_{ND} based on Hammers Maximum Probability Atlas revealed an interaction effect between ROI and age ($F_{5,190}$=9.94, p<0.001), in addition to a main effect of ROI but no main effect of age. Post-hoc correlation analyses between regional NET BP_{ND} and age revealed strong negative correlations in the thalamus (r=-.54) and midbrain (r=-.42, p<0.05 corrected; Fig. 3) but these correlations did not differ between HC and ADHD patients. Handedness and smoking status had no effect on NET BP_{ND} or led to any significant interactions. Comparable results were observed for manually delineated ROIs, showing strong negative correlations between NET BP_{ND} and age in midbrain (r=-.53), LC (r=-.51) and hypothalamus (r=-.51, p<0.05 corrected). Additionally, no main or interaction effects were observed for clinical variables (CAARS-Inattentiveness, CAARS-Hyperactivity/Impulsivity) and ROI BP_{ND}. Finally, exclusion of three patients with previous MPH intake in childhood (intake duration was four, five and seven years) and two patients with previous ATX consumption in adulthood (intake duration was five and six months) did not change NET binding results. We further excluded two patients exhibiting predominantly inattentive symptoms and one exhibiting predominantly hyperactivity/impulsivity symptoms and, in a separate analysis, two patients with past drug abuse. Again, exclusion of these subjects did not significantly change results.

Discussion

This is the first PET study to investigate differences in brain NET distribution and availability in adults with ADHD. We show no significant differences in the BP_{ND} of *(S,S)*-[^{18}F]FMeNER-D_2 between ADHD patients and HC. Further, exclusion of patients exhibiting either predominantly inattentive or predominantly hyperactivity/impulsivity subtype and patients with previous ADHD pharmacotherapy or past drug abuse did not change results. We corroborate an age related decrease in brain NET availability in the healthy human brain (47) and extend it to also show a decrease in brain NET availability with age in adults with ADHD.

Randomized, placebo controlled studies have repeatedly shown that MPH, AMPH and ATX significantly decrease symptoms in adult ADHD patient cohorts (48-50). The clinical efficacy of a pharmaceutical implies that the mechanism of action through which it attains a response is relevant to the pathophysiology and resulting symptomology of a particular disease. Therefore, modulation of the noradrenergic system by ATX, AMPH and MPH suggests noradrenergic pathology in ADHD.

In addition, executive functions such as response inhibition, vigilance, working memory and planning are typically impaired in ADHD (51, 52). The association of these functions with the PFC, which exhibits pronounced noradrenergic innervation once again implicates, more generally, the noradrenergic system in ADHD (53).

However, investigations into the involvement of other neurotransmitter systems in ADHD are similarly inconclusive. Firstly, current data available on dopaminergic contribution to ADHD pathophysiology is wrought with inconsistency. As is the case with NET, therapeutic doses of MPH have been shown to reduce radiotracer striatal DAT binding in a dose dependent manner in HC subjects using PET (54, 55). MPH induced DAT blockade has been causally linked to an increase in striatal extracellular dopamine in the human brain (12), and this effect has been associated with therapeutic responses to MPH in

ADHD (56). Moreover, striatal DAT availability in ADHD patients was correlated with improvement of clinical symptoms after MPH treatment (57). Brain imaging studies, however, have reported an array of partially contradictory results ranging from DAT increases (29, 57-59), to a lack of change (60) to decreases (27, 61) in the brain of adults with ADHD (61). While methodological factors such as tracer choice and patient characteristics including presence of prior medication, comorbidities and differing sample sizes (27, 28) have been suggested to account for this variability in results, investigations of other components of the dopaminergic system, such as the D2 and D3 receptors are similarly inconsistent (27, 30). Additionally, serotonergic alterations have been discussed in the context of ADHD pathophysiology (62), primarily based on the relationship between serotonergic innervation and impulsivity and hyperactivity, two core ADHD symptoms (63). However, serotonergic involvement in ADHD is contradicted by data showing the limited clinical efficacy of SSRIs in the improvement of ADHD symptoms. Further, recent SERT imaging studies showed no difference in SERT distribution between ADHD patients and healthy controls (61, 64). Therefore, though existing evidence neither affirms, nor disproves the neurotransmitter systems discussed above to be involved in ADHD, background pharmacologic evidence supporting, in particular dopaminergic and noradrenergic, contribution is strong. Del Campo et al. have recently suggested that ADHD related dopaminergic changes may reflect associated symptoms, rather than a disease specific endophenotype (30). Therefore, other approaches, which step away from the concept of endophenotypical noradrenergic changes in ADHD and focus on changes associated with ADHD symptoms may prove valuable. However, the fact that exclusion of patients exhibiting predominantly inattentive subtype and predominantly hyperactivity/impulsivity subtype did not change our main findings strongly suggests that our results reflect a lack of changes in NET in ADHD in general, rather than a subtype-specific phenomenon. In this context, future studies may profit from incorporating cognitive tests and genetic data into analysis for further symptom oriented and phenotypical classification of subjects.

However, despite the well-established link between NET psychopharmacology and improvement of ADHD symptoms, supported by recent genetic studies implicating the NET gene in ADHD (65), our study did not reveal differences in NET distribution between ADHD patients and HC. Interestingly, ATX, MPH and AMPH modulation of the NET has yet to be investigated in ADHD patients. Therefore, one cannot exclude the possibility that pharmacologic mechanisms of stimulants and ATX in ADHD patients differ from those in HC, as has been proposed to be the case by some (66), though not by others (67). On the other hand, the result of this study may also be interpreted to suggest that, despite the proposed involvement in the efficacy of ADHD pharmaceuticals, the NET may not be integral to ADHD pathophysiology. Nevertheless, the missing difference in NET between groups would not necessarily exclude the involvement of other components of the noradrenergic system in ADHD. In fact, guanfacine, an α2-adrenoceptor agonist and novel ADHD treatment option shows efficacy comparable to that of stimulant treatment (68). While this finding does not necessarily imply that α2-adrenoceptors are integral to ADHD, it again underlines the link between noradrenergic innervation and ADHD symptomology while proposing that ADHD symptoms may also be modulated by other noradrenergic elements.

However, a variety of characteristics attributed to the NET limit PET investigations into its role in ADHD and therefore must be considered. Firstly, while cortical and subcortical regions express NET, levels of expression are generally considered to be low (32, 70, 71), particularly in frontal cortical regions.

Therefore, comparability between subject groups is limited in these regions. Further, evaluation of NET levels in lateral cortical regions, including frontal regions, is made challenging by skull bound radioactivity, which spills over into adjacent regions and has been associated with *(S,S)*-[^{18}F]FMeNER-D_2 (40, 42). Therefore, due to generally low frontal cortex NET levels, together with image contamination as a result of spill over from bone uptake, NET levels in lateral frontal cortical regions cannot be evaluated with *(S,S)*-[^{18}F]FMeNER-D_2. Thus, we cannot exclude the possibility of NET differences between ADHD patients and HC subjects in these regions.

Neuroanatomical traits intrinsic to the noradrenergic system further limit interpretability. On the one hand, partial volume effects resulting from the LC's small size together with current standards of PET spatial-resolution may result in an underestimation of NET levels within this region (32). Accordingly, autoradiography studies have shown LC NET values to be 10 times higher than those of other cortical and subcortical regions, including the thalamus (39), while our findings confirm recent PET studies applying *(S,S)*-[^{18}F]FMeNER-D_2, showing only slightly differences between the LC and thalamus (32, 36). These method-dependent differences speak for distortion of LC values through partial volume effects. In addition, we cannot exclude the possibility that similar effects may influence NET values measured in the small thalamic sub-nuclei evaluated.

In conclusion, the lack of differences in NET distribution between ADHD patients and HC we show does not necessarily exclude noradrenergic pathology in ADHD, as only one molecular and not all regional aspects of the noradrenergic system were investigated. To further clarify NET involvement in ADHD, cortical brain regions must be investigated while occupancy studies must be carried out to solidify the relationship between pharmacologically induced clinical improvement and noradrenergic changes.

Acknowledgements:

This research was supported by a grant from the Austrian Science Fund Grant (P22981) to R Lanzenberger. We thank Stamenkovic M, Klier C, Hackenberg B, Konstantinidis A, Baldinger P, Meshkat D, Losak J and Gößler R for medical support. Further we thank PET-Team, especially Karanikas G, Nics L, Häusler D, Philippe C for the technical support. For administrative support, we thank Gryglewski G, Cotton M, Unterholzer J, and Godbersen MG. Rupert Lanzenberger had full access to all of the data in the study and takes responsibility for the integrity of the data and the accuracy of the data analysis.

Conflict of interest:

Without any relevance to this work, S. Kasper declares that he has received grant/research support from Eli Lilly, Lundbeck A/S, Bristol-Myers Squibb, Servier, Sepracor, GlaxoSmithKline, Organon, Dr. Willmar Schwabe GmbH & Co. KG and has served as a consultant or on advisory boards for AstraZeneca, Austrian Sick Found, Bristol-Myers Squibb, German Research Foundation (DFG), GlaxoSmithKline, Eli Lily, Lundbeck A/S, Pfizer, Organon, Sepracor, Janssen, and Novartis, and has served on speakers' bureaus for AstraZeneca, Eli Lilly, Lundbeck A/S, Servier, Sepracor and Janssen. R. Lanzenberger has received travel grants and conference speaker honoraria from AstraZeneca, Lundbeck A/S and Roche Austria GmbH. T. Vanicek has received a travel grant from Sanova. M. Spies and G.S. Kranz received trave grants from Roche and AOP Orphan. M. Hacker has received conference speaker honoraria from Covidian, GE Healthcare, IBA and Endocyte and consults advisory boards of Endocyte. W. Wadsak has received research support from Rotem GmbH, ABX, Iason, Advion and Raytest Austria and has served as a consultant/trainer for Bayer and THP. A. Kutzelnigg has received travel grants from Eli Lilly and Company, Affiris AG, Novartis Pharmaceuticals Corporation, and AstraZeneca, payment for lectures including service on speakers' bureaus from Eli Lilly and Company, Novartis Pharmaceuticals Corporation, AstraZeneca and Affiris AG and has served as a consultant and on advisory boards for the Austrian Federal Ministry of Health, Eli Lilly and Company, Biogen-Idec and Medice Arzneimittel GmbH. The authors N.D.Volkow, M. Mitterhauser, C. Rami-Mark, M. Savli, A. Hahn, A. Höflich and T. Traub-Weidinger report no financial relationships with commercial interests.

References:

1. American Psychiatric Association, editor. Diagnostic and statistical manual of mental health disorders: DSM-5 (5th ed.). Washington, DC American Psychiatric Publishing.; 2013.
2. Biederman J, Faraone SV. Attention-deficit hyperactivity disorder. Lancet. 2005;366(9481):237-48.
3. Barbaresi WJ, Colligan RC, Weaver AL, Voigt RG, Killian JM, Katusic SK. Mortality, ADHD, and psychosocial adversity in adults with childhood ADHD: a prospective study. Pediatrics. 2013;131(4):637-44.
4. Getahun D, Jacobsen SJ, Fassett MJ, Chen W, Demissie K, Rhoads GG. Recent trends in childhood attention-deficit/hyperactivity disorder. JAMA Pediatr;167(3):282-8.
5. Goldman LS, Genel M, Bezman RJ, Slanetz PJ. Diagnosis and treatment of attention-deficit/hyperactivity disorder in children and adolescents. Council on Scientific Affairs, American Medical Association. JAMA. 1998;279(14):1100-7.
6. Mannuzza S, Klein RG, Bessler A, Malloy P, LaPadula M. Adult psychiatric status of hyperactive boys grown up. Am J Psychiatry. 1998;155(4):493-8.
7. Kessler RC, Adler L, Barkley R, Biederman J, Conners CK, Demler O, et al. The prevalence and correlates of adult ADHD in the United States: results from the National Comorbidity Survey Replication. Am J Psychiatry. 2006;163(4):716-23.
8. Bymaster FP, Katner JS, Nelson DL, Hemrick-Luecke SK, Threlkeld PG, Heiligenstein JH, et al. Atomoxetine increases extracellular levels of norepinephrine and dopamine in prefrontal cortex of rat: a potential mechanism for efficacy in attention deficit/hyperactivity disorder. Neuropsychopharmacology. 2002;27(5):699-711.
9. Carboni E, Silvagni A, Vacca C, Di Chiara G. Cumulative effect of norepinephrine and dopamine carrier blockade on extracellular dopamine increase in the nucleus accumbens shell, bed nucleus of stria terminalis and prefrontal cortex. J Neurochem. 2006;96(2):473-81.
10. Castells X, Ramos-Quiroga JA, Rigau D, Bosch R, Nogueira M, Vidal X, et al. Efficacy of methylphenidate for adults with attention-deficit hyperactivity disorder: a meta-regression analysis. CNS drugs. 2011;25(2):157-69.
11. Chamberlain SR, Hampshire A, Muller U, Rubia K, Del Campo N, Craig K, et al. Atomoxetine modulates right inferior frontal activation during inhibitory control: a pharmacological functional magnetic resonance imaging study. Biol Psychiatry. 2009;65(7):550-5.
12. Volkow ND, Wang G, Fowler JS, Logan J, Gerasimov M, Maynard L, et al. Therapeutic doses of oral methylphenidate significantly increase extracellular dopamine in the human brain. J Neurosci. 2001;21(2):RC121.
13. Volkow ND, Wang GJ, Fowler JS, Ding YS. Imaging the effects of methylphenidate on brain dopamine: new model on its therapeutic actions for attention-deficit/hyperactivity disorder. Biol Psychiatry. 2005;57(11):1410-5.
14. Del Campo N, Chamberlain SR, Sahakian BJ, Robbins TW. The roles of dopamine and noradrenaline in the pathophysiology and treatment of attention-deficit/hyperactivity disorder. Biol Psychiatry. 2011;69(12):e145-57.
15. Berridge CW, Devilbiss DM, Andrzejewski ME, Arnsten AF, Kelley AE, Schmeichel B, et al.

Methylphenidate preferentially increases catecholamine neurotransmission within the prefrontal cortex at low doses that enhance cognitive function. Biol Psychiatry. 2006;60(10):1111-20.

16. Hannestad J, Gallezot JD, Planeta-Wilson B, Lin SF, Williams WA, van Dyck CH, et al. Clinically relevant doses of methylphenidate significantly occupy norepinephrine transporters in humans *in vivo*. Biol Psychiatry.2010;68(9):854-60.
17. Valentini V, Frau R, Di Chiara G. Noradrenaline transporter blockers raise extracellular dopamine in medial prefrontal but not parietal and occipital cortex: differences with mianserin and clozapine. J Neurochem. 2004;88(4):917-27.
18. Logan J, Wang GJ, Telang F, Fowler JS, Alexoff D, Zabroski J, et al. Imaging the norepinephrine transporter in humans with *(S,S)*-[^{11}C]O-methyl reboxetine and PET: problems and progress. Nucl Med Biol. 2007;34(6):667-79.
19. Urben S, Baumann P, Barcellona S, Hafil M, Preuss U, Peter-Favre C, et al. Cognitive efficacy of quetiapine in early-onset first-episode psychosis: a 12-week open label trial. Psychiatr Q. 2012;83(3):311-24.
20. Nyberg S, Jucaite A, Takano A, Kagedal M, Cselenyi Z, Halldin C, et al. Norepinephrine transporter occupancy in the human brain after oral administration of quetiapine XR. Int J Neuropsychopharmacol. 2013;16(10):2235-44.
21. Dickstein SG, Bannon K, Castellanos FX, Milham MP. The neural correlates of attention deficit hyperactivity disorder: an ALE meta-analysis. J Child Psychol Psychiatry. 2006;47(10):1051-62.
22. Bush G. Attention-deficit/hyperactivity disorder and attention networks. Neuropsychopharmacology. 2010;35(1):278-300.
23. Brennan AR, Arnsten AF. Neuronal mechanisms underlying attention deficit hyperactivity disorder: the influence of arousal on prefrontal cortical function. Ann N Y Acad Sci. 2008;1129:236-45.
24. Berridge CW, Waterhouse BD. The locus coeruleus-noradrenergic system: modulation of behavioral state and state-dependent cognitive processes. Brain Res Brain Res Rev. 2003;42(1):33-84.
25. Sallee FR, McGough J, Wigal T, Donahue J, Lyne A, Biederman J. Guanfacine extended release in children and adolescents with attention-deficit/hyperactivity disorder: a placebo-controlled trial. J Am Acad Child Adolesc Psychiatry. 2009;48(2):155-65.
26. Gamo NJ, Wang M, Arnsten AF. Methylphenidate and atomoxetine enhance prefrontal function through alpha2-adrenergic and dopamine D1 receptors. J Am Acad Child Adolesc Psychiatry. 2010;49(10):1011-23.
27. Volkow ND, Wang GJ, Kollins SH, Wigal TL, Newcorn JH, Telang F, et al. Evaluating dopamine reward pathway in ADHD: clinical implications. JAMA. 2009;302(10):1084-91.
28. Volkow ND, Wang GJ, Newcorn J, Fowler JS, Telang F, Solanto MV, et al. Brain dopamine transporter levels in treatment and drug naive adults with ADHD. Neuroimage. 2007;34(3):1182-90.
29. Spencer TJ, Biederman J, Madras BK, Dougherty DD, Bonab AA, Livni E, et al. Further evidence of dopamine transporter dysregulation in ADHD: a controlled PET imaging study using altropane. Biol Psychiatry. 2007;62(9):1059-61.

30. del Campo N, Fryer TD, Hong YT, Smith R, Brichard L, Acosta-Cabronero J, et al. A positron emission tomography study of nigro-striatal dopaminergic mechanisms underlying attention: implications for ADHD and its treatment. Brain. 2013;136(Pt 11):3252-70.
31. Jucaite A, Fernell E, Halldin C, Forssberg H, Farde L. Reduced midbrain dopamine transporter binding in male adolescents with attention-deficit/hyperactivity disorder: association between striatal dopamine markers and motor hyperactivity. Biol Psychiatry. 2005;57(3):229-38.
32. Arakawa R, Okumura M, Ito H, Seki C, Takahashi H, Takano H, et al. Quantitative analysis of norepinephrine transporter in the human brain using PET with *(S,S)*-[^{18}F]-FMeNER-D$_2$. J Nucl Med. 2008;49(8):1270-6. Neuropsychologia. 1971;9(1):97-113.
33. Oldfield RC. The assessment and analysis of handedness: the Edinburgh inventory. Neuropsychologia. 1971;9(1):97-113.
34. Salmaso D, Longoni AM. Problems in the assessment of hand preference. Cortex. 1985;21(4):533-49.
35. Formann AK, Waldherr, K. & Piswanger, K., editor. Wiener Matrizen-Test 2. Manual. Göttingen: Beltz Test GmbH; 2011.
36. Takano A, Varrone A, Gulyas B, Karlsson P, Tauscher J, Halldin C. Mapping of the norepinephrine transporter in the human brain using PET with *(S,S)*-[^{18}F]-FMeNER-D$_2$. Neuroimage. 2008;42(2):474-82.
37. Seneca N, Gulyas B, Varrone A, Schou M, Airaksinen A, Tauscher J, et al. Atomoxetine occupies the norepinephrine transporter in a dose-dependent fashion: a PET study in nonhuman primate brain using *(S,S)*-[^{18}F]-FMeNER-D$_2$. Psychopharmacology (Berl). 2006;188(1):119-27.
38. Rami-Mark C, Zhang MR, Mitterhauser M, Lanzenberger R, Hacker M, Wadsak W. [18F]FMeNER-D2: reliable fully-automated synthesis for visualization of the norepinephrine transporter. Nuclear medicine and biology. 2013;40(8):1049-54.
39. Schou M, Halldin C, Pike VW, Mozley PD, Dobson D, Innis RB, et al. Post-mortem human brain autoradiography of the norepinephrine transporter using *(S,S)*-[^{18}F]-FMeNER-D$_2$. Eur Neuropsychopharmacol. 2005;15(5):517-20.
40. Schou M, Halldin C, Sovago J, Pike VW, Hall H, Gulyas B, et al. PET evaluation of novel radiofluorinated reboxetine analogs as norepinephrine transporter probes in the monkey brain. Synapse. 2004;53(2):57-67.
41. Innis RB, Cunningham VJ, Delforge J, Fujita M, Gjedde A, Gunn RN, et al. Consensus nomenclature for *in vivo* imaging of reversibly binding radioligands. J Cereb Blood Flow Metab. 2007;27(9):1533-9.
42. Takano A, Gulyas B, Varrone A, Karlsson P, Schou M, Airaksinen AJ, et al. Imaging the norepinephrine transporter with positron emission tomography: initial human studies with *(S,S)*-[^{18}F]-FMeNER-D$_2$. Eur J Nucl Med Mol Imaging. 2008;35(1):153-7.
43. Hammers A, Allom R, Koepp MJ, Free SL, Myers R, Lemieux L, et al. Three-dimensional maximum probability atlas of the human brain, with particular reference to the temporal lobe. Hum Brain Mapp. 2003;19(4):224-47.
44. Maldjian JA, Laurienti PJ, Kraft RA, Burdette JH. An automated method for neuroanatomic and cytoarchitectonic atlas-based interrogation of fMRI data sets. Neuroimage. 2003;19(3):1233-9.

45. Keren NI, Lozar CT, Harris KC, Morgan PS, Eckert MA. *In vivo* mapping of the human locus coeruleus. Neuroimage. 2009;47(4):1261-7.
46. Akaike H. A new look at the statistical model identification. System identification and time-series analysis. IEEE Trans Automatic Control 1974;AC-19 716–23.
47. Ding Y-S, Singhal T, Planeta-Wilson B, Gallezot J-D, Nabulsi N, Labaree D, et al. PET imaging of the effects of age and cocaine on the norepinephrine transporter in the human brain using *(S,S)*-[^{11}C]O-methylreboxetine and HRRT. Synapse. 2010;64(1):30-8.
48. Volkow ND, Swanson JM. Clinical practice: Adult attention deficit-hyperactivity disorder. N Engl J Med. 2013;369(20):1935-44.
49. Faraone SV, Spencer T, Aleardi M, Pagano C, Biederman J. Meta-analysis of the efficacy of methylphenidate for treating adult attention-deficit/hyperactivity disorder. J Clin Psychopharmacol. 2004;24(1):24-9.
50. Adler LA, Spencer T, Brown TE, Holdnack J, Saylor K, Schuh K, et al. Once-daily atomoxetine for adult attention-deficit/hyperactivity disorder: a 6-month, double-blind trial. J Clin Psychopharmacol. 2009;29(1):44-50.
51. Willcutt E, Doyle A, Nigg J, Faraone S, Pennington B. Validity of the executive function theory of attention-deficit/hyperactivity disorder: a meta-analytic review. Biol Psychiatry. 2005;57(11):1336 - 46.
52. Lijffijt M, Kenemans J, Verbaten M, van Engeland H. A meta-analytic review of stopping performance in attention-deficit/hyperactivity disorder: deficient inhibitory motor control? J Abnorm Psychol. 2005;114(2):216 - 22.
53. Arnsten AF, Li BM. Neurobiology of executive functions: catecholamine influences on prefrontal cortical functions. Biol Psychiatry. 2005;57(11):1377-84.
54. Volkow ND, Wang GJ, Fowler JS, Gatley SJ, Logan J, Ding YS, et al. Dopamine transporter occupancies in the human brain induced by therapeutic doses of oral methylphenidate. Am J Psychiatry. 1998;155(10):1325-31.
55. Volkow ND, Wang GJ, Fowler JS, Logan J, Franceschi D, Maynard L, et al. Relationship between blockade of dopamine transporters by oral methylphenidate and the increases in extracellular dopamine: therapeutic implications. Synapse. 2002;43(3):181-7.
56. Volkow ND, Wang GJ, Tomasi D, Kollins SH, Wigal TL, Newcorn JH, et al. Methylphenidate-elicited dopamine increases in ventral striatum are associated with long-term symptom improvement in adults with attention deficit hyperactivity disorder. J Neurosci. 2012;32(3):841-9.
57. Dresel S, Krause J, Krause KH, LaFougere C, Brinkbaumer K, Kung HF, et al. Attention deficit hyperactivity disorder: binding of [^{99}mTc]TRODAT-1 to the dopamine transporter before and after methylphenidate treatment. Eur J Nucl Med. 2000;27(10):1518-24.
58. Dougherty DD, Bonab AA, Spencer TJ, Rauch SL, Madras BK, Fischman AJ. Dopamine transporter density in patients with attention deficit hyperactivity disorder. Lancet. 1999;354(9196):2132-3.
59. Krause KH, Dresel SH, Krause J, Kung HF, Tatsch K. Increased striatal dopamine transporter in adult patients with attention deficit hyperactivity disorder: effects of methylphenidate as

measured by single photon emission computed tomography. Neurosci Lett. 2000;285(2):107-10.

60. van Dyck CH, Quinlan DM, Cretella LM, Staley JK, Malison RT, Baldwin RM, et al. Unaltered dopamine transporter availability in adult attention deficit hyperactivity disorder. Am J Psychiatry. 2002;159(2):309-12.
61. Hesse S, Ballaschke O, Barthel H, Sabri O. Dopamine transporter imaging in adult patients with attention-deficit/hyperactivity disorder. Psychiatry Res. 2009;171(2):120-8.
62. Kranz GS. Reduced serotonin transporter binding in adult ADHD investigated by PET and [^{11}C]DASB. 26th European College of Neuropsychopharmacology (ECNP); 2013 5 - 9 October 2013: Barcelona, Spain.
63. Castellanos FX, Elia J, Kruesi MJ, Gulotta CS, Mefford IN, Potter WZ, et al. Cerebrospinal fluid monoamine metabolites in boys with attention-deficit hyperactivity disorder. Psychiatry Res. 1994;52(3):305-16.
64. Karlsson L, Tuominen L, Huotarinen A, Leppamaki S, Sihvola E, Helin S, et al. Serotonin transporter in attention-deficit hyperactivity disorder--preliminary results from a positron emission tomography study. Psychiatry Res. 2013;212(2):164-5.
65. Thakur GA, Sengupta SM, Grizenko N, Choudhry Z, Joober R. Comprehensive phenotype/genotype analyses of the norepinephrine transporter gene (SLC6A2) in ADHD: relation to maternal smoking during pregnancy. PloS one. 2012;7(11):e49616.
66. Millard WJ, Standish LJ. The paradoxical effect of central nervous system stimulants on hyperactivity: a paradox unexplained by the rate-dependent effect. J Nerv Ment Dis. 1982;170(8):499-501.
67. Rapoport JL, Inoff-Germain G. Responses to methylphenidate in Attention-Deficit/Hyperactivity Disorder and normal children: update 2002. J Atten Disord. 2002;6 Suppl 1:S57-60.
68. Taylor FB, Russo J. Comparing guanfacine and dextroamphetamine for the treatment of adult attention-deficit/hyperactivity disorder. J Clin Psychopharmacol. 2001;21(2):223-8.
69. Wang GJ, Volkow ND, Wigal T, Kollins SH, Newcorn JH, Telang F, et al. Long-term stimulant treatment affects brain dopamine transporter level in patients with attention deficit hyperactive disorder. PloS one. 2013;8(5):e63023.
70. Smith HR, Beveridge TJ, Porrino LJ. Distribution of norepinephrine transporters in the non-human primate brain. Neuroscience. 2006;138(2):703-14.
71. Gross-Isseroff R, Israeli M, Biegon A. Autoradiographic analysis of [^{3}H]desmethylimipramine binding in the human brain postmortem. Brain Res. 1988;456(1):120-6.

Tables:

	ADHD	HC
age	30.7 ±10.4	30.9 ±10.6
sex	15 M/7 F	15 M, 7 F
current smokers	7	11
handedness	20 r/2 l	17 r/5 l
CAARS		
Inattention	18.8 ±5.2*	0.1 ±0.4
Hyperactive/Impulsive	19.6 ±5.6*	0.2 ±0.6
Past psychopharmacological treatment	4 patients were using stimulants, 2 patients were using SNRI 1 patient was using stimulants and AD	
past comorbidities	7 patients suffered from depression and are currently under remission, 2 patients abused drugs in the past	

Table 1. Epidemiological and clinical data of participants. Age and CAARS-Inattention and Hyperacitvity/Impulsivity scores are given in mean ± standard deviation. * marks significant differences between ADHD patients and HC, $p<0.0001$. *CAARS* Conners' Adult ADHD Rating Scale, *SNRI* Selective Noradrenalin Reuptake Inhibitors, *AD* Antidepressants

	HC	ADHD
Hammers Maximum Probability Atlas ROIs		
Thalamus	0.370 ±0.096	0.355 ±0.075
Hippocamus	0.110 ±0.061	0.120 ±0.065
Midbrain with Pons	0.256 ±0.106	0.250 ±0.111
Putamen	0.178 ±0.047	0.184 ±0.058
Pallidum	0.218 ±0.057	0.226 ±0.063
Cerebellum	0.163 ±0.077	0.152 ±0.103
MNI T1 single subject brain delineated ROIs		
Midbrain without Pons	0.460 ±0.137	0.501 ±0.117
Locus Coeruleus	0.386 ±0.131	0.408 ±0.122
Claustrum	0.175 ±0.053	0.182 ±0.062
Hypothalamus	0.284 ±0.103	0.293 ±0.109
Manually delinated individual ROIs		
Thalamus	0.495 ±0.123	0.308 ±0.132
Locus Coeruleus	0.469 ±0.104	0.348 ±0.138
Thalamic sub-nuclei ROIs delinated with WFU Pickatlas Tool		
Lateral Dorsal Nucleus	0.231 ±0.170	0.159 ±0.198
Lateral Geniculum Body	0.312 ±0.118	0.341 ±0.129
Lateral Posterior Nucleus	0.403 ±0.121	0.370 ±0.114
Mammillary Body	0.547 ±0.155	0.590 ±0.136
Medial Dorsal Nucleus	0.537 ±0.153	0.512 ±0.413
Medial Geniculum Body	0.472 ±0.165	0.519 ±0.177
Midline Nucleus	0.126 ±0.171	0.060 ±0.213
Pulvinar	0.333 ±0.126	0.318 ±0.129
Subthalamic Nucleus	0.362 ±0.123	0.401 ±0.144
Ventral Anterior Nucleus	0.165 ±0.115	0.116 ±0.123
Ventral Lateral Nucleus	0.394 ±0.093	0.368 ±0.095
Ventral Posterior Lateral Nucleus	0.593 ±0.130	0.605 ±0.146
Ventral Posterior Medial Nucleus	0.733 ±0.160	0.752 ±0.135

Table 2. Binding potential by region of interest. Mean NET BP_{ND} and standard deviations are listed from Hammers Maximum probability Atlas ROIs, MNI T1 single subject brain delineated ROIs, manually delineated individual ROIs and thalamic sub-nuclei ROIs for ADHD patients and HCs. No significant differences could be detected in NET BP_{ND} between groups.

Figures:

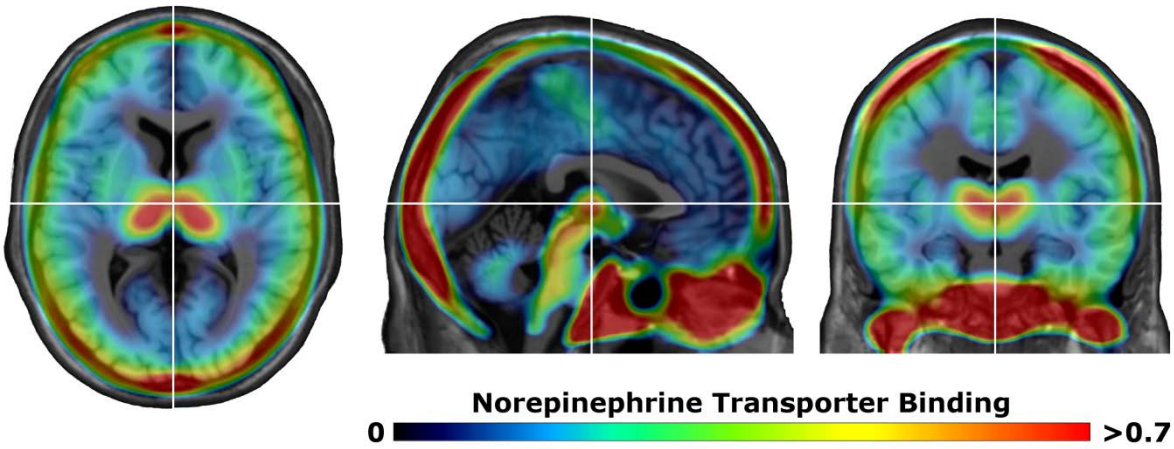

Fig 1. Average *(S,S)*-[$_{18}$F]FMeNER-D$_2$ distribution in 22 healthy controls normalized to MNI T1 template. High NET BP_{ND} is found in thalamus and midbrain ROIs, lowest in the basal ganglia. The figure shows highest NET uptake in bones, a phenomenon associated with tracer specific deflourination. The colour table represent binding potential at each voxel, blue indicates lowest and red highest NET BP_{ND}. Crosshair is set on thalamus.

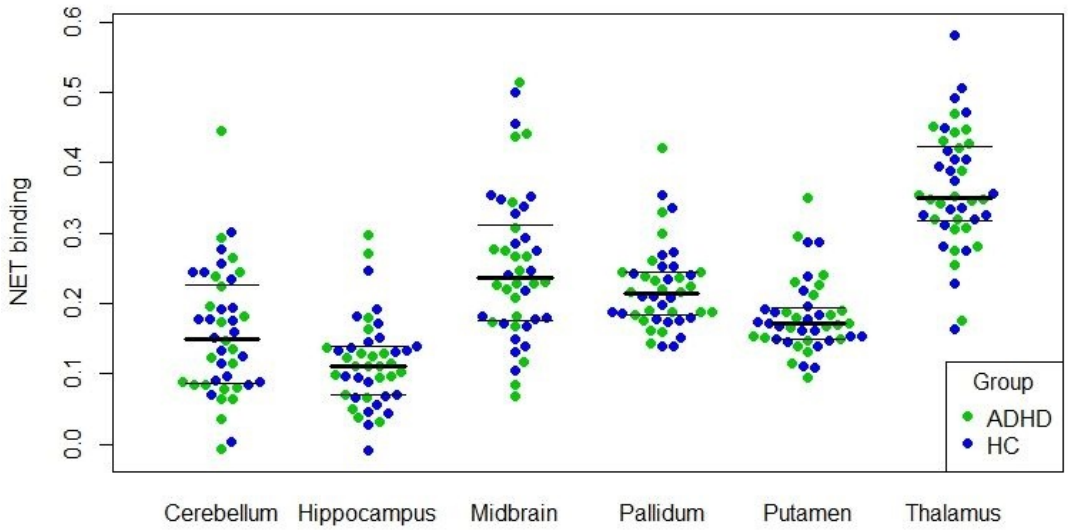

Fig. 2 NET BP_{ND} in selected ROIs. Scatterplots depict NET BP_{ND}, given in mean and standard deviations, in exemplified regions: cerebellum, hippocampus, midbrain, pallidum, putamen and thalamus. There were no significant differences between ADHD patients and healthy controls.

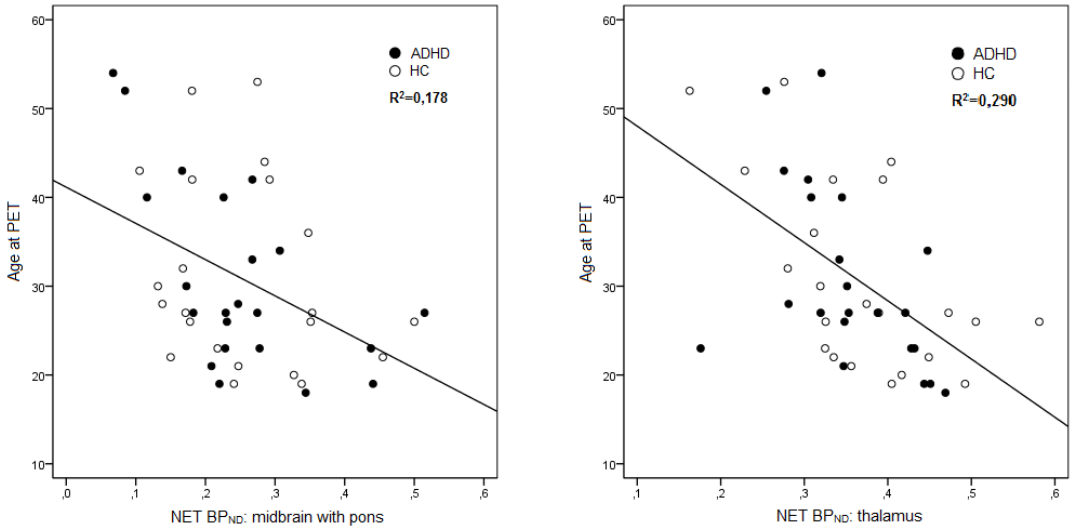

Fig. 3 Negative correlation of NET BP_{ND} and age in thalamus and midbrain/pons. Scatterplots showing a significant negative correlation between $NETBP_{ND}$ and age in thalamus (R^2=0.290) and midbrain/pons (R^2=0.178). ROIs were extracted from Hammers Maximum Probability Atlas. Age is given in years, significance level was set to $p<0.05$ and results were Bonferroni corrected for multiple comparisons.

3.1.5 Manuscript #4

SYNTHESIS AND *IN SILICO* EVALUATION OF NOVEL COMPOUNDS FOR PET BASED INVESTIGATIONS OF THE NOREPINEPHRINE TRANSPORTER

Molecules, 2015, 20, 1712-1730.

Catharina Neudorfer [1,2,*], Amir Seddik [3], Karem Shanab [1,2], Andreas Jurik [3], **Christina Rami-Mark** [1], Wolfgang Holzer [2], Gerhard Ecker [3], Markus Mitterhauser [1], Wolfgang Wadsak [1], Helmut Spreitzer [2,*]

[1]Medical University of Vienna, Department of Biomedical Imaging and Image-guided Therapy, Division of Nuclear Medicine, Waehringer Guertel 18-20, 1090 Vienna, Austria

[2]University of Vienna, Faculty of Life Sciences, Department of Pharmaceutical Chemistry, Division of Drug Synthesis, Althanstraße 14, 1090 Vienna, Austria

[3]University of Vienna, Faculty of Life Sciences, Department of Pharmaceutical Chemistry, Division of Drug Design and Medicinal Chemistry, Althanstraße 14, 1090 Vienna, Austria

*****Author to whom correspondence should be addressed; E-Mail: catharina.neudorfer@gmail.com; Tel.: +43-4277-55629; Fax: +43-4277-855629 (C. Neudorfer). E-Mail: helmut.spreitzer@univie.ac.at; Tel.: +43-4277-55621; Fax: +43-4277-855621 (H. Spreitzer).

Molecules [IF: 2.095]

Keywords: NET; ADHD; Cocaine dependence; BAT; PET; FAPPI

Abstract: Since the NET is involved in a variety of diseases, the investigation of underlying dysregulation-mechanisms of the NE system is of major interest. Based on the previously described highly potent and selective NET ligand 1-(3-(methylamino)-1-phenylpropyl)-3-phenyl-1,3-dihydro-2*H*-benzimidazol-2-one (Me@APPI), this paper aims at the development of several fluorinated methylamine based analogs of this compound. The newly synthesized compounds were computationally evaluated for their interactions with the monoamine transporters and represent reference compounds for PET based investigation of the NET.

1. Introduction

Abnormal regulation of the norepinephrine transporter (NET) or NET dysfunction, respectively, cause either increased or decreased levels of norepinephrine (NE) in the synaptic cleft. Since NE is a fundamental neurochemical messenger, its accurate regulation is of major importance. Thus, the NET, responsible for NE equilibrium in the synaptic cleft, is representing the reuptake site and considered to be involved in a variety of neurological/psychiatric disorders,[1,2] but also plays a pivotal role in cardiovascular[1,2,3] and metabolic diseases.[3-5] Reduced NET levels go along with neurological disorders like major depression,[6,7] Parkinson's disease (PD), Alzheimer's disease (AD)[8-18], and cardiovascular diseases such as hypertension, cardiomyopathy, and heart failure.[5,13] Furthermore, a dysfunction of the NE system was reported in Attention Deficit Hyperactivity Disorder (ADHD),[9,17,19] suicide,[1,12,20] substance abuse (cocaine dependence),[16] and schizophrenia.[10] A more recent discovery is the involvement of the NET in diseases like diabetes and obesity, due to its presence in brown adipose tissue (BAT) and the proposed activation thereof via NE.[4,5,21]

Based on the fact that the NET is involved in such a variety of diseases, the investigation of the underlying dysregulation-mechanism of the NE system is of major interest. For this purpose, information about the transporter abundance and density in healthy and pathological living human brains is required. The most suitable and accurate technique to gain this information is positron emission tomography (PET). As a non-invasive molecular imaging technique, it represents a suitable approach towards the collection of missing data in the living organism and direct quantification of receptor/transporter densities *in vivo*. To fully gain insight in the molecular changes of the noradrenergic system *via* PET, however, prior development of suitable NET PET radioligands is required.

So far, radiolabeled NET binding reboxetine analogs [^{11}C]MeNER, [^{11}C]MRB, ((*S*,*S*)-2-(α-(2-[^{11}C]methoxyphenoxy)benzyl) morpholine) and [^{18} F]FMeNER-D_2 ((*S,S*)-2-(α-(2-[^{18}F]Fluoro[$^{2}H_2$] methoxyphenoxy)benzyl) morpholine) have been described, which however display certain limitations such as metabolic stability, complex radiosynthesis, or late equilibrium.[22-26]

Recently, Zhang *et al*[26] evaluated a series of benzimidazolone based propanamines with *in vitro* inhibitory activity on the human norepinephrine transporter (hNET). The results of these investigations suggested that compounds containing a phenyl moiety directly at the benzimidazolone ring (e.g. **1**) (figure 1) were the most potent, representing a half maximal inhibitory concentration (IC_{50}) below 10 nM (IC_{50} < 10 nM). Furthermore, hNET selectivity over hSERT (human serotonin transporter) turned out (> 300-fold) superior to those of reboxetine and atomoxetine (16- and 81-fold).[26] Fluorination at position 2 of the phenyl moiety, attached to the benzimidazolone ring (e.g. **2**) (figure 1), indicated similar hNET potency, comparable to its non-fluorinated analogs (e.g. **1**) and additionally exhibited hNET selectivity over hSERT (80-fold) similar to atomoxetine.[26]

Both benzimidazolone derived propanamines with a phenyl moiety (**1**), as well as a fluorinated phenyl moiety (**2**) indicated excellent hNET selectivity over hDAT (human dopamine transporter) with < 50% inhibition of the cocaine analog [^{3}H]WIN-35,428, binding to hDAT at a concentration of 10 µM.[26]

Given those findings, both described benzimidazolone based propanamines (**1** and **2**) represent

excellent candidates for selective and potent NET inhibition with high affinity and low unspecific binding. Thus, on the basis of the results of Zhang *et al*[26] the methylamino moiety of core compound **1** has been radiolabeled with ^{11}C and tested by our research group.[27] All investigated preclinical parameters, such as affinity, blood brain barrier penetration, lipophilicity, metabolic degradation, and selectivity showed excellent results, thus suggesting suitability of ^{11}C radiolabeled 1-(3-(methylamino)-1-phenylpropyl)-3-phenyl-1,3-dihydro-2*H*-benzimidazole-2-one ([^{11}C]Me@APPI) (**3**) (figure 1) as a NET radioligand for the employment in PET.

Figure 1. Chemical structure of the highly potent and selective NET ligands 1-(3-(methylamino)-1-phenylpropyl)-3-phenyl-1,3-dihydro-2*H*-benzimidazol-2-one (Me@APPI) (**1**) and 4-fluoro-1-(2-fluorophenyl)-3-(3-(methylamino)-1-phenylpropyl)-1,3-dihydro-2*H*-benzimidazol-2-one (**2**) as well as radiolabeled analog [^{11}C]Me@APPI (**3**).

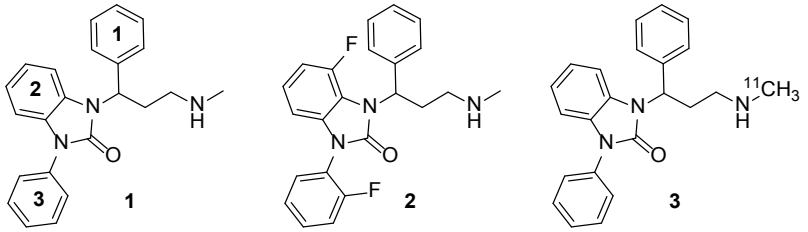

Due to successful preclinical testing of [^{11}C]Me@APPI (**3**) and given the excellent *in vitro* results of compound **2**, shown by Zhang *et al*,[26] the aim of this paper is the synthesis and docking studies of several fluorinated analogs (**4-6**) of compound **1** (figure 2) as reference compounds for their later prepared radioactive analogs. All methylamine derived benzimidazolone derivatives (**4-6**) will be subjected to affinity, selectivity, and lipophilicity studies towards the NET as well as blood brain barrier penetration experiments at the Medical University of Vienna. The most promising NET ligands will then be selected for the development of new, selective PET tracers for the NET. Thereby, radiolabeling with both, ^{11}C and ^{18}F will be subject of further experiments.

Figure 2. Chemical structure of envisaged reference compounds **4-6** (FAPPI: 1-3).

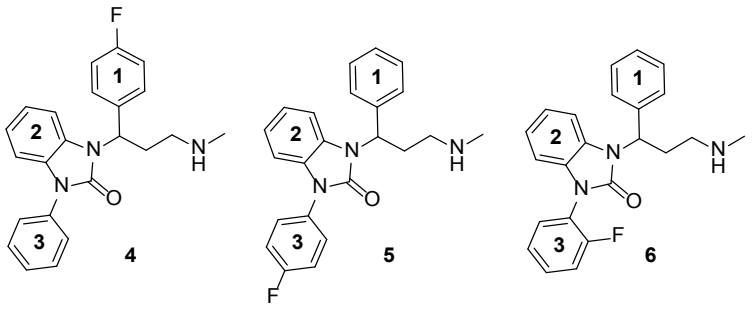

2. Results and Discussion

The synthesis of reference compounds **4-6** first required the preparation of side chains **11** and **12**, as well as core compounds **16-18**. After successful preparation, side chain **11** was merged in a condensation reaction with core compound **16**, whereas side chain **12** was reacted with core compounds **17** and **18**, prior to halogen exchange and substitution with methylamine (scheme 1).

For the synthesis of side chains **11** and **12**, the keto group of commercially available compounds **7** and **8** was reduced with sodium borohydride, in order to obtain intermediate alcohols **9** and **10**. Subsequent bromination of **9** and **10** with aqueous hydrogen bromide led to the formation of products **11** and **12**, respectively.

Scheme 1. Reactions and conditions for: (i) THF, EtOH, $NaBH_4$, -10°C → -5°C, 10 min, yields for **9**: 95%, **10**: 100%; (ii) aqu. HBr, rt, 3 h, yields for **11**: 64%, **12**: 86%; (iii) 1,1'-carbonyldiimidazol, anhyd. THF, rt, overnight, yields for **16**: 74%, **17**: 61%, **18**: 69%; (iv) 1,1'-carbonyldiimidazol, anhyd. DMF, 90°C, 2 h, yields for **17**: 80%, **18**: 80%; (v) K_2CO_3, DMF, rt, 30 min → addition of **11** and **12** → rt, 30 min, yields for **19**: 32%, **20**: 63%, **21**: 55%; (vi) NaI, acetone, reflux, 24 h, yields for **22**: 82%, **23**: 76%, **24**: 53%; (vii) NH_3 in isopropanol, 80°C, 3 h, yield for **25**: 50%; (viii) methylamine in EtOH, 80°C, 3 h, yields for **4**: 48%, **5**: 29%, **6**: 30%.

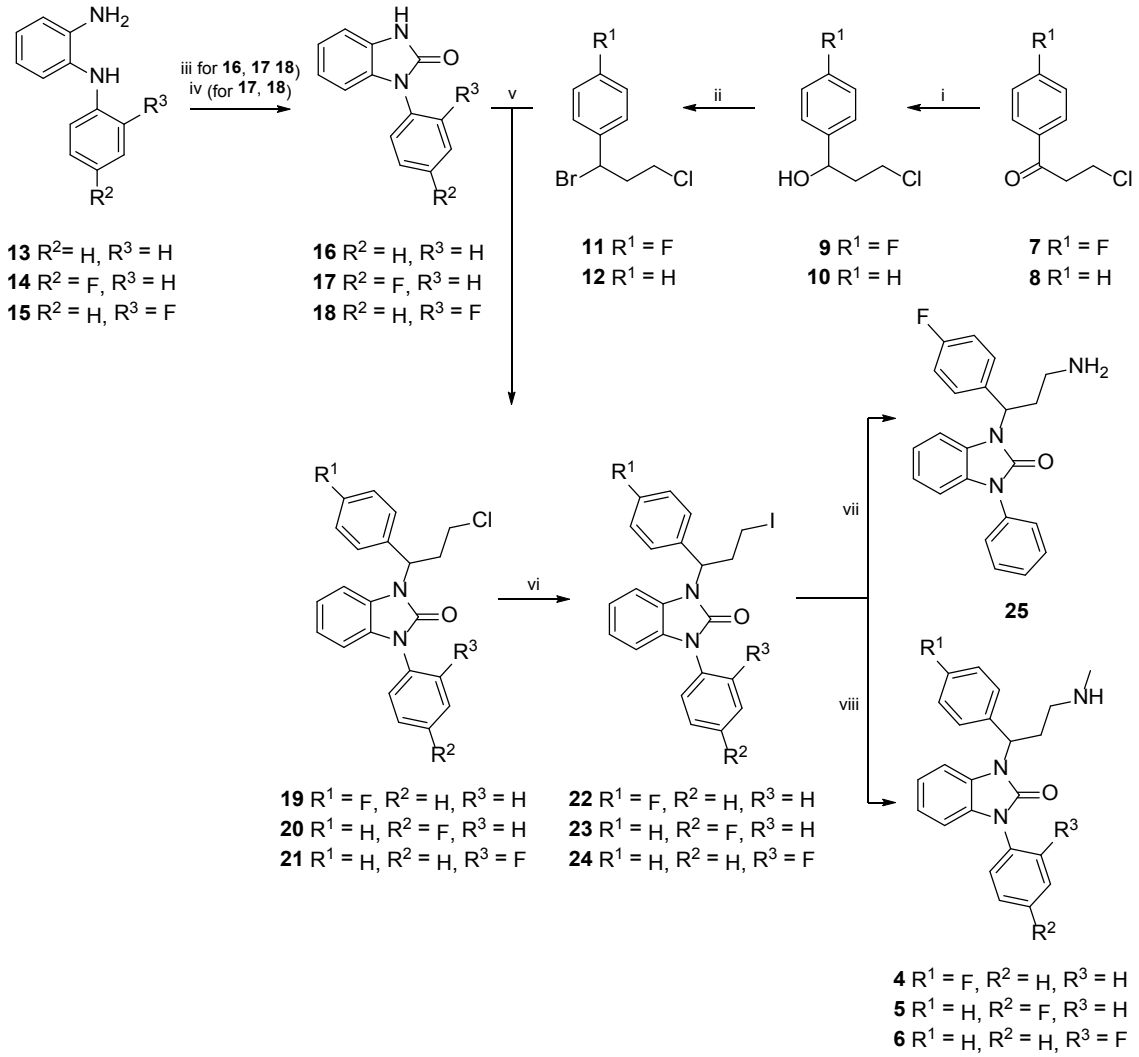

.

Core compound **16** was prepared by the reaction of commercially available *N*-phenylbenzene-1,2-diamine (**13**) with 1,1'-carbonyldiimidazole. For the preparation of **17** and **18** however, **14** and **15** first had to be made accessible (scheme 2). Thus, 1-fluoro-2-nitrobenzene (**26**) reacted with commercially available fluoroanilines **27** and **28**, respectively, to obtain disubstituted amines **29** and **30**. Therefore, two different methods were applied (scheme 2): The first method (i) was conducted by heating **26** and

27 with anhydrous potassium fluoride and potassium carbonate in a microwave oven. Since an alternative method -conventional heating at 180 °C- gave compound **29** in higher yields, this approach (ii) was chosen for the large scale synthesis of **29** as well as for the preparation of **30**.

Scheme 2. Reactions and conditions for (i) anhyd. KF, K_2CO_3, microwave oven, 900 W, 10 min, yields for **29**: 58%; (ii) anhyd. KF, K_2CO_3, 180°C, 2 d, yields for **29**: 68%, **30**: 52%; (iii) Zn, AcOH, 0°C → rt, 2 h, yields for **14**: 93%, **15**: n.d.

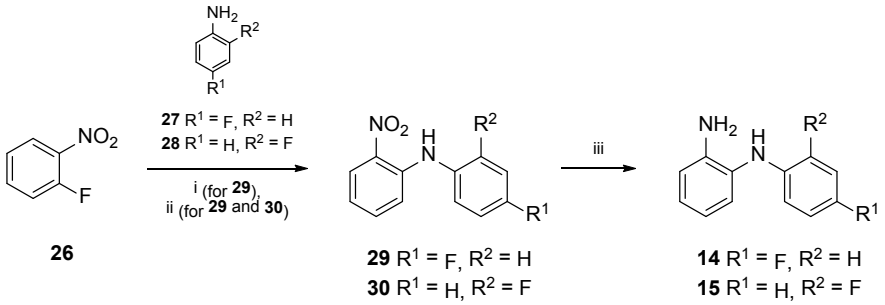

In the next reaction step, the nitro groups of both disubstituted amines (**29** and **30**) were reduced. For this purpose **29** or **30** were added to a mixture of zinc/acetic acid. The resulting amines **14** or **15** were obtained in excellent yields (scheme 2).

Freshly prepared intermediates **14** and **15** were then subjected to a cyclization reaction with 1,1'-carbonyldiimidazol in DMF under anhydrous conditions (scheme 1). DMF was preferred over THF in order to ensure higher yields and shorter reaction times.

Condensation reactions of benzimidazolones **16**, **17**, and **18** with side chains **11** and **12**, respectively were performed under basic conditions (scheme 1). After purification, the chloro substituted derivatives **19**-**21** were converted into the iodo compounds (**22**-**24**) in a Finkelstein reaction. Target compounds **4**-**6** (FAPPI:1-3) were then made accessible by heating derivatives **22**-**24** in a solution of methylamine in ethanol in a sealed tube for 3 h. Additionally to reference compounds **4-6**, free amine **25** was synthesized by dissolving **22** in a solution of ammonia in isopropanol and heating the resulting mixture in a sealed tube for 3 h. As compound **25** features a free amine moiety, it can be considered a precursor for radiosynthesis.

Since compounds **4** and **5** comprise a novel fluoro substitution, a computational docking study was performed to assess if these compounds still would fit in the binding site of the NET. Furthermore, we aimed at creating a binding mode hypothesis which allows gaining insights into the molecular basis of binding and selectivity towards the monoamine transporters. As the basic scaffold has been shown to act in an enantioselective manner, the respective (*R*) enantiomers were used throughout the docking studies.[26] The ligands were docked in the substrate binding site (S1) of the outward-open conformation of the transporter models (see Experimental Section for details), since related inhibitors, such as nortriptyline, sertraline, mazindol, etc. were also shown to fit in the S1 of the *Drosophila* DAT (dDAT) and the "SERT"-ized leucine transporter ("LeuBAT") in the same protein conformation.[28,29] Interestingly, the co-crystallized ligand in dDAT, nortriptyline (**31**), has the same ranking of human NET, SERT and

DAT activity as reference compound **1**, i.e. 4.4, 18 and 1149 nM K_D vs. 9, 2995 and >10000 nM IC_{50}, respectively.[26,30] Additionally, nortriptyline shares important structural features with the benzimidazolones, i.e. two aromatic moieties and an *N*-methyl-ethylenamine side chain. Therefore their binding mode can be expected to be similar.

Figure 3. Chemical structure of nortriptyline (co-crystallized ligand from the template (PDB code 4M48).[28]

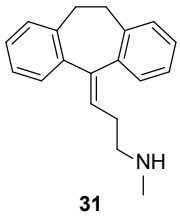

31

Common scaffold clustering[31] revealed two binding hypotheses (see Experimental Section) which indicated that compounds **4-6** fit in the S1 of all three transporters. Hence, additional fluorination does not seem to cause steric clashes. In both hypotheses, the most prominent protein-ligand interaction was the cationic nitrogen atom placed in the A sub pocket,[32] located between the central Asp75/98/79 side chain as a salt-bridge and the Phe72/95/76 side chain as a cation-*pi* interaction in NET/SERT/DAT, respectively. This is well in accordance with the X-ray structures of the templates. Additional *pi-pi* stacking interactions with Phe152/176/156 and Phe323/355/341 further promote the binding in both hypotheses obtained.

Hypothesis 1: the benzimidazolone heterocycle (ring 2) is placed in the B sub pocket and ring 3 in the C pocket, whereas ring 1 is solvent exposed (see figure in Experimental Section).

Hypothesis 2: Ligand ring 1 is placed in the B pocket whereas ring 2 is placed at the same height (measured from the membrane-water interface) and overlap with the rings of nortriptyline (**31**).The solvent exposed Tyr151/Tyr175/Phe155 in NET/SERT/DAT, resp. T-stacks with ring 2 whereas ring 3 points extracellularly (Table 1, Figure 4).

Table 1. Sequence alignment of all distinct monoamine transporter residues located in sub sites (reference **32**) in the vicinity of the docked compounds. Red: hydrophilic side chain, green: lipophilic side chain, bold: bulkier side chain.

	B site				C site		Outer site		
hNET	S420	M424	G149	V148	A145	F72	D473	Y151	A477
hSERT	**T439**	L443	**A173**	**I172**	A177	Y95	**E493**	Y175	**T497**
hDAT	A423	M427	G153	V152	S149	F76	D476	F155	A480

Figure 4. Overlay of compounds **1**, **2**, and **4-6** (maroon) in binding hypothesis 2 in hNET showing agreement with the co-crystal pose of nortriptyline (**31**) (green). Val148 and Asp473 allow more space than Ile172 and Glu439 in hSERT, resp., whereas Tyr151 might induce a more potent stacking interaction as compared to Phe155 in hDAT. The angle between ligand ring 2 and 3 is almost 90° in all poses. The extracellular space is located above.

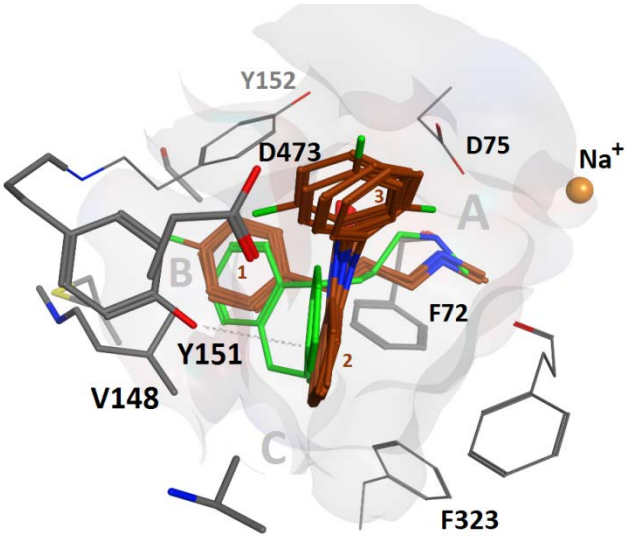

As binding hypothesis 2 is in close agreement with the co-crystallized ligands in dDAT and LeuBAT, we focus further analysis on this proposed binding mode.

Binding hypothesis 2 indicates why the investigated compounds (**4-6**) show weaker affinity to SERT and DAT than to NET: lower SERT affinity may be due to Ile172 and Glu439, allowing less space for the ligand to be accommodated as compared to in NET, that comprises a valine and an aspartate at the homologous positions, respectively. Lower DAT affinity could be ascribed to weaker T stacking interactions of Phe155 as compared to Tyr151 in NET, based on previous findings that a Tyr-Phe pair has a stronger binding energy than a Phe-Phe pair.[34]

3. Experimental Section

3.1. General

The NMR spectra were recorded from $CDCl_3$ or DMSO-d_6 solutions on a Bruker DPX200 spectrometer (200 MHz for ^1H, 50 MHz for ^{13}C) or on a Bruker Avance III 400 spectrometer (400 MHz for ^1H, 100 MHz

for ^{13}C, 40 MHz for ^{15}N, 376 MHz for ^{19}F) at 25 °C. The center of the solvent (residual) signal was used as an internal standard which was related to TMS with δ 7.26 ppm (^{1}H in $CDCl_3$), δ 2.49 ppm (^{1}H in DMSO-d_6), δ 77.0 ppm (^{13}C in $CDCl_3$) and δ 39.5 ppm (^{13}C in DMSO-d_6). ^{15}N NMR spectra (gs-HMBC, gs-HSQC) were referenced against neat, external nitromethane, ^{19}F NMR spectra by absolute referencing via *Ξ* ratio. Digital resolutions were 0.25 Hz/data point in the ^{1}H and 0.3 Hz/data point in the ^{13}C-NMR spectra. Coupling constants (*J*) are quoted in Hz. The following abbreviations were used to show the multiplicities: s: singlet, d: doublet, t: triplet, q: quadruplet, dd: doublet of doublet, m: multiplet. Mass spectra were obtained on a Shimadzu QP 1000 instrument (EI, 70 eV), high-resolution mass spectrometry was carried out on a Finnigan MAT 8230 (EI, 10 eV) or Finnigan MAT 900 S (ESI, 4 kV, 3 µA, CH_3CN/MeOH) electrospray ionization mass spectrometer with a micro-TOF analyzer. Microwave experiments were carried out in a Synthos 3000 microwave oven (Anton Paar, SXQ80 rotor) with an internal temperature probe.

3.2. Syntheses

Compound purity: All compounds synthesized featured a purity of at least 95%.

General procedure for the synthesis of 9 and 10

Starting materials **7** or **8**, respectively (1 mmol) was dissolved in THF (1 ml) and EtOH (1 ml) was added. The mixture was cooled to -10°C and $NaBH_4$ (1.05 mmol) was slowly added at this temperature. The solution was stirred at -5°C for 10 min and thereafter, poured into a mixture of saturated aqueous ammonium chloride (3 ml) in ice (1.5 g). The product was extracted with diethyl ether, dried over Na_2SO_4 and evaporated to dryness. The crude product was employed directly in the subsequent reaction step without further purification.

3-Chloro-1-(4-fluorophenyl)propan-1-ol (9) Yield: 4.78 g (95%), pale yellow oil, analytical data are in complete accordance with literature values.[35]

3-Chloro-1-phenylpropan-1-ol (10) Yield: 4.61 g (99%), light yellow oil, analytical data are in complete accordance with literature values.[36]

General procedure for the synthesis of 11 and 12

To starting material **5** or **6**, respectively (1 mmol) was added 48% aqueous HBr (3 ml) and the mixture was stirred for 3h at room temperature. Thereafter, the solution was poured into a mixture of K_2CO_3 (1 g) in ice (5.5 g) and additional solid K_2CO_3 was added for neutralization (pH 7). The crude reaction product was extracted with diethyl ether, the combined organic layers were dried with $MgSO_4$ and evaporated to dryness. The crude product was employed directly in the subsequent reaction step without further purification.

1-(1-Bromo-3-chloropropyl)-4-fluorobenzene (11) Yield: 64%, pale yellow oil, analytical data are in complete accordance with literature values.[37]

(1-Bromo-3-chloropropyl)benzene (12) Yield: 5.64 g (86%), yellow oil, analytical data are in complete accordance with literature values.[36]

General procedure for the synthesis of 29 and 30

4-Fluoroaniline or 2-fluoroaniline, respectively (1 mmol), anhydrous KF (1 mmol), and K_2CO_3 (1 mmol) were well powdered with a mortar and a pestle, then 1-fluoro-2-nitrobenzene (1 mmol) was added and the mixture was stirred for 2 days at 180°C. Thereafter, water (5 ml) and CH_2Cl_2 (5 ml) were added and the organic layer was washed with 10% HCl (5 ml) and brine (5 ml). The combined organic layers were dried over Na_2SO_4 and evaporated to dryness prior to purification by column chromatography.

***N*-(4-Fluorophenyl)-2-nitroaniline (29)** Yield: 68%, dark orange crystals, mp. 82°C-83°C, purification: silica gel 60, petrol ether/ethyl acetate 9:1 and RP-18 silica gel, methanol/water 7:3, analytical data are in complete accordance with literature values.[38]

2-Fluoro-*N*-(2-nitrophenyl)aniline (30) Yield: 52%, orange crystals, mp. 79°C-80°C, purification: silica gel 60, petrol ether/ethyl acetate 9:1, analytical data are in complete accordance with literature values.[39]

Alternative procedure for the synthesis of 29

4-Fluoroaniline (7.89 g, 70.87 mmol), anhydrous KF (4.13 g, 70.87 mmol), and K_2CO_3 (9.81 g, 70.87 mmol) were well powdered with a mortar and a pestle, then 1-fluoro-2-nitrobenzene (10.00 g, 70.87 mmol) was added and the mixture was irradiated in the microwave (900 W, 10 min). Thereafter, water and CH_2Cl_2 were added and the organic layer was washed with 10% HCl and brine. The combined organic layers were dried over Na_2SO_4 and evaporated to dryness prior to purification by column chromatography (silica gel 60, petrol ether/ethyl acetate 9.5:0.5). Yield: 9.51 g (58%), dark orange crystals, mp. 82°C-83°C

General procedure for the synthesis of 14 and 15

To a solution of $Zn^{ø}$ (13.8 mmol) in glacial acetic acid (1 ml) was added starting material **28** or **29** (1 mmol) at 0°C under argon atmosphere. After the addition, the mixture was allowed to warm to room temperature and was stirred for 2 h. $Zn^{ø}$ was filtered off and the pH of the solution was adjusted to pH 9 with 2N NaOH. Thereafter, the aqueous layer was extracted three times with CH_2Cl_2, the combined organic layers were dried over $MgSO_4$ and evaporated to dryness.

***N*-(4-Fluorophenyl)benzene-1,2-diamine (14)** Yield: 93%, dark orange-reddish oil, purification: silica gel 60, petrol ether/ethyl acetate 9:1, analytical data are in complete accordance with literature values.[40]

***N*-(2-Fluorophenyl)benzene-1,2-diamine (15)** The crude reaction product was subjected to the next reaction step without further purification.

General procedure for the synthesis of 16-18

To a solution of starting materials **13**, **14**, or **15** (1 mmol) in THF was added 1,1'-carbonyldiimidazole (1.4 mmol) under argon atmosphere and the mixture was stirred at room temperature overnight. Thereafter, the crude reaction product was purified by column chromatography.

1-Phenyl-1,3-dihydro-2*H*-benzimidazol-2-one (16) Yield: 0.85 g (74%), pink crystals, mp. 201°C-202°C, THF: 10 ml, purification: silica gel 60, petrol ether/ethyl acetate 1:1, analytical data are in

complete accordance with literature values.[41]

1-(4-Fluorophenyl)-1,3-dihydro-2*H*-benzimidazol-2-one (17) Yield: 61%, brown resin, THF: 25 ml, purification: silica gel 60, petrol ether/ethyl acetate 9:1, **^{1}H-NMR** (200 MHz, $CDCl_3$): δ (ppm) 6.74-6.81 (m, 2H), 6.89-7.11 (m, 2H), 7.14-7.23 (m, 2H), 7.48-7.59 (m, 1H), 7.73-7.78 (m, 1H), 9.03 (br s, 1H), **^{13}C-NMR** (50 MHz, $CDCl_3$): δ (ppm) 108.5, 110.0, 116.3, 116.8, 121.4, 121.7, 122.3, 128.0, 128.2, 130.4, 135.1, 155.1, 159.3, 164.2, **MS**: m/z (%) 228 (M^+, 100), 199 (31), 172 (8), 114 (9), 95 (10), 75 (17), 51 (10), **HRMS**: m/z calculated for $C_{13}H_{10}FN_2O$ $[M + H]^+$: 229.0772. Found: 229.0769.

1-(2-Fluorophenyl)-1,3-dihydro-2*H*-benzimidazol-2-one (18) Yield: 69%, brown resin, THF: 20 ml, purification: silica gel 60, petrol ether/ethyl acetate 9:1, **^{1}H-NMR** (200 MHz, $CDCl_3$): δ (ppm) 6.82-6.85 (m, 1H), 7.00-7.19 (m, 3H), 7.26−7.88 (m, 2H), 7.43−7.60 (m, 2H), 10.54 (br s, 1H), **^{13}C-NMR** (50 MHz, $CDCl_3$): δ (ppm) 108.9, 110.1, 117.0, 117.4, 121.5, 121.9, 122.4, 124.9, 125.0, 128.2, 129.6, 130.4, 154.8, 155.4, 160.5, **MS**: m/z (%) 228 (M^+, 33), 199 (9), 181 (15), 149 (17), 111 (22), 97 (20), 71 (41), 69 (100), 55 (53), 43 (56), **HRMS**: m/z calculated for $C_{13}H_9FN_2NaO$ $[M + Na]^+$: 251.0597. Found: 251.0592.

Alternative procedure for the synthesis of 17 and 18

A solution of 1,1'-carbonyldiimidazole (1.4 mmol) in DMF (4 ml) was slowly added to a mixture of **14** or **15** (1 mmol) in DMF (4 ml) under argon atmosphere. The resulting solution was stirred at 90°C for 2 h. After completion of the reaction, the solvent was evaporated *in vacuo*, the slurry was taken up in water, filtered and dried.

1-(4-Fluorophenyl)-1,3-dihydro-2*H*-benzimidazol-2-one (17) Yield: 80%, brown resin

1-(2-Fluorophenyl)-1,3-dihydro-2*H*-benzimidazol-2-one (18) Yield: 80%, brown resin

General procedure for the synthesis of 19-21

Starting materials **16-18** (1 mmol) and K_2CO_3 (2 mmol) were suspended in DMF (1.8 ml) and stirred at 25°C for 30 min. **11** and **12**, respectively (1.5 mmol) were added after 30 min and the solution was stirred at room temperature overnight. To the mixture was added ethyl acetate (5 ml) and water (5 ml). The aqueous layer was extracted several times with ethyl acetate and the combined organic layers were washed with brine, dried over $MgSO_4$ and evaporated to dryness.

1-(3-Chloro-1-(4-fluorophenyl)propyl)-3-phenyl-1,3-dihydro-2*H*-benzimidazol-2-one (19) Yield: 32%, white oil, purification: silica gel 60, petrol ether/ethyl acetate 8:2, **^{1}H-NMR** (200 MHz, $CDCl_3$): δ (ppm) 2.70-2.87 (m, 1H), 3.12-3.30 (m, 1H), 3.60-3.66 (m, 2H), 5.73 (m, 1H), 7.00-7.11 (m, 6H), 7.38-7.57 (m, 7H), **^{13}C-NMR** (50 MHz, $CDCl_3$): δ (ppm) 34.3, 42.0, 53.8, 108.7, 109.0, 115.5, 115.9, 121.7, 122.0, 126.0, 127.8, 129.2, 129.4, 129.5, **MS**: m/z (%) 380 (M^+, 21), 210 (100), 181 (8), 167 (12), 135 (9), 115 (5), 109 (58), 77 (12), **HRMS**: m/z calculated for $C_{22}H_{18}ClFN_2ONa$ $[M + Na]^+$: 403.0989. Found: 403.0989.

1-(3-chloro-1-phenylpropyl)-3-(4-fluorophenyl)-1,3-dihydro-2*H*-benzimidazol-2-one (20) Yield: 63%, dark orange resin, purification: silica gel 60, petrol ether/ethyl acetate 9:1 and RP-18 silica gel,

methanol, **^{1}H-NMR** (400 MHz, $CDCl_3$): δ (ppm) 2.80-2.88 (m, 1H, 2'-CH_2), 3.17-3.26 (m, 1H, 2'-CH_2), 3.62-3.70 (m, 2H, 3'-CH_2), 5.79 (dd, *J* = 10.0 Hz and 5.6 Hz, 1H, 1'-CH), 7.04-7.09 (m, 4H, benzim 4-CH, benzim 5-CH, benzim 6-CH, benzim 7-CH), 7.21-7.26 (m, 2H, f-phen 3-CH, f-phen 5-CH), 7.31-7.33 (m, 1H, phen 4-CH), 7.36-7.40 (m, 2H, phen 3-CH, phen 5-CH), 7.52-7.56 (m, 4H, f-phen 2-CH, f-phen 6-CH, phen 2-CH, phen 6-CH), **^{13}C-NMR** (100 MHz, $CDCl_3$): δ (ppm) 34.1 (2'-CH_2), 42.0 (3'-CH_2), 54.4 (1'-CH), 108.6 (benzim 4-CH), 109.0 (benzim 7-CH), 116.4 (d, *J* = 22.9 Hz, f-phen 3-CH, 116.4 (d, *J* = 22.9 Hz, f-phen 5-CH), 121.6 (benzim 5-CH), 122.1 (benzim 6-CH), 127.4 (phen 2-CH), 127.4 (phen 6-CH), 127.9 (d, *J* = 8.6 Hz, f-phen 2-CH), 127.9 (d, *J* = 8.6 Hz, f-phen 6-CH), 128.1 (phen 4-CH), 128.7 (benzim 7a-C), 128.8 (phen 3-CH), 128.8 (phen 5-CH), 129.4 (benzim 3a-C), 130.3 (d, *J* = 3.1 Hz, f-phen 1-C), 138.4 (phen 1-C), 153.2 (benzim 2-CO), 161.6 (d, *J* = 247.7 Hz, f-phen 4-CF), **^{19}F-NMR** (471 MHz, $CDCl_3$): δ (ppm) -113.31 (m, 5-CF), **MS**: m/z (%) 380 (M^+, 2), 228 (100), 199 (11), 185 (16), 153 (6), 117 (14), 91 (73), 75 (8), **HRMS**: m/z calculated for $C_{22}H_{19}ClFN_2O$ $[M + H]^+$: 381.1170. Found: 381.1176.

1-(3-chloro-1-phenylpropyl)-3-(2-fluorophenyl-1,3-dihydro-2*H*-benzimidazol-2-one (21) Yield: 55%, orange resin, purification: silica gel 60, petrol ether/ethyl acetate 9:1, **^{1}H-NMR** (400 MHz, $CDCl_3$): δ (ppm) 2.78-2.86 (m, 1H, 2'-CH_2), 3.23 (br s, 1H, 2'-CH_2), 3.64-3.68 (m, 2H, 3'-CH_2), 5.79 (br s, 1H, 1'-CH), 6.85-6.87 (m, 1H, benzim 4-CH) 7.05-7.06 (m, 3H, benzim 5-CH, benzim 6-CH, benzim 7-CH), 7.28-7.40 (m, 5H, f-phen 3-CH, f-phen 6-CH, phen 3-CH, phen 4-CH, phen 5-CH), 7.43-7.48 (m, 1H, f-phen 4-CH), 7.52-7.56 (m, 3H, f-phen 5-CH, phen 2-CH, phen 6-CH), **^{13}C-NMR** (100 MHz, $CDCl_3$): δ (ppm) 34.2 (2'-CH_2), 41.9 (3'-CH_2), 54.5 (1'-CH), 108.8 (d, *J* = 1.7 Hz, benzim 4-CH), 109.0 (benzim 7-CH), 117.1 (d, *J* = 19.5 Hz, f-phen 3-CH), 121.6 (benzim 5-CH), 121.9 (f-phen 1-C), 122.0 (benzim 6-CH), 124.8 (d, *J* = 3.9 Hz, f-phen 6-CH), 127.3 (phen 2-CH), 127.3 (phen 6-CH), 128.1 (phen 4-CH), 128.8 (phen 3-CH), 128.8 (phen 5-CH), 129.4 (benzim 3a-C), 129.5 (f-phen 5-CH), 130.2 (d, *J* = 7.8 Hz, f-phen 4-CH), 138.4 (phen 1-C), 153.0 (benzim 2-CO), 157.9 (d, *J* = 253.2 Hz, f-phen 2-CF), due to limited resolution of the measuring apparatus, quaternary carbon benzim 7a-C could not be detected, **^{19}F-NMR** (471 MHz, $CDCl_3$): δ (ppm) -118.39 (m, f-phen 2-CF), **MS**: m/z (%) 380 (M^+, 12), 228 (100), 199 (5), 153 (3), 117 (7), 91 (49), 75 (5), **HRMS**: m/z calculated for $C_{22}H_{19}ClFN_2O$ $[M + H]^+$: 381.1170. Found: 381.1164.

General procedure for the synthesis of 22-24

A solution of starting materials **19**, **20**, or **21** (1 mmol) and NaI (1.03 g, 6.89 mmol) in acetone (7 ml) was refluxed for 24 h. The precipitate formed was filtered and the solvent was removed *in vacuo*.

1-(1-(4-Fluorophenyl)-3-iodopropyl)-3-phenyl-1,3-dihydro-2*H*-benzimidazol-2-one (22) Yield: 82%, yellow resin, **^{1}H-NMR** (200 MHz, $CDCl_3$): δ (ppm) 2.77-2.92 (m, 1H), 3.14-3.31 (m, 3H), 5.63-5.70 (m, 1H), 7.01-7.10 (m, 6H), 7.36-7.56 (m, 7H), **^{13}C-NMR** (50 MHz, $CDCl_3$): δ (ppm) 2.3, 35.3, 57.0, 108.8, 108.9, 115.5, 115.9, 121.6, 122.0, 126.0, 127.7, 128.5, 129.1, 129.3, 129.4, 134.0, 134.1, 134.3, 153.0, 159.9, 164.8, **MS**: m/z (%) 472 (M^+, 32), 317 (8), 210 (100), 181 (11), 167 (23), 140 (3), 135 (43), 115 (8), 109 (34), 77 (15), 51 (7), **HRMS**: m/z calculated for $C_{22}H_{18}FIN_2ONa$ $[M + Na]^+$: 495.0346. Found: 495.0353.

1-(4-fluorophenyl)-3-(3-iodo-1-phenylpropyl)-1,3-dihydro-2*H*-benzimidazol-2-one (23) Yield: 76%,

yellow crystals, mp. 39°C-41°C, purification: silica gel 60, petrol ether/ethyl acetate 9:1, **^{1}H-NMR** (200 MHz, $CDCl_3$): δ (ppm) 2.81-2.99 (m, 1H, 2'-CH_2), 3.11-3.35 (m, 3H, 2'-CH_2, 3'-CH_2), 5.70 (dd, *J* = 6 Hz and 2 Hz, 1H, 1'-CH), 7.04-7.09 (m, 4H, benzim 4-CH, benzim 5-CH, benzim 6-CH, benzim 7-CH), 7.17-7.42 (m, 5H, f-phen 3-CH, f-phen 5-CH, phen 4-CH, phen 2-CH, phen 5-CH), 7.51-7.57 (m, 4H, f-phen 2-CH, f-phen 6-CH, phen 2-CH, phen 6-CH), **^{13}C-NMR** (50 MHz, $CDCl_3$): δ (ppm) 2.4 (2'-CH_2), 35.2 (3'-CH_2), 57.6 (1'-CH), 108.6 (benzim 4-CH), 109.2 (benzim 7-CH), 116.4 (d, *J* = 23 Hz, f-phen 3-CH), 116.4 (d, *J* = 23 Hz, f-phen 5-CH), 121.6 (benzim 5-CH), 122.1 (benzim 6-CH), 127.3 (phen 2-CH), 127.3 (phen 6-CH), 127.8 (phen 4-CH), 128.1 (d, *J* = 5 Hz, f-phen 2-CH), 128.1 (d, *J* = 5 Hz, f-phen 6-CH), 128.5 (benzim 7a-C), 128.8 (phen 3-CH), 128.8 (phen 5-CH), 129.4 (benzim 3a-C), 130.3 (d, *J* = 3Hz, f-phen 1-C), 138.1 (phen 1-C), 153.2 (benzim 2-CO), 161.6 (d, *J* = 247 Hz, f-phen 4-CF), **MS**: m/z (%) 472 (M^+, 13), 317 (5), 228 (100), 185 (15), 117 (47), 103 (2), 91 (40), 75 (8), 55 (5), **HRMS**: m/z calculated for $C_{22}H_{19}FIN_2O$ $[M + H]^+$: 473.0526. Found: 473.0506.

1-(2-fluorophenyl)-3-(3-iodo-1-phenylpropyl)-1,3-dihydro-2*H*-benzimidazol-2-one (24) Yield: 53%, yellow crystals, mp. 38°C-39°C, purification: silica gel 60, petrol ether/ethyl acetate 9:1, **^{1}H-NMR** (200 MHz, $CDCl_3$): δ (ppm) 2.80-2.98 (m, 1H, 2'-CH_2), 3.13-3.36 (m, 3H, 2'-CH_2, 3'-CH_2), 5.67-5.74 (m, 1H, 1'-CH), 6.85-6.88 (m, 1H, benzim 4-CH) 6.99-7.07 (m, 3H, benzim 5-CH, benzim 6-CH, benzim 7-CH), 7.26-7.45 (m, 5H, f-phen 3-CH, f-phen 6-CH, phen 3-CH, phen 4-CH, phen 5-CH), 7.47-7.58 (m, 4 H, f-phen 4-CH, f-phen 5-CH, phen 2-CH, phen 6-CH), **^{13}C-NMR** (50 MHz, $CDCl_3$): δ (ppm) 2.3 (2'-CH_2), 35.4 (3'-CH_2), 57.6 (1'-CH), 108.9 (d, *J* = 1.5 Hz, benzim 4-CH), 109.1 (benzim 7-CH), 117.1 (d, *J* = 19 Hz, f-phen 3-CH), 121.6 (benzim 5-CH), 121.9 (f-phen 1-C), 122.0 (benzim 6-CH), 124.8 (d, *J* = 3.5 Hz, f-phen 6-CH), 127.3 (phen 2-CH), 127.3 (phen 6-CH), 128.1 (phen 4-CH), 128.8 (phen 3-CH), 128.8 (phen 5-CH), 129.5 (f-phen 5-CH), 130.2 (d, *J* = 8 Hz, f-phen 4-CH), 138.2 (phen 1-C), 153.0 (benzim 2-CO), 157.8 (d, *J* = 251.5 Hz, f-phen 2-CF), **MS**: m/z (%) 472 (M^+, 9), 317 (5), 241 (4), 228 (100), 199 (5), 185 (10), 117 (37), 91 (29), 75 (7), **HRMS**: m/z calculated for $C_{22}H_{19}FIN_2O$ $[M + H]^+$: 473.0526. Found: 473.0532.

General procedure for the synthesis of 1-(3-Amino-1-(4-fluorophenyl)propyl)-3-phenyl-1,3-dihydro-2*H*-benzimidazol-2-one (25)

1-(1-(4-fluorophenyl)-3-iodopropyl)-3-phenyl-1,3-dihydro-2*H*-benzimidazol-2-one (0.26 g, 0.55 mmol) and a solution of NH_3 in isopropanol (2 M, 22 ml) were heated in a sealed tube for 3 h at 80°C. After evaporation of the solvent, the crude product was purified by column chromatography (silica gel 60, CH_2Cl_2/MeOH 9:1). Yield: 0.10 g (50%), light brown crystals, mp. 87°C-88°C

^{1}H-NMR (400 MHz, $CDCl_3$): δ (ppm) 2.74-2.84 (m, 3H, 2'-CH_2, 3'-CH_2), 2.98-3.04 (m, 1H, 3'-CH_2), 5.74-5.78 (m, 1H, 1'-CH), 6.79-6.81 (m, 1H, benzim 7-CH), 6.96-7.01 (m, 5H, benzim 4-CH, benzim 5-CH, benzim 6-CH, f-phen 3-CH, f-phen 5-CH), 7.30-7.33 (m, 1H, phen 4-CH), 7.40-7.48 (m, 4H, f-phen 2-CH, f-phen 6-CH, phen 3-CH, phen 5-CH), 7.52-7.54 (m, 2H, phen 2-CH, phen 6-CH), due to limited resolution of the measuring apparatus, protons NH_2 could not be detected, **^{13}C-NMR** (100 MHz, $CDCl_3$): δ (ppm) 30.3 (2'-CH_2), 37.8 (3'-CH_2), 52.7 (1'-CH), 109.2 (benzim 4-CH), 110.0 (benzim 7-CH), 115.7 (d, *J* = 21.5 Hz, f-phen 3-CH), 115.7 (d, *J* = 8.2 Hz, f-phen 5-CH), 122.0 (benzim 5-CH), 122.3 (benzim 6-CH), 126.4 (phen 2-CH), 126.4 (phen 6-CH), 127.5 (benzim 7a-C), 128.1 (phen 4-CH), 129.2 (d, *J* =

8.2 Hz, f-phen 2-CH), 129.2 (d, *J* = 8.2 Hz, f-phen 6-CH), 129.5 (benzim 3a-C), 129.7 (phen 3-CH), 129.7 (phen 5-CH), 133.3 (d, *J* = 3.2 Hz, f-phen 1-C), 134.0 (phen 1-CH), 153.8 (benzim 2-CO), 162.3 (d, *J* = 247.4 Hz, f-phen 4-CF), **^{19}F-NMR** (471 MHz, $CDCl_3$): δ (ppm) -113.68 (m, f-phen CF), **MS**: m/z (%) 361 (M^+, 17), 331 (10), 210 (100), 181 (15), 167 (16), 149 (29), 128 (17), 77 (19), 57 (20), 43 (12), **HRMS**: m/z calculated for $C_{22}H_{21}FN_3O$ $[M + H]^+$: 362.1669. Found: 362.1674.

General procedure for the synthesis of 4-6

Starting materials **18**, **19** or **20** (1 mmol) and a solution of methylamine in EtOH (12.5 ml, 8 M) were heated in a sealed tube for 3 h at 80°C. After evaporation of the solvent, the crude reaction product was purified by column chromatography.

1-(1-(4-Fluorophenyl)-3-(methylamino)propyl)-3-phenyl-1,3-dihydro-2*H*-benzimidazol-2-one (4) Yield: 48%, light orange resin, purification: silica gel 60, dichloromethane/methanol 9:1 and dichloromethane/ethyl acetate/methanol 7:2:1, **^{1}H-NMR** (400 MHz, $CDCl_3$): δ (ppm) 2.42 (s, 3H, $NHCH_3$), 2.57-2.74 (m, 4H, 2'-CH_2, 3'-CH_2), 3.15 (br s, 1H, $NHCH_3$), 5.76-5.79 (m, 1H, 1'-CH), 6.88-6.90 (m, 1H, benzim 7-CH), 6.97-7.05 (m, 4H, benzim 5-CH, benzim 6-CH, f-phen 3-CH, f-phen 5-CH), 7.07-7.10 (m, 1H, benzim 4-CH), 7.39-7.43 (m, 1H, phen 4-CH), 7.46-7.57 (m, 6H, f-phen 2-CH, f-phen 6-CH, phen 2-CH, phen 3-CH, phen 5-CH, phen 6-CH), **^{13}C-NMR** (100 MHz, $CDCl_3$): δ (ppm) 30.6 (2'-CH_2), 35.9 ($NHCH_3$), 48.3 (3'-CH_2), 53.1 (1'-CH), 108.9 (benzim 4-CH), 109.5 (benzim 7-CH), 115.5 (d, *J* = 21.5 Hz, f-phen 3-CH), 115.5 (d, *J* = 21.5 Hz, f-phen 5-CH) 121.4 (benzim 5-CH), 121.8 (benzim 6-CH), 126.0 (phen 2-CH), 126.0 (phen 6-CH), 127.7 (phen 4-CH), 128.0 (benzim 7a-C), 129.0 (d, *J* = 8.1 Hz, f-phen 2-CH), 129.0 (d, *J* = 8.1 Hz, f-phen 6-CH), 129.4 (benzim 3a-C), 129.5 (phen 3-CH), 129.5 (phen 5-CH), 134.4 (phen 1-CH), 134.6 (d, *J* = 3.4 Hz, f-phen 1-CH), 153.5 (benzim 2-CO), 162.1 (d, *J* = 246.7 Hz, f-phen 4-CF), **^{19}F-NMR** (471 MHz, $CDCl_3$): δ (ppm) -114.36 (m, f-phen 4-CF), **MS**: m/z (%) 375 (M^+, 16), 210 (57), 181 (10), 167 (12), 150 (10), 109 (22), 97 (16), 71 (27), 57 (78), 44 (100), **HRMS**: m/z calculated for $C_{23}H_{23}FN_3O$ $[M + H]^+$: 376.1825. Found: 376.1821.

1-(4-fluorophenyl)-3-(3-(methylamino)-1-phenylpropyl)-1,3-dihydro-2*H*-benzimidazol-2-one (5) Yield: 29%, light yellow crystals, mp. 100°C-102°C, purification: silica gel 60, dichloromethane/methanol 9:1 and RP-18 silica gel methanol/water 9:1 and 7:3, **^{1}H-NMR** (200 MHz, $CDCl_3$): δ (ppm) 2.53 (s, 3H, $NHCH_3$), 3.13 (br s, 4H, 2'-CH_2, 3'-CH_2), 5.77-5.81 (m, 1H, 1'-CH), 6.96-7.03 (m, 4H, benzim 4-CH, benzim 5-CH, benzim 6-CH, benzim 7-CH), 7.16-7.34 (5H, f-phen 3-CH, f-phen 5-CH, phen 4-CH, phen 2-CH, phen 5-CH), 7.49-7.56 (m, 4H, f-phen 2-CH, f-phen 6-CH, phen 2-CH, phen 6-CH), due to limited resolution of the measuring apparatus, proton NH could not be detected, **^{13}C-NMR** (50 MHz, $CDCl_3$): δ (ppm) 27.6 (2'-CH_2), 33.1 ($NHCH_3$), 47.0 (3'-CH_2), 54.2 (1'-CH), 108.8 (benzim 4-CH), 109.9 (benzim 7-CH), 116.6 (d, *J* = 23 Hz, f-phen 3-CH), 116.6 (d, *J* = 23 Hz, f-phen 5-CH), 122.1 (benzim 5-CH), 122.6 (benzim 6-CH), 127.2 (phen 2-CH), 127.2 (phen 6-CH), 127.7 (phen 4-CH), 128.3 (d, *J* = 6 Hz, f-phen 2-CH), 128.3 (d, *J* = 6 Hz, f-phen 6-CH), 128.4 (benzim 7a-C), 128.9 (phen 3-CH), 128.9 (phen 5-CH), 129.2 (benzim 3a-C), 129.7 (d, *J* = 3 Hz, f-phen 1-C), 136.9 (phen 1-C), 153.4 (benzim 2-CO), 161.7 (d, *J* = 248 Hz, f-phen 4-CF), **MS**: m/z (%) 375 (M^+, 11), 330 (7), 228 (50), 199 (7), 185 (9), 147 (17), 128 (26), 117 (8), 91 (13), 58 (34), 44 (100), **HRMS**: m/z calculated for $C_{23}H_{23}FN_3O$ $[M + H]^+$: 376.1825. Found: 376.1828.

1-(2-fluorophenyl)-3-(3-(methylamino)-1-phenylpropyl)-1,3-dihydro-2*H*-benzimidazol-2-one (6) Yield: 30%, yellow crystals, mp. 92°C-93°C, purification: silica gel 60, dichloromethane/methanol 9:1 and RP-18 silica gel methanol/water 9:1 and 7:3, **^{1}H-NMR** (200 MHz, $CDCl_3$): δ (ppm) 2.57 (s, 3H, $NHCH_3$), 3.01-3.15 (m, 4H, 2'-CH_2, 3'-CH_2), 5.75-5.86 (m, 1H, 1'-CH), 6.83-6.87 (m, 1H, benzim 4-CH) 6.98-7.05 (m, 3H, benzim 5-CH, benzim 6-CH, benzim 7-CH), 7.25-7.42 (m, 5H, f-phen 3-CH, f-phen 6-CH, phen 3-CH, phen 4-CH, phen 5-CH), 7.48-7.61 (m, 4 H, f-phen 4-CH, f-phen 5-CH, phen 2-CH, phen 6-CH), due to limited resolution of the measuring apparatus, proton $NHCH_3$ could not be detected, **^{13}C-NMR** (50 MHz, $CDCl_3$): δ (ppm) 27.7 (2'-CH_2), 33.2 (NHCH3), 46.9 (3'-CH_2), 53.5 (1'-CH), 109.0 (benzim 4-CH), 110.1 (benzim 7-CH), 117.1 (d, *J* = 19.5 Hz, f-phen 3-CH), 122.2 (benzim 5-CH), 122.7 (benzim 6-CH), 125.1 (d, *J* = 3.0 Hz, f-phen 6-CH), 127.3 (phen 2-CH), 127.1 (phen 6-CH), 128.3 (phen 4-CH), 128.9 (phen 3-CH), 128.9 (phen 5-CH), 129.5 (f-phen 5-CH), 130.7 (d, *J* = 4.5 Hz, f-phen 4-CH), 136.5 (phen 1-C), 153.6 (benzim 2-CO), 157.6 (d, *J* = 250.5 Hz, f-phen 2-CF), due to limited resolution of the measuring apparatus, quaternary carbon f-phen 1-C could not be detected, **MS**: m/z (%) 375 (M^+, 17), 318 (10), 228 (82), 199 (9), 185 (9), 147 (16), 128 (35), 117 (9), 91 (20), 58 (43), 44 (100), **HRMS**: m/z calculated for $C_{23}H_{23}FN_3O$ $[M + H]^+$: 376.1825. Found: 376.1822.

3.3. Computational Methods

The ligand structures were built in the protonated form using Molecular Operating Environment (MOE) 2013.[42] Homology models of human NET, SERT and DAT were obtained from the *Drosophila* dopamine transporter template ($dDAT_{cryst}$, PDB id 4M48[43]), by selecting the model with the most favorable Discrete Optimized Protein Energy (DOPE) of 250 generated by Modeller 9.11.[44] The co-crystallized inhibitor nortriptyline was retained during model generation and the compounds were docked in the same site using Genetic Optimization for Ligand Docking (GOLD) 5.2.[45] One hundred poses per ligand (i.e. five hundred poses per protein target) were generated based on the GoldScore scoring function, while keeping the ligand flexible and the protein rigid.

The common chemical scaffold, i.e. the reference compound, was extracted from the resulting poses, analogous to the methods of our previous study.[46] Cluster analysis was performed based on Euclidian distance and complete linkage of the root-mean square deviation of the ligand's heavy atoms matrix using XLStat.[47] The dendrogram was cut at eight clusters and the ones containing all five ligands were selected.

Figure 5. *Left column*: Overlay of compounds **1**, **2**, and **4-6** (maroon) in binding hypothesis 1 and comparison with the co-crystal pose of nortriptyline (**31**) (green). In NET, V148 allows more space than I172 in SERT. The angle between ligand ring 2 and 3 is ca. 60° in all poses. *Right column*: Overlay of compounds **1**, **2**, and **4-6** (maroon) in binding hypothesis 2. In NET, V148 still allows more space than in hSERT, whereas E439 might disrupt ligand ring 3. DAT lacks a more potent stacking interaction due to F155 as compared to NET[Y151] and SERT[Y175]. Binding mode 2 poses are more in agreement with the co-crystal pose. The angle between ligand ring 2 and 3 is almost 90° in all poses. The extracellular space is located above in all figures.

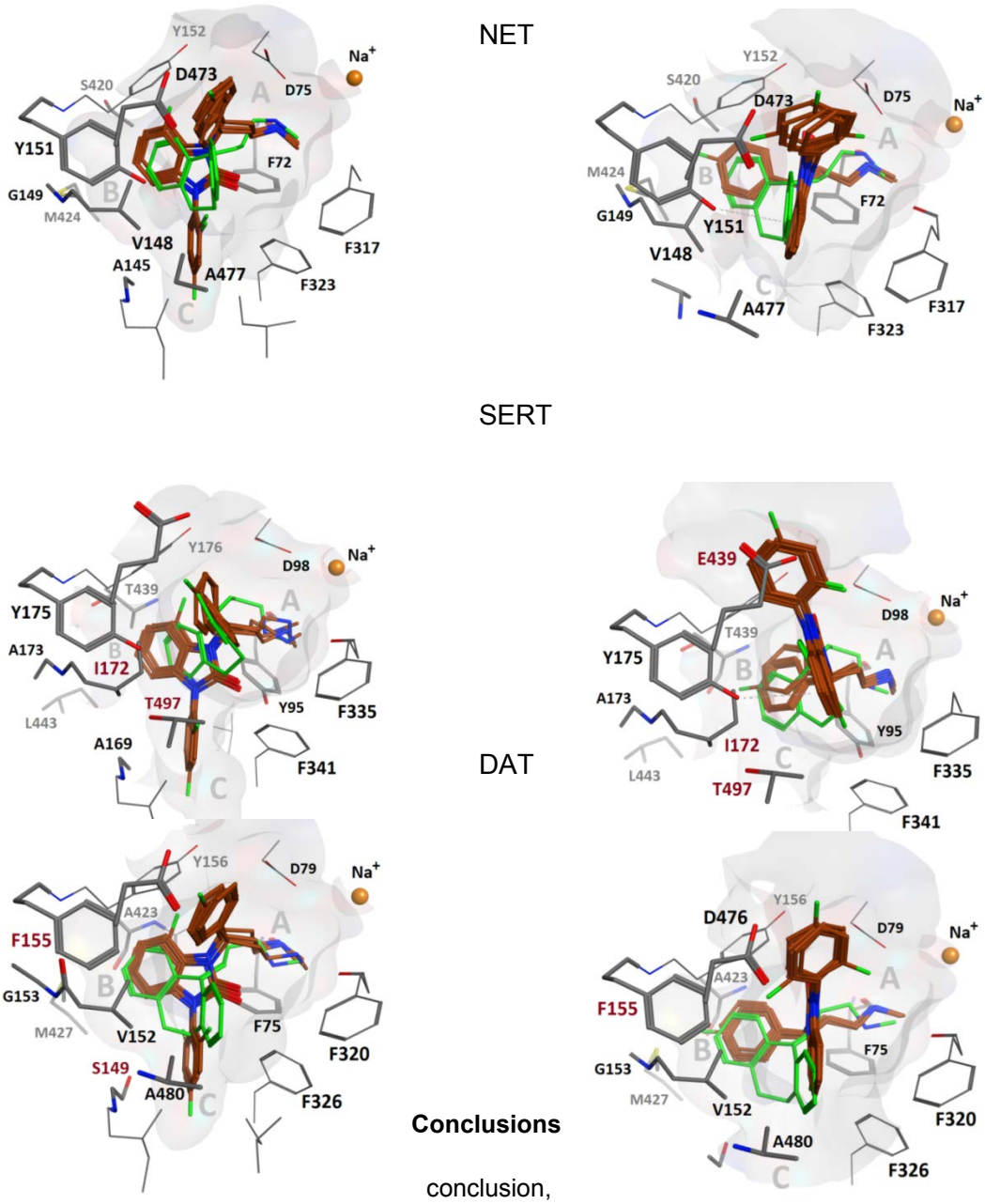

4. Conclusions

In conclusion, four new final compounds have been synthesized within the scope of this work, which aimed at the development of new, selective, high affinity references for the imaging of the NET system *via* PET. Whilst methylamines **4-6** (FAPPI:1-3) represent reference compounds for their later prepared radioactive analogs, additionally prepared free amine **25** (APPI:1) will serve as precursor for

radiolabeling. Compounds **4**-**6** will be evaluated for affinity and selectivity towards the NET and additionally will be subject of lipophilicity and blood brain barrier penetration experiments at the Medical University of Vienna. Docking studies indicate that fluorinated methyl amines **4-6** (FAPPI:1-3) bind in an analogous way to the NET as reference compound **1**. Thus these compounds (**4-6**) are promising candidates for biological evaluation. The most promising derivatives regarding their suitability as NET ligands will then be selected for the further development of new and selective PET tracers for the NET, which will comprise either a [^{11}C]methylamine, [^{18}F]fluoroalkyl amine or [^{18}F]fluorobenzene radiolabel, respectively. The results of ongoing studies on affinity, selectivity and lipophilicity of the discussed compounds, will be published in a following paper.

Acknowledgments

AS, AJ, and GFE acknowledge financial support provided by the Austrian Science Fund, grants AW/0123221 and F3502.

Conflicts of Interest

The authors declare no conflict of interest.

References and Notes

1. Sung, U.; Apparsundram, S.; Galli, A.; Kahlig, K. M.; Savchenko, V.; Schroeter, S.; Quick, M. W.; Blakely, R. D. *J. Neurosci*, **2003**, 23, 1697.
2. Kim, C. H.; Hahn, M. K., Joung, Y.; Anderson, S. L.; Steele, A. H.; Mazei-Robinson, M. S.; Gizer, I.; Teicher, M. H.; Cohen, B. M.; Robertson, D.; Walman, I. D.; Blakely, R. D.; Kim, K. S. *PNAS*, **2006**, 103, 19164.
3. Hahn, M. K.; Robertson, D.; Blakely, R. D. *J. Neurosci*., **2003**, 23, 4470.
4. Mirbolooki, M. R.; Upadhyay, S. K.; Constantinescu, C. C.; Pan, M. L.; Mukherjee, J. *Nucl. Med. Biol.*, **2014**, 41, 10.
5. Lin, S. L; Fan, X.; Yeckel, C. W.; Weinzimmer, D.; Mulnix, T.; Gallezot, J. D.; Carson, R. E.; Sherwin, R. S.; Ding, Y. S *Nuc. Med. Biol.*, **2012**, 39, 1081.
6. Stöber, G.; Nöthen, M. M.; Pörzgen, P.; Brüss, M.; Bönisch, H.; Knapp, M.; Beckmann, H.; Propping, P. *American Jounal of Medical Genetics (Neuropsychiatric Genetics)*, **1996**, 67, 523.
7. Young, J. B.; Landsberg, L. *Catecholamines and the adrenal medulla*. In: Williams Textbook of Endocrinology, 9th Ed., Wilson, J. D., Foster, D. W. (Eds.) W. B. Saunders Co., Philadelphia, **1998**, 680.
8. Tellioglu, T.; Robertson, D. *Exp. Rev. Mol. Med*., **2001**, 1.
9. Blakely, R. D.; Bauman, A. L., *Curr. Opin. Neurobiol.*, **2000**, 10, 328.
10. Zhu, M. Y.; Shamburger, S.; Li, J.; Ordway, G. A. *Journal of Pharmacology and Experimental Therapeutics*, **2000**, 295, 951.

11. Moron, J. A.; Grockington, A.; Wise, R. A.; Rocha, B. A.; Hope, B. T. *J. Neurosci.*, **2002**, 22, 386.

12. Schroeter, S.; Apparsundaram, S.; Wiley, R. G.; Miner, L. H.; Sesack, S. R.; Blakely, R. D. *The Journal of comparative neurology*, **2000**, 420, 211.

13. Torres, G. E.; Gainetdinov, R. R.; Caron, M. G. *Nature Reviews Neuroscience*, **2003**, 4, 13.

14. Ordway, G. A.; Stockmeier, C. A.; Cason, G. W.; Klimek, V. *J. Neurosci.*, **1997**, 17, 1710.

15. Smith, H. R.; Beveridge, T. J. R.; Porrino, L. J. *Neuroscience*, **2006**, 138, 703.

16. Zhou, J. *Drugs Future*, **2004**, 29, 1235.

17. Curatolo, P.; D'Agati, E.; Moavero, R. *Ital. J. Pediatr.*, **2010**, 36, 79.

18. Mash, D. C.; Ouyang, Q.; Qin, Y.; Pablo, J. *Neurosci. Methods*, **2005**, 143, 79.

19. Barr, C. L.; Kroft, J.; Feng, Y.; Wigg, K.; Roberts, W.; Malone, M.; Ickowicz, A.; Schachar, R.; Tannock, R.; Kennedy, J. L. *American Journal of Medical Genetics (Neuropsychiatric Genetics)*, **2002**, 114, 255.

20. Klimek, V.; Stockmeier, C.; Overholser, J.; Meltzer, H. Y.; Kalka, S.; Dilley, G.; Ordway, G. A. *J. Neurosci.*, **1997**, 17, 8451.

21. Nedergaard, J.; Cannon, B. *Cell Metabolism*, **2010**, 11, 268.

22. Gulyas, B.; Brockschnieder, D.; Nag, S.; Pavlova, E.; Kasa, P.; Beliczai, Z.; Legradi, A.; Gulya, K.; Thiele, A.; Dyrks, T.; Halldin, C. *Neurochem Int* 56, 789-798.

23. Wilson, A. A.; Johnson, D. P.; Mozley, D.; Hussey, D.; Ginovart, N.; Nobrega, J.; Garcia, A.; Meyer, J.; Houle, S. *Nucl Med Biol.*, **2003**, 30, 85.

24. Takano, A.; Gulyas, B.; Varrone, A.; Halldin, C. *Eur. J. Nucl. Med. Mol. Imaging*, **2009**, 36, 1885.

25. Schou, M.; Zoghbi, S. S.; Shetty, H. U.; Shchukin, E.; Liow, J. S.; Hong, J.; Andrée, B. A.; Gulyás, B.; Farde, L.; Innis, R. B.; Pike, V. W.; Halldin, C. Mol Imaging Biol. **2009**, 11, 23.

26. Zhang, P.; Terefenko, E. A.; McComas, C. C.; Mahaney, P. E.; Vu, A.; Trybulski, E.; Koury, E.; Johnston, G.; Bray, J.; Deecher, D. *Bioorg. Med. Chem. Lett.*, **2008**, 18, 6067.

27. Mark, C.; Bornatowicz, B.; Mitterhauser, M.; Hendl, M.; Nics, L.; Haeusler, D.; Lanzenberger, R.; Berger, M. L.; Spreitzer, H.; Wadsak, W. *Nucl. Med. Biol.*, **2013**, 40, 295.

28. Penmatsa, A.; Wang, K. H.; Gouaux, E. *Nature*, **2013**, 503, 85.

29. Wang, H.; Goehring, A.; Wang, K. H.; Penmatsa, A.; Ressler, R.; Gouaux, E. *Nature*, **2013**, 503, 141.

30. Tatsumi, M.; Groshan, K.; Blakely, R. D.; Richelson, E. *European Journal of Pharmacology*, **1997**, 340, 249.

31. Richter, L.; de Graaf, C.; Sieghart, W.; Varagic, Z.; Morzinger, M.; de Esch, I. J.; Ecker, G. F.; Ernst, M., *Nature chemical biology*, **2012**, 8, 455-64.

32. Andersen, J.; Olsen, L.; Hansen, K. B.; Taboureau, O.; Jorgensen, F. S.; Jorgensen, A. M.; Bang-Andersen, B.; Egebjerg, J.; Stromgaard, K.; Kristensen, A. S. *The Journal of biological chemistry*, **2010**, 285, 2051.

33. Bissantz, C.; Kuhn, B.; Stahl, M. *J. Med. Chem.*, **2010**, 53, 5061.

34. Chelli, R.; Gervasio, F. L.; Procacci, P.; Schettino, V. *J. Am. Chem. Soc.*, **2002**, 124, 6133.

35. Yu, F.; Zhou, J. N.; Zhang, X. C.; Sui, Y. Z.; Wu, F. F.; Xie, L. J.; Chan, A. S. C.; Wu, J. *Chemistry - A European Journal*, **2011**, 17, 14234.

36. Varney, M. D.; Romines, W. H.; Boritzki, T.; Margosiak, S. A.; Barlett, C.; Howland, E. J. *J. Heterocyclic Chem.*, **1995**, 32, 1493.

37. La Regina, G.; Diodata D'Auria, F.; Tafi, A.; Piscitelli, F.; Olla, S.; Caporuscio, F.; Nencioni, L.; Cirilli, R.; La Torre, F.; Rodrigues De Melo, N.; Kelly, S. L.; Lamb, D. C.; Artico, M.; Botta, M.; Palamara, A. T.; Silvestri, R. *J. Med. Chem.*, **2008**, 51, 3841.

38. Xu, Z. B.; Lu, Y.; Guo, Z. R. *Synlett*, **2003**, 4, 564.

39. Panagopoulos, A. M.; Steinman, D.; Goncharenko, A.; Geary, K.; Schleisman, C.; Spaargaren, E.; Zeller, M.; Becker, D. P. *JOC*, **2013**, 78, 3532.

40. Wang, X. J.; Xi, M. Y.; Fu, J. H.; Zhang, F. R.; Cheng, G. F.; Yin, D. L.; You, Q. D. *Chinese Chemical Letters*, **2012**, 23, 707.

41. Liu, P.; Wang, Z.; Hu, X. *European Journal of Organic Chemistry*, **2012**, 10, 1994.

42. Molecular Operating Environment (MOE), C. C. G. I., 1010 Sherbooke St. West, Suite #910, Montreal, QC, Canada, H3A 2R7, **2013**.

43. Penmatsa, A.; Wang, K. H.; Gouaux, E. *Nature*, **2013**, 503, 85.

44. Sali, A.; Potterton, L.; Yuan, F.; van Vlijmen, H.; Karplus, M. *Proteins*, **1995,** 23, 318.

45. Jones, G.; Willett, P.; Glen, R. C.; Leach, A. R.; Taylor, R. *Journal of Molecular Biology*, **1997,** 267, 727.

46. Richter, L.; de Graaf, C.; Sieghart, W.; Varagic, Z.; Morzinger, M.; de Esch, I. J.; Ecker, G. F.; Ernst, M. *Nature Chemical Biology*, **2012**, 8, 455.

47. Addinsoft Inc., N. Y., NY. USA.

Sample Availability: Samples of the compounds **4-6**, **9-25**, and **29** and **30** are available from the authors.

3.1.6 Manuscript #5

COMPARATIVE IN VITRO EVALUATION OF THE NOREPINEPHRINE TRANSPORTER PET-LIGANDS [^{11}C]ME@APPI AND [^{18}F]FMENER-D2

J Nucl Med, 2015, in review.

Christina Rami-Mark[a,b], Cecile Philippe[a], Chrysoula Vraka[a], Lukas Nics[a], Monika Dumanic[a], Helmut Spreitzer[c], Rupert Lanzenberger[d], Marcus Hacker[a], Wolfgang Wadsak[a,b*] and Markus Mitterhauser[a,e]

[a] *Department of Biomedical Imaging und Image-guided Therapy, Division of Nuclear Medicine, Medical University of Vienna, Austria.*

[b] *Department of Inorganic Chemistry, University of Vienna, Austria.*

[c] *Department of Pharmaceutical Chemistry, Division of Drug Synthesis, University of Vienna, Austria.*

[d] *Department of Psychiatry and Psychotherapy, Division of Biological Psychiatry, Medical University of Vienna, Austria.*

[e] *Department of Pharmaceutical Technology and Biopharmaceutics, University of Vienna, Austria*

Word Count: 4990 words

Short Title: ^{11}C-Me@APPI vs. ^{18}F-FMeNER-D2

* **Corresponding Author:**
Prof. Dr. Wolfgang Wadsak,
Department of Biomedical Imaging und Image-guided Therapy, Division of Nuclear Medicine, Medical University of Vienna, Austria.
Tel.: +43-1-40400-55330; fax: +43-1-40400-15590; e-mail: wolfgang.wadsak@meduniwien.ac.at

Journal of Nuclear Medicine [IF= 5.774]

First Author:

Christina Rami-Mark MSc., phD student,
Department of Biomedical Imaging und Image-guided Therapy, Division of Nuclear Medicine, Medical University of Vienna, Austria.
Tel.: +43-1-40400-78350; fax: +43-1-40400-15590; e-mail: christina.rami-mark@meduniwien.ac.at

ABSTRACT

The norepinephrine transporter (NET) is involved in a plethora of psychiatric and neurological diseases. For gaining in vivo insight in the NET system and its pathological perturbations, molecular imaging using positron emission tomography can be used. Therefore, specific NET-PET ligands are required. Recently the radiosynthesis of the novel PET tracer ^{11}C-Me@APPI for the NET was described.

Methods:

This study addresses the comparative evaluation of the NET-PET tracers ^{11}C-Me@APPI and [^{18}F]FMeNER-D2 regarding their metabolic stability, passive diffusion through blood-brain-barrier (BBB) and binding behavior in in vitro autoradiography.

Results:

^{11}C-Me@APPI displayed outstanding metabolic stability, high affinity and is likely to passively penetrate the BBB in in vitro experiments. Moreover, selective NET binding in in vitro autoradiography was observed in human and rat brain tissue as well as in murine heart samples. All values were comparable or enhanced to those obtained with so far used [^{18}F]FMeNER-D2. Interestingly, binding enhancement was observed for ^{11}C-Me@APPI in brain regions.

Conclusion*:*

All tested preclinical parameters indicate that ^{11}C-Me@APPI is a suitable NET-PET-tracer and will be further evaluated in in vivo studies.

Keywords:

Norepinephrine transporter • PET • NET • radiochemistry • autoradiography

INTRODUCTION

The norepinephrine transporter (NET) is a presynaptic monoamine transporter and facilitates the reuptake of noradrenalin from the synaptic cleft into the cytosol – thereby terminating the noradrenergic action on postsynaptic adrenoreceptors. The involvement of the NET is reported in various psychiatric and neurodegenerative disorders, like attention deficit hyperactivity disorder, major depression or Alzheimer's dementia (*1-3*). Furthermore, a profound influence of noradrenaline, and more specifically, the NET in the arising of motor disturbances of Parkinson's disease is discussed (*4-8*). Besides, reduced NET levels were also described in cardiovascular diseases such as hypertension, cardiomyopathy, and heart failure (*9, 10*).

The NET distribution throughout the brain is rather low, peaking in the highest density in locus coeruleus (LC) (*11*) – the major noradrenergic nucleus in brain. From this area noradrenergic axons project to and modulate all areas of the brain (*12*), as well as it elicits control over the cardiovascular system (*10)*. Thus, precise NET-localization is essential for the comprehension of the role of altered neurotransmission in these illnesses. Effective therapy monitoring on a molecular level and deeper understanding of the underlying (patho-)physiological mechanisms is particularly feasible in vivo. Hence, there is an increasing need for non-invasive imaging techniques to visualize the functionality and abundance of NET in humans and animal models. To gain insight in the molecular perturbations in the noradrenergic system, positron emission tomography (PET) is the method of choice. Therefore, specific NET-PET tracers have to be developed meeting certain requirements (*13)*:

Firstly, the density of the NET in human brain is rather low, considering a B_{max} value of 4.4 nM for NET in the human insular cortex (*3*). Given the paucity of NET in utmost human brain regions, the affinity of the NET-PET tracers must be high, to guarantee reliable imaging. In other regions, such as the LC, NET-density is 4-8 fold higher. Thus, imaging of these regions might be possible also with slightly lower affinity NET-PET-ligands (*14-16)*, i.e. <10nM.

Secondly, high selectivity of the candidate tracers is mandatory. Due to the high degree of similarity of the NET to the dopamine transporter (DAT) and serotonin transporter (SERT), both highly abundant in human brain, the majority of NET ligands tend to bind also to a certain degree to these monoamine transporters (*17-20)*. This non-target binding presents a large challenge to newly developed tracers.

Moreover, PET-tracers need to be highly stable to assure an optimum signal-to-noise-ratio. Although stability in human blood, plasma or against human enzymes is the ultimate goal, it is important not to overlook the metabolic stability in small animals. To foster a better understanding of molecular mechanisms, small animal studies are often the method of choice. Potential brain metabolites are only assessable in a preclinical model, and therefore metabolic stability should be also assessed in the respective animal model.

Furthermore, the likelihood of blood brain barrier (BBB) penetration should be evaluated closely in cerebral PET tracer development. Therefore, high throughput methods for quantification of passive diffusion through the BBB, such as immobilized artificial membrane (IAM) chromatography can be used. It is noteworthy that also other mechanisms attribute to BBB penetration.

These methods enable a classification of candidate tracers without the use of animal studies (21). It is evident that logP values as such are insufficient for prediction of BBB passage (22), but might still provide useful information regarding non-specific binding.

To complete the preclinical portfolio, candidate tracers have to be tested in vitro in autoradiographic experiments to determine their binding characteristics. Upon successful murine tissue autoradiography, also human post mortem tissue can be used to obtain a first impression of the NET-PET-tracer binding behavior in humans. Superposition of Nissl-stained tissue slices enables morphological allocation of images.

So far, radiolabeled reboxetine analogs ^{11}C-MeNER, ^{11}C-MeNET and ^{18}F-FMeNER-D$_2$ (Fig.1) have been described (*23-34)*. Since these compounds display distinct limitations (metabolic stability, late equilibrium, complex radiosynthesis, unexplainable striatal uptake) (*23, 35*), which put some constraints on their applicability in clinical trials, more suitable NET-PET ligands - not based on reboxetine - are still of interest.

We therefore recently published the automated radiosynthesis of a new benzo[d]imidazolone derivative ^{11}C-Me@APPI (Fig.1) (*36)*. The central question to be examined in this paper is whether [^{11}C]Me@APPI displays comparable or even improved behavior as NET-PET radioligand in comparison to the gold standard ^{18}F-FMeNER-D2 using preclinical methods.

On these grounds, the following issues are addressed in this study: Affinity and selectivity of ^{11}C-Me@APPI and ^{18}F-FMeNER-D2 are compared, metabolic stability is tested in vitro in murine and human models; blood brain barrier penetration is predicted using IAM chromatography; a comparative in vitro autoradiography in human brain slices and murine brain and heart slices is performed and the morphology of the used tissues is allocated with Nissl staining as well as the NET-distribution is confirmed by immunohistochemical staining with a NET-specific antibody.

MATERIALS AND METHODS

NET, DAT and SERT expressing membrane preparations were obtained from Perkin Elmer. The ODP-50 column (20x4.0 mm, 5µm) was purchased from Shodex® (Showa Denko Europe GmbH). For prediction of BBB-penetration a Redistech IAM.PC.DD2 column (Regis Technologies Inc.) was used.

Microsomal preparations (human/rat liver microsomes) for stability testing were obtained from BD Bioscience. Pooled human and rat plasma was obtained from Innovative Research.

The human post mortem tissue (7-9h post mortem time, no history of neurological diseases) was obtained from the neurobio-bank of the Medical University of Vienna and approved by the local ethics committee ('Molecular neuropathologic investigation of neurodegenerative diseases' Nr.396/2011) following the principles of the Helsinki declaration. Research using animal tissue was carried out under institutional approval in accordance with the Austrian Animal Care Law.

All other chemicals were obtained from Sigma Aldrich.

Affinity and Selectivity

Affinity of Me@APPI was tested on membranes expressing the human NET (hNET membrane, 3µg

protein/unit, RBHNETM 400AU, Perkin Elmer) in a harvesting protocol as outlined recently (36). For selectivity testing, respective membranes expressing human DAT (12.7 µg protein/unit, RBHDATM400UA, Perkin Elmer) or SERT (9 µg protein/unit, RBHSTM400UA, Perkin Elmer) were used.

Radiochemistry

The radioligand ^{18}F-FMeNER-D2 was prepared as previously published *(37)*. Briefly, a two-step synthesis starting from ^{18}F-fluoride, dibromomethane-d2 and norethylreboxetin was carried out, followed by HPLC and SPE purification. The product was sterile formulated in Phosphate buffered saline (PBS) containing 8.5% Ethanol. Radiochemical and chemical purity were assessed via HPLC and TLC, osmolality and pH were in a physiological range. Specific activity was determined for every experiment. The radiosynthesis was carried out directly before to the autoradiographic experiments.
The NET-PET-tracer ^{11}C-Me@APPI was synthesised as presented in 2013 (*36*). Briefly, a ^{11}C-methylation via ^{11}C-methyl triflate in acetonitrile was performed. Subsequently, a HPLC purification and solid phase extraction using a C8 SepPak cartridge were done, and the final product was formulated physiologically (PBS, 8.5% Ethanol). After sterile filtration, quality control was done ensuring pH and osmolality in a physiological range, (radio-)chemical purity > 98% and sufficient specific activity for further studies.

LogD Analysis and IAM Chromatography

Lipophilicity was tested using HPLC according to an established protocol *(38)*. The substances were injected in toluene and triphenylene (known logD and k') in a polymeric ODP-50 column (20x4.0mm, 5µm) using a linear gradient from 10% MeOH /90% 25mM phosphate buffer to 100% methanol within 9.4min at a flow-rate of 1.5mL/min. As logD values are poor predictors of BBB penetration, an additional calculation of tPSA (total polar surface area) was performed according to Yoon et al. (*39)*. For IAM chromatography, a Redistech IAM.PC.DD2 column (150x4.6mm) was eluted isocratically with 0.01M phosphate buffer and acetonitrile (ACN) in different ratios (1mL/min). The resulting Pm (permeability) and Km (membrane partition coefficient) were obtained after data analysis and the data were compared with those derived from DASB and PIB as external standards.

Metabolic Stability Testing

Metabolic degradation was assessed using human and murine plasma, human and rat liver microsomes (CYP P450 enzymes) and carboxylic esterase (human and porcine) (*36, 40)*. For details see supplementary information.

Autoradiography

In vitro autoradiography on tissue slices from rat and human origin was performed in a modified protocol from Schou et al. (*11, 41, 42*). Briefly, slices were pre-incubated for 20min, radioligand and competitors

were added and incubation was done for 60min at RT. After washing and development on phosphor imaging films regions of interest (ROI) were analyzed and the percentage of total specific binding was calculated. For further details see supplementary information.

Nissl Staining and Immunhistochemistry

Post-autoradiographic processing of the slices was done by Nissl staining and immunohistochemistry in order to facilitate morphological mapping of hot areas in the autoradiography *(43-45)*. For details see supplementary information.

Statistical analysis

All experiments, if not stated otherwise, were performed in triplicates. All quantitative data were stated as arithmetic means ± standard deviation. Differences in parametric data was assessed using a two-tailed student t-test; p-values <0.05 were considered to be significant and indicated in tables and figures with *. Error bars represent the standard deviation; if not visible they are within the margin of the symbol.

RESULTS

Affinity and Selectivity

Affinity and selectivity for both tracers are high. Using, hNET expressing membranes, Me@APPI displays a binding affinity of Ki=3.2±0.6nM towards NET. Selectivity was found to be excellent with Ki(DAT)≥10000nM and Ki(SERT)≥669nM, tested in vitro on hDAT or hSERT membranes. Both affinity and selectivity of Me@APPI was comparable to FMeNER-D2: K_i(NET): 3.1nM, Ki(SERT) & Ki(DAT)≥1.000nM.

Lipophilicity and BBB penetration

Analysis of lipophilicity using OPD-chromatography revealed $logD_{HPLC}$ values of 3.08 for Me@APPI and 2.73 for FMeNER-D2, respectively. Furthermore, tPSA values were calculated as 35.58 for Me@APPI and FMeNER-D2 39.72. According to literature, a possible BBB-penetration is suspected when tPSA does not exceed 60 (*39*). Moreover, passive diffusion through immobilized artificial phospholipids was tested in IAM-chromatography. Permeability Pm was determined as 0.55 for Me@APPI and 0.48 for FMeNER-D2.

Metabolic Stability

Metabolic stability of both radiolabelled compounds was tested in vitro in a multi enzyme complex, single enzymes and plasma. [^{11}C]Me@APPI was highly stable in all tested systems, whereas ^{18}F-FMeNER-D2 showed significant metabolic instability. In murine and human plasma, both tracers displayed high

stability (99.5% intact, 1h) (Table 1).
In pooled human liver microsomes, ^{11}C-Me@APPI revealed no significant metabolism (1h, 99.5% intact), and also 93.5±1.2% of ^{18}F-FMeNER-D2 were found to be intact. Using rat liver microsomes, no radiometabolites were found using ^{11}C-Me@APPI after 1h. However, incubation of ^{18}F-FMeNER-D2 under the same conditions, lead to a rapid degradation. After 5min 3.2±1.0% remained unmetabolized; and less than 1% of the radiotracer (0.93±0.12%) was found to be intact after 10min.

Autoradiography, Immunohistochemistry and Nissl Staining

NET-autoradiography using ^{11}C-Me@APPI and ^{18}F-FMeNER-D2 revealed highest uptake in the same regions. Blocking was done with non-radioactive NET-ligands FMeNER-D2, Me@APPI and Nisoxetin in different concentrations (1nM,10nM,100nM,1µM). A concentration dependent binding displacement was observed using ^{18}F-FMeNER-D2 with all blocking compounds in all tested tissues (Fig 2). Binding enhancement was observed using ^{11}C-Me@APPI under the same conditions in brain, but displacement in rat heart. Table 2 presents a broad overview of the specific binding of NET ligands and fmol/mm^2 values of relative receptor density on human and rat tissues. All values are given in % as mean n≥9.
To address the issue of observed binding enhancement using ^{11}C-Me@APPI, harvesting experiments using hNET expressing membranes were conducted according to the affinity testing protocol, while applying ^{11}C-Me@APPI as radioligand. Hereby, binding displacement was observed concentration-dependently; using the same competitors as for in-vitro autoradiography. In figure **3**, the dependence of binding to concentration of competitors is shown, all counts were corrected for decay.
Subsequently, the morphology of cryo-slices was visualized using Cresyl violet and thus allow anatomical identification of hot regions in autoradiography. In figure 4, a superposition of a Nissl stain and the specific binding of ^{18}F-FMeNER-D2 on a coronal rat brain slice (baseline - blocking with 100nM Me@APPI) is shown.
In immunohistochemical staining NET-antibody-dye complexes were found strongly in heart fibers, hippocampus, thalamus and hypothalamus, and to a fewer extent in all other brain regions (Fig. 5). NET-staining in rat coronal brain was observed especially in the hippocampus, hypothalamus and thalamus.

DISCUSSION

The impact of the NET-involvement in various pathophysiological diseases has fostered the chase for improved imaging agents. Thereby the central importance of a non-invasive imaging techniques (such as PET) for the investigation of these molecular changes is evident. Therefore, this study is concerned with the issue whether ^{11}C-Me@APPI could become an enhanced NET-PET-tracer compared to reboxetine-based ligands. In detail, Me@APPI and FMeNER-D2 were tested regarding their affinity, lipophilicity and passive BBB penetration, stability and in vitro binding behavior.
Affinity for both tested compounds was proven to be high, with excellent selectivity, which should allow an in vivo quantification of NET also in lower density regions. Radiosynthetic availability of ^{11}C-Me@APPI is superior than for ^{18}F-FMeNER-D2, due to facile ^{11}C-*N*-methylation compared to the complex radiosynthesis of the reboxetine derivative.

Furthermore, logD values of both candidate tracers (logD=Me@APPI 3.08, FMeNER-D2 2.73) are in the discussed range for ideal cerebral PET tracers (*46*), indicating a high probability of Me@APPI to penetrate BBB. Since lipophilicity does not solely influence passive diffusion through BBB, there is growing support for immobilized artificial membrane chromatography (*21, 22*). Therefore, we wanted to provide also permeability values for passive diffusion through artificial phospholipids. Results of these measurements revealed Pm values of 0.48 for FMeNER-D2 (already known to penetrate BBB) and 0.55 for Me@APPI. Thus, these data corroborate the hypothesis that Me@APPI could be able to penetrate BBB.

The main arguments against reboxetine derived NET-PET ligands focus on their lack of in vivo stability. Therefore, we tested both Me@APPI and FMeNER-D2 in a plethora of human and murine enzymes and plasma. These experiments revealed >99% intact Me@APPI in all tested systems after 1h, highlighting the outstanding stability for our novel NET-PET tracer. Using [^{18}F]FMeNER-D2, we found good stability in vitro in the human enzymes (93.5%, 1h). However, using this ligand in clinical trials, an unexpected uptake behavior was observed vicinal to cortical areas, hampering a quantification of NET in these regions (28). Assuming that this intense accumulation originates from an arising radio-metabolite, a more stable NET-PET tracer, such as Me@APPI, is pivotal for further PET imaging applications. Incubation of both candidate PET-tracers in murine liver microsomes, revealed again high stability for ^{11}C-Me@APPI, but strikingly low metabolic stability for ^{18}F-FMeNER-D2. After 5min, less than 4% of the fluorinated tracer were intact, after more than 10min almost no intact tracer could be detected. Unfortunately, these findings put some constraints on the applicability of ^{18}F-FMeNER-D2 in an in vivo µPET study in rats. However, no concerns were found using ^{11}C-Me@APPI in a small animal model.

Since all data gathered in these preceding methods indicated that Me@APPI is as an improved NET-PET tracer, in vitro autoradiography was performed. Hereby, human brain tissue (hippocampus, thalamus und hypothalamus) and rat tissue (coronal brain slices, heart) were incubated with both freshly prepared radioligands. On rat heart cryo-slices binding displacement was observed using both radioligands when blocked with three different NET ligands. Interestingly, competition with other NET-ligands on brain slices lead to binding enhancement using ^{11}C-Me@APPI, but to binding displacement using ^{18}F-FMeNER-D2. The same percentage of enhancement/displacement was observed in the respective ROIs. On the one hand, this could be due to much lower concentrations of ^{18}F-FMeNER-D2 (~0,2 pM) as compared to ^{11}C-Me@APPI (~8nM). However, this problem cannot be addressed properly, as specific activity is much higher for fluorinated ligands than for C-11 labeled ones. Dilution of the radiolabeled product is also possible but only to a certain extent, since C-11 is rather short lived and therefore the radioactivity is limited. Thus, we have to deal with the heterogeneity of the radioligand molarity, although the extent to which this reflects the cause remains unclear.

Another view to propound is the binding position of the tracers within the binding pocket of the NET. It could be different for Me@APPI and FMeNER-D2. However, taking into account the evidence, that Me@APPI was able to displace ^{18}F-FMeNER-D2 in autoradiography and normal blocking behavior on heart slices, we could probably turn this idea down.

Besides, these findings raised the question if this altered binding behavior would also be observed in a cell membrane binding assay (using hNET cell membranes). Same conditions as for the in vitro autoradiography were used (same concentrations of competitors, same incubation time). Interestingly,

we could not confirm the binding enhancement on a cellular level; on the contrary, regular concentration dependent binding displacement was observed. On these grounds, only ex vivo autoradiography and in vivo µPET studies can further elucidate the observed binding behavior.
Moreover, preliminary experiments regarding striatal binding of 11C-Me@APPI were conducted. So far, no uptake of 11C-Me@APPI was observed using in vitro autoradiography.

CONCLUSION

To sum up, all tested preclinical parameters indicate that ^{11}C-Me@APPI is a suitable NET-PET-tracer. Affinity and selectivity, as well as outstanding stability foster future application of our novel NET-ligand. The observed binding enhancement in in vitro brain autoradiography will be further elucidated in ex vivo autoradiography experiments and in vivo µPET studies.

Acknowledgements

The authors thank Birgit Bornatowicz for the syntheses of cold compounds. Special thanks to Thomas Vanicek for his efforts in the NET-project. The authors thank Neydher Berroteran, Thomas Zenz and Paul Otter for their support.

Disclosures

Disclosure of potential conflicts of interest

The authors declare that they have no conflict of interest.

Parts of this projects were funded by the Austrian Science Fund (P22981 awarded to Prof.Dr.Lanzenberger).

Research involving Human Participants and/or Animals

Statement on human rights:
All procedures performed in studies involving human participants were in accordance with the ethical standards of the institutional and/or national research committee and with the 1964 Helsinki declaration and its later amendments or comparable ethical standards.

Statement on the welfare of animals:
All applicable international, national, and/or institutional guidelines for the care and use of animals were followed.

REFERENCES:

1. Zhou J. Norepinephrine transporter inhibitors and their therapeutic potential. *Drugs Future.* 2004;29:1235–1244.
2. Curatolo P, D'Agati E, Moavero R. The neurobiological basis of ADHD. *Italian Journal of Pediatrics.* 2010;36:79.
3. Mash DC, Ouyang Q, Qin Y, Pablo J. Norepinephrine transporter immunoblotting and radioligand binding in cocaine abusers. *Journal of Neuroscience Methods.* 2005;143:79-85.
4. Pifl C, Hornykiewicz O, Blesa J, Adánez R, Cavada C, Obeso JA. Reduced noradrenaline, but not dopamine and serotonin in motor thalamus of the MPTP primate: relation to severity of Parkinsonism. *Journal of Neurochemistry.* 2013;125:657-662.
5. Vazey EM, Aston-Jones G. The emerging role of norepinephrine in cognitive dysfunctions of Parkinson's disease. *Frontiers in Behavioral Neuroscience.* 2012;6:48.
6. Ostock CY, Lindenbach D, Goldenberg AA, Kampton E, Bishop C. Effects of noradrenergic denervation by anti-DBH-saporin on behavioral responsivity to l-DOPA in the hemi-parkinsonian rat. *Behavioural Brain Research.* 2014;270:75-85.
7. Harik S, Duckrow R, LaManna J, Rosenthal M, Sharma V, Banerjee S. Cerebral compensation for chronic noradrenergic denervation induced by locus ceruleus lesion: recovery of receptor binding, isoproterenol- induced adenylate cyclase activity, and oxidative metabolism. *The Journal of Neuroscience.* 1981;1:641-649.
8. Rommelfanger KS, Edwards GL, Freeman KG, Liles LC, Miller GW, Weinshenker D. Norepinephrine loss produces more profound motor deficits than MPTP treatment in mice. *Proceedings of the National Academy of Sciences of the United States of America.* 2007;104:13804-13809.
9. Schroeder C, Jordan J. Norepinephrine transporter function and human cardiovascular disease. *American Journal of Physiology - Heart and Circulatory Physiology.* 2012;303:H1273-H1282..
10. Moldovanova I, Schroeder C, Jacob G, et al. Hormonal Influences on Cardiovascular Norepinephrine Transporter responses in healthy women. *Hypertension.* 2008;51:1203-1209.
11. Schou M, Halldin C, Pike VW, et al. Post-mortem human brain autoradiography of the norepinephrine transporter using (S,S)-[18F]FMeNER-D2. *European Neuropsychopharmacology.* 2005;15:517-520.
12. Grandoso L, Pineda J, Ugedo L. Comparative study of the effects of desipramine and reboxetine on locus coeruleus neurons in rat brain slices. *Neuropharmacology.* 2004;46:815-823.
13. Wadsak W, Mitterhauser M. Basics and principles of radiopharmaceuticals for PET/CT. *European journal of radiology.* 2010;73:461-469.
14. Smith HR, Beveridge TJR, Porrino LJ. Distribution of norepinephrine transporters in the non-human primate brain. *Neuroscience.* 2006;138:703-714.
15. Logan J, Wang G-j, Telang F, et al. Imaging the norepinephrine transporter in humans with (S,S)-[11C]O-methyl reboxetine and PET: problems and progress. *Nuclear Medicine and Biology.* 2007;34:667-679.
16. Donnan GA, Kaczmarczyk SJ, Paxinos G, et al. Distribution of catecholamine uptake sites in human brain as determined by quantitative [3H] mazindol autoradiography. *The Journal of Comparative Neurology.* 1991;304:419-434.
17. Fowler JS, Volkow ND, Wang GJ, Gatley SJ, Logan J. [11C]Cocaine: PET studies of cocaine pharmacokinetics, dopamine transporter availability and dopamine transporter occupancy. *Nucl Med Biol.* 2001;28:561-572.
18. Pristupa ZB, Wilson JM, Hoffman BJ, Kish SJ, Niznik HB. Pharmacological heterogeneity of the cloned and native human dopamine transporter: disassociation of [3H]WIN 35,428 and [3H]GBR 12,935 binding. *Molecular Pharmacology.* 1994;45:125-135.
19. Tejani-Butt SM. [3H]nisoxetine: a radioligand for quantitation of norepinephrine uptake sites by autoradiography or by homogenate binding. *Journal of Pharmacology and Experimental Therapeutics.* 1992;260:427-436.
20. Bock N, Quentin DJ, Hüther G, Moll GH, Banaschewski T, Rothenberger A. Very early treatment with fluoxetine and reboxetine causing long-lasting change of the serotonin but not the noradrenaline transporter in the frontal cortex of rats. *World Journal of Biological Psychiatry.* 2005;6:107-112.
21. Tavares AA, Lewsey J, Dewar D, Pimlott SL. Radiotracer properties determined by high performance liquid chromatography: a potential tool for brain radiotracer discovery. *Nucl Med Biol.* 2012;39:127-135.
22. Vraka C, Nics L, Weiss V, et al. Combination of High Throughput HPLC Methods for Rapid Prediction of Blood Brain Barrier Penetration of Newly Developed Radiotracers - EANM 14.

European Journal of Nuclear Medicine and Molecular Imaging. 2014;41:442.

23. Wilson AA, Patrick Johnson D, Mozley D, et al. Synthesis and in vivo evaluation of novel radiotracers for the in vivo imaging of the norepinephrine transporter. *Nuclear Medicine and Biology.* 2003;30:85-92.

24. Takano A, Gulyás B, Varrone A, Halldin C. Comparative evaluations of norepinephrine transporter radioligands with reference tissue models in rhesus monkeys: (S,S)-[18F]FMeNER-D2; and (S,S)-[11C]MeNER. *European Journal of Nuclear Medicine and Molecular Imaging.* 2009;36:1885-1891.

25. Schou M, Halldin C, Sóvágó J, et al. PET evaluation of novel radiofluorinated reboxetine analogs as norepinephrine transporter probes in the monkey brain. *Synapse.* 2004;53:57-67.

26. Gulyás B, Brockschnieder D, Nag S, et al. The norepinephrine transporter (NET) radioligand (S,S)-[18F]FMeNER-D2 shows significant decreases in NET density in the human brain in Alzheimer's disease: A post-mortem autoradiographic study. *Neurochemistry International.*56:789-798.

27. Vanicek T, Spies M, Rami-Mark C, et al. The norepinephrine transporter in attention-deficit/hyperactivity disorder investigated with positron emission tomography. *JAMA Psychiatry.* 2014.

28. Vanicek T, Spies M, Rami-Mark C, et al. THe norepinephrine transporter in attention-deficit/hyperactivity disorder investigated with positron emission tomography. *JAMA Psychiatry.* 2014;71:1340-1349.

29. Stehouwer JS, Jarkas N, Zeng F, et al. Synthesis, radiosynthesis, and biological evaluation of fluorine-18-labeled 2β-carbo(fluoroalkoxy)-3β-(3′-((Z)-2-haloethenyl)phenyl) nortropanes: Candidate radioligands for in vivo imaging of the serotonin transporter with positron emission tomography. *Journal of Medicinal Chemistry.* 2008;51:7788-7799.

30. Zeng F, Jarkas N, Owens MJ, Kilts CD, Nemeroff CB, Goodman MM. Synthesis and monoamine transporter affinity of front bridged tricyclic 3β-(4′-halo or 4′-methyl)phenyltropanes bearing methylene or carbomethoxymethylene on the bridge to the 2β-position. *Bioorganic & Medicinal Chemistry Letters.* 2006;16:4661-4663.

31. Zeng F, Jarkas N, Stehouwer JS, et al. Synthesis, in vitro characterization, and radiolabeling of reboxetine analogs as potential PET radioligands for imaging the norepinephrine transporter. *Bioorganic & Medicinal Chemistry.* 2008;16:783-793.

32. Zeng F, Mun J, Jarkas N, et al. Synthesis, Radiosynthesis, and Biological Evaluation of Carbon-11 and Fluorine-18 Labeled Reboxetine Analogues: Potential Positron Emission Tomography Radioligands for in Vivo Imaging of the Norepinephrine Transporter. *Journal of Medicinal Chemistry.* 2008;52:62-73.

33. Zeng F, Stehouwer JS, Jarkas N, et al. Synthesis and biological evaluation of 2beta,3alpha-(substituted phenyl)nortropanes as potential norepinephrine transporter imaging agents. *Bioorg Med Chem Lett.* 2007;17:3044-3047.

34. Zeng F, Voll RJ, Crowe RJ, Waldrep MS, Dolph KB, Goodman MM. An improved synthesis of [11C]MENET via Suzuki coupling with [11C]methyl iodide. *Journal of labelled compounds & radiopharmaceuticals.* 2013;56:307-309.

35. Schou M, Zoghbi S, Shetty H, et al. Investigation of the metabolites of (S,S)-[11C]MeNER in humans, monkeys and rats. *Molecular Imaging and Biology.* 2009;11:23-30.

36. Mark C, Bornatowicz B, Mitterhauser M, et al. Development and automation of a novel NET-PET tracer: [11C]Me@APPI. *Nucl Med Biol.* 2013;40:295-303.

37. Rami-Mark C, Zhang MR, Mitterhauser M, Lanzenberger R, Hacker M, Wadsak W. [18F]FMeNER-D2: reliable fully-automated synthesis for visualization of the norepinephrine transporter. *Nucl Med Biol.* 2013;40:1049-1054.

38. Donovan SF, Pescatore MC. Method for measuring the logarithm of the octanol–water partition coefficient by using short octadecyl–poly(vinyl alcohol) high-performance liquid chromatography columns. *Journal of Chromatography A.* 2002;952:47-61.

39. Yoon CH, Kim SJ, Shin BS, Lee KC, Yoo SD. Rapid screening of blood-brain barrier penetration of drugs using the immobilized artificial membrane phosphatidylcholine column chromatography. *Journal of Biomolecular Screening.* 2006;11:13-20.

40. Nics L, Vraka C, Hendl M, et al. In-vitro stability of [18F]FE@SUPPY and [18F]FE@SUPPY:2 against human liver-microsomes and human plasma. *Nuklearmed-Nucl Med.* 2011;50, A176.

41. Gulyás B, Brockschnieder D, Nag S, et al. The norepinephrine transporter (NET) radioligand (S,S)-[18F]FMeNER-D2 shows significant decreases in NET density in the human brain in Alzheimer's disease: A post-mortem autoradiographic study. *Neurochemistry International.*

2010;56:789-798.
42. Philippe C, Haeusler D, Fuchshuber F, et al. Comparative autoradiographic in vitro investigation of melanin concentrating hormone receptor 1 ligands in the central nervous system. *Eur J Pharmacol.* 2014;735:177-183.
43. Kádár A, Wittmann G, Liposits Z, Fekete C. Improved method for combination of immunocytochemistry and Nissl staining. *Journal of neuroscience methods.* 2009;184:115-118.
44. Fukuda T, Koelle GB. The cytological localization of intracellular neuronal acetylcholinesterase. *The Journal of Biophysical and Biochemical Cytology.* 1959;5:433-440.
45. Hofman F. Immunohistochemistry. *Current Protocols in Immunology.* 2001; 21.4.1-21.4.23
46. Pike VW. PET Radiotracers: crossing the blood-brain barrier and surviving metabolism. *Trends in pharmacological sciences.* 2009;30:431-440.

FIGURES:

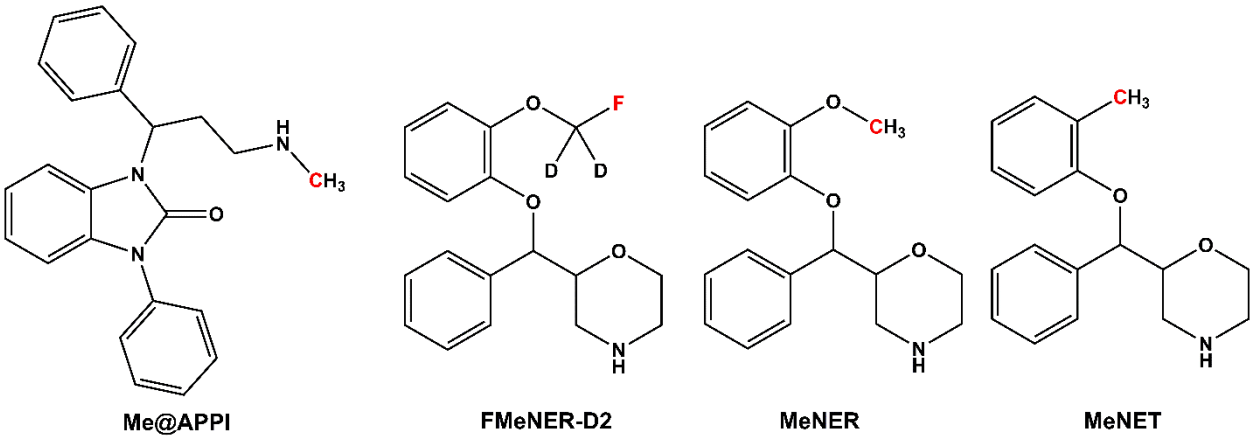

FIGURE 1: Chemical Structures of the two tested NET-PET ligands **Me@APPI** (1-(3-(methylamino)-1-phenylpropyl)-3-phenyl-1,3-dihydro-2H-benzo[d]imidazol-2-one) and **FMeNER-D2** (S,S)-((2-(fluoromethoxy-d2)phenoxy)(phenyl)methyl) morpholine). The red colored atom indicates the position of the radioisotope introduced by radiolabeling.

FIGURE 2: NET-autoradiography of ^{18}F-FMeNER-D2. Upper line displays coronal rat brain slices (10µm), and the lower line rat heart slices (10µm). Left to right: Nissl staining, baseline incubation (0.02pM ^{18}F-FMeNER-D2) and blocking with 100nM Me@APPI, 100nM Nisoxetine and 100nM FMeNER-D2. The scale shows the radioactivity from high (red) to low levels of radiotracer present on the Phosphor imager film.

FIGURE 3: NET-binding of ^{11}C-Me@APPI on human NET expressing cell membranes using a harvesting protocol. Competition was done using different concentrations of Me@APPI, FMeNER-D2 and Nisoxetine (1,3,10,30,100 and 1000nM).

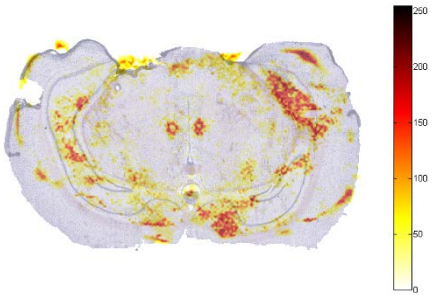

FIGURE 4: Subtraction image (^{18}F-FMeNER-D2 Baseline – blocking with 100nM Me@APPI) of NET-autoradiography superimposed on Nissl staining, implicating the specific NET-binding only. The scale depicts the specific binding on coronal rat brain slices

FIGURE 5:

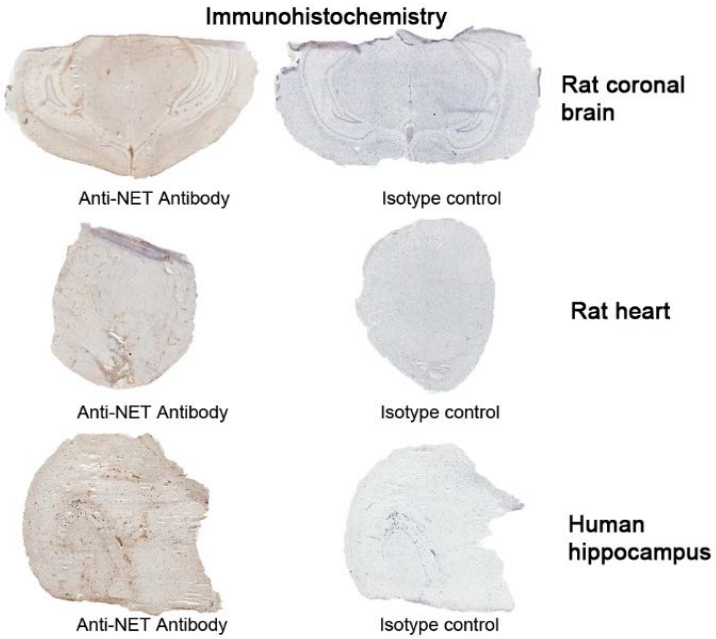

Immunohistochemistry on rat and human tissue using a NET-specific antibody (left column) and rabbit antibody isotype control (right column) and was colored with DAB (brown). Counterstaining (blue colored) was done with Mayers Hemalaun on both columns.

TABLES:

TABLE 1: An overview of all tested preclinical parameters for Me@APPI and FMeNER-D2.
[#] Schou et al. 2008.

TABLE 1	Me@APPI	FMeNER-D2
AFFINITY		
Ki NET [nM]	3.03 ± 1.8	3,1[#]
Ki SERT [nM]	>669	1000[#]
Ki DAT [nM]	>10000	1000[#]
LIPOPHILICITY AND BBB-PENETRATION		
log D (HPLC)	3.08 ± 0.01	2.73 ± 0.01
Total Polar Surface Area (tPSA)	35.58	39.72
Permeability (IAM)	0.55	0.48
RADIOSYNTHESIS		
Yield [GBq]	1.25 ± 0.72	1.53 ± 0.6
% Yield (corr for decay)	8.8 ± 4.3	12.0 ± 5.2
Specific Activity [GBq/µmol]	54.35 ± 8	589.9 ± 352
IN VITRO STABILITY (60min)		
human liver microsomes	99.5 ± 0.2	93.5 ± 1.2
rat liver microsomes	99.5 ± 0.1*	<1% after 10 min*
pooled human plasma	99.9 ± 0.1	99.9 ± 0.1
pooled rat plasma	99.8 ± 0.1	99.9 ± 0.1

TABLE 2: Specific NET binding of ^{11}C-Me@APPI and ^{18}F-FMeNER-D2 using different competitors

TABLE 2	^{11}C-Me@APPI		^{18}F-FMeNER-D2	
	% BL-Competitor	*fmol*	*% BL-Competitor*	*fmol*
Rat whole brain				
FMeNER	127.5±8.2 *	n.d.	52.51±7.3*	0.0398
Nisoxetin	127.3±14.7*	n.d.	68.00±6.3	0.0268
Me@APPI	169.3±19.5	n.d.	83.55±11.2	0.0138
Rat heart				
FMeNER	38.28±6.7	1.679	63.71±6.4	1.532
Nisoxetin	48.53±10.6	1.392	74.42±8.9	1.246
Me@APPI	38.82±8.4	1.664	72.02±2.4	1.478
Human hippocampus				
FMeNER	167.5±22.3	n.d.	36.84±9.4	0.075
Nisoxetin	146.8±17.6	n.d.	48.46±5.7	0.061
Me@APPI	173.3±15.3	n.d.	59.21±11.5	0.049
Human hypothalamus				
FMeNER	114.4±7.5	n.d.	82.48±4.5	0.724
Nisoxetin	112.6±12.6	n.d.	95.75±5.7	0.176
Me@APPI	115.7±6.8	n.d.	85.86±6.8	0.584
Human thalamus				
FMeNER	134.5±14.3	n.d.	36.78±9.6*	0.076
Nisoxetin	118.7±12.5	n.d.	53.28±7.6	0.056
Me@APPI	141.2±16.4	n.d.	57.85±8.1	0.051

3.1.7 Manuscript #6

RADIOSYNTHESIS AND FIRST PRECLINICAL EVALUATION OF THE NOVEL NOREPINEPHRINE TRANSPORTER PET-LIGANDS [^{11}C]ME@HAPTHI'

European Journal of Nuclear Medicine and Molecular Imaging Research, 2015, in review.

Christina Rami-Mark[1,2], Neydher Berroteran[1,2], Cecile Philippe[1], Stefanie Foltin[1], Chrysoula Vraka[1], Alexander Hoepping[3], Rupert Lanzenberger[4], Marcus Hacker[1], Markus Mitterhauser[1*] and Wolfgang Wadsak[1,2]

[1]*Medical University of Vienna, Department of Biomedical Imaging and Image-guided Therapy, Division of Nuclear Medicine, Vienna, Austria*

[2]*University of Vienna, Department of Inorganic Chemistry, Vienna, Austria*

[3] *ABX Advanced Biochemical Compounds, Radeberg, Germany*

[4]*Department of Psychiatry and Psychotherapy, Division of Biological Psychiatry, Medical University of Vienna, Austria.*

*****Author to whom correspondence should be addressed:
Prof. Dr. Markus Mitterhauser,
Department of Biomedical Imaging und Image-guided Therapy, Division of Nuclear Medicine, Medical University of Vienna, Austria.
Tel.: +43-1-40400-55340; fax: +43-1-40400-15590; e-mail: markus.mitterhauser@meduniwien.ac.at

EJNMMI Res [IF: 5.14]

Keywords: NET; PET; autoradiography, radiosynthesis; HAPTHI

Abstract:

Background:

The norepinephrine transporter (NET) has been demonstrated to be relevant to a multitude of neurological, psychiatric and cardiovascular pathologies. Due to the wide range of possible applications for PET imaging of the NET together with the limitations of currently available radioligands, novel PET tracers for imaging of the cerebral NET with improved pharmacological and pharmacodynamic properties are needed.

Methods:

The present study addresses the radiosynthesis and first preclinical evaluation of the novel NET PET tracer [^{11}C]Me@HAPTHI by describing its affinity, selectivity, metabolic stability, plasma free fraction, blood brain barrier (BBB) penetration and binding behavior in *in vitro* autoradiography.

Results:

[^{11}C]Me@HAPTHI was prepared and displayed outstanding affinity and selectivity as well as excellent *in vitro* metabolic stability and it is likely to penetrate the BBB. Moreover, selective NET binding in *in vitro* autoradiography was observed in human brain and rat heart tissue samples.

Conclusion:

All preclinical results and radiosynthetic key-parameters indicate that the novel benzothiadiazole dioxide-based PET tracer [^{11}C]Me@HAPTHI is a feasible and improved NET radioligand and might prospectively ease clinical NET imaging.

1. Background:

The noradrenergic system – and specifically the presynaptic norepinephrine transporter (NET) – is proposed to be altered in a variety of neurological, neuropsychiatric and cardiovascular diseases. For example, alterations have been shown in Alzheimer's disease, Morbus Parkinson, major depressive disorder, and attention deficit hyperactivity disorder [1-9]. Therefore, a reliable non-invasive molecular imaging technique – such as positron emission tomography (PET) – would be of great benefit for early stage *in vivo* diagnostics, visualization of treatment response, and further elucidation of underlying pathophysiological mechanisms.

Great efforts have been made to develop PET tracers for the NET over the last two decades. Focus was primarily placed on Reboxetine derived ligands [10-14]. However, previous studies have shown that the *in vivo* and *in vitro* behavior of these Reboxetine analogues, more specifically [^{11}C]MeNER ([^{11}C]MRB, ((S,S)-2-(α-(2-[^{11}C]methoxyphenoxy)benzyl)morpholine), [^{11}C]MeNET and [^{18}F]FMeNER-D$_2$ ((*S,S*)-2-(α-(2-[^{18}F]Fluoro[^{2}H$_2$] methoxyphenoxy)benzyl) morpholine), is not favorable for viable imaging of the NET by PET. Limitations include their metabolic stability, late reaching of equilibrium, unexplainable striatal uptake, and complexity of radiosynthesis [10, 15-18]. Recently, we aimed at the preparation of a benzo[d]imidazolone derivative – [^{11}C]Me@APPI as new NET-PET tracer [19]. Despite its favorable properties and straightforward production, its affinity was not sufficient and its lipophilicity to high. Hence, there is ample demand for a novel, enhanced radioligand for *in vivo* NET imaging.

Therefore, this study highlights a novel, non-Reboxetine based NET-PET tracer based on a benzothiadiazole scaffold: [^{11}C]Me@HAPTHI ((S)-1-(3-hydroxy-4-([^{11}C]methylamino)butyl)-3-phenyl-1,3-dihydrobenzo[c][1,2,5]thiadiazole 2,2-dioxide) (figure 1). In general, the designed benzothidiazole dioxides shows excellent affinity and selectivity as well as slightly reduced flexibility compared to other previously published benzoimidazolones [20, 21]. Hence, these substances offer an ideal basis for the further development of novel NET-ligands for PET imaging.

The objectives of this investigation were:

- The set-up of a small scale radiosynthetic procedure for the preparation of the carbon-11 labelled [^{11}C]Me@HAPTHI and its optimization;
- The up-scaling and set-up of a fully automated preparation of [^{11}C]Me@HAPTHI, including purification and formulation;
- The *in-vitro* evaluation of Me@HAPTHI and its precursor HAPTHI. Evaluation includes binding studies for the determination of affinity and selectivity of both Me@HAPTHI and its precursor HAPTHI towards NET using NET, serotonin transporter (SERT) and dopamine transporter (DAT) expressing membranes, metabolic stability testing *in-vitro* against Cytochrom P 450 enzymes, logP analysis and IAM chromatography for indirect measurement of blood-brain-barrier (BBB) penetration, and determination of plasma free fraction.
- Comparative *in vitro* autoradiography on human and rodent tissue slices

2. Materials and Methods:

2.1 Materials

Precursor, HAPTHI ((S)-1-(4-amino-3-hydroxybutyl)-3-phenyl-1,3-dihydrobenzo[c] [1,2,5]thiadiazole 2,2-dioxide, and cold reference compound Me@HAPTHI ((S)-1-(3-hydroxy-4-(methylamino)butyl)-3-

phenyl-1,3-dihydrobenzo[c][1,2,5]thiadiazole 2,2-dioxide) were custom-synthesized by ABX advanced biochemical compounds (Radeberg, Germany). Briefly, synthesis of (2S)-4-(2,2-Dioxido-3-phenyl-2,1,3-benzothiadiazol-1(3H)-yl)-1-(methylamino)butan-2-ol followed the route described by Neill et. al.[20, 21]. For more details, see supplementary information.

2-Butanone (MEK, <99.0% ACS reagent), acetonitrile (ACN, HPLC grade), dimethylsulfoxide (DMSO), tetrabutylammonium hydroxide 30-hydrate (TBAH), ammonium formate, ammonium acetate, sodium hydroxide, triethylamine and ethanol (absolute) were purchased from Sigma Aldrich (Vienna, Austria) in highest available grades. In addition, iodine (sublimated grade for analysis; ACS, Pharm.Eur.) was obtained from Merck (Darmstadt, Germany). Silver triflate impregnated carbon was prepared by reaction of 1 g of silver trifluoromethanesulfonate (Sigma Aldrich, Vienna, Austria) in 20 mL ACN with 3 g of Graphpac-GC (80/100 mesh, Alltech, Deerfield, USA). The suspension was stirred under protection from light and in an argon atmosphere for 30 min. After removal of the solvent, the resulting powder was dried under protection from light for further 2 h under reduced pressure.

For formulation of the product 0.9% saline solution from B. Braun (Melsungen, Germany), 3% saline solution (Landesapotheke Salzburg, Austria) and sodium dihydrogenphosphate-monohydrate and disodiumhydrogenphosphate-dihydrate (both from Merck, Darmstadt, Germany) were used. Sterile water was purchased from Meditrade Medicare Medizinprodukte (Kufstein, Austria). Phosphate buffer (125 mM) was prepared by dissolving 0.224 g sodium dihydrogenphosphate-monohydrate and 1.935 g disodiumhydrogenphosphate-dihydrate in 100 mL sterile water. For solid phase extraction C18 plus SepPak® cartridges were purchased from Waters (Waters® Associates Milford, USA). Low-protein binding Millex® GS 0.22 µm sterile filters were obtained from Millipore (Bedford, USA).

All other chemicals and solvents for the radiosyntheses were obtained from Merck (Darmstadt, Germany) and Sigma-Aldrich (Vienna, Austria) with at least analytical grade and used without further purification.

NET, DAT and SERT expressing membrane preparations were obtained from Perkin Elmer (MA, USA). An ODP-50 column (20x4.0 mm, 5µm) was purchased from Shodex® (Showa Denko Europe GmbH, Munich, Germany). For prediction of BBB penetration, a Redistech IAM.PC.DD2 column (Regis Technologies Inc., Morton Grove, USA) was used.

Microsomal preparations (human/rat liver microsomes) for stability testing were obtained from BD Bioscience (NJ, USA). Pooled human and rat plasma was obtained from Innovative Research (MI, USA). The human post mortem tissue (7-9 h post mortem time, no history of neurological diseases) was obtained from the Neurobiobank of the Medical University of Vienna and approved by the local ethics committee ('Molecular neuropathologic investigation of neurodegenerative diseases' Nr.396/2011) following the principles of the Helsinki declaration. Wild-type male rats were deeply anesthesized by isoflurane and sacrificed by decapitation. The organs of interest (i.e. brain, heart and testis) were removed and quick-frozen in *i*-pentan. Research using animal tissue was carried out under institutional approval in accordance with the Austrian Animal Care Law. Tissues were cut at -20°C in a micro-cryotome (Microm HM 560, Thermo Scientific, Austria). Frozen slices were thaw-mounted onto superfrost slides (Menzel-Gläser SUPERFROST plus microscopy slides, Thermo Scientific, Germany). A barrier pen (Mini PAP Pen, Invitrogen, USA) was used for immunohistochemistry only,. For detection of autoradiography a Cyclone Phospho-Imager (Cyclone Plus Storage Phosphor System, Perkin Elmer,

Germany) and Phosphor Imager plates (Multisensitive Phosphor Screens Long Type MS, PPN 7001724, Perkin Elmer, Germany) were used. The lead shielded and light-protected cassettes (Fisher Biotech Autoradiography Cassette FBCS 1417) were purchased from Fisher Scientific (PA, USA).

The NET-antibody (SLC6A2 Antibody H-67, sc-67216) was purchased from Santa Cruz Biotechnology (Texas, USA). An endogenous Avidin-Biotin blocking kit (ab64212), as well as the DAB (=3,3'-diaminobenzidine) substrate kit (94665) were obtained from abcam (Cambridge, UK). A rabbit primary antibody isotype control was purchased from Invitrogen (CA, USA). A peroxidase based Vectastain ABC kit (Rabbit IgG, PK-4001) was obtained from Vector Laboratories (CA, USA). Phosphate buffered saline (PBS pH 7.4, 10 fold concentrate, 11237) was obtained from Morphisto Evolutionsforschung und Anwendung GmbH (Germany). Mayer's Hemalaun solution was purchased from Merck Millipore (Germany). Histofluid (Marienfeld Superior, Germany) was used as a mounting medium. Coverslips from Menzel Gläser (24x60 mm, Thermo Fisher Scientific, Germany) were used for conservation of mounted slides. All other chemicals were obtained from Sigma Aldrich.

2.2 Instrumentation

$[^{11}C]CO_2$ was produced within a GE PETtrace cyclotron (General Electric Medical System, Uppsala, Sweden) by a $^{14}N(p,\alpha)^{11}C$ nuclear reaction under irradiation of a gas target filled with N_2 (+1% O_2) (Air Liquide Austria GmbH, Schwechat, Austria).

The evaluation of the reaction conditions was performed manually with starting activities <2 GBq. After optimization of the reaction parameters, [^{11}C]Me@HAPTHI-synthesis was transferred to the TRACERlab™ FX C Pro synthesizer and a fully automated synthesis was established.

Crude [^{11}C]Me@HAPTHI was purified by semi-preparative reversed phase HPLC using the built-in semi-preparative HPLC system equipped with a radioactivity and a UV detector (Linear Instruments Model 200 Detector UV/VIS) and a LaPrep HPLC pump (VWR International, Radnor, USA). A Supelcosil™ LC-ABZb, 5 µm, 250x10 mm (Supelco®, Belfonte,PA, USA) column was used with a mobile phase of ACN/0.1 M ammonium acetate 40/60 v/v% at a flow rate of 6 mL/min.

The analytical HPLC was performed on a Merck-Hitachi LaChrom HPLC system (L-7100 pump; LaChrom L-7400 UV detector) using a NaI radio-detector (Bertholdt Technologies, Bad Wildbach, Germany) and a GinaStar® processing software (Raytest, Straubenhardt, Germany). A Phenomenex® Prodigy, Phenyl-3(PH-3), 5 µm, 250x4.6 mm (Phenomenex®, Aschaffenburg, Germany) column with a mobile phase consisting of ACN/0.1 M ammonium formate 50/50 v/v% at a flow rate of 2 mL/min was used while detection of the cold compounds was performed at 280nm.

The osmolality of the final sterile product was measured with a Wescor osmometer Vapro® 5600 (Sanova Medical Systems, Vienna, Austria).

2.3 Methods:

2.3.1 Radiochemistry

Production of $[^{11}C]CH_3I$ and $[^{11}C]CH_3OTf$

The cyclotron production of $[^{11}C]CO_2$ was terminated at desired target activities between 40-50 GBq at currents between 48 and 53 µA (20-25 min) and trapped upon delivery on a molecular sieve (4 Å) within the Tracerlab FxC Pro synthesizer. Subsequently, $[^{11}C]CO_2$ was converted into $[^{11}C]CH_4$ by a Ni-catalysed reduction with H_2 at 400°C. $[^{11}C]CH_3I$ was produced within the same synthesizer using the

dry-method (gas phase conversion) described by Larsen et al. [22] with adopted modifications described by Kniess et al. [23]. Briefly, the resulting [^{11}C]CH_4 was reacted with sublimated iodine at 738°C in a recirculating process for 4 min to give [^{11}C]CH_3I. The produced [^{11}C]CH_3I was trapped on-line on a Porapak® N column and finally released by heating the trap to 200°C. [^{11}C]CH_3OTf was prepared on-line at the passage of [^{11}C]CH_3I through a pre-heated (190°C) column containing 300 mg silver triflate impregnated graphitized carbon at a flow rate of 40 mL/min [24].

Small scale reactions:

For optimization of reaction conditions, small-scale reactions using [^{11}C]CH_3I or [^{11}C]CH_3OTf were performed. Either [^{11}C]CH_3I or [^{11}C]CH_3OTf was trapped in 500 µL of the solvent of choice at room temperature (RT) and aportioned for further experiments in 1mL Wheaton v-vials. All evaluation reactions were performed manually (shielded hood; starting activity <2 GBq). The influence of various reaction conditions was investigated:

- → Reaction temperature: 25°C, 75°C
- → Base as catalyst: NaOH, triethylamine (TEA) and TBAH
- → Precursor concentration: 1mg/mL or 2mg/mL
- → Solvent: MEK or DMSO

Finale reaction volumes of small-scale reactions were 100 - 200 µL. The reactions were quenched with an equivolume solution of ammonium acetate (aq., pH 3.5) and the radiochemical incorporation yield (RCI) was determined using analytical radio-HPLC. In figure 2 the reaction scheme is presented.

Full automation of radiosyntheses:

The automation of the *N*-^{11}C-methylation reaction was done on the TRACERlab™ FX C Pro (GE Healthcare) [25]. A schematic flowchart of the synthesis is depicted in figure 3.

After conversion of cyclotron-produced [^{11}C]CO_2 to [^{11}C]methane [^{11}C]methyl iodide, and [^{11}C]CH_3OTf, it was trapped at RT in a glass reactor containing precursor HAPTHI (1 mg, 3 µmol) and 0.5 µL of an aqueous NaOH-solution (5M) in 500 µL MEK. After heating of the sealed reaction vessel to 75°C for 2 min, the crude reaction mixture was cooled to 25° and quenched by addition of 1 mL HPLC eluent. The entire volume was then transferred to the 5 mL injection loop. The crude mixture was (fluid detector controlled) injected into the semi-preparative HPLC column (figure 4). The pure [^{11}C]Me@HAPTHI peak was cut into a round bulb, containing 80 mL of distilled water. The now predominantly aqueous product solution was subjected to solid phase extraction by transferring over a preconditioned (10 mL EtOH, air, 20 mL water, air) C18 SPE cartridge. After rinsing of the C18 SepPak® with water (V6) for complete removal of residual HPLC solvents, the pure product was eluted with 1.5 mL EtOH (V5) into a two-neck vial and the cartridge and transfer lines rinsed with further 5 mL 0.9% saline into the same vial. After formulation with 9 mL 0.9% saline, 1 mL 3% saline and 1 mL 125 mM phosphate buffer, sterile filtration (0.22 µm) was performed under aseptic conditions (laminar air flow hot cell, class A) to avoid microbial contamination.

Quality control

Chemical and radiochemical impurities were assessed using analytical radio- and UV-HPLC according to the monograph in the European Pharmacopoeia [26]. Radiochemical identity and purity were measured via analytical radio-HPLC by comparison of retention times with authentic samples. Specific radioactivity was determined by quantification of the non-radioactive product (HPLC UV channel at

280 nm) and inclusion of the overall radiochemical yield (GBq at end of synthesis). Sterility, absence of endotoxins, pH, osmolality and residual solvents were determined by standard procedures routinely performed at the PET Centre of the Vienna General Hospital/ Medical University of Vienna and follow the respective monograph in the European Pharmacopoeia [26].

Statistical analysis

All quantitative data described in the text and figures are specified as arithmetic mean ± standard deviation. For the determination of significance, a student two-tailed t-test (α=0.95) was performed using Microsoft® Excel. P values of < 0.05 were considered to be significant. Unless otherwise stated, error bars in figures represent the standard deviation; if not visual, they are within the icon margin.

2.3.2 NET-expressing membrane binding studies

The affinity of new radiolabeled ligand was determined in a NET-expressing membrane binding protocol [27-29]. For details see supplementary information.

Data from the competition plots (as arithmetic means of values derived from three different assays, each in triplicate for each compound) were analyzed and subsequently IC_{50} and K_i values were calculated using GraphPad Prism® software (San Diego, USA).

Assays similar to those described for NET were performed in order to determine the selectivity of the tested compounds towards NET in comparison to DAT and SERT. IC_{50} and K_i values were obtained in analogy to NET experiments. Ratios DAT/NET and SERT/NET were determined.

2.3.3 LogD analysis, IAM chromatography and blood-brain-barrier-penetration

LogD values were assessed using a HPLC-based protocol according to Donovan and Pescatore [30]. All compounds (as cold reference standards) were injected together with two known compounds – with known logD and k' values – according to a standard protocol. A polymeric ODP-50 column was used; a linear gradient from 10% MeOH 90% 25 mM phosphate buffer (pH 7.4)to 100% methanol within 9.4 min at a flow-rate of 1.5 mL/min was applied. Internal standards were triphenylene and toluene; detection was performed at 260 nm and 285 nm.

As lipophilicity alone was shown to be a tenuous predictor for blood brain barrier penetration other *in vitro* methods have been described, such as immobilized artificial membrane (IAM) chromatography and further calculation of tPSA (total polar surface area) values [31-33]. Therefore, IAM chromatography was performed using a Redistech IAM.PC.DD2 column (15 cm x 4.6 mm) according to previously published methods [19, 34-36]. For analysis, 0.01 M phosphate buffer (pH 7.4) and ACN (in different ratios) were used isocratically as mobile phase at a flow rate of 1 mL/min. Resulting K_m (membrane partition coefficient) and P_m (permeability) values were obtained after data analysis using Microsoft Excel. The resulting data were compared with those derived from compounds known to penetrate BBB as external standard. Additionally, tPSA values were determined *in silico* using Chem Bio Draw Ultra (Cambridge Software, Perkin Elmer, USA).

2.3.4 Metabolic stability testing

Liver microsomes are subcellular fractions that are rich in endoplasmatic reticuli, which contain many drug-metabolizing enzymes, e.g. cytochrome P450s, flavin monooxygenases, and epoxide hydrolase. Microsomal incubations were performed in order to investigate the metabolization of [^{11}C]Me@HAPTHI. As results, both the percentage of test compound metabolized after a certain time and the biological

half-life were determined.

2.3.5 Plasma protein binding

For the determination of free fraction in human pooled plasma an ultrafiltration protocol according to previously published methods was used [37-40]. Briefly, aliquots of pooled human plasma were spiked with [^{11}C]Me@HAPTHI and centrifuged using ultrafiltration vials (Amicon Centrifree; Millipore, Bedford, USA). The plasma free fraction was calculated and the percentage of unspecific binding of [^{11}C]Me@HAPTHI to the filter matrix evaluated. For a detailed method, see the supplementary information.

2.3.6 *Autoradiography, Nissl Staining and Immunohistochemistry*

Human brain tissue (cortex, thalamus, hippocampus, cerebellum, and hypothalamus) was obtained deeply frozen from the Neurobiobank of the Medical University Vienna and was stored at -80 °C. Before cutting, tissue blocks were thawed slowly within 12 h to -20 °C. The organs were cut at -20°C in a micro-cryotome into 10 µm thick slices and thaw mounted onto object slides. Slices were again stored at -80°C until the beginning of the experiment.

In vitro autoradiography was performed with slight modifications according to previously published protocols [29, 41-43]. Non-specific binding was determined by co-incubation with excess Nisoxetine (10 µM). For competition experiments, non-radioactive FMeNER-D2, an established NET-PET tracer, and Me@HAPTHI were added to the incubation solution in different concentrations. After 1h at room temperature, incubation was stopped and slices were processed on phosphor imaging films. All data was exported to Microsoft Excel for statistical analysis and the percentage of total specific binding was calculated.

Post-autoradiographic processing of the slices was done by Nissl staining in order to facilitate morphological mapping of hot areas in the autoradiography. The same tissue slices were stained after autoradiography with cresyl violet [29, 44, 45] to demonstrate the Nissl substance in the neurons and cell nuclei. For a detailed procedure, see supplementary information.

Immunohistochemical staining experiments were performed on rat and human tissue cryo-slices, vicinal to the slices used for autoradiographic experiments. The staining procedure was a modification of a general protocol as published previously in detail [29, 46].

3. Results

3.1 Radiochemistry

The optimal parameters were examined in small-scale reactions. Thus, the influence of different ^{11}C-methylation agents, solvent, precursor concentration, reaction temperature and base were investigated (figure 5a-d). Radiochemical incorporation yields (RCIY) of [^{11}C]Me@HATPHI were below 6 % for all examined conditions using [^{11}C]CH_3I as methylation agent. Hereby, DMSO proved to be the best solvent for the SN_2 reaction using [^{11}C]methyl iodide. In contrast, very promising results were obtained using [^{11}C]CH_3OTf as radio-methylation agent (figure 5c-d). Interestingly, the use of DMSO as solvent did not result in high incorporation, less than 1 % RCIY was observed using [^{11}C]CH_3OTf. Applying 2-butanone resulted in high radiochemical incorporation yields. Furthermore, the influence of basic catalysis was examined: TBAH catalysis could not shift the reaction kinetics to favourable outcomes, as it did not result in any methylation of HAPTHI. Up to 12.8 ± 4.7 % RCIY was observed

when using 0.5 µL triethylamine instead. Conducting the experiments with 0.5 µL of 1 M NaOH (aq.), however, yielded 42.9 ± 5.2 % radiochemical incorporation with 1 mg/mL precursor concentration and even above 50 % RCI were obtained with 2 mg/mL precursor concentration. A further increase in basicity – facilitated by 0.5 µL 5 M NaOH (aq.) instead of 1 M NaOH (aq.) – did not lead to improved results (in a total reaction volume of 100 µL); only <0.5 % RCIY were obtained.

Hence, best results were obtained with NaOH-catalysis in 2-butanone for 2 min at 75°C using 2 mg/mL precursor HAPTHI. Thereby, 54.0 ± 8.3 % radiochemical incorporation was achieved.

Therefore, these optimum reaction parameters were transferred to the fully automated radiosynthesis within the Tracerlab FxC Pro synthesizer. In table 1, an overview on the automated syntheses, their conversion and yield is given. The crude reaction mixture was purified via semi-preparative radio-HPLC using isocratic conditions (0.1 M ammonium acetate and acetonitrile (60/40; v/v)) at a flow rate of 5 mL/min. An exemplary semi-preparative HPLC chromatogram is outlined in figure 4a. The precursor HAPTHI was found to be eluted at a retention time of 4.5 min (k'=0.55) and the product [^{11}C]Me@HAPTHI at 7.6 min (k'=1.62), respectively.

Overall, 7 large scale radiosyntheses were performed, yielding 2.2±2.0 GBq (18.9±13.3%, corrected for decay to EOB) of sterile, formulated [^{11}C]Me@HAPTHI within 41 min including 5 min of radiopharmaceutical quality control. A mean specific activity of 46.8±28.5 GBq/µmol was found in the large-scale syntheses. A representative analytical HPLC chromatogram of the purified, sterile [^{11}C]Me@HAPTHI is shown in figure 4b. The retention times in the analytical HPLC assay were 3.37 min (k'=2,17) for precursor HAPTHI, 1.8 min (k'=0.7) for [^{11}C]MeOH, 2.7 min (k'=1.55) for [^{11}C]CH_3OTf and 3.1 min (k'=1.9) for [^{11}C]CH_3I, respectively. The product [^{11}C]Me@APPI was eluted at a retention time of 4.38 min (k'=3.08). Radiochemical purity always exceeded 98%. Osmolality and pH values were at all times found to be in a physiological range. Residual solvent analysis using GC revealed MEK <5 ppm and ACN <20 ppm, besides 8.5% ethanol present in the product formulation (total product volume: 17.5 mL). Moreover, sterility and absence of endotoxins was approved for all produced batches of [^{11}C]Me@HAPTHI upon complete decay of radioactivity as *in-process* control.

3.2 Affinity and selectivity testings

Affinity of reference compounds (Me@HAPTHI and its radiolabeling progenitor HAPTHI) was determined using human NET membranes as Kd= 0.21 ± 0.07 nM for Me@HAPTHI and 24.2 ± 10.9 nM for HAPTHI, respectively (n≥9 triplicates). For determination of selectivity, the affinity of both reference substances was assessed on human DAT and SERT membranes and revealed >10 µM for both compounds for DAT and 409 ± 43 nM (Me@HAPTHI) and 10274 ± 1207 nM (HAPTHI) towards SERT, respectively, (n≥5 triplicates). Hence, selectivity of Me@HAPTHI towards NET was determined as DAT/NET>1947.6 and SERT/NET=9757. Both values clearly elucidate the ideal binding properties of our novel NET-PET ligand [^{11}C]Me@HAPTHI.

3.3 LogD analysis, IAM chromatography and blood-brain-barrier penetration

The lipophilicity of the novel NET-PET radioligand Me@HAPTHI was found to be in a decent range (logD= 2.27 ± 0.01) for a potential penetration of the BBB. The precursor HAPTHI showed a logD value of 2.30 ± 0.01. Additionally, BBB penetration experiments using IAM chromatography revealed a permeability of Pm=1.15 ± 0.25 for Me@HAPTHI and Pm=1.14 ± 0.27 for the precursor HAPTHI, respectively. Both values were within the identical, ideal range (Pm= 0.01-4.21) from other PET tracers,

known to easily penetrate the BBB [36].

3.4 Metabolic stability testing

Stability testing using human liver microsomes (n=4), revealed no significant metabolism of [^{11}C]Me@HAPTHI within the tested timeframe. After 60 min, 99.6±0.3 % of the tracer was found to be still intact. Incubation of [^{11}C]Me@HAPTHI with pooled male rat liver microsomes revealed a higher metabolic degradation. The percentage of intact tracer over time is presented in figure 6. Overall, 29.3±1.9 % tracer was still intact after 1 h incubation time. Thus, the stability of the novel NET PET tracer [^{11}C]Me@HAPTHI is encouraging in a human and rodent setting and superior to the established Reboxetine-derived PET tracer [^{18}F]FMeNER-D2 [29].

3.5 Plasma protein binding

The mean percentage of plasma free fraction (ff) and percentage of unspecific binding to the filter matrix of the Centrifee vials was determined. A plasma free fraction of ff = 8.2 ± 0.3 % (n=7 triplicates) as well as an unspecific filter retention of 51.26 ± 0.78 % was found. Overall, the ff of our novel NET-PET tracer [^{11}C]Me@HAPTHI was in the same range as that of [^{11}C]ADAM [37].

3.6 In vitro autoradiography, immunohistochemistry and Nissl staining

In the autoradiographic experiments, the highest uptake of [^{11}C]Me@HAPTHI was observed in NET-rich regions identified with immunohistochemistry (figure 7). Blocking was performed with non-radioactive NET-ligands FMeNER-D2 and Me@HAPTHI in two different concentrations each (100nM, 1µM). A concentration dependent binding displacement was observed using human tissue samples for both cold competitors. In table 2, an overview on the percentage of specific displaceable binding of [^{11}C]Me@HAPTHI and fmol/mm^2 values of relative transporter protein density on the different tissue sections is given. All values are given in % as mean n≥3 triplicates. Autoradiography of human cerebellum revealed NET specific uptake in NET-rich regions identified with IHC, though blocking experiments were not possible due to the enourmous inhomogeneity of the tissue samples. In human nucleus caudatus , a region known to be low in NET density, only unspecific binding was observed.

Immunohistochemical staining was used to allocate areas with high uptake in autoradiography with regions known high NET abundance. Hence, the NET antibody-dye complexes were found highly abundant in heart fibers, hippocampus, thalamus and hypothalamus, and to a fewer extent in all other brain regions (figure 7). NET specificity of staining was validated using a rabbit antibody isotype control.

Moreover, harvesting experiments with [^{11}C]Me@APPI using hNET expressing membranes were performed according to the affinity testing protocol. Thereby, a concentration dependent displacement of [^{11}C]Me@HAPTHI was observed for all tested competitor substances (cold FMeNER-D2 or Me@HAPTHI),and the counts were corrected for decay (figure 8). Using Graph Pad Prism, data correlation revealed akin binding displacement behaviour for both cold Me@HAPTHI as well as the established NET ligand FMeNER-D2 (n≥3 triplicates).

4. Discussion:

[^{11}C]Me@HAPTHI presents a large stride towards an improved, novel, feasibly producible PET tracer for NET imaging. This study comprises the first radiochemical preparation, quality control and *in vitro* evaluation of this novel candidate PET-tracer. We describe its affinity, selectivity, lipophilicity, its potential to penetrate the BBB as well as metabolic stability. Moreover, the *in vitro* binding behaviour of

[^{11}C]Me@HAPTHI to human NET cell membranes as well as human and rodent tissue slices was examined.

The excellent affinity of Me@HAPTHI (K_d hNET=0.21 ± 0.07 nM) and exceptional selectivity of our candidate NET-PET ligand, present the ideal ground for a further evaluation of this tracer. Moreover, a lower non-specific binding can be expected, as the described radioligand is less lipophilic than previous NET-PET tracers based on reboxetine (logD Me@HAPTHI=2.21, logD FMeNER-D2= 2.73). Based on the *in vitro* data acquired, successful BBB penetration by [^{11}C]Me@HAPTHI may be expected. This assumption is supported by immobilized artificial membrane chromatography results showing Me@HAPTHI to be within the discussed range of permeability Pm values.

Additionally, the high radiochemical yields and feasible radiosynthetic availability favour our newly developed NET radioligand. The employed ^{11}C-methylation reaction can be implemented at any PET facility with a cyclotron. Hence, this study presents a large stride towards a highly affine, selective and routine available radiotracer. Moreover, *in vitro* stability of [^{11}C]Me@HAPTHI against human liver microsomes, containing all human liver cytochrome P450 enzymes, is excellent (99.6±0.3 % intact tracer after 60min). In contrast, other existing PET tracers show significant metabolic degradation within this timeframe (e.g., [^{11}C]MeNER, [^{11}C]DASB or [^{11}C]WAY-100635 [15, 47, 48]). Also in the murine setting, where highly increased turn-over rates of the enzymes are present, a sufficient metabolic stability of [^{11}C]Me@HAPTHI was observed (29.26±1.95 % intact, 60 min).

Furthermore, a plasma free fraction of 8.4% was determined in ultrafiltration experiments, which was which was in a similar range with other clinically successful PET-tracers (e.g., [^{11}C]ADAM).

In vitro binding studies revealed specific displaceable binding in human brain regions and rat heart, indicating towards a promising further use of this tracer in *in vivo* studies. In competition experiments, a displacement was observed for blocking both with the established NET ligand FMeNER-D2 and Me@HAPTHI in a concentration dependent manner. The high radiotracer uptake areas matched with the high NET-density regions identified by immunohistochemistry. Therefore, specific NET uptake of [^{11}C]Me@HAPTHI can be affirmed. While this specific NET binding may be valid on *ex vivo* tissue, the question of binding behaviour on a cellular level was raised. Therefore, *in vitro* binding studies on human NET membranes were performed in a cell harvesting protocol. In these cell based experiments, which used the same parameters as autoradiography studies (i.e. incubation time, buffer etc.), a comparable concentration dependent binding displacement was found for both competitors FMeNER-D2 and Me@HAPTHI. Therefore, selective NET-uptake for our novel PET ligand [^{11}C]Me@HAPTHI could be confirmed on a cellular and on a human and rat tissue level.

Thus, [^{11}C]Me@HAPTHI was showing highly promising results *in vitro* so far and might therefore become an improved, routine NET PET tracer. As a next step, small animal experiments will be performed to further elucidate the *in vivo* behaviour of [^{11}C]Me@HAPTHI.

5. Conclusion:

A number of key properties have been discussed in the presented study, indicating that the benzothiadiazole dioxide [^{11}C]Me@HAPTHI presents a viable and improved NET-PET tracer.

We demonstrated its outstanding affinity & selectivity, its great stability in human liver microsomes, as well as promising results from *in vitro* autoradiography. Therefore, these data encourage us for an *in*

vivo application of this compound in small animal PET experiments in the future. On these grounds, [^{11}C]Me@HAPTHI, might improve clinical NET imaging.

6. Competing interests:

Dr. Alexander Hoepping is full employee at ABX Advanced Biochemical Compounds. No other conflicts of interest were present in the context of this paper.

7. Authors contributions

CRM: performed all radiosyntheses and preclinical in vitro experiments, autoradiography, immunohistochemistry and writing of the paper. NB: contributed to all radiosyntheses and metabolite studies. CP: contributed to in vitro autoradiography and immunohistochemistry. SF: contributed to the affinity and selectivity testing procedures. CV: contributed to IAM chromatography experiments and plasma free fraction. AH: performed the synthesis of the cold reference standard Me@HAPTHI and the precursor HAPTHI. RL: participated in the design of the study and proofread the manuscript. MH: Designed parts of the research and proofread the manuscript. MM: Conceived and supervised the preclinical experiments and proofread the manuscript. WW: Conceived and supervised the radiosyntheses and proofread the manuscript. All authors read and approved the manuscript.

8. Acknowledgements

The authors would like to thank Vanessa Fröhlich and Thomas Zenz for their practical and technical support. The authors are grateful to Marie Spies, MD, for native English editing.

9. References

1. Zhou J. Norepinephrine transporter inhibitors and their therapeutic potential. Drugs Future. 2004;29:1235–44.

2. Zhou J, Zhang A, Klaess T, Johnson KM, Wang CZ, Ye YP, et al. Biaryl Analogues of Conformationally Constrained Tricyclic Tropanes as Potent and Selective Norepinephrine Reuptake Inhibitors: Synthesis and Evaluation of Their Uptake Inhibition at Monoamine Transporter Sites. J Med Chem. 2003;46:1997-2007. doi:10.1021/jm020596w.

3. Curatolo P, D'Agati E, Moavero R. The neurobiological basis of ADHD. Italian Journal of Pediatrics. 2010;36:79.

4. Mash DC, Ouyang Q, Qin Y, Pablo J. Norepinephrine transporter immunoblotting and radioligand binding in cocaine abusers. Journal of Neuroscience Methods. 2005;143:79-85. doi:10.1016/j.jneumeth.2004.09.013.

5. Schlessinger A, Geier E, Fan H, Irwin JJ, Shoichet BK, Giacomini KM, et al. Structure-based discovery of prescription drugs that interact with the norepinephrine transporter, NET. Proceedings of the National Academy of Sciences of the United States of America. 2011;108:15810-5. doi:10.1073/pnas.1106030108.

6. Vazey EM, Aston-Jones G. The emerging role of norepinephrine in cognitive dysfunctions of Parkinson's disease. Frontiers in Behavioral Neuroscience. 2012;6:48. doi:10.3389/fnbeh.2012.00048.

7. Moldovanova I, Schroeder C, Jacob G, Hiemke C, Diedrich A, Luft FC, et al. Hormonal Influences on Cardiovascular Norepinephrine Transporter Responses in Healthy Women. Hypertension. 2008;51:1203-9. doi:10.1161/hypertensionaha.107.107433.

8. Harik S, Duckrow R, LaManna J, Rosenthal M, Sharma V, Banerjee S. Cerebral compensation for chronic noradrenergic denervation induced by locus ceruleus lesion: recovery of receptor binding, isoproterenol- induced adenylate cyclase activity, and oxidative metabolism. The Journal of Neuroscience. 1981;1:641-9.

9. Rommelfanger KS, Edwards GL, Freeman KG, Liles LC, Miller GW, Weinshenker D. Norepinephrine loss produces more profound motor deficits than MPTP treatment in mice. Proceedings of the National Academy of Sciences of the United States of America. 2007;104:13804-9. doi:10.1073/pnas.0702753104.

10. Wilson AA, Patrick Johnson D, Mozley D, Hussey D, Ginovart N, Nobrega J, et al. Synthesis and in vivo evaluation of novel radiotracers for the in vivo imaging of the norepinephrine transporter. Nuclear Medicine and Biology. 2003;30:85-92. doi:10.1016/s0969-8051(02)00420-1.

11. Takano A, Gulyás B, Varrone A, Halldin C. Comparative evaluations of norepinephrine transporter radioligands with reference tissue models in rhesus monkeys: (S,S)-[18F]FMeNER-D2; and (S,S)-[11C]MeNER. European Journal of Nuclear Medicine and Molecular Imaging. 2009;36:1885-91. doi:10.1007/s00259-009-1194-x.

12. Schou M, Halldin C, Sóvágó J, Pike VW, Hall H, Gulyás B, et al. PET evaluation of novel radiofluorinated reboxetine analogs as norepinephrine transporter probes in the monkey brain. Synapse. 2004;53:57-67. doi:10.1002/syn.20031.

13. Gulyás B, Brockschnieder D, Nag S, Pavlova E, Kása P, Beliczai Z, et al. The norepinephrine transporter (NET) radioligand (S,S)-[18F]FMeNER-D2 shows significant decreases in NET density in

the human brain in Alzheimer's disease: A post-mortem autoradiographic study. Neurochemistry International.56:789-98. doi:10.1016/j.neuint.2010.03.001.

14. Rami-Mark C, Zhang MR, Mitterhauser M, Lanzenberger R, Hacker M, Wadsak W. [18F]FMeNER-D2: reliable fully-automated synthesis for visualization of the norepinephrine transporter. Nucl Med Biol. 2013;40:1049-54. doi:10.1016/j.nucmedbio.2013.08.007.

15. Schou M, Zoghbi S, Shetty H, Shchukin E, Liow J-S, Hong J, et al. Investigation of the Metabolites of (S,S)-[11C]MeNER in Humans, Monkeys and Rats. Molecular Imaging and Biology. 2009;11:23-30. doi:10.1007/s11307-008-0175-y.

16. Zeng F, Jarkas N, Stehouwer JS, Voll RJ, Owens MJ, Kilts CD, et al. Synthesis, in vitro characterization, and radiolabeling of reboxetine analogs as potential PET radioligands for imaging the norepinephrine transporter. Bioorganic & Medicinal Chemistry. 2008;16:783-93. doi:10.1016/j.bmc.2007.10.025.

17. Zeng F, Mun J, Jarkas N, Stehouwer JS, Voll RJ, Tamagnan GD, et al. Synthesis, Radiosynthesis, and Biological Evaluation of Carbon-11 and Fluorine-18 Labeled Reboxetine Analogues: Potential Positron Emission Tomography Radioligands for in Vivo Imaging of the Norepinephrine Transporter. Journal of Medicinal Chemistry. 2008;52:62-73. doi:10.1021/jm800817h.

18. Zeng F, Stehouwer JS, Jarkas N, Voll RJ, Williams L, Camp VM, et al. Synthesis and biological evaluation of 2β,3α-(substituted phenyl)nortropanes as potential norepinephrine transporter imaging agents. Bioorganic & Medicinal Chemistry Letters. 2007;17:3044-7. doi:10.1016/j.bmcl.2007.03.056.

19. Mark C, Bornatowicz B, Mitterhauser M, Hendl M, Nics L, Haeusler D, et al. Development and automation of a novel NET-PET tracer: [11C]Me@APPI. Nucl Med Biol. 2013;40:295-303. doi:10.1016/j.nucmedbio.2012.11.009.

20. O'Neill DJ, Adedoyin A, Bray JA, Deecher DC, Fensome A, Goldberg JA, et al. Discovery of Novel Selective Norepinephrine Inhibitors: 1-(2-Morpholin-2-ylethyl)-3-aryl-1,3-dihydro-2,1,3-benzothiadiazole 2,2-Dioxides (WYE-114152). Journal of Medicinal Chemistry. 2011;54:6824-31. doi:10.1021/jm200733r.

21. O'Neill DJ, Adedoyin A, Alfinito PD, Bray JA, Cosmi S, Deecher DC, et al. Discovery of novel selective norepinephrine reuptake inhibitors: 4-[3-aryl-2,2-dioxido-2,1,3-benzothiadiazol-1(3H)-yl]-1-(methylamino)butan-2-ols (WYE-103231). J Med Chem. 2010;53:4511-21. doi:10.1021/jm100053t.

22. Larsen P, Ulin J, Dahlstrøm K, Jensen M. Synthesis of [11C]iodomethane by iodination of [11C]methane. Applied Radiation and Isotopes. 1997;48:153-7. doi:10.1016/s0969-8043(96)00177-7.

23. Kniess T, Rode K, Wuest F. Practical experiences with the synthesis of [11C]CH3I through gas phase iodination reaction using a TRACERlabFXC synthesis module. Applied Radiation and Isotopes. 2008;66:482-8. doi:10.1016/j.apradiso.2007.06.005.

24. Jewett DM. A simple synthesis of [11C]methyl triflate. International Journal of Radiation Applications and Instrumentation Part A Applied Radiation and Isotopes. 1992;43:1383-5. doi:10.1016/0883-2889(92)90012-4.

25. GE Healthcare U, Sweden.

26. Radioactive pharmaceuticals (Radiopharmaceutica, 6.0/0125), . European Pharmacopoeia (Europäisches Arzneibuch): Verlag Österreich GmbH; 2008. p. 995 ff.

27. Zeng F, Jarkas N, Owens MJ, Kilts CD, Nemeroff CB, Goodman MM. Synthesis and monoamine transporter affinity of front bridged tricyclic 3β-(4′-halo or 4′-methyl)phenyltropanes bearing methylene or carbomethoxymethylene on the bridge to the 2β-position. Bioorganic & Medicinal Chemistry Letters. 2006;16:4661-3. doi:10.1016/j.bmcl.2006.05.098.
28. Tejani-Butt SM. [3H]nisoxetine: a radioligand for quantitation of norepinephrine uptake sites by autoradiography or by homogenate binding. Journal of Pharmacology and Experimental Therapeutics. 1992;260:427-36.
29. Rami-Mark C, Philippe C, Vraka C, Nics L, Dumanic M, Spreitzer H, et al. Comparative In Vitro Evaluation of the Norepinephrine Transporter PET-ligands 11C-Me@APPI and 18F-FMeNER-D2. Journal of Nuclear Medicine. 2015:in review.
30. Donovan SF, Pescatore MC. Method for measuring the logarithm of the octanol–water partition coefficient by using short octadecyl–poly(vinyl alcohol) high-performance liquid chromatography columns. Journal of Chromatography A. 2002;952:47-61. doi:10.1016/s0021-9673(02)00064-x.
31. Naik P, Cucullo L. In vitro blood–brain barrier models: Current and perspective technologies. Journal of Pharmaceutical Sciences. 2012;101:1337-54. doi:10.1002/jps.23022.
32. Neuhaus W, Freidl M, Szkokan P, Berger M, Wirth M, Winkler J, et al. Effects of NMDA receptor modulators on a blood–brain barrier in vitro model. Brain Research. 2011;1394:49-61. doi:10.1016/j.brainres.2011.04.003.
33. Yoon CH, Kim SJ, Shin BS, Lee KC, Yoo SD. Rapid Screening of Blood-Brain Barrier Penetration of Drugs Using the Immobilized Artificial Membrane Phosphatidylcholine Column Chromatography. Journal of Biomolecular Screening. 2006;11:13-20. doi:10.1177/1087057105281656.
34. Tavares AA, Lewsey J, Dewar D, Pimlott SL. Radiotracer properties determined by high performance liquid chromatography: a potential tool for brain radiotracer discovery. Nucl Med Biol. 2012;39:127-35. doi:10.1016/j.nucmedbio.2011.06.011.
35. Rami-Mark C, Bornatowicz B, Fink C, Otter P, Ungersboeck J, Vraka C, et al. Synthesis, radiosynthesis and first in vitro evaluation of novel PET-tracers for the dopamine transporter: [(11)C]IPCIT and [(18)F]FE@IPCIT. Bioorg Med Chem. 2013;21:7562-9. doi:10.1016/j.bmc.2013.10.046.
36. Vraka C, Nics L, Weiss V, Wagner K-H, Hacker M, Wadsak W, et al. Combination of High Throughput HPLC Methods for Rapid Prediction of Blood Brain Barrier Penetration of Newly Developed Radiotracers - EANM 14. European Journal of Nuclear Medicine and Molecular Imaging. 2014;41:442. doi:10.1007/s00259-014-2901-9.
37. Huang Y, Hwang D-R, Narendran R, Sudo Y, Chatterjee R, Bae S-A, et al. Comparative Evaluation in Nonhuman Primates of Five PET Radiotracers for Imaging the Serotonin Transporters[colon] [lsqb]11C[rsqb]McN 5652, [lsqb]11C[rsqb]ADAM, [lsqb]11C[rsqb]DASB, [lsqb]11C[rsqb]DAPA, and [lsqb]11C[rsqb]AFM. J Cereb Blood Flow Metab. 2002;22:1377-98.
38. Gandelman MS, Baldwin RM, Zoghbi SS, Zea-Ponce Y, Innis RB. Evaluation of ultrafiltration for the free-fraction determination of single photon emission computed tomography (SPECT) radiotracers: beta-CIT, IBF, and iomazenil. J Pharm Sci. 1994;83:1014-9.
39. Price JC, May berg HS, Dannals RF, Wilson AA, Ravert HT, Sadzot B, et al. Measurement of Benzodiazepine Receptor Number and Affinity in Humans Using Tracer Kinetic Modeling, Positron

Emission Tomography, and [11C]Flumazenil. J Cereb Blood Flow Metab. 1993;13:656-67.
40. Sadzot B, Price JC, Mayberg HS, Douglass KH, Dannals RF, Lever JR, et al. Quantification of Human Opiate Receptor Concentration and Affinity Using High and Low Specific Activity [11C]Diprenorphine and Positron Emission Tomography. J Cereb Blood Flow Metab. 1991;11:204-19.
41. Schou M, Halldin C, Pike VW, Mozley PD, Dobson D, Innis RB, et al. Post-mortem human brain autoradiography of the norepinephrine transporter using (S,S)-[18F]FMeNER-D2. European Neuropsychopharmacology. 2005;15:517-20. doi:10.1016/j.euroneuro.2005.01.007.
42. Gulyás B, Brockschnieder D, Nag S, Pavlova E, Kása P, Beliczai Z, et al. The norepinephrine transporter (NET) radioligand (S,S)-[18F]FMeNER-D2 shows significant decreases in NET density in the human brain in Alzheimer's disease: A post-mortem autoradiographic study. Neurochemistry International. 2010;56:789-98. doi:http://dx.doi.org/10.1016/j.neuint.2010.03.001.
43. Philippe C, Haeusler D, Fuchshuber F, Spreitzer H, Viernstein H, Hacker M, et al. Comparative autoradiographic in vitro investigation of melanin concentrating hormone receptor 1 ligands in the central nervous system. Eur J Pharmacol. 2014;735:177-83. doi:10.1016/j.ejphar.2014.04.020.
44. Kádár A, Wittmann G, Liposits Z, Fekete C. Improved method for combination of immunocytochemistry and Nissl staining. Journal of neuroscience methods. 2009;184:115-8. doi:10.1016/j.jneumeth.2009.07.010.
45. Fukuda T, Koelle GB. The Cytological Localization of Intracellular Neuronal Acetylcholinesterase. The Journal of Biophysical and Biochemical Cytology. 1959;5:433-40.
46. Hofman F. Immunohistochemistry. Current Protocols in Immunology. 2001. doi:10.1002/0471142735.im2104s49.
47. Någren K, Halldin C, Pike VW, Allonen T, Hietala J, Swahn CG, et al. Radioactive metabolites of the 5-HT1A receptor pet radioligand, [carbonyl-11C]way-100635, measured in human plasma samples. Journal of Labelled Compounds and Radiopharmaceuticals. 2001;44:S472-S4. doi:10.1002/jlcr.25804401167.
48. Parsey RV, Ojha A, Ogden RT, Erlandsson K, Kumar D, Landgrebe M, et al. Metabolite Considerations in the In Vivo Quantification of Serotonin Transporters Using 11C-DASB and PET in Humans. Journal of Nuclear Medicine. 2006;47:1796-802.

10. Illustrations and Figures:

Figure 1: Chemical Structures of Reboxetine, and ^{11}C-labelled NET PET tracers [^{11}C]Me@APPI and [^{11}C]MeNER, [11C]MeNET and our novel NET-PET ligand [^{11}C]ME@HAPTHI. The red colored atom indicates the position of the radioisotope introduced by radiolabeling

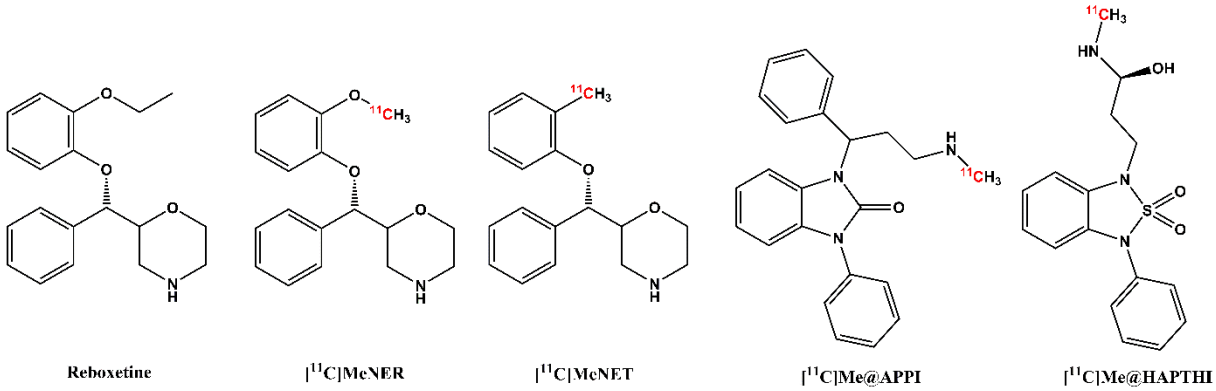

Figure 2: Radiosynthesis of [^{11}C]Me@HAPTHI starting from the precursor molecule HAPTHI

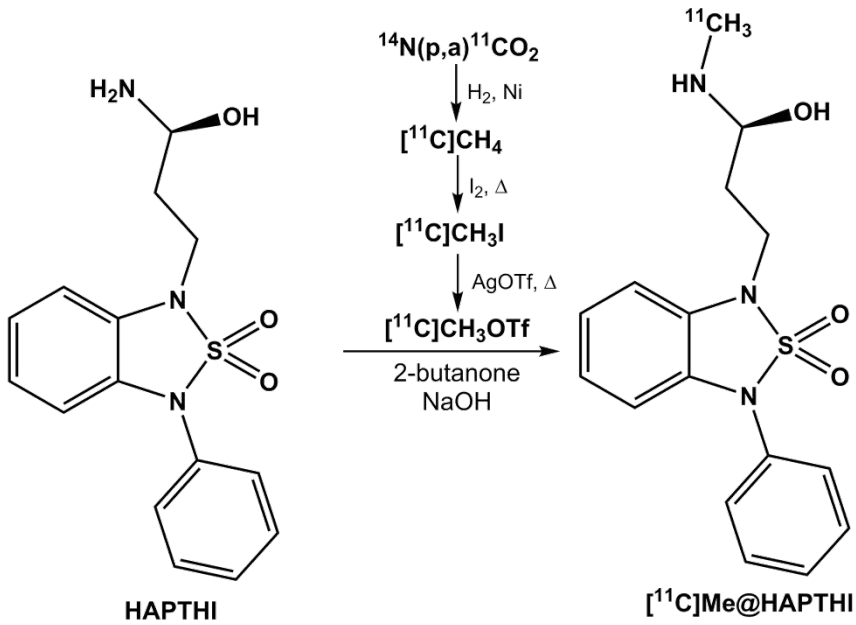

Figure 3: Flowscheme of the fully-automated radiosynthesis of [^{11}C]Me@HAPTHI

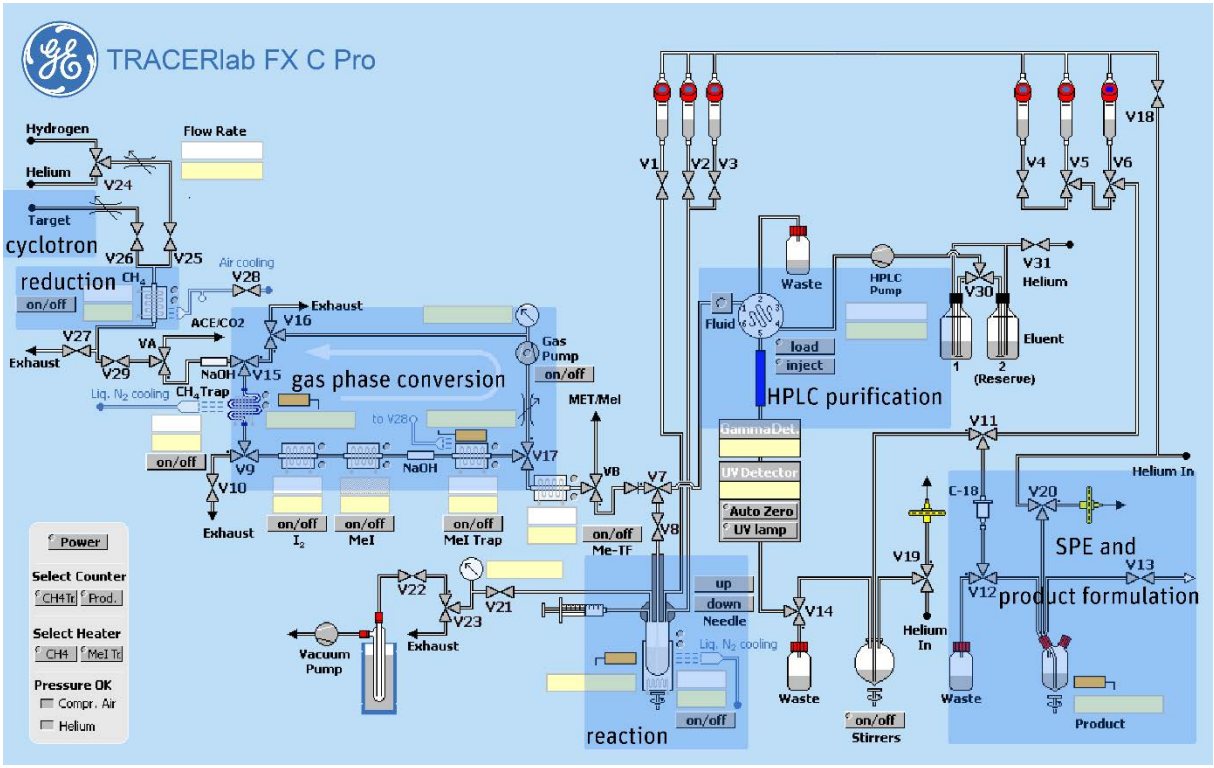

Figure 4: a) semi-preparative and b) analytical HPLC chromatogram

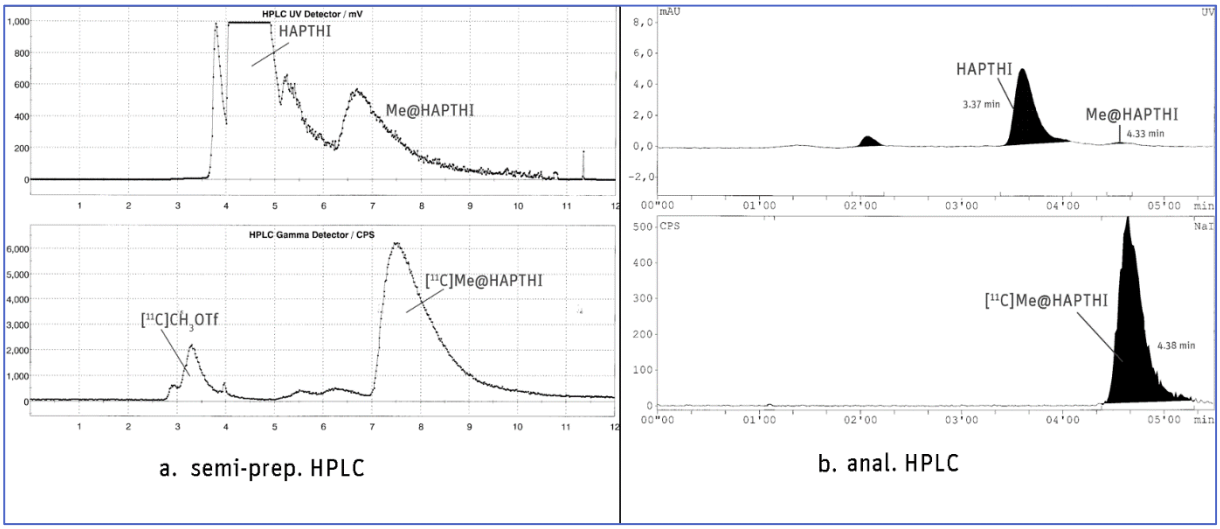

Figure 5: Dependence of the radiochemical incorporation yield of [^{11}C]Me@HAPTHI (n ≥ 3) on the ^{11}C-methylation agent (a) [^{11}C]methyliodide or (b) [^{11}C]methyltriflate) in DMSO and 2 butanone using different bases (NaOH, triethylamine or TBAH) at 2 min reaction time.

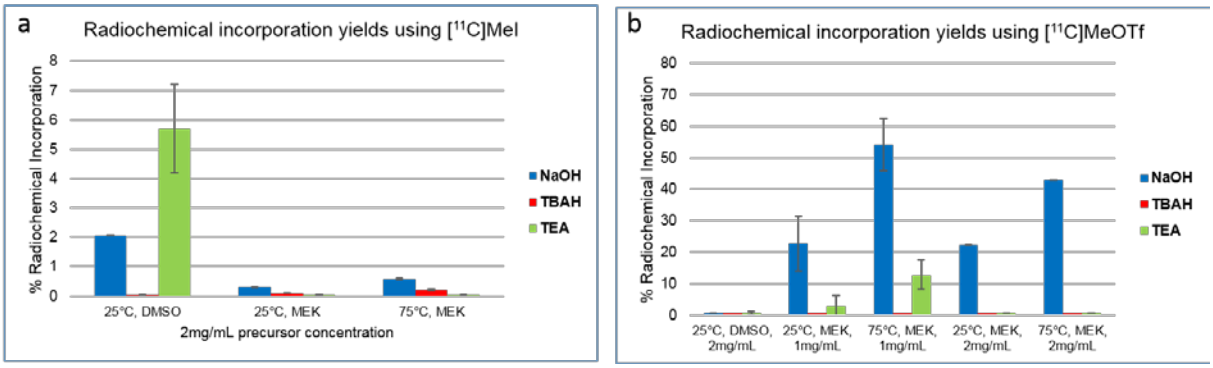

Figure 6: Metabolic stability of [^{11}C]Me@HAPTHI against human and rat liver microsomes

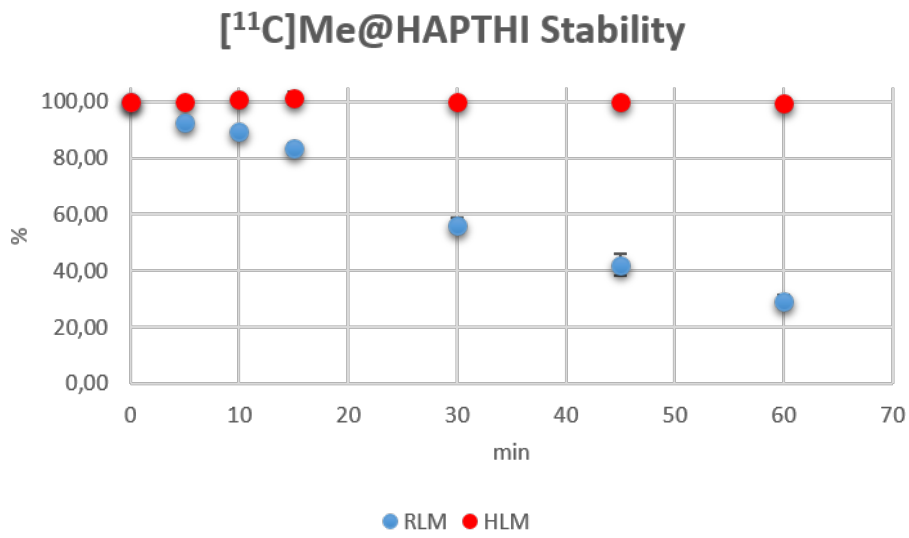

Figure 7: (a) NET-autoradiography and (b) immunohistochemistry of [^{11}C]Me@HAPTHI on 10µm slices of human cortex, thalamus, hypothalamus, cerebellum and nucleus caudatus as well as rat heart tissue and blocking with 100nM FMeNER-D2, 1µM FMeNER-D2, 100nM Me@HAPTHI and 1µM Me@HAPTHI. The scale shows the radioactivity from high (red) to low levels of radiotracer present on the Phosphor imager film.

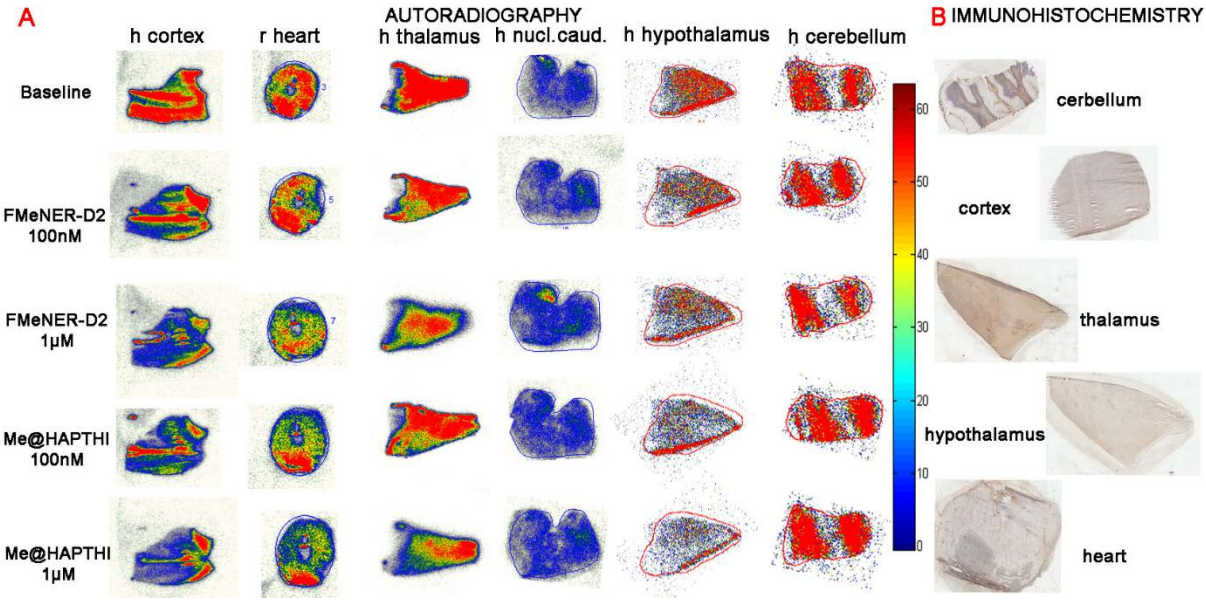

Figure 8: NET-binding of [^{11}C]Me@HAPTHI on human NET expressing cell membranes using a harvesting protocol. Competition was done using different concentrations of Me@HAPTHI and FMeNER-D2 (1,3,10,30,100 and 1000nM).

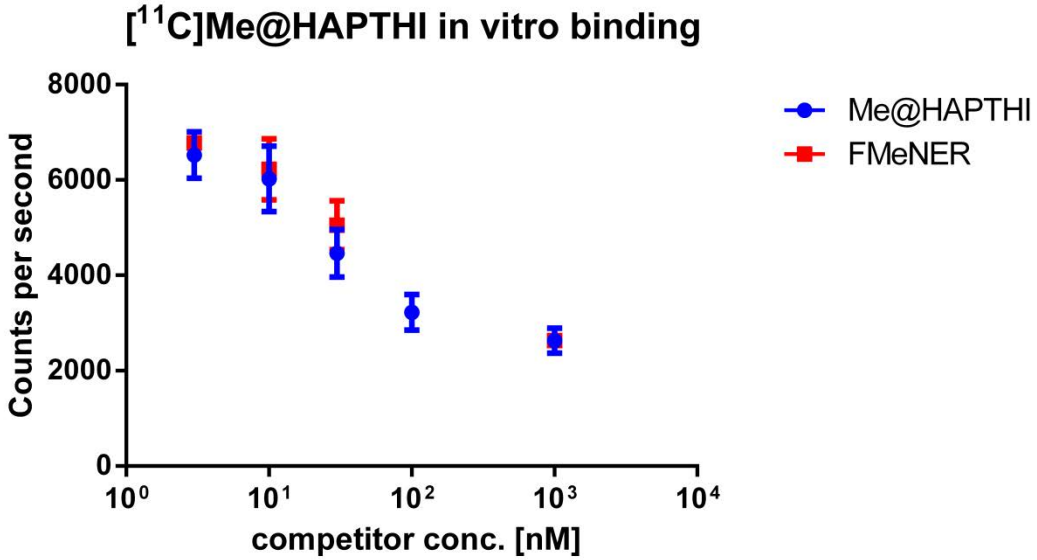

11. Tables and Captions

Table 1: Overview on the fully automated, large-scale radiosyntheses of [^{11}C]Me@HAPTHI. Reaction conditions: [11C]MeOTf, NaOH, MEK, 2mg/mL precursor concentration. EOS: end of synthesis, EOB: end of bombardment

[^{11}C]Me@HAPTHI (n=7)	*mean*	*SD*	*median*
starting activity [^{11}C]CO_2	53.4	2.4	53.9
trapped [^{11}C]CH_4	34.6	4.6	32
trapped [^{11}C]CH_3I	29.6	2.4	29
trapped [^{11}C]CH_3OTf in Reactor	16.6	5.5	17.2
after quenching	8.8	3.6	8.9
loss during injection in loop waste	1.0	0.5	0.8
product [^{11}C]Me@HAPTHI (EOS)	2.2	2.0	1.9
yield (decay corr. to EOB)	13.7	13.5	15.9
specific activity [GBq/µmol] (EOS)	43.4	29.7	59.2

Table 2: Overview of specific NET binding of the radioligand [^{11}C]Me@HAPTHI vs. Me@HAPTHI and, FMeNER-D2 on rat and human tissue origin. fmol values reflect calculated relative concentration (fmol/mm^2) of transporter protein). n.d.= not determined, limit of detection=0.01 fmol

TABLE 2	[^{11}C]Me@HAPTHI	
n≥3	*% BL-Competitor*	*fmol*
Rat heart		
FMeNER 1µM	88.8±11.2	<0.01
FMeNER 100nM	99.00±0.07	<0.01
Me@HAPTHI 1µM	92.5±7.5*	<0.01
Me@HAPTHI 100nM	104.5±4.5	<0.01
Human cortex		
FMeNER 1µM	71.9±7.9*	0.86
FMeNER 100nM	86.3±11.2*	<0.01
Me@HAPTHI 1µM	66.3±5.9*	1.32
Me@HAPTHI 100nM	82.1±13.9*	0.02
Human thalamus		
FMeNER 1µM	68.36±2.11	0.71
FMeNER 100nM	77.6±9.8	0.47
Me@HAPTHI 1µM	85.9±18.5	0.09
Me@HAPTHI 100nM	92.5±17.3	0.26
Human hypothalamus		
FMeNER 1µM	77.4±14.5	0.02
FMeNER 100nM	97.8±14.6	0.11
Me@HAPTHI 1µM	62.0±3.6*	0.04
Me@HAPTHI 100nM	83.7±1.7*	0.05
Human hippocampus		
FMeNER 1µM	67.3±8.2	<0.01
FMeNER 100nM	97.1±10.3	<0.01
Me@HAPTHI 1µM	68.3±5.3	<0.01
Me@HAPTHI 100nM	84.1±9.3	<0.01
Human nucleus caudatus		
FMeNER 1µM	107.6±17.7	n.d.
FMeNER 100nM	102.6±14.5	n.d.
Me@HAPTHI 1µM	110.0±21.0	n.d.
Me@HAPTHI 100nM	93.5±12.5	nd
Human cerebellum		
FMeNER 1µM	108.2±17.3	n.d.
FMeNER 100nM	103.9±12.2	n.d.
Me@HAPTHI 1µM	107.2±20.8	n.d.
Me@HAPTHI 100nM	124.7±10.8	n.d.

Captions:

Figure 1: Chemical Structures of Reboxetine, and ^{11}C-labelled NET PET tracers [^{11}C]Me@APPI and [^{11}C]MeNER, [11C]MeNET and our novel NET-PET ligand [^{11}C]ME@HAPTHI. The red colored atom indicates the position of the radioisotope introduced by radiolabelingFigure 2: Radiosynthesis of [^{11}C]Me@HAPTHI starting from the precursor molecule HAPTHI

Figure 3: Flowscheme of the fully-automated radiosynthesis of [^{11}C]Me@HAPTHI

Figure 4: a) semi-preparative and b) analytical HPLC chromatogram

Figure 5: Dependence of the radiochemical incorporation yield of [^{11}C]Me@HAPTHI (n ≥ 3) on the ^{11}C-methylation agent (a) [^{11}C]methyliodide or (b) [^{11}C]methyltriflate) in DMSO and 2 butanone using different bases (NaOH, triethylamine or TBAH) at 2 min reaction time.

Figure 6: Metabolic stability of [^{11}C]Me@HAPTHI against human and rat liver microsomes

Figure 7: (a) NET-autoradiography and (b) immunohistochemistry of [^{11}C]Me@HAPTHI on 10µm slices of human cortex, thalamus, hypothalamus, cerebellum and nucleus caudatus as well as rat heart tissue and blocking with 100nM FMeNER-D2, 1µM FMeNER-D2, 100nM Me@HAPTHI and 1µM Me@HAPTHI. The scale shows the radioactivity from high (red) to low levels of radiotracer present on the Phosphor imager film.

Figure 8: NET-binding of [^{11}C]Me@HAPTHI on human NET expressing cell membranes using a harvesting protocol. Competition was done using different concentrations of Me@HAPTHI and FMeNER-D2 (1,3,10,30,100 and 1000nM).

Table 1: Overview on the fully automated, large-scale radiosyntheses of [^{11}C]Me@HAPTHI. Reaction conditions: [11C]MeOTf, NaOH, MEK, 2mg/mL precursor concentration. EOS: end of synthesis, EOB: end of bombardment

Table 2: Overview of specific NET binding of the radioligand [^{11}C]Me@HAPTHI vs. Me@HAPTHI and, FMeNER-D2 on rat and human tissue origin. fmol values reflect calculated relative concentration (fmol/mm^2) of transporter protein. n.d.= not determined, limit of detection=0.01 fmol

3.2 UNPUBLISHED DATA

3.2.1 NET-ligand Database

Background:

The assessment of a structure activity relationship (SAR) for NET PET tracers urges for a database comprising all so far existing NET radioligands. Therefore, a substance library of 32 candidate tracers – not based on reboxetine - for the NET was set up based on previously described lead structures [236, 237, 239, 243, 244, 246, 333]. Thus, several additional benzo[d]imidazolone derivatives (FMe@APPI, FAPPI), 9 phenoxyisochromen derivatives (PHOXI), 4 indolinyl derivatives (DIMAP), 5 thiadiazole derivatives (HAPTHI) and 5 indolinole derivatives (MAPPI) have been designed (table 5). Amongst those, 21 have already been custom-synthesized by ABX Advanced Biochemical Compounds (Radeberg, Germany).

Table 5: Overview on the novel, potential NET-PET ligands

LEAD STRUCTURE	R1=	R2=	R3=	COMPOUND
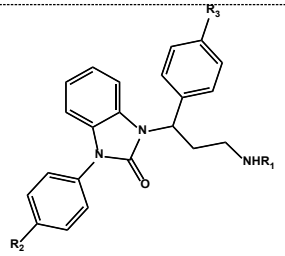	H	H	H	**APPI:0**
	CH_3	H	H	**Me@APPI**
	CH_2F	H	H	**FMe@APPI**
	CH_2CH_2F	H	H	**FE@APPI**
	CH_3	H	F	**FAPPI:1**
	CH_3	p-F	H	**FAPPI:2**
	CH_3	o-F	H	**FAPPI:3**
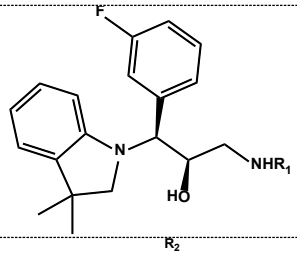	H	-	-	**DIMAP**
	CH_3	-	-	**Me@DIMAP**
	CH_2F	-	-	**FMe@DIMAP**
	CH_2CH_2F	-	-	**FE@DIMAP**
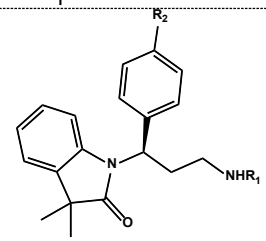	H	H	-	**MAPPI**
	CH_3	H	-	**Me@MAPPI**
	CH_2F	H	-	**FMe@MAPPI**
	CH_2CH_2F	H	-	**FE@MAPPI**
	CH_3	F	-	**MeF@MAPPI**
	H	H	-	**HAPTHI**
	CH_3	H	-	**Me@HAPTHI**

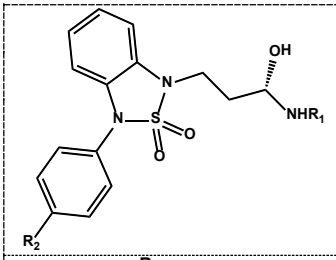	CH_2F	H	-	**FMe@HAPTHI**
	CH_2CH_2F	H	-	**FE@HAPTHI**
	CH_3	F	-	**MeF@HAPTHI**
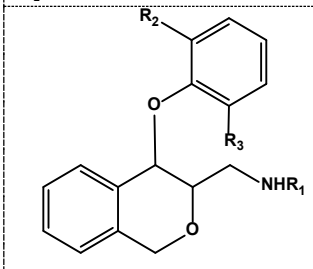	H	CH_3	H	**Phoxi 1**
	CH_3	CH_3	H	**Me@Phoxi1**
	CH_2F	CH_3	H	**FMe@Phoxi1**
	CH_2CH_2F	CH_3	H	**FE@Phoxi1**
	H	CF_3	H	**Phoxi 2**
	CH_3	CF_3	H	**Me@Phoxi 2**
	CH_2F	CF_3	H	**FMe@Phoxi 2**
	CH_2CH_2F	CF_3	H	**FE@Phoxi 2**
	H	CF_3	F	**Phoxi 3**
	CH_3	CF_3	F	**Me@Phoxi 3**
	CH_2F	CF_3	F	**FMe@Phoxi 3**
	CH_2CH_2F	CF_3	F	**FE@Phoxi 3**

Methods:

All available NET ligands were tested *in silico* for the determination of total polar surface area and *in vitro* for their binding affinity and selectivity; lipophilicity as well as their BBB penetration in IAM-chromatography. On these grounds, promising radioligands were identified and further evaluated. Hence, the radiosynthesis of these ligands was set up and optimized in small scale experiments and the optimum parameters used for automation of radiosynthesis for routine use. Upon a successful achievement of a fully automated radiosynthesis, a quality control following the guidelines of the European Pharmacopoeia was set up [1]. The radiolabeled NET-PET-tracers were subsequently tested for their *in vitro* stability against human and murine enzymes and their *in vitro* binding behavior was examined in competitive autoradiographic studies on *ex vivo* tissue samples of human and rat origin.

Results:

From the first data, based on affinity and selectivity values as well as logD, Pm and tPSA values, a structure - activity relationship can be proposed.

Table 6: First *in vitro* data of the tested novel NET-ligands (n≥6)

	Mol.weight	logD	tPSA	Km	Pm	Ki (NET)	Ki (DAT)	Ki (SERT)
APPI:0	343, 43	3.08±0.01	49,57			19.3±2.9	>5000	485±105
Me@APPI	357,46	3,14±0,001	35,58	197,87	0,55	3,03±1.2	10000	669
FE@APPI	375,45	3,70±0,01	35,58	1377,3	3,67	9,02±4,9	n.d.	
FAPPI:1	375,45	3,42±0,07	35,58	1168,4	3,11	46,88±56,9		
FAPPI:3	375,45	3,18±0,02	35,58	798,83	2,13	23,86±19,7		
Me@DIMAP	328,43	3,66±0,05	35,5	1539,41	4,69	3,34±1,0	>10000	
MAPPI	330,86	2,05±0,004	46,33	240,63	0,73	1350±325	>10000	
Me@MAPPI	308,43	2,15±0,01	32,34	269,37	0,87	60,97±20,4	>10000	
FE@MAPPI	340,44	2,77±0,0004	32,34	436,93	1,28	32181*	>10000	
HAPTHI	333,41	2,3±0,01	86,87	307,68	0,93	24,19±10,9	>10000	10274±1207
Me@HAPTHI	347,43	2,27±0,01	72,88	327,03	0,94	0,20±0,06	>10000	409±43
FE@HAPTHI	379,45	3,05±0,01	72,88	477,67	1,26	519,8±185	> 10000	

Highest affinity was observed for the methylated substances (table 6). Moreover, fluoroethylated candidates showed significantly lower affinity, indicating that the bulkiness of the fluoroethyl group might interfere with the binding pocket. Thus, we aimed for the fluoromethylated species to grasp whether a shorter FMe-group would be sterically tolerated or not. This fluorination would enable a radiolabelling with F-18, fostering a better availability of the novel PET-ligands. Unfortunately, in first experiments it turned out, that the stability of the FMe-derivatives is meager and a synthesis not viably yielding suitable amounts of cold reference compounds so far.

Thus, best *in vitro* results were obtained for Me@HAPTHI, Me@APPI and Me@DIMAP. Therefore, radiosynthesis of the ^{11}C-methylated HAPTHI and APPI was set-up, optimized and fully automated (manuscript #1 and #6). With the radiolabelled ^{11}C-NET PET tracers, stability testing was performed, indicating towards highly stable candidate ligands (both [^{11}C]Me@HAPTHI and [^{11}C]Me@APPI, respectively). A selective NET-binding was observed in *in vitro* autoradiography for both ligands. However, binding studies using [^{11}C]Me@HAPTHI showed a concentration dependent binding displacement, whilst [^{11}C]Me@APPI showed a binding enhancement when competed with cold NET ligands. However, using both NET-PET tracers in a cell based competition binding study, a concentration dependent binding displacement was observed for both ligands. Thus, a selective NET uptake can be supposed for both [^{11}C]Me@HAPTHI and [^{11}C]Me@APPI.

Due to a lack of the suitable precursor for the radiolabeling of DIMAP, a radiosynthesis could not be attained yet, but will be accomplished in the near future.

Conclusion:

A substance library for potential NET-PET ligands was set up, and a clear structure-activity relationship can be observed. Based on the *in vitro* results, a methyl amino group at the aliphatic chain seems to be inevitable for high NET affinity and optimal pharmacological properties. So far, the best candidate NET-ligands were [^{11}C]Me@HAPTHI and [^{11}C]Me@APPI. These two radiotracers showed highly promising results regarding their

in vitro stability and binding behavior in *in vitro* autoradigraphy. Thus, two novel, auspicious NET-PET ligands were identified and will be evaluated *in vivo* in future studies.

3.2.2 [^{18}F]FE@APPI

Aim and Background:

Since the methylated benzo[d]imidazolones showed promising results so far, we aimed at the preparation of a fluoroethylated derivative – FE@APPI (figure 33). There is ample support for a radiofluorinated NET PET tracer, not merely enabling a reasonable satellite distribution to other facilities due to the longer half-life of ^{18}F but rather facilitating improved PET images (i.e. the slowly reachable binding equilibrium urges a use of longer-lived radionuclides).

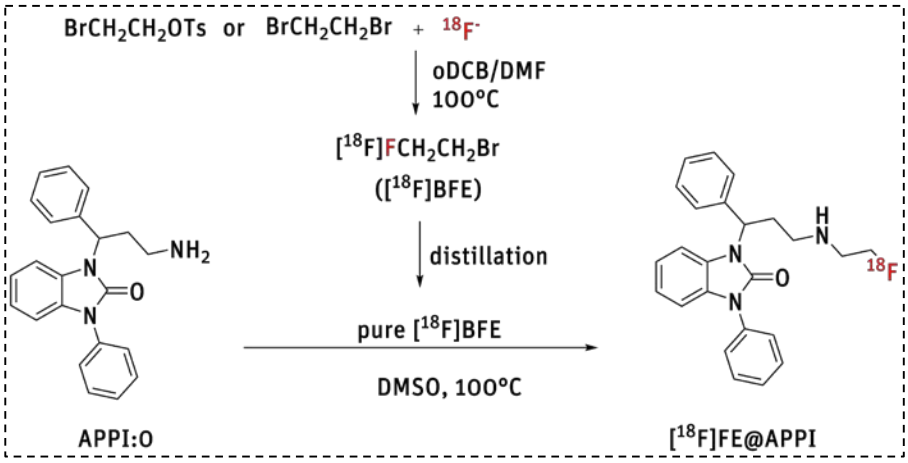

Figure 33: radiosynthesis of [^{18}F]FE@APPI

Methods:

Therefore, small scale experiments were performed using [^{18}F]fluoroethyltosylate and 1-bromo-2-[^{18}F]fluoroethane as [^{18}F]fluoroethylation synthons (figure 33). The nucleophilic substitution of the respective progenitor (1,2-dibromoethane or ethane-1,2-diyl-bis(4-methylbenzenesulfonate)) with azeotropically dried [^{18}F]fluoride was achieved almost quantitatively. However, a purification step between the two reaction steps was essentially required. Thus, the first SN_2-reaction was carried out in solvents with high boiling point (*N,N*-

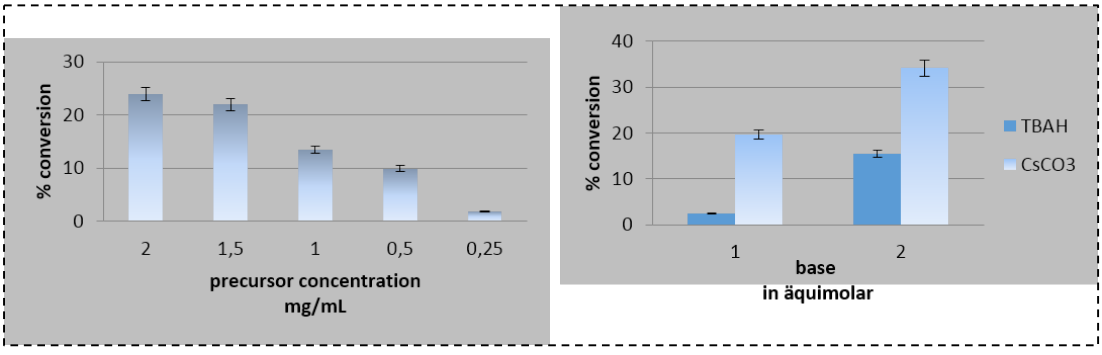

Figure 34: dependency of the radiochemical incorporation yield of [18F]FE@APPI on a) precursor concentration and b) base used as catalyst (n≥4)

dimethylformamide (DMF) or ortho-dichlorobenzene (o-DCB)) at 100°C for 10 minutes and subsequently the prepared 1-bromo-2-[^{18}F]fluoroethane distilled at 100°C with a supportive He-stream.

To avoid spill-over traces within the next reaction, an empty vial was interconnected between the two reaction vials. The [^{18}F]fluoroalkylation synthons were trapped in dimethylsulfoxide (DMSO) for the subsequent nucleophilic reaction with APPI:0 (precursor, figure 33) following the previously established principle of rapid translation from 11C-methylated to 18F-fluoroethylated tracers using the same precursor molecule [42]. To achieve higher conversion yields, the influence of base and precursor concentration was tested. In figure 34, the tested parameters are outlined.

Results:

For small scale reactions, optimum parameters were:

- dibromomethane and [^{18}F]fluoride, 10 Min 100°C, subsequent distillation
- Trapping of [^{18}F]BFE in DMSO
- 1,5 mg/mL Precursor, 100°C, 20 Min reaction time
- Basic catalysis with Cs_2CO_3 (aqueous, 2mg/µL)

With these parameters, a maximum radiochemical incorporation yield of 34±5.6% [^{18}F]FE@APPI was obtained in small scale experiments. On logic grounds, there was no compelling reason to perform upscaled reactions, necessary to achieve suitable yields for a latter (pre-)clinical application. Interestingly, it was found that radiochemical yield decreased with increase in reaction volumes (figure 35). Even, further increase or decrease of base or precursor concentration did not result in improved behavior.

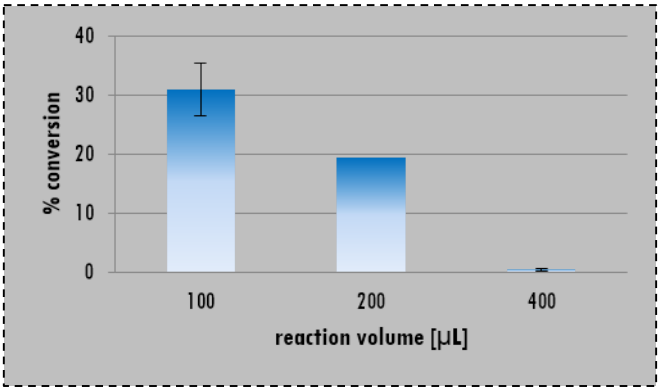

Figure 35: effect of increasing reaction volume on conversion yields (n=4)

Conclusion:

A clinical application cannot be supported with these observed radiochemical yields. However, the lipophilicity and affinity of this [^{18}F]fluoroethylated APPI-derivative were not promising as well (logD=3.49±0,01, K_i hNET=246±37nM, K_i hDAT>10000nM, K_i hSERT >1000nM). Therefore, a further future evaluation of [^{18}F]FE@APPI is not planned.

3.2.3 [^{11}C]FAPPI and [^{18}F]FAPPI

Aim and Background:

Along similar lines, an additional approach of labeling the benzoimidazolone scaffold with ^{11}C and ^{18}F is presented with the FAPPI derivatives. A closer look at the molecular structure enables a mulitnuclide radiolabeling strategy. Therefore, the 5 different radio-topoisomers, depicted in figure 36, were designed, tested for their *in vitro* properties and suitable labeling precursors were designed.

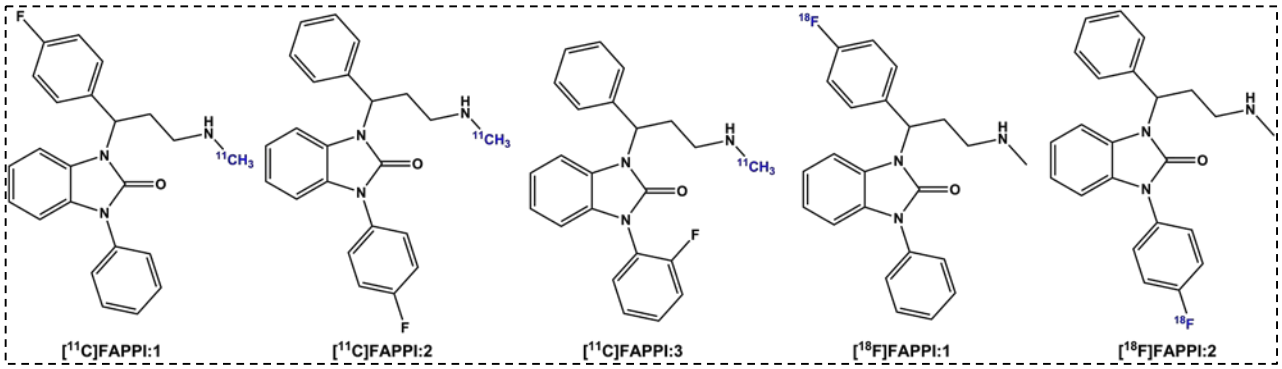

Figure 36: Overview on the different FAPPI radiolabeling positions

Methods:

Radiolabeling with carbon-11 can be reached straightforwardly via nucleophilic substitution of the primary phenylpropyl amine using [^{11}C]CH_3I or [^{11}C]CH_3OTf. Introduction of a fluorine-18 can be accomplished in a more complex manner via Stille coupling or Buchwald Hartwig amination using the respective precursors (figure 37).

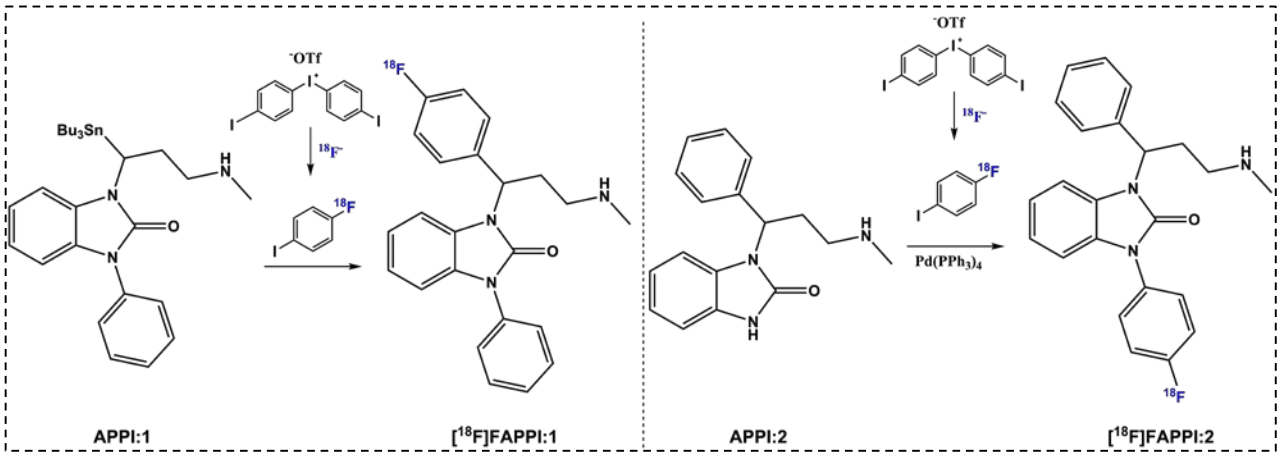

Figure 37: Radiolabeling strategy for the ^{18}F-labeled FAPPI radioligands

For these metal catalyzed coupling reactions, the labeling synthon 1-[^{18}F]fluoro-4-iodobenzene needs to be prepared freshly from bis(4-iodophenyl)iodonium triflate for each batch.

However, before a radiosynthesis is attempted, *in vitro* tests regarding the suitability of the novel NET-PET tracers are required. Thus, only upon a reasonable NET affinity and selectivity, as well as decent lipophilicity

and BBB-permeability, a radiosynthesis is performed.

Therefore, lipophilicity was tested using a HPLC based method for determination of lipophilicity [334]. Thereby, a short octadecyl–poly(vinyl alcohol) polymeric column was used with a rapid MeOH/ aqueous phosphate buffer gradient at a flow rate of 1mL/min. By using two internal standards (i.e. toluene and triphenylene) the retention time can be converted in the logD value of the respective tested substance.

Moreover, affinity and selectivity of the FAPPIs was tested in membrane binding experiments using a cell harvester. The human NET and DAT membrane preparations were incubated in competition experiment with a tritiated radioligand with known affinity to the respective target. Using different competitor concentrations (i.e. FAPPIs), the resulting hNET or hDAT membrane bound activity of the ^{3}H-ligand on the glass fiber filter is determined in a beta-counter. Subsequently, the affinity of the candidate compounds can be deduced via the sigmoidal competition curve using Graph Pad Prism software (San Diego, USA).

For determination of permeability through the BBB, a slightly modified HPLC protocol from Tavares et al. was used [283, 335]. Therefore, an artificial phosphatidyl choline coated column was used isocratically with different ratios of ACN/aqueous phosphate buffer at a flow rate of 1 mL/min. Depending on the interactions of the candidate substance with the phosphatidyl choline scaffold – mimicking passive diffusion- the retention time varies. Extrapolation of the retention time to purely aqueous, physiological conditions and factoring in the molecular weight of the test compound as well as the column parameters, the partition coefficient and the permeability can be calculated.

Results:

Affinity of the three cold FAPPI reference molecules revealed a moderate to high affinity for hNET in membrane binding experiments using a cell harvester (Ki_{NET}=9.02±4.9nM for FAPPI:1, Ki_{NET}=46.88±56.9nM for FAPPI:2 and Ki_{NET}=23.86±19.7nM for FAPPI:3). Affinity towards hDAT was <10 µM for all three compounds. Moreover, a $logD_{HPLC}$ of 3.7±0.01, 3.42±0.01 and 3.18±0.07 was obtained for FAPPI:1, FAPPI:2 and FAPPI:3, respectively. In IAM-chromatography experiments, a BBB-permeability of Pm= 3.669 was determined for FAPPI:1, and Pm= 3.112 for FAPPI:2 as well as Pm=2.12 for FAPPI:3. Moreover, a total polar surface area of 35.58 was calculated for all three compounds using ChemBioDraw Ultra (Camebridge Soft, Perkin Elmer).

Conclusion:

The low density of NET in human brain, requires an affinity in the single-digit nM range of the candidate compounds. Therefore, radiolabeling of FAPPI:2 and FAPPI:3 was omitted. Moreover, the high Pm values for all tested compounds indicate towards a poor BBB-penetration, only the low affinity FAPPI:3 showed a permeability in a more reasonable range. With a high logD value (logD> 3) for all three FAPPIs, the unspecific binding is estimated to be high and BBB penetration might be hampered. Therefore, a radiolabeling of the FAPPI compounds will not be performed. Unfortunately, these novel compounds did not show the expected favorable properties.

3.2.4 [^{18}F]FMeNER-D2 and its metabolic stability

Aim and Background:

Present understanding of the metabolic stability of [^{18}F]FMeNER-D2 is limited, but uptake of its metabolite(s) is severely interfering with the interpretation of the NET-PET signal in areas adjacent to the skull (see manuscript #3, figure 38). Hitherto, the arising radio-metabolite(s) are still unidentified, but alleged to be [^{18}F]fluoride - thus resulting in bone uptake or meningeal uptake in cortical regions. To gain insight in the enzymatic mechanisms of [^{18}F]FMeNER-D2 degradation, a systematic evaluation of the metabolic cleavage of the NET-PET-tracer was performed using various enzymes and the binding behavior of the parent compound as well as the radiometabolites to human bone matter (diaphysis) as well as inorganic bone mineral matrix (hydroxyapatite (HA)) was examined.

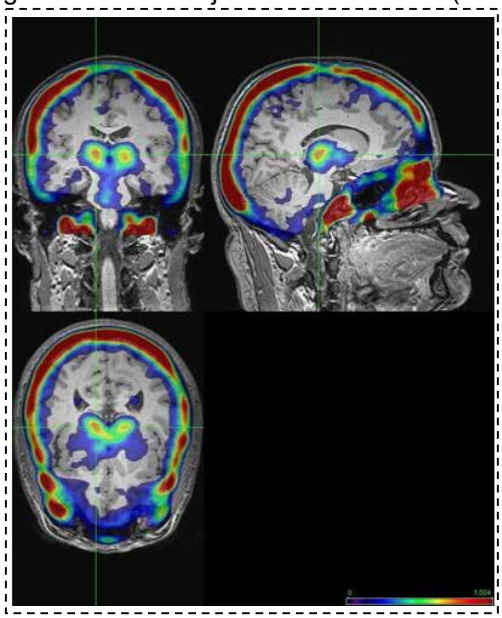

Figure 38: human PET-scan of [^{18}F]FMeNER-D2 in a healthy volunteer [manuscript#3]

Methods:

Incubation of the radiotracer preparation (containing <0.1% ethanol in the final incubation solution) with a selected single enzyme or a multi enzyme complex were performed under physiological conditions (10mM phosphate buffer, pH 7.4, 37°C). The tested enzymes were:

multi-enzyme complexes:

- human liver microsomes (HLM)
- rat liver microsomes (RLM)
- human carboxylesterase (CES) (hCES 1; hCES 2 and hCES 3)

single enzymes:

- monoaminooxidase A (MAO A)
- monoaminooxidase B (MAO B)
- catechyl-*O*-methyltransferase (COMT)
- CYP 1A1
- CYP 3A4
- CYP 2A6
- CYP 2E1
- CYP 1B1
- CYP 2C19
- CYP 2D6

After 5min pre-incubation of the enzymes, which require NADP(H) as co-factor, with a NADPH-generating system (solution-A: $NADP^+$, Glucose-6-phosphate and magnesium-chloride in H_2O and solution-B: Glucose-6-phosphate dehydrogenase in sodium citrate) under physiological conditions, 10µL of the freshly prepared

radiotracer was added and placed in a thermomixer at 37°C and 350rpm. The incubation of [^{18}F]FMeNER-D2 was stopped at certain time-points (depending on the degradation kinetics) by quenching of an aliquot with an equivolume of an ice-cooled ACN/MeOH (9/1) mixture. The mixture was centrifuged at 22600xg for 4 min at 4°C and the supernatant analyzed by analytical HPLC and thin layer chromatography (TLC, Silica Gel, 70/30 ACN/H_2O). The ratio of intact tracer to radiometabolites was determined and the obtained data processed with Microsoft Excel.

Results:

Incubation of [^{18}F]FMeNER-D2 with rat liver microsomes revealed a rapid cleavage, which lead to the formation of three different radio-metabolites. In figure 39, the percentage of intact tracer over time is outlined. After 3 min incubation time, only 5.36±5.6% of tracer were found to be unmetabolized, and after 10 min no intact radiotracer was detectable. From TLC analysis, the formation of free [^{18}F]fluoride can be vastly excluded (0% $^{18}F^-$, at all timepoints). Thus, these findings do not at all corroborate the suspected bone uptake through the expected defluorination, but purport a specific uptake of the radiometabolite(s) in cortical/meningeal regions.

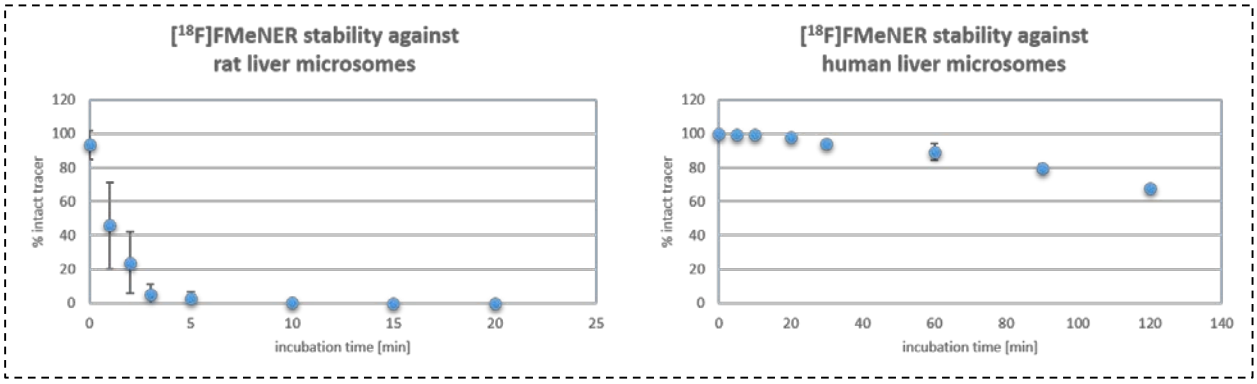

Figure 39: Metabolic stability of [18F]FMeNER-D2 over time against rat and human liver microsomes

Using the akin set-up for human liver microsomes, a higher metabolic stability was observed – reflecting the lower turn-over numbers from HLMs compared to RLMs (figure 39). Thus, after 90 min incubation of [^{18}F]FMeNER-D2 with HLMs still 79.6±2.5% of the radiotracer was found to be intact. Also in this species, no defluorination was detectable, pinpointing towards a species independent enzymatic reaction.
To identify the responsible singe enzyme(s) involved in the metabolic breakdown of the radiotracer, incubation with different CYPs and other enzymes was performed. Thereby, no metabolites were formed with COMT, MAO A, MAO B, CES, CYP 1A1, CYP 2E1, CYP2A6 and CYP 2B1 within 240 min (n≥2). Thus, the metabolic instability of [^{18}F]FMeNER-D2 is probably not attributed to any of the aforementioned enzymes.

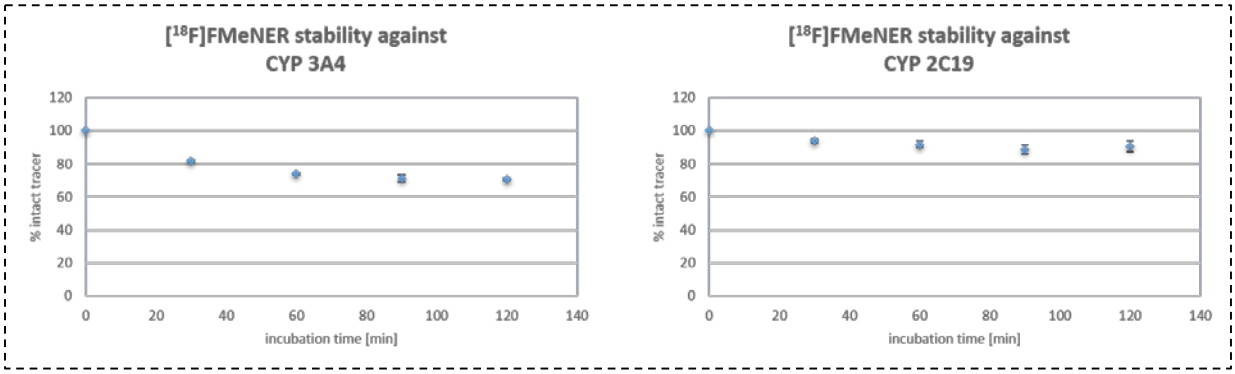

Figure 40: Metabolic stability of [^{18}F]FMeNER-D2 over time against human CYP 3A4 and CYP 2C19

In contrast, incubation of [^{18}F]FMeNER-D2 with CYP 3A4 lead to a significant cleavage, outlined in figure 40. Incubation with human CYP 2C19 lead to a metabolic degradation of 11.4±2.4% of [^{18}F]FMeNER-D2 after 90 min. Data gathered from incubation with CYP 3A4 yielded 70.7±0.7% intact tracer after 90 minutes.

The question whether these two single enzymes are responsible for the overall degradation of [^{18}F]FMeNER-D2 in RLM or HLM was addressed next. Selective enzyme inhibitors were added to the liver microsomal preparation and preincubated for 5 min, and the [^{18}F]FMeNER-D2 added. The change in metabolic stability was determined.

For CYP 3A4 (and to less extent also CYP 2C19) ketoconazole, for CYP 2C19 benzylnirvanone and for CYP 2D6 quinidine were added in different concentration (2,5,10 µM) to inhibit the single CYP in the multienzyme complex. As negative control, inhibitors of CYP single enzymes (i.e. quinidine, montelukast, furafyllin) - not able to degrade [^{18}F]FMeNER-D2 - were employed, and did not result in any change of metabolic degradation.

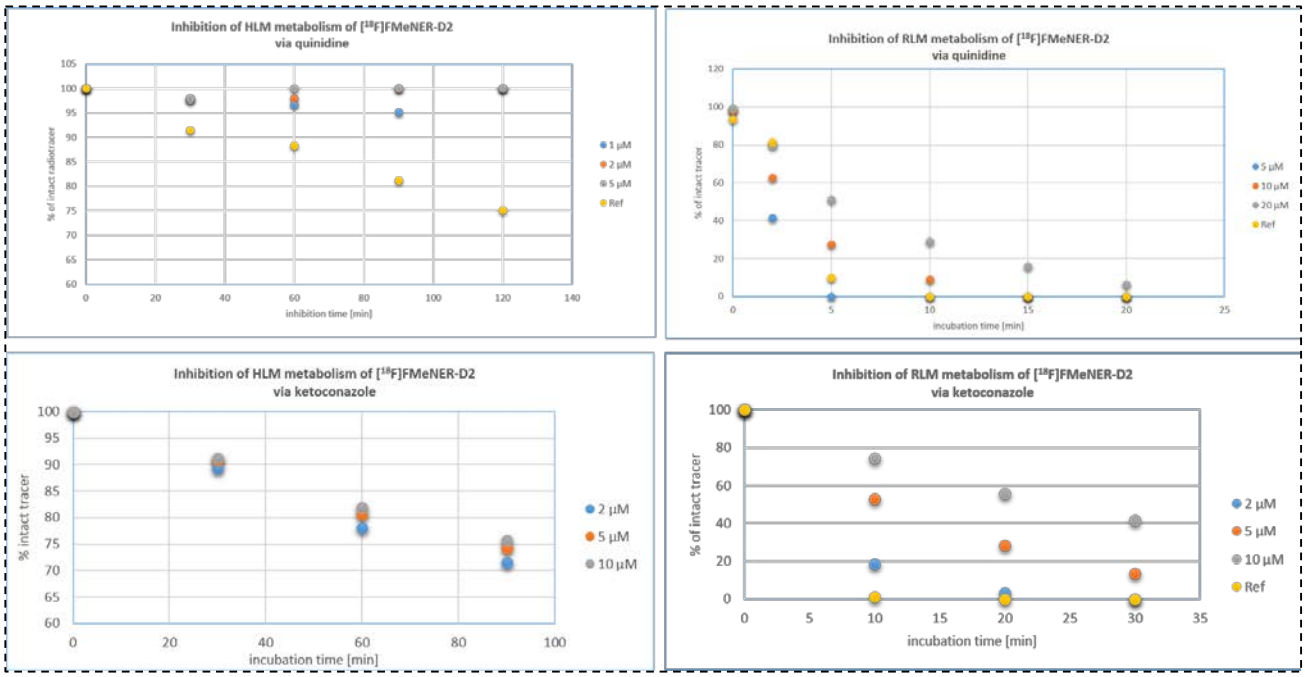

Figure 41: Inhibition of single enyzmes in the RLM and HLM over time against rat and human liver microsomes

As clearly outlined in figure 41, a concentration dependent inhibition of the respective single enzyme within the HLM and RLM was obtained, fostering a potential key role of these two single enzymes involved in the xenobiotic cleavage of the radiolabelled Reboxetine-derivative [^{18}F]FMeNER-D2.

In bone binding studies, no significant uptake was observed for the intact radiotracer [^{18}F]FMeNER-D2 when incubation with hydroxylapatite (HA) or human diaphysis (5.76±2.1 % binding, comparable to [^{18}F]FDG) This uptake is suggesting only a non-specific binding. As positive control (99.8% binding) [^{18}F]NaF and as negative control [^{18}F]FDG (2-3% binding) were used. Incubation of the metabolized tracer from RLMs (100% cleavage) resulted in less uptake in bone matter (HA:1.5±0.3%, diaphysis: 1.3±0.01%). Therefore, only a non-specific uptake can be assumed for both intact [^{18}F]FMeNER-D2 and the radiometabolites with decreased polarity.

Conclusion:

The metabolic stability of the NET-PET tracer [^{18}F]FMeNER-D2 is rather limited in the human and strongly retrenched in an animal metabolic model. The impact of arising radiometabolites on human and small animal PET scans is known to hamper a proper quantification in cortical areas. This metabolic degradation could be primarily attributed to CYP enzymes within the liver (CYP 3A4 and 2D6), but not to central occurring enzymes (MAO A+B, COMT). The formation of fluoride can be utterly excluded, and no specific bone uptake could be observed for both intact [^{18}F]FMeNER-D2 and its radiometabolites.

Thus, the impeding uptake in cortical areas in the human PET scan might be attributed to uptake in cortical tissue or meninges via still unknown mechanisms.

4 SUMMARY AND DISCUSSION

This thesis has highlighted the importance of the norepinephrine transporter in a variety of neurological, psychiatric and cardiac diseases. To comprehend the molecular mechanisms involved in NET-dysregulation and their *in vivo* impact on patient treatment, non-invasive PET imaging can detail the complex patho-physiological interactions on a molecular level. Within this thesis, several new NET-PET radioligands – for the first time not based on the Reboxetine structure - were successfully synthesized and evaluated. These novel PET-imaging probes, especially the methylated NET-PET tracers [^{11}C]Me@APPI and [^{11}C]Me@HAPTHI, will help to facilitate an early stage *in vivo* diagnosis and treatment control in numerous neurological and psychiatric diseases as well as cardiovascular maladies. The enhanced stability and rather different metabolites arising by CYPs and other enzymes should therefore enable a quantification of brain-NET without impeding bone/meningeal uptake, as observed for so-far described fluorinated Reboxetine-based radiotracers [172].

4.1. REBOXETINE DERIVED NET-PET-TRACER: [^{18}F]FMENER-D2

In vivo imaging in a clinical human setting requires a complete toxicological analysis and full assessment of biological activity and safety of the newly developed tracer. Unfortunately, only established NET-PET tracer based on Reboxetine are so far fulfilling the respective criteria. Therefore, aim of this thesis was an improvement of the rather complex radiosynthesis of [^{18}F]FMeNER-D2 for routine clinical applications. To facilitate a reliable pharmaceutical production, a fully automated preparation of this NET-PET tracer was set-up for the first time, allowing a reproducible synthesis for human studies. The radiosynthesis was optimized successfully, yielding high amounts of product - considering the complex radiosynthesis – and excellent specific activities. Moreover, a large reduction in radiation burden for the radiochemists was reached through a remotely controlled, automated production.

Autoradiography on human and murine tissue samples was performed. Competition experiments with known and newly developed NET ligands resulted in a concentration dependent binding displacement and therefore selective NET-uptake.

However, the detriment of the Reboxetine-derived PET tracers is their high metabolic cleavage – resulting in impeding signals in the PET scans which hamper a proper quantification of NET in cortical regions. To comprehend the arising uptake, a metabolic stability testing was performed *in vitro* using a plethora of human and murine enzymes. Hereby, no metabolism was observed using central occurring enzymes, like MAO A, MAO B or COMT. Though, incubation of [^{18}F]FMeNER-D2 with CYP P450 enzymes, predominantly located in the liver, lead to a significant and fast metabolism of the tracer. Moreover, the arising three radiometabolites were found to be more polar than [^{18}F]FMeNER-D2. Surprisingly, no formation of free [^{18}F]fluoride was been observed. On these grounds, the interfering uptake in cortical regions, but not in bone matter, might be attributed to these emerging radiometabolites. Further research on these radiometabolites might include an analysis of human blood samples after injection of the radiotracer, to draw a firm conclusion about the metabolic

fate of [^{18}F]FMeNER-D2. However, the interfering signals in NET-PET scans cannot be eliminated - therefore better ligands for NET-PET imaging are still of high interest.

4.2. ^{11}C AND ^{18}F LABELED BENZOIMIDAZOLONE DERIVATIVES

The development of NET-PET tracers based on a benzoimidazolone scaffold, lead to several candidate substances. These compounds were evaluated *in vitro* regarding their affinity, selectivity and lipophilicity prior to a potential radiolabeling. Best results were obtained for the methylated compound, Me@APPI. Its high affinity, selectivity and stability favor this NET-PET tracer for a future *in vivo* application. Moreover, high NET-affinity was found for the fluoroethylated compound FE@APPI, but unfortunately lipophilicity and selectivity turned out to be poor. Thus, other ^{18}F-fluorinated substances were designed: the FAPPI derivatives. However, the fluorination of the aryl rings resulted in lower affinity towards NET (FAPPI 1+3), therefore no radiosynthesis was set up. As outlined in the unpublished data, fluoromethylated derivatives would present a highly interesting alternative to the ^{11}C methylated tracers, enabling a longer equilibration time due to the longer half-life of the fluorine-18. However, all trials to accomplish the synthesis of reference standards of the FMe-substances did, so far, not result in sufficient substance quantities – indicating towards an overall low stability of these fluoromethylated compounds.

The radiosyntheses of [^{11}C]Me@APPI was successfully established in small scale and large scale automated experiments. Sufficient quantities of radioactivity (~1.5Gq) were produced in a routine manner, allowing a further preclinical evaluation of this tracer. Moreover, the synthesis of [^{18}F]FE@APPI was set-up successfully in small scale reaction. Interestingly, an upscaling of the reaction volume of the [^{18}F]FE@APPI synthesis could not be achieved at all. Therefore, this ^{18}F-fluoroethylated analogue of Me@APPI could not be produced in sufficient quantities for (pre-)clinical applications.

The preclinical evaluation of the [^{11}C]Me@APPI revealed an excellent metabolic stability in a human and murine setting. Moreover, data from IAM chromatography are encouraging and point towards a possible BBB penetration of this NET-PET tracer. In autoradiographic experiments on rodent and human brain tissue and rat heart, selective binding of [^{11}C]Me@APPI in NET-rich regions was observed and regions identified by immunohistochemistry and Nissl staining. However, competition experiments on ex vivo tissue samples, with known NET-PET tracers, resulted in unexplainable binding enhancement. Additionally, the high lipophilicity of [^{11}C]Me@APPI leads to a higher non-specific binding to lipophilic tissue samples and might therefore hamper a proper quantification. Nevertheless, a decision upon the suitability of the NET-PET radioligand [^{11}C]Me@APPI can be feasibly made only after *in vivo* experiments in small animal models.

4.3. ^{11}C-LABELED BENZOTHIADIAZOLE DERIVATIVED PET TRACERS

Rational design of novel NET ligands lead to the synthesis of benzothiadiazole derivatives – HAPTHI. Within this thesis, three HAPTHI derivatives were tested for their affinity and selectivity, lipophilicity and their potential to penetrate the BBB. Best results were obtained for the methylated compound, Me@HAPTHI. Its outstanding affinity and selectivity, as well as ideal lipophilicity for a cerebral PET tracer, favor this NET-ligand. Lower affinity was obtained for the free amine HAPTHI and worst affinity was found for the fluoroethylated compound, FE@HAPTHI. The fluoromethylated substance could not be obtained in sufficient quantities, indicating towards a poor stability of FMe@HAPTHI.

Therefore, the radiosynthesis for the methylated benzothiadiazole dioxide [^{11}C]Me@HAPTHI was set up in small scale reactions and subsequently transferred to an automated, routine syntheziser. With this fully automated radiosynthesis, high yields of [^{11}C]Me@HAPTHI could be obtained enabling further evaluation of the radiotracer. A pharmaceutical quality control was set up and all produced batches of [^{11}C]Me@HAPTHI passed the strict requirements.

In preclinical evaluations, high metabolic stability was found in the human setting, where no significant radiometabolites were observed within one hour. In *in vitro* autoradiography on human brain tissue and rat heart, a selective, concentration dependent binding displacement of [^{11}C]Me@HAPTHI was observed using known NET ligands as competitors. In NET-deprived regions, identified by IHC, no significant uptake of [^{11}C]Me@HAPTHI was observed (i.e. striatum, nucleus caudatus). Only in NET-rich areas selective uptake was observed. Moreover, binding experiments on a cellular level were performed in a harvesting protocol. In these competition experiments, a concentration dependent binding displacement, as obtained in prior autoradiographic experiments, was observed. On these grounds, [^{11}C]Me@HAPTHI present a viable, improved, non-Reboxetine NET-PET tracer and will be evaluated in the future in small animal models using µPET/CT.

5 CONCLUSION AND OUTLOOK

Within this thesis, the first non-Reboxetine based NET-radioligands for PET imaging were designed and preclinically evaluated regarding their lipophilicity, NET affinity and selectivity, BBB-penetration and metabolic stability. The radiosyntheses of 4 candidate NET-PET-probes were established in small scale experiments, and for the most favorable compounds successfully transferred to a fully-automated, routine radiosynthesis. The radiochemical yield and purity, as well as the specific activity was reasonable for all promising radioligands, enabling a latter preclinical testing. Moreover, a feasible quality control was set-up ensuring sufficient quality for (pre-)clinical application of the produced NET-PET probes. Furthermore, *in vitro* binding of [^{18}F]FMeNER-D2, [^{11}C]Me@APPI and [^{11}C]Me@HAPTHI on *ex vivo* material of human and rodent specimen was evaluated. These experiments revealed selective, NET-specific binding on human and murine tissue, pointing towards a potential use as clinical NET-PET-tracer. Due to organizational issues, µPET and biodistribution experiments are lacking so far, but planned in the near future.

Overall, the experimental results within this thesis were included within 6 articles submitted to peer-reviewed journals with high visibility and impact in their respective fields. Amongst them, 4 publications have already been accepted by the following target journals:

Nuclear Medicine and Biology	(2 peer-reviewed publications, impact factor 2013: 2.408)
JAMA Psychiatry	(1 peer-reviewed publication, impact factor 2014: 14.721)
Molecules	(1 peer-reviewed publication, impact factor 2015: 2.095)

Moreover, two manuscripts are concurrently under review: one in the Journal of Nuclear Medicine (impact factor 2015: 5.774) and one in the European Journal of Nuclear Medicine and Molecular Imaging Research (impact factor 2015: 5.14). Furthermore, the hitherto unpublished results included in chapter 3.2 will be submitted for publication after completion of remaining *in vitro* and *vivo* experiments in the near future.

This thesis has not only pinpointed the importance of NET-PET imaging for diagnosis and understanding of a variety of neurological and pathophysiological diseases, but also highlighted the benefits and drawbacks of the existing and newly developed NET-PET-tracers. While initial findings are auspicious, further *in vivo* experiments have to be performed to elucidate the *in vivo* binding behavior of the two utmost promising novel NET-PET tracers [^{11}C]Me@APPI and [^{11}C]Me@HAPTHI.

Present understanding of NET-influence in a plethora of dysregulations and diseases is limited. However, this thesis has provided ample support for the centrality of NET imaging to comprehend the involved molecular mechanisms. However, the available routine NET ligands are limited and display impeding uptake in striatal and cortical areas due to arising radiometabolites. The development of novel NET-PET tracers with enhanced affinity, selectivity and metabolic stability might facilitate precise NET-imaging in the future.

Therefore, a NET ligand database was set-up, enabling a first structure activity relationship of candidate

ligands. Present data indicates towards a high NET activity for aliphatic methylamino-substituted ligands. In the future, several additional substances will be evaluated and included in the database, to generalize the preliminary findings.

Moreover, a highly aspiring new research area will present the NET-imaging of BAT *in vivo* using NET-radioligands. The high impact of NET in BAT dysregulation fosters a potential therapeutic effect in diabetes and obesity. In preliminary Western blot experiments, a high content of NET in rodent BAT tissue samples was found. However, existing BAT cells – post-differentiated and classified via their UCP-1 expression - displayed only tenuous NET density – indicating towards a poor model to feasibly study the NET-BAT-nexus. Moreover, *in vitro* autoradiographic studies on BAT tissue is not possible, due to the physiology and morphology of the tissue. Thus, only small animal imaging with the novel NET-PET tracers [^{11}C]Me@APPI and [^{11}C]Me@HAPTHI will help to elucidate the molecular mechanisms and impact of NET in brown adipose tissue.

6 REFERENCES

[1] Radioactive pharmaceuticals (Radiopharmaceutica, 6.0/0125), . European Pharmacopoeia (Europäisches Arzneibuch): Verlag Österreich GmbH; 2008, p. 995 ff.

[2] Radiopharmaceuticals for Positron Emission Tomography. Radiochemical Syntheses: John Wiley & Sons, Inc.; 2012.

[3] Schlyer DJ. PET tracers and radiochemistry. Annals of the Academy of Medicine, Singapore 2004;33:146-54.

[4] Ametamey SM, Honer M, and Schubiger PA. Molecular imaging with PET. Chemical reviews 2008;108:1501-16.

[5] Pichler BJ, Judenhofer MS, and Pfannenberg C. Multimodal imaging approaches: PET/CT and PET/MRI. Handbook of experimental pharmacology 2008:109-32.

[6] Zaidi H and Del Guerra A. An outlook on future design of hybrid PET/MRI systems. Medical physics 2011;38:5667-89.

[7] Cole EL, Stewart MN, Littich R, Hoareau R, and Scott PJ. Radiosyntheses using fluorine-18: the art and science of late stage fluorination. Current topics in medicinal chemistry 2014;14:875-900.

[8] Wuest F. Fluorine-18 labeling of small molecules: the use of 18F-labeled aryl fluorides derived from no-carrier-added [18F]fluoride as labeling precursors. Ernst Schering Research Foundation workshop 2007:51-78.

[9] Mulliken RS. The Nature of the Chemical Bond. By Linus Pauling. The Journal of Physical Chemistry 1940;44:827-8.

[10] Munich Molecular Imaging Handbook Series Pharmaceutical Radiochemistry (I): Scintomics, Fürstenfeldbruck, Germany,2010.

[11] Bishop A, Satyamurthy N, Bida G, and Barrio JR. Chemical reactivity of the 18F electrophilic reagents from the 18O(p,n) 18F gas target systems. Nucl Med Biol 1996;23:559-65.

[12] Bishop A, Satyamurthy N, Bida G, Hendry G, Phelps M, and Barrio JR. Proton irradiation of [18O]O2: production of [18F]F2 and [18F]F2 + [18F] OF2. Nucl Med Biol 1996;23:189-99.

[13] Bishop A, Satyamurthy N, Bida G, Phelps M, and Barrio JR. Metals suitable for fluorine gas target bodies: first use of aluminum for the production of [18F]F2. Nucl Med Biol 1996;23:181-8.

[14] Bishop A, Satyamurthy N, Bida G, Phelps M, and Barrio JR. Identification and quantitation of gaseous compounds of fluorine generated in [18F]F2 target systems. Nucl Med Biol 1996;23:391-405.

[15] Bishop A, Satyamurthy N, Bida G, Phelps M, and Barrio JR. Production of [18F]F2 using the 16O(3He,p)18F reaction. Nucl Med Biol 1996;23:385-9.

[16] Nolting DD, Nickels ML, Guo N, and Pham W. Molecular imaging probe development: a chemistry perspective. American Journal of Nuclear Medicine and Molecular Imaging 2012;2:273-306.

[17] Hamacher K, Coenen HH, and Stocklin G. Efficient stereospecific synthesis of no-carrier-added 2-[18F]-fluoro-2-deoxy-D-glucose using aminopolyether supported nucleophilic substitution. Journal of nuclear medicine : official publication, Society of Nuclear Medicine 1986;27:235-8.

[18] Block D, Coenen HH, and Stoecklin G. The N.C.A. nucleophilic 18F-fluorination of 1,N-disubstituted alkanes as fluoroalkylation agents. J. Labelled Compd. Radiopharm. 1987;24:1029-42.
[19] Coenen HH, Schüller M, Stöcklin G, Klatte B, and Knöchel A. Preparation of N.C.A. [17-18F]-fluoroheptadecanoic acid in high yields via aminopolyether supported, nucleophilic fluorination. Journal of Labelled Compounds and Radiopharmaceuticals 1986;23:455-66.
[20] Moon BS, Park JH, Lee HJ, Kim JS, Kil HS, Lee BS, et al. Highly efficient production of [(18)F]fallypride using small amounts of base concentration. Applied radiation and isotopes : including data, instrumentation and methods for use in agriculture, industry and medicine 2010;68:2279-84.
[21] Chaly T and Dahl JR. Thin layer chromatographic detection of kryptofix 2.2.2 in the routine synthesis of [18F]2-fluoro-2-deoxy-D-glucose. International journal of radiation applications and instrumentation. Part B, Nuclear medicine and biology 1989;16:385-7.
[22] Moerlein SM, Brodack JW, Siegel BA, and Welch MJ. Elimination of contaminant Kryptofix 2.2.2 in the routine production of 2-[18F]fluoro-2-deoxy-D-glucose. International journal of radiation applications and instrumentation. Part A, Applied radiation and isotopes 1989;40:741-3.
[23] Lemaire C, Guillaume M, Cantineau R, and Christiaens L. No-carrier-added regioselective preparation of 6-[18F]fluoro-L-dopa. Journal of nuclear medicine : official publication, Society of Nuclear Medicine 1990;31:1247-51.
[24] Zhao X, Zhuang W, Fang D, Xue X, and Zhou J. A Highly Efficient Conversion of Primary or Secondary Alcohols into Fluorides with n-Perfluorobutanesulfonyl Fluoride-Tetrabutylammonium Triphenyldifluorosilicate. Synlett 2009;2009:779-82.
[25] Maslan FD and Stoddard EA. Acetonitrile–Water Liquid–Vapor Equilibrium. The Journal of Physical Chemistry 1956;60:1146-7.
[26] Wessmann SH, Henriksen G, and Wester HJ. Cryptate mediated nucleophilic 18F-fluorination without azeotropic drying. Nuklearmedizin 2012;51:1-8.
[27] Lee SJ, Oh SJ, Chi DY, Kang SH, Kil HS, Kim JS, et al. One-step high-radiochemical-yield synthesis of [18F]FP-CIT using a protic solvent system. Nucl Med Biol 2007;34:345-51.
[28] Kim DW, Choe YS, and Chi DY. A new nucleophilic fluorine-18 labeling method for aliphatic mesylates: reaction in ionic liquids shows tolerance for water. Nucl Med Biol 2003;30:345-50.
[29] Kim HW, Jeong JM, Lee YS, Chi DY, Chung KH, Lee DS, et al. Rapid synthesis of [18F]FDG without an evaporation step using an ionic liquid. Applied radiation and isotopes : including data, instrumentation and methods for use in agriculture, industry and medicine 2004;61:1241-6.
[30] Noyce DS and Virgilio JA. Synthesis and solvolysis of 1-phenylethyl disubstituted phosphinates. The Journal of Organic Chemistry 1972;37:2643-7.
[31] Jacobson O and Chen X. PET Designated Flouride-18 Production and Chemistry. Current topics in medicinal chemistry 2010;10:1048-59.
[32] Di Chiro G. Positron emission tomography using [18F] fluorodeoxyglucose in brain tumors. A powerful diagnostic and prognostic tool. Investigative radiology 1987;22:360-71.
[33] Fowler JS and Ido T. Initial and subsequent approach for the synthesis of 18FDG. Seminars in nuclear

medicine 2002;32:6-12.
[34] Ido T, Wan CN, Casella V, Fowler JS, Wolf AP, Reivich M, et al. Labeled 2-deoxy-D-glucose analogs. 18F-labeled 2-deoxy-2-fluoro-D-glucose, 2-deoxy-2-fluoro-D-mannose and 14C-2-deoxy-2-fluoro-D-glucose. Journal of Labelled Compounds and Radiopharmaceuticals 1978;14:175-83.
[35] Lu S, Lepore SD, Li SY, Mondal D, Cohn PC, Bhunia AK, et al. Nucleophile Assisting Leaving Groups: A Strategy for Aliphatic 18F-Fluorination. The Journal of Organic Chemistry 2009;74:5290-6.
[36] Herth MM, Debus F, Piel M, Palner M, Knudsen GM, Luddens H, et al. Total synthesis and evaluation of [18F]MHMZ. Bioorg Med Chem Lett 2008;18:1515-9.
[37] Hasler F, Kuznetsova OF, Krasikova RN, Cservenyak T, Quednow BB, Vollenweider FX, et al. GMP-compliant radiosynthesis of [18F]altanserin and human plasma metabolite studies. Applied radiation and isotopes : including data, instrumentation and methods for use in agriculture, industry and medicine 2009;67:598-601.
[38] Ungersboeck J, Richter S, Collier L, Mitterhauser M, Karanikas G, Lanzenberger R, et al. Radiolabeling of [18F]altanserin - a microfluidic approach. Nucl Med Biol 2012;39:1087-92.
[39] Ryzhikov NN, Seneca N, Krasikova RN, Gomzina NA, Shchukin E, Fedorova OS, et al. Preparation of highly specific radioactivity [18F]flumazenil and its evaluation in cynomolgus monkey by positron emission tomography. Nucl Med Biol 2005;32:109-16.
[40] Terrier F. Rate and equilibrium studies in Jackson-Meisenheimer complexes. Chemical reviews 1982;82:77-152.
[41] Artamkina GA, Egorov MP, and Beletskaya IP. Some aspects of anionic .sigma.-complexes. Chemical reviews 1982;82:427-59.
[42] Gomzina NA, Vasil'ev DA, and Krasikova RN. Use of 2-[18F]fluoroethyl bromide in synthesis of O-(2′-[18F]fluoroethyl)-L-tyrosine, a radiotracer for PET diagnostics of brain tumors. Radiochemistry 2007;49:299-304.
[43] Wadsak W, Mien LK, Ettlinger DE, Eidherr H, Haeusler D, Sindelar KM, et al. 18F fluoroethylations: different strategies for the rapid translation of 11C-methylated radiotracers. Nucl Med Biol 2007;34:1019-28.
[44] Wadsak W and Mitterhauser M. Basics and principles of radiopharmaceuticals for PET/CT. European journal of radiology 2010;73:461-9.
[45] Wadsak W, Wirl-Sagadin B, Mitterhauser M, Mien LK, Ettlinger DE, Keppler BK, et al. NCA nucleophilic radiofluorination on substituted benzaldehydes for the preparation of [18F]fluorinated aromatic amino acids. Applied radiation and isotopes : including data, instrumentation and methods for use in agriculture, industry and medicine 2006;64:355-9.
[46] Lin K-S, Ding Y-S, Kim S-W, and Kil K-E. Synthesis, enantiomeric resolution, F-18 labeling and biodistribution of reboxetine analogs: promising radioligands for imaging the norepinephrine transporter with positron emission tomography. Nuclear Medicine and Biology 2005;32:415-22.
[47] Mitterhauser M, Wadsak W, Mien L-K, Hoepping A, Viernstein H, Dudczak R, et al. Synthesis and biodistribution of [18F]FE@CIT, a new potential tracer for the dopamine transporter. Synapse 2005;55:73-9.
[48] Bauman G, Belhocine T, Kovacs M, Ward A, Beheshti M, and Rachinsky I. 18F-fluorocholine for prostate

cancer imaging: a systematic review of the literature. Prostate Cancer Prostatic Dis 2012;15:45-55.
[49] Iwata R, Pascali C, Bogni A, Furumoto S, Terasaki K, and Yanai K. [18F]Fluoromethyl triflate, a novel and reactive [18F]fluoromethylating agent: preparation and application to the on-column preparation of [18F]fluorocholine. Applied Radiation and Isotopes 2002;57:347-52.
[50] Kryza D. Synthesis of [18F]Fluorocholine ([18F]FCH). Radiochemical Syntheses: John Wiley & Sons, Inc.; 2012, p. 61-8.
[51] Litman Y, Pace P, Silva L, Hormigo C, Caro R, Gutierrez H, et al. Novel, simple and fast automated synthesis of 18F -choline in a single Synthera module. AIP Conference Proceedings 2012;1509:223-7.
[52] Neal TR, Apana S, and Berridge MS. Improved synthesis of [18F]fluoromethyl tosylate, a convenient reagent for radiofluoromethylations. Journal of Labelled Compounds and Radiopharmaceuticals 2005;48:557-68.
[53] Piel M, Bauman A, Baum RP, Höhnemann S, Klette I, Wortmann R, et al. Improved automated synthesis of [18F]fluoroethylcholine as a radiotracer for cancer imaging. Bioorganic & Medicinal Chemistry 2007;15:3171-5.
[54] Rodnick ME, Brooks AF, Hockley BG, Henderson BD, and Scott PJH. A fully-automated one-pot synthesis of [18F]fluoromethylcholine with reduced dimethylaminoethanol contamination via [18F]fluoromethyl tosylate. Applied Radiation and Isotopes 2013;78:26-32.
[55] Schmaljohann J, Schirrmacher E, Wängler B, Wängler C, Schirrmacher R, and Guhlke S. Fully automated SPE-based synthesis and purification of 2-[18F]fluoroethyl-choline for human use. Nuclear Medicine and Biology 2011;38:165-70.
[56] Shao X, Hockley BG, Hoareau R, Schnau PL, and Scott PJH. Fully automated preparation of [11C]choline and [18F]fluoromethylcholine using TracerLab synthesis modules and facilitated quality control using analytical HPLC. Applied Radiation and Isotopes 2011;69:403-9.
[57] Zhang M-R, Furutsuka K, Maeda J, Kikuchi T, Kida T, Okauchi T, et al. N-[18F]fluoroethyl-4-piperidyl acetate ([18F]FEtP4A) A PET tracer for imaging brain acetylcholinesterase in vivo. Bioorg. Med. Chem. 2003;11:2519-27.
[58] Zuhayra M, Alfteimi A, Papp L, Luetzen U, Luetzen A, Von FC, et al. Simplified fast and high yielding automated synthesis of [18F]fluoroethylcholine for prostate cancer imaging. Bioorg. Med. Chem. 2008;16:9121-6.
[59] Rami-Mark C, Zhang MR, Mitterhauser M, Lanzenberger R, Hacker M, and Wadsak W. [18F]FMeNER-D2: reliable fully-automated synthesis for visualization of the norepinephrine transporter. Nucl Med Biol 2013;40:1049-54.
[60] Murali D, Vandehey N, Christian B, Nickles J, Houser E, Converse A, et al. An efficient synthesis of F18-FECNT, a PET tracer for dopamine transporter. J NUCL MED MEETING ABSTRACTS 2008;49:288P-a-.
[61] Schou M, Halldin C, Sovago J, Pike VW, Hall H, Gulyas B, et al. PET evaluation of novel radiofluorinated reboxetine analogs as norepinephrine transporter probes in the monkey brain. Synapse (N. Y., NY, U. S.) 2004;53:57-67.
[62] Slaets D, De Bruyne S, Dumolyn C, Moerman L, Mertens K, and De Vos F. Reduced dimethylaminoethanol

in [18F]fluoromethylcholine: an important step towards enhanced tumour visualization. European Journal of Nuclear Medicine and Molecular Imaging 2010;37:2136-45.
[63] Chun J-H, Lu S, Lee Y-S, and Pike VW. Fast and High-Yield Microreactor Syntheses of ortho-Substituted [18F]Fluoroarenes from Reactions of [18F]Fluoride Ion with Diaryliodonium Salts. The Journal of Organic Chemistry 2010;75:3332-8.
[64] Carroll MA, Nairne J, and Woodcraft JL. Diaryliodonium salts: a solution to 3-[18F]fluoropyridine. Journal of Labelled Compounds and Radiopharmaceuticals 2007;50:452-4.
[65] Pike VW and Aigbirhio FI. Reactions of cyclotron-produced [18F]fluoride with diaryliodonium salts-a novel single-step route to no-carrier-added [18]fluoroarenes. Journal of the Chemical Society, Chemical Communications 1995:2215-6.
[66] Moon BS, Kil HS, Park JH, Kim JS, Park J, Chi DY, et al. Facile aromatic radiofluorination of [18F]flumazenil from diaryliodonium salts with evaluation of their stability and selectivity. Organic & Biomolecular Chemistry 2011;9:8346-55.
[67] Wüst FR and Kniess T. Synthesis of 4-[18F]fluoroiodobenzene and its application in sonogashira cross-coupling reactions. Journal of Labelled Compounds and Radiopharmaceuticals 2003;46:699-713.
[68] Wüst FR and Kniess T. No-carrier added synthesis of 18F-labelled nucleosides using Stille cross-coupling reactions with 4-[18F]fluoroiodobenzene. Journal of Labelled Compounds and Radiopharmaceuticals 2004;47:457-68.
[69] Wüst FR and Kniess T. N-Arylation of indoles with 4-[18F]fluoroiodobenzene: synthesis of 18F-labelled σ2 receptor ligands for positron emission tomography (PET). Journal of Labelled Compounds and Radiopharmaceuticals 2005;48:31-43.
[70] Guram AS, Rennels RA, and Buchwald SL. A Simple Catalytic Method for the Conversion of Aryl Bromides to Arylamines. Angewandte Chemie International Edition in English 1995;34:1348-50.
[71] Berridge MS and Tewson TJ. Chemistry of fluorine-18 radiopharmaceuticals. International journal of radiation applications and instrumentation. Part A, Applied radiation and isotopes 1986;37:685-93.
[72] Furuya T, Kuttruff CA, and Ritter T. Carbon-fluorine bond formation. Current opinion in drug discovery & development 2008;11:803-19.
[73] Groult H. Electrochemistry of fluorine production. Journal of Fluorine Chemistry 2003;119:173-89.
[74] Oberdorfer F, Hofmann E, and Maier-Borst W. Preparation of a new 18F-labelled precursor: 1-[18F]fluoro-2-pyridone. International Journal of Radiation Applications and Instrumentation. Part A. Applied Radiation and Isotopes 1988;39:685-8.
[75] Ogawa M, Hatano K, Oishi S, Kawasumi Y, Fujii N, Kawaguchi M, et al. Direct electrophilic radiofluorination of a cyclic RGD peptide for in vivo alpha(v)beta3 integrin related tumor imaging. Nucl Med Biol 2003;30:1-9.
[76] Chirakal R, Firnau G, Schrobilgen GJ, McKay J, and Garnett ES. The synthesis of [18F]Xenon difluoride from [18F]fluoride gas. The International Journal of Applied Radiation and Isotopes 1984;35:401-4.
[77] Satyamurthy N, Bida GT, Phelps ME, and Barrio JR. N-[18F]fluoro-N-alkylsulfonamides: novel reagents for mild and regioselective radiofluorination. International journal of radiation applications and instrumentation. Part A, Applied radiation and isotopes 1990;41:733-8.

[78] Diksic M and Jolly D. New high-yield synthesis of 18F-labelled 2-deoxy-2-fluoro-D-glucose. Int J Appl Radiat Isot 1983;34:893-6.
[79] Dolle F, Demphel S, Hinnen F, Fournier D, Vaufrey F, and Crouzel C. 6-[18F]Fluoro-L-DOPA by radiofluorodestannylation: a short and simple synthesis of a new labelling precursor. Journal of Labelled Compounds and Radiopharmaceuticals 1998;41:105-14.
[80] Namavari M, Bishop A, Satyamurthy N, Bida G, and Barrio JR. Regioselective radiofluorodestannylation with [18F]F2 and [18F]CH3COOF: a high yield synthesis of 6-[18F]Fluoro-L-dopa. International journal of radiation applications and instrumentation. Part A, Applied radiation and isotopes 1992;43:989-96.
[81] de Vries EFJ, Luurtsema G, Brüssermann M, Elsinga PH, and Vaalburg W. Fully automated synthesis module for the high yield one-pot preparation of 6-[18F]fluoro-l-DOPA. Applied Radiation and Isotopes 1999;51:389-94.
[82] Marik J and Sutcliffe JL. Click for PET: rapid preparation of [18F]fluoropeptides using CuI catalyzed 1,3-dipolar cycloaddition. Tetrahedron Letters 2006;47:6681-4.
[83] Kettenbach K, Schieferstein H, and Ross TL. 18F-Labeling Using Click Cycloadditions. BioMed Research International 2014;2014:16.
[84] Ramil CP and Lin Q. Bioorthogonal chemistry: strategies and recent developments. Chemical communications (Cambridge, England) 2013;49:11007-22.
[85] Best MD. Click chemistry and bioorthogonal reactions: unprecedented selectivity in the labeling of biological molecules. Biochemistry 2009;48:6571-84.
[86] Sletten EM and Bertozzi CR. From mechanism to mouse: a tale of two bioorthogonal reactions. Accounts of chemical research 2011;44:666-76.
[87] Ferrieri R A and Wolf A P. The Chemistry of Positron Emitting Nucleogenic (Hot) Atoms with Regard to Preparation of Labelled Compounds of Practical Utility. Radiochimca Acta; 1983, p. 69.
[88] Wolf AP and Redvanly CS. Carbon-11 and radiopharmaceuticals. The International Journal of Applied Radiation and Isotopes 1977;28:29-48.
[89] Andersson J, Truong P, and Halldin C. In-target produced [11C]methane: Increased specific radioactivity. Applied Radiation and Isotopes 2009;67:106-10.
[90] Comar D, Maziere M, and Crouzel C. Radiopharmaceuticals and Labelled Compounds. Vol. 1IAEA, Vienna 1973:461.
[91] Marazano C, Maziere M, Berger G, and Comar D. Synthesis of methyl iodide-11C and formaldehyde-11C. The International Journal of Applied Radiation and Isotopes 1977;28:49-52.
[92] Larsen P, Ulin J, Dahlstrøm K, and Jensen M. Synthesis of [11C]iodomethane by iodination of [11C]methane. Applied Radiation and Isotopes 1997;48:153-7.
[93] Link JM, Krohn KA, and Clark JC. Production of [11C]CH3I by single pass reaction of [11C]CH4 with I2. Nucl Med Biol 1997;24:93-7.
[94] Jewett DM. A simple synthesis of [11C]methyl triflate. International Journal of Radiation Applications and Instrumentation. Part A. Applied Radiation and Isotopes 1992;43:1383-5.
[95] Holschbach M and Schüller M. An on-line method for the preparation of n.c.a.

[11CH3]trifluoromethanesulfonic acid methyl ester. Applied Radiation and Isotopes 1993;44:897-8.
[96] Arai T, Zhang M-R, Ogawa M, Fukumura T, Kato K, and Suzuki K. Efficient and reproducible synthesis of [1-11C]acetyl chloride using the loop method. Applied Radiation and Isotopes 2009;67:296-300.
[97] Matarrese M, Salimbeni A, Turolla EA, Turozzi D, Moresco RM, Poma D, et al. 11C-Radiosynthesis and preliminary human evaluation of the disposition of the ACE inhibitor [11C]zofenoprilat. Bioorganic and Medicinal Chemistry 2004;12:603-11.
[98] Luthra SK, Pike VW, and Brady F. Preparation of some NCA [1-11C]acid chlorides as labelling agents. International Journal of Radiation Applications and Instrumentation. Part A. Applied Radiation and Isotopes 1990;41:471-6.
[99] Matarrese M, Sudati F, Soloviev D, Todde S, Turolla EA, Kienle MG, et al. Automation of [11C]acyl chloride syntheses using commercially available 11C-modules. Applied Radiation and Isotopes 2002;57:675-9.
[100] Zhang M-R, Ogawa M, Yoshida Y, and Suzuki K. Selective synthesis of [2-11C]2-iodopropane and [1-11C]iodoethane using the loop method by reacting methylmagnesium bromide with [11C]carbon dioxide. Applied Radiation and Isotopes 2006;64:216-22.
[101] Rami-Mark C, Ungersboeck J, Haeusler D, Nics L, Philippe C, Mitterhauser M, et al. Reliable set-up for in-loop (1)(1)C-carboxylations using Grignard reactions for the preparation of [carbonyl-(1)(1)C]WAY-100635 and [(1)(1)C]-(+)-PHNO. Applied radiation and isotopes : including data, instrumentation and methods for use in agriculture, industry and medicine 2013;82:75-80.
[102] Walborsky HM. Mechanism of Grignard reagent formation. The surface nature of the reaction. Acc. Chem. Res 1990:286-93.
[103] Krasikova RN, Andersson J, Truong P, Nag S, Shchukin EV, and Halldin C. A fully automated one-pot synthesis of [carbonyl-11C]WAY-100635 for clinical PET applications. Applied radiation and isotopes : including data, instrumentation and methods for use in agriculture, industry and medicine 2009;67:73-8.
[104] McCarron JA, Turton DR, Pike VW, and Poole KG. Remotely-controlled production of the 5-HT1A receptor radioligand, [carbonyl-11C]WAY-100635, via 11C-carboxylation of an immobilized Grignard reagent. Journal of Labelled Compounds and Radiopharmaceuticals 1996;38:941-53.
[105] Långström B, Itsenko O, and Rahman O. [11C]Carbon monoxide, a versatile and useful precursor in labelling chemistry for PET-ligand development. Journal of Labelled Compounds and Radiopharmaceuticals 2007;50:794-810.
[106] Hostetler ED, Terry GE, and Donald Burns H. An improved synthesis of substituted [11C]toluenes via Suzuki coupling with [11C]methyl iodide. Journal of Labelled Compounds and Radiopharmaceuticals 2005;48:629-34.
[107] Hosoya T, Sumi K, Doi H, Wakao M, and Suzuki M. Rapid methylation on carbon frameworks useful for the synthesis of 11CH3-incorporated PET tracers: Pd(0)-mediated rapid coupling of methyl iodide with an alkenyltributylstannane leading to a 1-methylalkene. Org Biomol Chem 2006;4:410-5.
[108] Krasikova R. Synthesis modules and automation in F-18 labeling. Ernst Schering Research Foundation workshop 2007:289-316.
[109] Padgett HC, Schmidt DG, Luxen A, Bida GT, Satyamurthy N, and Barrio JR. Computer-controlled

radiochemical synthesis: a chemistry process control unit for the automated production of radiochemicals. International journal of radiation applications and instrumentation. Part A, Applied radiation and isotopes 1989;40:433-45.
[110] Alexoff DL, Russell JA, Shiue CY, Wolf AP, Fowler JS, and MacGregor RR. Modular automation in PET tracer manufacturing: application of an autosynthesizer to the production of 2-deoxy-2-[18F]fluoro-D-glucose. International journal of radiation applications and instrumentation. Part A, Applied radiation and isotopes 1986;37:1045-61.
[111] Jacobson M, Steichen R, and Peller P. PET Radiochemistry and Radiopharmacy. In: P Peller, R Subramaniam, and A Guermazi editors. PET-CT and PET-MRI in Oncology: Springer Berlin Heidelberg; 2012, p. 19-30.
[112] Kuhar M. Neurotransmitter. In: I Stolerman editor. Encyclopedia of Psychopharmacology: Springer Berlin Heidelberg; 2010, p. 876-.
[113] Andrews A, Gerhardt G, and Daws L. Neurotransmitter Transporters. In: I Stolerman editor. Encyclopedia of Psychopharmacology: Springer Berlin Heidelberg; 2010, p. 876-.
[114] Gether U, Andersen PH, Larsson OM, and Schousboe A. Neurotransmitter transporters: molecular function of important drug targets. Trends in Pharmacological Sciences 2006;27:375-83.
[115] Pradhan T, Jung HS, Jang JH, Kim TW, Kang C, and Kim JS. Chemical sensing of neurotransmitters. Chemical Society Reviews 2014;43:4684-713.
[116] Anden NE, Dahlstrom A, Fuxe K, and Larsson K. Mapping out of catecholamine and 5-hydroxytryptamine neurons innervating the telencephalon and diencephalon. Life sciences 1965;4:1275-9.
[117] Carlsson A, Dahlstroem A, Fuxe K, and Lindqvist M. HISTOCHEMICAL AND BIOCHEMICAL DETECTION OF MONOAMINE RELEASE FROM BRAIN NEURONS. Life sciences 1965;4:809-16.
[118] Carlsson A, Lindqvist M, Dahlstrom A, Fuxe K, and Masuoka D. Effects of the amphetamine group on intraneuronal brain amines in vivo and in vitro. The Journal of pharmacy and pharmacology 1965;17:521-3.
[119] Dahlstrom A and Fuxe K. Evidence for the existence of an outflow of noradrenaline nerve fibres in the ventral roots of the rat spinal cord. Experientia 1965;21:409-10.
[120] Fuxe K. EVIDENCE FOR THE EXISTENCE OF MONOAMINE NEURONS IN THE CENTRAL NERVOUS SYSTEM. IV. DISTRIBUTION OF MONOAMINE NERVE TERMINALS IN THE CENTRAL NERVOUS SYSTEM. Acta physiologica Scandinavica. Supplementum 1965:Suppl 247:37+.
[121] Fuxe K and Nilsson BY. Mechanoreceptors and adrenergic nerve terminals. Experientia 1965;21:641-2.
[122] Fuxe K and Owman C. Cellular localization of monoamines in the area postrema of certain mammals. J Comp Neurol 1965;125:337-53.
[123] Satoh K, Tohyama M, Yamamoto K, Sakumoto T, and Shimizu N. Noradrenaline innervation of the spinal cord studied by the horseradish peroxidase method combined with monoamine oxidase staining. Experimental brain research 1977;30:175-86.
[124] Yamamoto T, Ishikawa M, and Tanaka C. Catecholaminergic terminals in the developing and adult rat cerebellum. Brain Res 1977;132:355-61.
[125] Björklund A and Lindvall O. Dopamine-containing systems in the CNS. Handbook of chemical

neuroanatomy 1984;2:55-122.
[126] Nieuwenhuys R. Chemoarchitecture of the Brain. 1 ed.: Springer-Verlag Berlin Heidelberg,1985.
[127] Cooper J.R., Bloom FE, and Roth RH. The Biochemical Basis of Neuropharmacology: Oxford University Press New York,1977.
[128] Paxinos G. Foreword. In: G Paxinos editor. The Rat Nervous System (Third Edition). Burlington: Academic Press; 2004, p. xvii.
[129] Tang J, Li Z, Lu L, and Cho CH. β-Adrenergic system, a backstage manipulator regulating tumour progression and drug target in cancer therapy. Seminars in Cancer Biology 2013;23:533-42.
[130] Eisenhofer G, Kopin IJ, and Goldstein DS. Catecholamine Metabolism: A Contemporary View with Implications for Physiology and Medicine. Pharmacological Reviews 2004;56:331-49.
[131] Tellioglu T and Robertson D. Genetic or acquired deficits in the norepinephrine transporter: current understanding of clinical implications. Expert Reviews in Molecular Medicine 2001;3:1-10.
[132] GLOWINSKI J and BALDESSARINI RJ. METABOLISM OF NOREPINEPHRINE IN THE CENTRAL NERVOUS SYSTEM. Pharmacological Reviews 1966;18:1201-38.
[133] Berridge CW and Waterhouse BD. The locus coeruleus-noradrenergic system: modulation of behavioral state and state-dependent cognitive processes. Brain research. Brain research reviews 2003;42:33-84.
[134] Curatolo P, D'Agati E, and Moavero R. The neurobiological basis of ADHD. Italian Journal of Pediatrics 2010;36:79.
[135] Mash DC, Ouyang Q, Qin Y, and Pablo J. Norepinephrine transporter immunoblotting and radioligand binding in cocaine abusers. Journal of Neuroscience Methods 2005;143:79-85.
[136] Siddiqui N, Andalip, Bawa S, Ali R, Afzal O, Akhtar M, et al. Antidepressant potential of nitrogen-containing heterocyclic moieties: An updated review. Journal of Pharmacy and Bioallied Sciences 2011;3:194-212.
[137] Zhou J. Norepinephrine transporter inhibitors and their therapeutic
potential. Drugs Future 2004;29:1235–44.
[138] Harik S, Duckrow R, LaManna J, Rosenthal M, Sharma V, and Banerjee S. Cerebral compensation for chronic noradrenergic denervation induced by locus ceruleus lesion: recovery of receptor binding, isoproterenol- induced adenylate cyclase activity, and oxidative metabolism. The Journal of Neuroscience 1981;1:641-9.
[139] Ostock CY, Lindenbach D, Goldenberg AA, Kampton E, and Bishop C. Effects of noradrenergic denervation by anti-DBH-saporin on behavioral responsivity to l-DOPA in the hemi-parkinsonian rat. Behavioural Brain Research 2014;270:75-85.
[140] Klimek V, Stockmeier C, Overholser J, Meltzer HY, Kalka S, Dilley G, et al. Reduced Levels of Norepinephrine Transporters in the Locus Coeruleus in Major Depression. The Journal of Neuroscience 1997;17:8451-8.
[141] Westfall T and Westfall D. Goodman and Gilman's The Pharmacological Basis of Therapeutics. 12 ed.,2011.
[142] VOGT M. NOREPINEPHRINE AND EPINEPHRINE IN THE CENTRAL NERVOUS SYSTEM. Pharmacological Reviews 1954;6:31-2.

[143] Rang H, Ritter J, Flower R, and Henderson G. Rang & Dale's Pharmacology. 7 ed.: Churchill Livingstone, Elsevier, London,2011.
[144] Dorn GW. Adrenergic Signaling Polymorphisms and Their Impact on Cardiovascular Disease. Physiological Reviews 2010;90:1013-62.
[145] Small KM, McGraw DW, and Liggett SB. PHARMACOLOGY AND PHYSIOLOGY OF HUMAN ADRENERGIC RECEPTOR POLYMORPHISMS. Annual Review of Pharmacology and Toxicology 2003;43:381-411.
[146] Goldstein D. Catecholamines: Bridging Basic Science with Clinical Medicine: Academic Press, San Diego,1998.
[147] Madamanchi A. β-Adrenergic receptor signaling in cardiac function and heart failure. McGill Journal of Medicine : MJM 2007;10:99-104.
[148] Bristow MR. β-Adrenergic Receptor Blockade in Chronic Heart Failure. Circulation 2000;101:558-69.
[149] Carson PE. Beta blocker treatment in heart failure. Progress in Cardiovascular Diseases 1999;41:301-21.
[150] Sung U, Apparsundaram S, Galli A, Kahlig KM, Savchenko V, Schroeter S, et al. A Regulated Interaction of Syntaxin 1A with the Antidepressant-Sensitive Norepinephrine Transporter Establishes Catecholamine Clearance Capacity. The Journal of Neuroscience 2003;23:1697-709.
[151] Blakely RD, De Felice LJ, and Hartzell HC. Molecular physiology of norepinephrine and serotonin transporters. Journal of Experimental Biology 1994;196:263-81.
[152] Bönisch H and Brüss M. The Norepinephrine Transporter in Physiology and Disease. In: H Sitte and M Freissmuth editors. Neurotransmitter Transporters: Springer Berlin Heidelberg; 2006, p. 485-524.
[153] Torres GE, Gainetdinov RR, and Caron MG. Plasma membrane monoamine transporters: structure, regulation and function. Nat Rev Neurosci 2003;4:13-25.
[154] Hertting G and Axelrod J. Fate of Tritiated Noradrenaline at the Sympathetic Nerve-Endings. Nature 1961;192:172-3.
[155] Pacholczyk T, Blakely RD, and Amara SG. Expression cloning of a cocaine-and antidepressant-sensitive human noradrenaline transporter. Nature 1991;350:350-4.
[156] Zahniser NR and Doolen S. Chronic and acute regulation of Na+/Cl–-dependent neurotransmitter transporters: drugs, substrates, presynaptic receptors, and signaling systems. Pharmacology & Therapeutics 2001;92:21-55.
[157] Nguyen TT and Amara SG. N-Linked Oligosaccharides Are Required for Cell Surface Expression of the Norepinephrine Transporter but Do Not Influence Substrate or Inhibitor Recognition. Journal of Neurochemistry 1996;67:645-55.
[158] Melikian HE, Ramamoorthy S, Tate CG, and Blakely RD. Inability to N-glycosylate the human norepinephrine transporter reduces protein stability, surface trafficking, and transport activity but not ligand recognition. Molecular Pharmacology 1996;50:266-76.
[159] Zhu M-Y, Shamburger S, Li J, and Ordway GA. Regulation of the Human Norepinephrine Transporter by Cocaine and Amphetamine. Journal of Pharmacology and Experimental Therapeutics 2000;295:951-9.

[160] Lee C, Javitch J, and Snyder S. Recognition sites for norepinephrine uptake: regulation by neurotransmitter. Science 1983;220:626-9.
[161] Kim C-H, Hahn MK, Joung Y, Anderson SL, Steele AH, Mazei-Robinson MS, et al. A polymorphism in the norepinephrine transporter gene alters promoter activity and is associated with attention-deficit hyperactivity disorder. Proceedings of the National Academy of Sciences 2006;103:19164-9.
[162] Vazey EM and Aston-Jones G. The emerging role of norepinephrine in cognitive dysfunctions of Parkinson's disease. Frontiers in Behavioral Neuroscience 2012;6:48.
[163] Moldovanova I, Schroeder C, Jacob G, Hiemke C, Diedrich A, Luft FC, et al. Hormonal Influences on Cardiovascular Norepinephrine Transporter Responses in Healthy Women. Hypertension 2008;51:1203-9.
[164] Schroeder C and Jordan J. Norepinephrine transporter function and human cardiovascular disease,2012.
[165] Mirbolooki MR, Constantinescu CC, Pan M-L, and Mukherjee J. Targeting presynaptic norepinephrine transporter in brown adipose tissue: A novel imaging approach and potential treatment for diabetes and obesity. Synapse 2013;67:79-93.
[166] CANNON B and NEDERGAARD J. Brown Adipose Tissue: Function and Physiological Significance. Physiological Reviews 2004;84:277-359.
[167] Li C-sR, Potenza MN, Lee DE, Planeta B, Gallezot J-D, Labaree D, et al. Decreased norepinephrine transporter availability in obesity: Positron Emission Tomography imaging with (S,S)-[11C]O-methylreboxetine. NeuroImage 2014;86:306-10.
[168] Lin S-f, Fan X, Yeckel CW, Weinzimmer D, Mulnix T, Gallezot J-D, et al. Ex Vivo and In Vivo Evaluation of the Norepinephrine Transporter Ligand [11C]MRB for Brown Adipose Tissue Imaging. Nuclear Medicine and Biology 2012;39:1081-6.
[169] Nedergaard J and Cannon B. The Changed Metabolic World with Human Brown Adipose Tissue: Therapeutic Visions. Cell Metabolism 2010;11:268-72.
[170] Shannon JR, Flattem NL, Jordan J, Jacob G, Black BK, Biaggioni I, et al. Orthostatic Intolerance and Tachycardia Associated with Norepinephrine-Transporter Deficiency. New England Journal of Medicine 2000;342:541-9.
[171] Cortese S. The neurobiology and genetics of Attention-Deficit/Hyperactivity Disorder (ADHD): what every clinician should know. European journal of paediatric neurology : EJPN : official journal of the European Paediatric Neurology Society 2012;16:422-33.
[172] Vanicek T, Spies M, Rami-Mark C, Savli M, Hoflich A, Kranz GS, et al. The Norepinephrine Transporter in Attention-Deficit/Hyperactivity Disorder Investigated With Positron Emission Tomography. JAMA Psychiatry 2014.
[173] Dickstein SG, Bannon K, Castellanos FX, and Milham MP. The neural correlates of attention deficit hyperactivity disorder: an ALE meta-analysis. Journal of child psychology and psychiatry, and allied disciplines 2006;47:1051-62.
[174] Bush G. Attention-deficit/hyperactivity disorder and attention networks. Neuropsychopharmacology : official publication of the American College of Neuropsychopharmacology 2010;35:278-300.
[175] Brennan AR and Arnsten AF. Neuronal mechanisms underlying attention deficit hyperactivity disorder:

the influence of arousal on prefrontal cortical function. Annals of the New York Academy of Sciences 2008;1129:236-45.
[176] Hauser TU, Iannaccone R, Ball J, Mathys C, Brandeis D, Walitza S, et al. Role of the medial prefrontal cortex in impaired decision making in juvenile attention-deficit/hyperactivity disorder. JAMA Psychiatry 2014;71:1165-73.
[177] Nyberg S, Jucaite A, Takano A, Kagedal M, Cselenyi Z, Halldin C, et al. Norepinephrine transporter occupancy in the human brain after oral administration of quetiapine XR. The international journal of neuropsychopharmacology / official scientific journal of the Collegium Internationale Neuropsychopharmacologicum (CINP) 2013;16:2235-44.
[178] Bjorkholm C, Jardemark K, Marcus MM, Malmerfelt A, Nyberg S, Schilstrom B, et al. Role of concomitant inhibition of the norepinephrine transporter for the antipsychotic effect of quetiapine. European neuropsychopharmacology : the journal of the European College of Neuropsychopharmacology 2013;23:709-20.
[179] Espay AJ, LeWitt PA, and Kaufmann H. Norepinephrine deficiency in Parkinson's disease: the case for noradrenergic enhancement. Movement disorders : official journal of the Movement Disorder Society 2014;29:1710-9.
[180] Rommelfanger KS, Edwards GL, Freeman KG, Liles LC, Miller GW, and Weinshenker D. Norepinephrine loss produces more profound motor deficits than MPTP treatment in mice. Proceedings of the National Academy of Sciences of the United States of America 2007;104:13804-9.
[181] Pifl C, Hornykiewicz O, Blesa J, Adánez R, Cavada C, and Obeso JA. Reduced noradrenaline, but not dopamine and serotonin in motor thalamus of the MPTP primate: relation to severity of Parkinsonism. Journal of Neurochemistry 2013;125:657-62.
[182] Wang Y, Chen X, Wang T, Sun YN, Han LN, Li LB, et al. Additional noradrenergic depletion aggravates forelimb akinesia and abnormal subthalamic nucleus activity in a rat model of Parkinson's disease. Life sciences 2014;119:18-27.
[183] Gatley SJ, Volkow ND, Wang GJ, Fowler JS, Logan J, Ding YS, et al. PET imaging in clinical drug abuse research. Current pharmaceutical design 2005;11:3203-19.
[184] Belej T, Manji D, Sioutis S, Barros HM, and Nobrega JN. Changes in serotonin and norepinephrine uptake sites after chronic cocaine: pre- vs. post-withdrawal effects. Brain Res 1996;736:287-96.
[185] Benmansour S, Tejani-Butt SM, Hauptmann M, and Brunswick DJ. Lack of effect of high-dose cocaine on monoamine uptake sites in rat brain measured by quantitative autoradiography. Psychopharmacology (Berl) 1992;106:459-62.
[186] Burchett SA and Bannon MJ. Serotonin, dopamine and norepinephrine transporter mRNAs: heterogeneity of distribution and response to 'binge' cocaine administration. Brain research. Molecular brain research 1997;49:95-102.
[187] Macey DJ, Smith HR, Nader MA, and Porrino LJ. Chronic cocaine self-administration upregulates the norepinephrine transporter and alters functional activity in the bed nucleus of the stria terminalis of the rhesus monkey. The Journal of neuroscience : the official journal of the Society for Neuroscience 2003;23:12-6.

[188] Beveridge TJ, Smith HR, Nader MA, and Porrino LJ. Effects of chronic cocaine self-administration on norepinephrine transporters in the nonhuman primate brain. Psychopharmacology (Berl) 2005;180:781-8.
[189] Ding YS, Singhal T, Planeta-Wilson B, Gallezot JD, Nabulsi N, Labaree D, et al. PET imaging of the effects of age and cocaine on the norepinephrine transporter in the human brain using (S,S)-[(11)C]O-methylreboxetine and HRRT. Synapse 2010;64:30-8.
[190] Schroeder C, Tank J, Boschmann M, Diedrich A, Sharma AM, Biaggioni I, et al. Selective Norepinephrine Reuptake Inhibition as a Human Model of Orthostatic Intolerance. Circulation 2002;105:347-53.
[191] Birkenfeld AL, Schroeder C, Boschmann M, Tank J, Franke G, Luft FC, et al. Paradoxical Effect of Sibutramine on Autonomic Cardiovascular Regulation. Circulation 2002;106:2459-65.
[192] Boschmann M, Schroeder C, Christensen NJ, Tank J, Krupp G, Biaggioni I, et al. Norepinephrine Transporter Function and Autonomic Control of Metabolism. The Journal of Clinical Endocrinology & Metabolism 2002;87:5130-7.
[193] Cannon B and Nedergaard JAN. Brown Adipose Tissue: Function and Physiological Significance. Physiological Reviews 2004;84:277-359.
[194] Lachance J and Page E. Hormonal factors influencing fat deposition in the interscapular brown adipose tissue of the white rat. Endocrinology 1953;52:57-64.
[195] Cohade C, Osman M, Pannu HK, and Wahl RL. Uptake in supraclavicular area fat ("USA-Fat"): description on 18F-FDG PET/CT. Journal of nuclear medicine : official publication, Society of Nuclear Medicine 2003;44:170-6.
[196] Cypess AM, Chen Y-C, Sze C, Wang K, English J, Chan O, et al. Cold but not sympathomimetics activates human brown adipose tissue in vivo. Proceedings of the National Academy of Sciences 2012;109:10001-5.
[197] Nedergaard J, Bengtsson T, and Cannon B. Unexpected evidence for active brown adipose tissue in adult humans. American journal of physiology. Endocrinology and metabolism 2007;293:E444-52.
[198] Enerback S. The origins of brown adipose tissue. The New England journal of medicine 2009;360:2021-3.
[199] Shimizu Y, Satoh S, Yano H, Minokoshi Y, Cushman SW, and Shimazu T. Effects of noradrenaline on the cell-surface glucose transporters in cultured brown adipocytes: novel mechanism for selective activation of GLUT1 glucose transporters. The Biochemical journal 1998;330 (Pt 1):397-403.
[200] Santalucia T, Camps M, Castello A, Munoz P, Nuel A, Testar X, et al. Developmental regulation of GLUT-1 (erythroid/Hep G2) and GLUT-4 (muscle/fat) glucose transporter expression in rat heart, skeletal muscle, and brown adipose tissue. Endocrinology 1992;130:837-46.
[201] UCP1_HUMAN P-. Uniprot Database. 2015.
[202] Carey AL, Formosa MF, Every B, Bertovic D, Eikelis N, Lambert GW, et al. Ephedrine activates brown adipose tissue in lean but not obese humans. Diabetologia 2013;56:147-55.
[203] Carey AL, Vorlander C, Reddy-Luthmoodoo M, Natoli AK, Formosa MF, Bertovic DA, et al. Reduced UCP-1 content in in vitro differentiated beige/brite adipocytes derived from preadipocytes of human subcutaneous white adipose tissues in obesity. PLoS One 2014;9:e91997.
[204] Li C-sR, Potenza MN, Lee DE, Planeta B, Gallezot J-D, Labaree D, et al. Decreased norepinephrine

transporter availability in obesity: Positron Emission Tomography imaging with (S,S)-[11C]O-methylreboxetine. NeuroImage.
[205] Lee ZSK, Critchley JAJH, Tomlinson B, Young RP, Thomas GN, Cockram CS, et al. Urinary epinephrine and norepinephrine interrelations with obesity, insulin, and the metabolic syndrome in Hong Kong Chinese. Metabolism: Clinical and Experimental 2001;50:135-43.
[206] Ziegler MG, Elayan H, Milic M, Sun P, and Gharaibeh M. Epinephrine and the metabolic syndrome. Current Hypertension Reports 2012;14:1-7.
[207] Gallezot J-D, Weinzimmer D, Nabulsi N, Lin S-F, Fowles K, Sandiego C, et al. Evaluation of [(11)C]MRB for assessment of occupancy of norepinephrine transporters: Studies with atomoxetine in non-human primates. NeuroImage 2011;56:268-79.
[208] Hannestad J, Gallezot J-D, Planeta-Wilson B, Lin S-F, Williams WA, van Dyck CH, et al. Clinically Relevant Doses of Methylphenidate Significantly Occupy the Norepinephrine Transporter in Humans In Vivo. Biological psychiatry 2010;68:854-60.
[209] Hwang J, Yeckel C, Gallezot J-D, Ersahin D, Belfort-Deaguiar R, Cheng D, et al. Imaging brown fat in humans with 11C-MRB, a selective norepinephrine transporter PET ligand. J NUCL MED MEETING ABSTRACTS 2014;55:235-.
[210] Javaid JI, Perel JM, and Davis JM. Inhibition of biogenic amines uptake by imipramine, desipramine, 2 OH-imipramine and 2 OH-desipramine in rat brain. Life sciences 1979;24:21-8.
[211] Waldmeier PC, Baumann PA, Hauser K, Maitre L, and Storni A. Oxaprotiline, a noradrenaline uptake inhibitor with an active and an inactive enantiomer. Biochem Pharmacol 1982;31:2169-76.
[212] Gehlert DR, Hemrick-Luecke SK, Schober DA, Krushinski J, Howbert JJ, Robertson DW, et al. (R)-thionisoxetine, a potent and selective inhibitor of central and peripheral norepinephrine uptake. Life sciences 1995;56:1915-20.
[213] Melloni P, Carniel G, Della Torre A, Bonsignori A, Buonamici M, Pozzi O, et al. Potential antidepressant agents, aryloxy-benzyl derivatives of ethanolamine and morpholine. Eur J Med Chem. 1984;19:235-42.
[214] Chumpradit S, Kung MP, Panyachotipun C, Prapansiri V, Foulon C, Brooks BP, et al. Iodinated tomoxetine derivatives as selective ligands for serotonin and norepinephrine uptake sites. J Med Chem 1992;35:4492-7.
[215] Wong DT, Threlkeld PG, Best KL, and Bymaster FP. A new inhibitor of norepinephrine uptake devoid of affinity for receptors in rat brain. The Journal of pharmacology and experimental therapeutics 1982;222:61-5.
[216] Bogeso KP, Christensen AV, Hyttel J, and Liljefors T. 3-Phenyl-1-indanamines. Potential antidepressant activity and potent inhibition of dopamine, norepinephrine, and serotonin uptake. J Med Chem 1985;28:1817-28.
[217] Blough BE, Holmquist CR, Abraham P, Kuhar MJ, and Carroll FI. 3alpha-(4-Substituted phenyl)nortropane-2beta-carboxylic acid methyl esters show selective binding at the norepinephrine transporter. Bioorg Med Chem Lett 2000;10:2445-7.
[218] Hoepping A, Johnson KM, George C, Flippen-Anderson J, and Kozikowski AP. Novel conformationally constrained tropane analogues by 6-endo-trig radical cyclization and stille coupling - switch of activity toward

the serotonin and/or norepinephrine transporter. J Med Chem 2000;43:2064-71.
[219] Maryanoff BE, McComsey DF, Gardocki JF, Shank RP, Costanzo MJ, Nortey SO, et al. Pyrroloisoquinoline antidepressants. 2. In-depth exploration of structure-activity relationships. J Med Chem 1987;30:1433-54.
[220] Hyttel J. Citalopram--pharmacological profile of a specific serotonin uptake inhibitor with antidepressant activity. Progress in neuro-psychopharmacology & biological psychiatry 1982;6:277-95.
[221] Mahaney PE, Gavrin LK, Trybulski EJ, Stack GP, Vu AT, Cohn ST, et al. Structure-Activity Relationships of the Cycloalkanol Ethylamine Scaffold: Discovery of Selective Norepinephrine Reuptake Inhibitors. J. Med. Chem. 2008;51:4038-49.
[222] Mahaney PE, Vu AT, McComas CC, Zhang P, Nogle LM, Watts WL, et al. Synthesis and activity of a new class of dual acting norepinephrine and serotonin reuptake inhibitors: 3-(1H-indol-1-yl)-3-arylpropan-1-amines. Bioorg. Med. Chem. 2006;14:8455-66.
[223] Kasper S, el Giamal N, and Hilger E. Reboxetine: the first selective noradrenaline re-uptake inhibitor. Expert opinion on pharmacotherapy 2000;1:771-82.
[224] Healy D and Healy H. The clinical pharmacologic profile of reboxetine: does it involve the putative neurobiological substrates of wellbeing? Journal of affective disorders 1998;51:313-22.
[225] Souery D and Sternon J. [Reboxetine (Edronax)]. Revue medicale de Bruxelles 1999;20:511-6.
[226] Hajós M, Fleishaker JC, Filipiak-Reisner JK, Brown MT, and Wong EHF. The Selective Norepinephrine Reuptake Inhibitor Antidepressant Reboxetine: Pharmacological and Clinical Profile. CNS Drug Reviews 2004;10:23-44.
[227] Schatzberg AF. Clinical efficacy of reboxetine in major depression. The Journal of clinical psychiatry 2000;61 Suppl 10:31-8.
[228] Dencker SJ. The need for new and better antidepressants: reboxetine a new option. Acta psychiatrica Scandinavica. Supplementum 2000;402:6-11.
[229] Cipriani A, Furukawa TA, Salanti G, Geddes JR, Higgins JP, Churchill R, et al. Comparative efficacy and acceptability of 12 new-generation antidepressants: a multiple-treatments meta-analysis. Lancet 2009;373:746-58.
[230] Wilson AA, Patrick Johnson D, Mozley D, Hussey D, Ginovart N, Nobrega J, et al. Synthesis and in vivo evaluation of novel radiotracers for the in vivo imaging of the norepinephrine transporter. Nuclear Medicine and Biology 2003;30:85-92.
[231] Schou M, Halldin C, Pike VW, Mozley PD, Dobson D, Innis RB, et al. Post-mortem human brain autoradiography of the norepinephrine transporter using (S,S)-[18F]FMeNER-D2. European Neuropsychopharmacology 2005;15:517-20.
[232] Schou M, Halldin C, Sóvágó J, Pike VW, Gulyás B, Mozley PD, et al. Specific in vivo binding to the norepinephrine transporter demonstrated with the PET radioligand, (S,S)-[11C]MeNER. Nuclear Medicine and Biology 2003;30:707-14.
[233] Schou M, Sóvágó J, Pike V, Gulyás B, Bøgesø K, Farde L, et al. Synthesis and Positron Emission Tomography Evaluation of Three Norepinephrine Transporter Radioligands: [C-11]Desipramine, [C-

11]Talopram and [C-11]Talsupram. Molecular Imaging and Biology 2006;8:1-8.
[234] Takano A, Gulyás B, Varrone A, Karlsson P, Schou M, Airaksinen A, et al. Imaging the norepinephrine transporter with positron emission tomography: initial human studies with (S,S)-[18F]FMeNER-D2. European Journal of Nuclear Medicine and Molecular Imaging 2008;35:153-7.
[235] McComas CC, Vu AT, Mahaney PE, Cohn ST, Fensome A, Marella MA, et al. Synthesis and activity of 1-(3-amino-1-phenylpropyl)indolin-2-ones: A new class of selective norepinephrine reuptake inhibitors. Bioorganic & Medicinal Chemistry Letters 2008;18:4929-31.
[236] McComas CC, Zhang P, Terefenko EA, Vu AT, and Cohn ST. Substituted propylamine derivatives and methods of their use in treating conditions ameliorated by monoamine reuptake. Wyeth, John, and Brother Ltd., USA . 2007, p. 43pp.
[237] Zhang P, Terefenko EA, Bray J, Deecher D, Fensome A, Harrison J, et al. 1- or 3-(3-Amino-2-hydroxy-1-phenyl propyl)-1,3-dihydro-2H-benzimidazol-2-ones: Potent, Selective, and Orally Efficacious Norepinephrine Reuptake Inhibitors†‡. Journal of Medicinal Chemistry 2009;52:5703-11.
[238] Zhang P, Terefenko EA, McComas CC, Mahaney PE, Vu A, Trybulski E, et al. Synthesis and activity of novel 1- or 3-(3-amino-1-phenyl propyl)-1,3-dihydro-2H-benzimidazol-2-ones as selective norepinephrine reuptake inhibitors. Bioorganic & Medicinal Chemistry Letters 2008;18:6067-70.
[239] Wu D, Pontillo J, Ching B, Hudson S, Gao Y, Fleck BA, et al. Discovery of a potent, selective, and less flexible selective norepinephrine reuptake inhibitor (sNRI). Bioorganic & Medicinal Chemistry Letters 2008;18:4224-7.
[240] Bymaster FP, Lee TC, Knadler MP, Detke MJ, and Iyengar S. The dual transporter inhibitor duloxetine: a review of its preclinical pharmacology, pharmacokinetic profile, and clinical results in depression. Current pharmaceutical design 2005;11:1475-93.
[241] Sauer JM, Ring BJ, and Witcher JW. Clinical pharmacokinetics of atomoxetine. Clinical pharmacokinetics 2005;44:571-90.
[242] Michelson D, Read HA, Ruff DD, Witcher J, Zhang S, and McCracken J. CYP2D6 and clinical response to atomoxetine in children and adolescents with ADHD. Journal of the American Academy of Child and Adolescent Psychiatry 2007;46:242-51.
[243] Hudson S, Kiankarimi M, Eccles W, Dwight W, Mostofi YS, Genicot MJ, et al. Structure–activity relationships of chiral selective norepinephrine reuptake inhibitors (sNRI) with increased oxidative stability. Bioorganic & Medicinal Chemistry Letters 2008;18:4491-4.
[244] Hudson S, Kiankarimi M, Eccles W, Mostofi YS, Genicot MJ, Dwight W, et al. Synthesis and structure–activity relationships of selective norepinephrine reuptake inhibitors (sNRI) with a heterocyclic ring constraint. Bioorganic & Medicinal Chemistry Letters 2008;18:4495-8.
[245] O'Neill DJ, Adedoyin A, Bray JA, Deecher DC, Fensome A, Goldberg JA, et al. Discovery of Novel Selective Norepinephrine Inhibitors: 1-(2-Morpholin-2-ylethyl)-3-aryl-1,3-dihydro-2,1,3-benzothiadiazole 2,2-Dioxides (WYE-114152). Journal of Medicinal Chemistry 2011;54:6824-31.
[246] O'Neill DJ, Adedoyin A, Alfinito PD, Bray JA, Cosmi S, Deecher DC, et al. Discovery of novel selective norepinephrine reuptake inhibitors: 4-[3-aryl-2,2-dioxido-2,1,3-benzothiadiazol-1(3H)-yl]-1-

(methylamino)butan-2-ols (WYE-103231). J Med Chem 2010;53:4511-21.
[247] Haka MS and Kilbourn MR. Synthesis and regional mouse brain distribution of [11C]nisoxetine, a norepinephrine uptake inhibitor. International journal of radiation applications and instrumentation. Part B, Nuclear medicine and biology 1989;16:771-4.
[248] Reith ME, Wang LC, and Dutta AK. Pharmacological profile of radioligand binding to the norepinephrine transporter: instances of poor indication of functional activity. J Neurosci Methods 2005;143:87-94.
[249] Petersen PV, Lassen N, Ammitzboll T, Moller Nielsen I, Nymark M, Pedersen V, et al. Further pharmacological studies of bicyclic thymoleptics. Acta pharmacologica et toxicologica 1970;28:241-8.
[250] Petersen PV, Lassen N, Hansen V, Huld T, Hjortkjaer J, Holmblad J, et al. Pharmacological studies of a new series of bicyclic thymoleptics. Acta pharmacologica et toxicologica 1966;24:121-33.
[251] McConathy J, Owens MJ, Kilts CD, Malveaux EJ, Camp VM, Votaw JR, et al. Synthesis and biological evaluation of [11C]talopram and [11C]talsupram: candidate PET ligands for the norepinephrine transporter. Nucl Med Biol 2004;31:705-18.
[252] Ding YS, Lin KS, and Logan J. PET imaging of norepinephrine transporters. Current pharmaceutical design 2006;12:3831-45.
[253] Schou M, Sovago J, Pike VW, Gulyas B, Bogeso KP, Farde L, et al. Synthesis and positron emission tomography evaluation of three norepinephrine transporter radioligands: [C-11]desipramine, [C-11]talopram and [C-11]talsupram. Molecular imaging and biology : MIB : the official publication of the Academy of Molecular Imaging 2006;8:1-8.
[254] Malizia AL, Melichar JK, Rhodes CG, Haida A, Reynolds AH, Jones T, et al. Desipramine binding to noradrenaline reuptake sites in cardiac sympathetic neurons in man in vivo. Eur J Pharmacol 2000;391:263-7.
[255] Ding YS, Lin KS, Logan J, Benveniste H, and Carter P. Comparative evaluation of positron emission tomography radiotracers for imaging the norepinephrine transporter: (S,S) and (R,R) enantiomers of reboxetine analogs ([11C]methylreboxetine, 3-Cl-[11C]methylreboxetine and [18F]fluororeboxetine), (R)-[11C]nisoxetine, [11C]oxaprotiline and [11C]lortalamine. J Neurochem 2005;94:337-51.
[256] Schou M, Zoghbi S, Shetty H, Shchukin E, Liow J-S, Hong J, et al. Investigation of the Metabolites of (S,S)-[11C]MeNER in Humans, Monkeys and Rats. Molecular Imaging and Biology 2009;11:23-30.
[257] Ding Y-S, Singhal T, Planeta-Wilson B, Gallezot J-D, Nabulsi N, Labaree D, et al. PET imaging of the effects of age and cocaine on the norepinephrine transporter in the human brain using (S,S)-[11C]O-methylreboxetine and HRRT. Synapse 2010;64:30-8.
[258] Severance AJ, Milak MS, Kumar JS, Prabhakaran J, Majo VJ, Simpson NR, et al. In vivo assessment of [11C]MRB as a prospective PET ligand for imaging the norepinephrine transporter. Eur J Nucl Med Mol Imaging 2007;34:688-93.
[259] Zeng F, Mun J, Jarkas N, Stehouwer JS, Voll RJ, Tamagnan GD, et al. Synthesis, Radiosynthesis, and Biological Evaluation of Carbon-11 and Fluorine-18 Labeled Reboxetine Analogues: Potential Positron Emission Tomography Radioligands for in Vivo Imaging of the Norepinephrine Transporter. J. Med. Chem. 2009;52:62-73.
[260] Zeng F, Jarkas N, Stehouwer JS, Voll RJ, Owens MJ, Kilts CD, et al. Synthesis, in vitro characterization,

and radiolabeling of reboxetine analogs as potential PET radioligands for imaging the norepinephrine transporter. Bioorganic & Medicinal Chemistry 2008;16:783-93.
[261] Zeng F, Mun J, Jarkas N, Stehouwer JS, Voll RJ, Tamagnan GD, et al. Synthesis, Radiosynthesis, and Biological Evaluation of Carbon-11 and Fluorine-18 Labeled Reboxetine Analogues: Potential Positron Emission Tomography Radioligands for in Vivo Imaging of the Norepinephrine Transporter. Journal of Medicinal Chemistry 2008;52:62-73.
[262] Seneca N, Gulyás B, Varrone A, Schou M, Airaksinen A, Tauscher J, et al. Atomoxetine occupies the norepinephrine transporter in a dose-dependent fashion: a PET study in nonhuman primate brain using (S,S)-[18F]FMeNER-D2. Psychopharmacology 2006;188:119-27.
[263] Takano A, Halldin C, Varrone A, Karlsson P, Sjoholm N, Stubbs JB, et al. Biodistribution and radiation dosimetry of the norepinephrine transporter radioligand (S,S)-[18F]FMeNER-D2: a human whole-body PET study. Eur J Nucl Med Mol Imaging 2008;35:630-6.
[264] Takano A, Varrone A, Gulyás B, Karlsson P, Tauscher J, and Halldin C. Mapping of the norepinephrine transporter in the human brain using PET with (S,S)-[18F]FMeNER-D2. NeuroImage 2008;42:474-82.
[265] Mark C, Bornatowicz B, Mitterhauser M, Hendl M, Nics L, Haeusler D, et al. Development and automation of a novel NET-PET tracer: [11C]Me@APPI. Nucl Med Biol 2013;40:295-303.
[266] Halldin C, Farde L, Högberg T, Mohell N, Hall H, Suhara T, et al. Carbon-11-FLB 457: A Radioligand for Extrastriatal D2 Dopamine Receptors. Journal of Nuclear Medicine 1995;36:1275-81.
[267] Bankstahl JP, Kuntner C, Abrahim A, Karch R, Stanek J, Wanek T, et al. Tariquidar-Induced P-Glycoprotein Inhibition at the Rat Blood–Brain Barrier Studied with (R)-11C-Verapamil and PET. Journal of Nuclear Medicine 2008;49:1328-35.
[268] Elsinga PH, Hendrikse NH, Bart J, Vaalburg W, and Waarde Av. PET Studies on P-Glycoprotein Function in the Blood-Brain Barrier: How it Affects Uptake and Binding of Drugs within the CNS. Current pharmaceutical design 2004;10:1493-503.
[269] Wagner CC, Bauer M, Karch R, Feurstein T, Kopp S, Chiba P, et al. A Pilot Study to Assess the Efficacy of Tariquidar to Inhibit P-glycoprotein at the Human Blood–Brain Barrier with (R)-11C-Verapamil and PET. Journal of Nuclear Medicine 2009;50:1954-61.
[270] Pike VW. PET Radiotracers: crossing the blood-brain barrier and surviving metabolism. Trends in pharmacological sciences 2009;30:431-40.
[271] Slifstein M. Affinity. In: I Stolerman editor. Encyclopedia of Psychopharmacology: Springer Berlin Heidelberg; 2010, p. 36-.
[272] Vallabhajosula S. Molecular Imaging - Radiopharmaceuticals for PET and SPECT. 1 ed.: Springer-Verlag Berlin Heidelberg,2009.
[273] Slifstein M. Equilibrium Dissociation Constant. In: I Stolerman editor. Encyclopedia of Psychopharmacology: Springer Berlin Heidelberg; 2010, p. 489-90.
[274] Cheng Y and Prusoff WH. Relationship between the inhibition constant (K1) and the concentration of inhibitor which causes 50 per cent inhibition (I50) of an enzymatic reaction. Biochem Pharmacol 1973;22:3099-108.

[275] Lombardo F, Shalaeva MY, Tupper KA, and Gao F. ElogDoct: A Tool for Lipophilicity Determination in Drug Discovery. 2. Basic and Neutral Compounds. Journal of Medicinal Chemistry 2001;44:2490-7.
[276] Scherrer RA and Howard SM. Use of distribution coefficients in quantitative structure-activity relationships. J Med Chem 1977;20:53-8.
[277] Lipinski CA, Lombardo F, Dominy BW, and Feeney PJ. Experimental and computational approaches to estimate solubility and permeability in drug discovery and development settings. Advanced drug delivery reviews 2001;46:3-26.
[278] Smith DA, Jones BC, and Walker DK. Design of drugs involving the concepts and theories of drug metabolism and pharmacokinetics. Medicinal research reviews 1996;16:243-66.
[279] Yoshida F and Topliss JG. QSAR model for drug human oral bioavailability. J Med Chem 2000;43:2575-85.
[280] Seelig A. The role of size and charge for blood-brain barrier permeation of drugs and fatty acids. Journal of molecular neuroscience : MN 2007;33:32-41.
[281] Gerebtzoff G and Seelig A. In silico prediction of blood-brain barrier permeation using the calculated molecular cross-sectional area as main parameter. Journal of chemical information and modeling 2006;46:2638-50.
[282] Yoon CH, Kim SJ, Shin BS, Lee KC, and Yoo SD. Rapid Screening of Blood-Brain Barrier Penetration of Drugs Using the Immobilized Artificial Membrane Phosphatidylcholine Column Chromatography. Journal of Biomolecular Screening 2006;11:13-20.
[283] Tavares AA, Lewsey J, Dewar D, and Pimlott SL. Radiotracer properties determined by high performance liquid chromatography: a potential tool for brain radiotracer discovery. Nucl Med Biol 2012;39:127-35.
[284] Kobayashi K, Urashima K, Shimada N, and Chiba K. SELECTIVITIES OF HUMAN CYTOCHROME P450 INHIBITORS TOWARD RAT P450 ISOFORMS: STUDY WITH cDNA-EXPRESSED SYSTEMS OF THE RAT. Drug Metabolism and Disposition 2003;31:833-6.
[285] Bayliss MK and Eddershaw PJ. Drug metabolism assays and their use in drug discovery. Ernst Schering Research Foundation workshop 2002:69-79.
[286] Lewis DF, Dickins M, Eddershaw PJ, Tarbit MH, and Goldfarb PS. Cytochrome P450 substrate specificities, substrate structural templates and enzyme active site geometries. Drug metabolism and drug interactions 1999;15:1-49.
[287] Lewis DF, Eddershaw PJ, Dickins M, Tarbit MH, and Goldfarb PS. Structural determinants of cytochrome P450 substrate specificity, binding affinity and catalytic rate. Chemico-biological interactions 1998;115:175-99.
[288] Lewis DF. Human cytochromes P450 associated with the phase 1 metabolism of drugs and other xenobiotics: a compilation of substrates and inhibitors of the CYP1, CYP2 and CYP3 families. Current medicinal chemistry 2003;10:1955-72.
[289] Guengerich FP. Cytochrome P450 and Chemical Toxicology. Chemical Research in Toxicology 2007;21:70-83.
[290] Lewis DF and Lake BG. Species differences in coumarin metabolism: a molecular modelling evaluation of CYP2A interactions. Xenobiotica; the fate of foreign compounds in biological systems 2002;32:547-61.

[291] Venkatakrishnan K, von Moltke LL, and Greenblatt DJ. Human cytochromes P450 mediating phenacetin O-deethylation in vitro: validation of the high affinity component as an index of CYP1A2 activity. J Pharm Sci 1998;87:1502-7.
[292] Petrulis JR, Chen G, Benn S, LaMarre J, and Bunce NJ. Application of the ethoxyresorufin-O-deethylase (EROD) assay to mixtures of halogenated aromatic compounds. Environmental toxicology 2001;16:177-84.
[293] Wang B, Yang LP, Zhang XZ, Huang SQ, Bartlam M, and Zhou SF. New insights into the structural characteristics and functional relevance of the human cytochrome P450 2D6 enzyme. Drug metabolism reviews 2009;41:573-643.
[294] Kawano S, Kamataki T, Yasumori T, Yamazoe Y, and Kato R. Purification of human liver cytochrome P-450 catalyzing testosterone 6 beta-hydroxylation. Journal of biochemistry 1987;102:493-501.
[295] Zhou SF, Liu JP, and Lai XS. Substrate specificity, inhibitors and regulation of human cytochrome P450 2D6 and implications in drug development. Current medicinal chemistry 2009;16:2661-805.
[296] Imai T. Human carboxylesterase isozymes: catalytic properties and rational drug design. Drug metabolism and pharmacokinetics 2006;21:173-85.
[297] Ross MK and Crow JA. Human carboxylesterases and their role in xenobiotic and endobiotic metabolism. Journal of biochemical and molecular toxicology 2007;21:187-96.
[298] Harris JE, Sloane JF, and King DT. New techniques in autoradiography. Nature 1950;166:25-6.
[299] Bundy DC. Autoradiography. Current protocols in protein science / editorial board, John E. Coligan ... [et al.] 2001;Chapter 10:Unit 10.1.
[300] Odeblad E. [New trends in autoradiography]. Nordisk medicin 1950;43:1056-8.
[301] Langstrom B, Andren PE, Lindhe O, Svedberg M, and Hall H. In vitro imaging techniques in neurodegenerative diseases. Molecular imaging and biology : MIB : the official publication of the Academy of Molecular Imaging 2007;9:161-75.
[302] Atweh SF and Kuhar MJ. Autoradiographic localization of opiate receptors in rat brain. III. The telencephalon. Brain Res 1977;134:393-405.
[303] Bourgeois JP, Popot JL, Ryter A, and Changeux JP. Consequences of denervation on the distribution of the cholinergic (nicotinic) receptor sites from Electrophorus electricus revealed by high resolution autoradiography. Brain Res 1973;62:557-63.
[304] Hafeez MA and Zerihun L. Autoradiographic localization of 3H-5-HTP and 3H-5-HT in the pineal organ and circumventricular areas in the rainbow trout, Salmo gairdneri Richardson. Cell and tissue research 1976;170:61-76.
[305] Hollt V, Dum J, Blasig J, Schubert P, and Herz A. Comparison of in vivo and in vitro parameters of opiate receptor binding in naive and tolerant dependent rodents. Life sciences 1975;16:1823-8.
[306] Maurer RA and Woolley DE. Demonstration of nuclear 3H-estradiol binding in hypothalamus and amygdala of female, androgenized-female, and male rats. Neuroendocrinology 1974;16:137-47.
[307] Mess B and Voros E. On the thyrotrophic area of the anterior hypothalamus. Acta biologica Academiae Scientiarum Hungaricae 1965;16:105-12.
[308] Mohler H, Battersby MK, Richards JG, Polc P, Cumin R, Pieri L, et al. Benzodiazepine receptor:

localization by photoaffinity labeling and isolation of a possible endogenous ligand. Advances in biochemical psychopharmacology 1980;21:295-9.
[309] Pert CB, Kuhar MJ, and Snyder SH. Autoradiograhic localization of the opiate receptor in rat brain. Life sciences 1975;16:1849-53.
[310] Pert CB, Kuhar MJ, and Snyder SH. Opiate receptor: autoradiographic localization in rat brain. Proc Natl Acad Sci U S A 1976;73:3729-33.
[311] Sheridan PJ. Cellular and subcellular localization of 3h-diethylstilboestrol in the central nervous system. Cell and tissue research 1977;183:379-84.
[312] Young WS, 3rd and Kuhar MJ. A new method for receptor autoradiography: [3H]opioid receptors in rat brain. Brain Res 1979;179:255-70.
[313] Fukuda T and Koelle GB. The Cytological Localization of Intracellular Neuronal Acetylcholinesterase. The Journal of Biophysical and Biochemical Cytology 1959;5:433-40.
[314] Kádár A, Wittmann G, Liposits Z, and Fekete C. Improved method for combination of immunocytochemistry and Nissl staining. Journal of neuroscience methods 2009;184:115-8.
[315] Bergstrom M, Awad R, Estrada S, Malman J, Lu L, Lendvai G, et al. Autoradiography with positron emitting isotopes in positron emission tomography tracer discovery. Molecular imaging and biology : MIB : the official publication of the Academy of Molecular Imaging 2003;5:390-6.
[316] Schou M, Halldin C, Sóvágó J, Pike VW, Hall H, Gulyás B, et al. PET evaluation of novel radiofluorinated reboxetine analogs as norepinephrine transporter probes in the monkey brain. Synapse 2004;53:57-67.
[317] Varrone A, Steiger C, Schou M, Takano A, Finnema SJ, Guilloteau D, et al. In vitro autoradiography and in vivo evaluation in cynomolgus monkey of [18F]FE-PE2I, a new dopamine transporter PET radioligand. Synapse (Hoboken, NJ, U. S.) 2009;63:871-80.
[318] Liu H, Jin H, Li J, Zhang X, Kaneshige K, Parsons SM, et al. In vitro and ex vivo characterization of (-)-TZ659 as a ligand for imaging the vesicular acetylcholine transporter. Eur J Pharmacol 2015.
[319] Cohen M, Varki NM, Jankowski MD, and Gagneux P. Using unfixed, frozen tissues to study natural mucin distribution. Journal of visualized experiments : JoVE 2012:e3928.
[320] Duran I, Mari-Beffa M, Santamaria JA, Becerra J, and Santos-Ruiz L. Freeze substitution followed by low melting point wax embedding preserves histomorphology and allows protein and mRNA localization techniques. Microscopy research and technique 2011;74:440-8.
[321] Fischer AH, Jacobson KA, Rose J, and Zeller R. Cryosectioning tissues. CSH protocols 2008;2008:pdb.prot4991.
[322] Bratthauer GL. Preparation of frozen sections for analysis. Methods in molecular biology (Clifton, N.J.) 2010;588:67-73.
[323] Halldin C, Bjurling P, Stalnacke CG, Jossan SS, Oreland L, and Langstrom B. 11C-labelling of dimethylphenethylamine in two different positions and biodistribution studies. International journal of radiation applications and instrumentation. Part A, Applied radiation and isotopes 1989;40:557-60.
[324] Kilbourn MR, Carey JE, Koeppe RA, Haka MS, Hutchins GD, Sherman PS, et al. Biodistribution, dosimetry, metabolism and monkey PET studies of [18F]GBR 13119. Imaging the dopamine uptake system in

vivo. International journal of radiation applications and instrumentation. Part B, Nuclear medicine and biology 1989;16:569-76.
[325] Shiue CY, Bai LQ, Teng RR, Arnett CD, and Wolf AP. No-carrier-added N-(3-[18F]fluoropropyl)spiroperidol: biodistribution in mice and tomographic studies in a baboon. Journal of nuclear medicine : official publication, Society of Nuclear Medicine 1987;28:1164-70.
[326] Welch MJ, Chi DY, Mathias CJ, Kilbourn MR, Brodack JW, and Katzenellenbogen JA. Biodistribution of N-alkyl and N-fluoroalkyl derivatives of spiroperidol; radiopharmaceuticals for PET studies of dopamine receptors. International journal of radiation applications and instrumentation. Part B, Nuclear medicine and biology 1986;13:523-6.
[327] Ingvar M, Eriksson L, Rogers GA, Stone-Elander S, and Widen L. Rapid feasibility studies of tracers for positron emission tomography: high-resolution PET in small animals with kinetic analysis. J Cereb Blood Flow Metab 1991;11:926-31.
[328] Bloomfield PM, Rajeswaran S, Spinks TJ, Hume SP, Myers R, Ashworth S, et al. The design and physical characteristics of a small animal positron emission tomograph. Physics in medicine and biology 1995;40:1105-26.
[329] Yao R, Lecomte R, and Crawford ES. Small-animal PET: what is it, and why do we need it? J Nucl Med Technol 2012;40:157-65.
[330] Schnockel U, Hermann S, Stegger L, Law M, Kuhlmann M, Schober O, et al. Small-animal PET: a promising, non-invasive tool in pre-clinical research. European journal of pharmaceutics and biopharmaceutics : official journal of Arbeitsgemeinschaft fur Pharmazeutische Verfahrenstechnik e.V 2010;74:50-4.
[331] Myers R and Hume S. Small animal PET. European Neuropsychopharmacology 2002;12:545-55.
[332] Riemann B, Schafers KP, Schober O, and Schafers M. Small animal PET in preclinical studies: opportunities and challenges. The quarterly journal of nuclear medicine and molecular imaging : official publication of the Italian Association of Nuclear Medicine (AIMN) [and] the International Association of Radiopharmacology (IAR), [and] Section of the So 2008;52:215-21.
[333] Zhang P, Terefenko EA, McComas CC, Mahaney PE, Vu A, Trybulski E, et al. Synthesis and activity of novel 1- or 3-(3-amino-1-phenyl propyl)-1,3-dihydro-2H-benzimidazol-2-ones as selective norepinephrine reuptake inhibitors. Bioorg. Med. Chem. Lett. 2008;18:6067-70.
[334] Donovan SF and Pescatore MC. Method for measuring the logarithm of the octanol–water partition coefficient by using short octadecyl–poly(vinyl alcohol) high-performance liquid chromatography columns. Journal of Chromatography A 2002;952:47-61.
[335] Vraka C, Nics L, Weiss V, Wagner K-H, Hacker M, Wadsak W, et al. Combination of High Throughput HPLC Methods for Rapid Prediction of Blood Brain Barrier Penetration of Newly Developed Radiotracers - EANM 14. European Journal of Nuclear Medicine and Molecular Imaging 2014;41:442.

7 APPENDIX

7.1 LIST OF ABBREVIATIONS

ABBREVIATION		ABBREVATION	
α	alpha particle	**G protein**	guanine nucleotide-binding proteins
β+	positron	**GC**	gas chromatography
µPET	microPET	**HEK**	human embryonic kidney
Å	angstroem	**HPLC**	high pressure liquid chromatography
ACN	acetonitrile	**IAM**	immobilized artificial membrane
AD	Alzheimer's disease	**IC50**	half maximum inhibitoric concentration
ADHD	attention deficient hyperactivity disorder	**K2.2.2.**	Kryptofix
ADME	absorption distribution metabolism excretion	**Kd**	equilibrium dissociation constant
AR	adrenoreceptor	**Ki**	equilibrium inhibition constant
ATX	atomoxetin	**LAL**	Limulus amebocyte lysate
BAT	brown adipose tissue	**LC**	locus ceruleus
BBB	blood-brain-barrier	**LOR**	line of response
cAMP	cyclic adenosin monophosphate	**MAO**	Monoaminooxidase
CES	carboxyl esterase	**MAP**	mitogen-activated protein
CNS	central nervous system	**MR**	magnetic resonance spectroscopy
COMT	catechyl-o-methyl transferase	**NADP(H)**	nicotinamide adenine dinucleotide phosphate
CT	computer tomography	**NE**	norepinephrine, noradrenalin
CYP	cytochrom P 450	**NET**	norepinephrine transporter
DA	dopamine	**NMDA**	N-methyl-D-aspartate
DAT	dopamine transporter	**oDCB**	ortho-dichlorobenzene
DMF	dimethylformamide	**PD**	Parkinson's disease

DMSO	dimethylsulfoxide	**PET**	positron emission tomography
FFA	free fatty acid	**PI3K**	phosphatidylinositide 3-kinase
Pm	permeability	**TLC**	thin layer chromatography
ROI	region of interest	**UCP-1**	uncoupling protein 1, thermogenin
SERT	serotonin transporter	**UV**	ultraviolet
SNar	aromatic nucleophilic substitution	**VMA**	vanillyl mandelic acid
SNRI	selective noradrenaline reuptake inhibitors	**VMAT**	vesicular monoamine transporter
SPE	solid phase extraction	**VOI**	volume of interest
SUV	standardized uptake value	**WAT**	white adipose tissue
t1/2	half-life		

7.2 CURRICULUM VITAE

CHRISTINA RAMI-MARK

PERSONAL INFORMATION

Date & Place of Birth: 18th June 1988, Kirchdorf/Krems, Austria

Marital Status: Married

Research Facility: Radiochemistry and Biomarker Development Unit, Division of Nuclear Medicine, Department of Biomedical Imaging and Image-guided Therapy, Medical University of Vienna, Austria

Contact: christina.rami-mark@meduniwien.ac.at

c.mark@mark.at

RESEARCH AND WORKING FIELD

•PET-Radiolabeling: Development of PET-tracers for neurotransmitter transporters and receptors (especially for NET, but also for DAT and SERT)

•SPECT-Radiolabeling: Development of 99mTc-labeled Antibodys

•Routine preparation: [carbonyl-^{11}C]WAY100635, [^{11}C]PHNO, [^{18}F]FMeNER-D2, [^{18}F]FET and [^{68}Ga]PSMA for clinical trials

•Preclinical research: Radiolabeling, biodistribution, binding studies, autoradiography, metabolite studies, µPET

EDUCATION

10/2011-2015 PhD- studies: Chemistry at the University of Vienna
(Scientific work in Radiochemistry at Division of Nuclear Medicine, Dept of Biomedical Imaging and Image-guided Therapy, Medical University of Vienna)

09/2011	Master Degree at Institute of Organic Chemistry, University of Vienna
10/2009- 09/2011	Master studies in Chemistry at the University of Vienna
06/2009	Bachelor Degree at the Institute of Inorganic Chemistry at the University of Vienna
10/2006-10/2009	Bachelor studies in Chemistry at the University of Vienna
1998-2006:	'Stiftsgymnasium Admont', 8911 Admont
1994-1998:	Elementary school: Volksschule Windischgarsten

SCIENTIFIC AND ACADEMICAL EXPERIENCES

01/2015	Assistant at the University of Vienna: radiochemistry practical course
10/2014	Lecture at the Medical University: Selbstorganisiertes Lernen - Chemie
10/2011-now	Employment as researcher at the Radiochemistry and Biomarker Development Unit, Division of Nuclear Medicine, Department of Biomedical Imaging and Image-guided Therapy, Medical University of Vienna
02/2011 – 09/2011	Scientific assistant and supervision of students during master thesis at the University of Vienna, Institute of Organic Chemistry, Währinger Straße 38 1090 Wien
02/2009 – 09/10	Tutor at the University of Vienna, Institute of Organic Chemistry, Währinger Straße 38, 1090 Wien

LANGUAGES

German (mother tongue)
English (B2 to C1 level)
Italian (B1 to B2 level)
French (B1 level)
Russian (A2 level)

7.3 LIST OF SCIENTIFIC PUBLICATIONS

PEER REVIEWED ARTICLES

1. **Mark C.**, Bornatowicz B., Mitterhauser M., Hendl M., Nics L., Haeusler D., Lanzenberger R., Berger ML., Spreitzer H., Wadsak W. Development and automation of a novel NET-PET tracer: [11C]Me@APPI. *Nucl Med Biol.,* **2013**, 40, 2, 295-303. IF=2.41

2. **Rami-Mark C.**,Bornatowicz B., Fink C., Otter P., Ungersboeck J., Vraka C., Haeusler D.,Nics L., Spreizer, H., Mitterhauser M., Wadsak W. Synthesis, radiosynthesis and first in-vitro evaluation of Novel PET-tracers for the dopamine transporter: [^{11}C]IPCIT and [^{18}F]FE@IPCIT. *Bioorg Med Chem.*, **2013**, 21, 7562-7569. IF =2.82

3. **Rami-Mark C.**, Zhang M.R., Mitterhauser M., Lanzenberger R., Wadsak W. [18F]FMeNER-D2: Reliable fully-automated synthesis for visualization of the norepinephrine transporter. *Nucl Med Biol.*, **2013,** 40, 1049-1054. IF=2.41

4. **Rami-Mark C.**, Ungersboeck J., Haeusler D., Nics L., Philippe C., Mitterhauser M,. Willeit M., Lanzenberger R., Karanikas G., Wadsak W. Reliable set-up for in-loop ^{11}C-carboxylations using Grignard reactions for the preparation of [carbonyl-^{11}C]WAY-100635 and [^{11}C]-(+)-PHNO. *Appl Radiat Isot.,* **2013**, 80: 75-80. IF=1.09

5. Kranz GS, **Rami-Mark C**, Kaufmann U, Baldinger P, Hahn A, Höflich A, Savli M, Stein P, Wadsak W, Mitterhauser M, Winkler D, Lanzenberger R, Kasper S. Effects of hormone replacement therapy on cerebral serotonin-1A receptor binding in postmenopausal women examined with [*carbonyl*-^{11}C]WAY-100635. *Psychoneuroendocrinology* **2014**, 45, 1-10. IF=3.53

6. Stein P, Baldinger P, Kaufmann U, **Rami-Mark C**, Hahn A, Höflich A, et al. Relation of progesterone and DHEAS serum levels to 5-HT1A receptor binding potential in pre- and postmenopausal women. Psychoneuroendocrinology, **2014,** 46, 52-63. IF =5.59

7. Vanicek T, Spies M, **Rami-Mark C**, Savli M, Höflich A, Kranz GS, Hahn A, Kutzelnigg A, Traub-Weidinger T, Mitterhauser M, Wadsak W, Hacker M, Volkow N, Kasper S, Lanzenberger R. The Norepinephrine Transporter in Attention-Deficit/Hyperactivity Disorder Investigated With Positron Emission Tomography. *JAMA Psychiatry,* **2014**, 71, 1340-1349. IF=12.01

8. Pia Baldinger, Anna S Höflich, Markus Mitterhauser, Andreas Hahn, **Christina Rami-Mark**, Marie Spies, Wolfgang Wadsak, Rupert Lanzenberger, Siegfried Kasper. Effects of Silexan on the serotonin-1A receptor and microstructure of the human brain: a randomized, placebo-controlled, double-blind, cross-over study with molecular and structural neuroimaging. International Journal of Neuropsychopharmacology, **2015**, 1-9. IF=5.26

9. Neudorfer C, Seddik A, Shanab K, Jurik A, **Rami-Mark C**, Holzer W, Ecker G, Mitterhauser M, Wadsak W, Spreitzer H. Synthesis and in silico evaluation of novel reference compounds for PET based investigations of the norepinephrine transporter. *Molecules* **2014,** 20, 1712-1730. IF=2.1

10. Pia Baldinger, Christoph Kraus, **Christina Rami-Mark**, Gregor Gryglewski, Georg S Kranz, Daniela Haeusler, Andreas Hahn, Marie Spies, Wolfgang Wadsak, Markus Mitterhauser, Dan Rujescu, Siegfried Kasper, Rupert Lanzenberger. Interaction between 5-HTTLPR and 5-HT1B genotype status enhances cerebral 5-HT1A receptor binding. NeuroImage, **2015**, in press. IF=6.13

11. **Christina Rami-Mark**, Cecile Philippe, Chrysoula Vraka, Lukas Nics, Monika Dumanic, Helmut Spreitzer, Rupert Lanzenberger, Marcus Hacker, Wolfgang Wadsak and Markus Mitterhauser. Comparative preclinical evaluation of the norepinephrine transporter PET ligands [11C]Me@APPI AND [18F]FMeNER-D2. J Nucl Med. **2015**, Submitted, in review.

12. **Christina Rami-Mark**, Neydher Berroteran, Cecile Philippe, Stefanie Folitn, Chrysoula Vraka, Alexander Hoepping, Rupert Lanzenberger, Marcus Hacker, Markus Mitterhauser and Wolfgang Wadsak. Radiosynthesis and first preclinical evaluation of the novel norepinephrine transporter PET ligand [11C]Me@HAPTHI. European Journal of Nuclear Medicine and Molecular Imaging Research, **2015**, Submitted, in review.

ORAL PRESENTATIONS

1. **Mark C.**, Bornatowicz B., Nics L., Hendl M., Otter P., Haeusler D., Berger M., Lanzenberger R., Spreitzer H., Mitterhauser M., Wadsak W. (2012): Radiosynthese und präklinische Evaluierung von neuen Norepinephrine Transporter Liganden, 20. Jahrestagung der Arbeitsgemeinschaft Radiochemie/ Radiopharmazie der DGN, Bad Honnef, Germany

2. **Rami-Mark C.**, Zhang M.R., Mitterhauser M., Lanzenberger R., Wadsak W. (2013) "Targeting the Norepinephrine Transporter" – [^{18}F]FMeNER-D2: Optimierung und Automatisierung der Radiosynthese zur klinischen Anwendung, 21. Jahrestagung der Arbeitsgemeinschaft Radiochemie/ Radiopharmazie der DGN, Pamhagen, Austria

3. **Rami-Mark C.**, D. Haeusler, F.Kiefer, M.R. Zhang, R. Lanzenberger, M. Hacker, M. Mitterhauser, W.Wadsak. (2014) „Targeting the Norepinephrine Transporter - [18F]FMeNER-D2: automation of synthesis, in-vitro and in-vivo evaluation in human/rat brain and periphery." *31st International Austrian Winter Symposium of Radioactive Isotopes in Molecular Imaging*, January 22 – 25, 2014, Zell am See, Austria

4. **Rami-Mark C.**, M. R. Zhang, M. Mitterhauser, R. Lanzenberger, M. Hacker, W. Wadsak. (2014) „Verbesserte Basis zur Norepinephrin-Transporter Bildgebung: Die vollautomatisierte Radiosynthese von [18F]FMeNER-D2" NuklearMedizin2014, 52. Jahrestagung der Deutschen Gesellschaft für Nuklearmedizin, 26.-29.3.2014, Hannover, Germany

POSTER PRESENTATIONS

1. **Mark C.**, Bornatowicz B., Ungersboeck J. Nics L., Haeusler D., Berger M., Lanzenberger R., Spreitzer H., Mitterhauser M., Wadsak W. Development of [11C]Me@APPI, a novel NET-PET tracer for the Norepinephrine Transporter,25th Annual Congress of the European Association of Nuclear Medicine; 27-31th Oct 2012; Milano, Italy: Eur J Nucl Med Mol Imaging, 2012, 39, Suppl 2: S409.

2. **Mark C.**, Bornatowicz B., Fink C., Haeusler D., Berger M., Spreitzer H. Mitterhauser M., Wadsak W. Novel PET-tracers for the dopamine transporter: [11C]IPCIT and [18F]FE@IPCIT, 20th International Symposium of Radiopharmaceutical Sciences, 12-17th May 2013, Jeju, Korea: Label Compd Radiopharm 2013; 56,Suppl 1:S148, P-061.

3. **Rami-Mark C.**, Vraka C., Nics L., Haeusler D., Lanzenberger R., Bornatowicz B., Spreitzer H., Hacker M., Mitterhauser M., Wadsak W. [18F]FMeNER-D2 vs. [11C]Me@APPI – a comparative preclinical evaluation of PET tracers for the norepinephrine transporter. 27th Annual Congress of the European Association of Nuclear Medicine; 18th-22nd Oct 2014; Gothenburg, Sweden. Eur J Nucl Med Mol Imaging, 2014, 41, Suppl 2: S420 P220.

4. **Rami-Mark C.**, Fazekas J., Singer J., Willmann M., Wadsak W., Jensen-Jarolim E., Mitterhauser M. A 99mTc-labelled antibody for the canine EGF-receptor: radiolabelling, quality control, stability testing and binding studies. 27th Annual Congress of the European Association of Nuclear Medicine; 18th-22nd Oct 2014; Gothenburg, Sweden. Eur J Nucl Med Mol Imaging, 2014, 41, Suppl 2: S446, P305.